FAR-FIELD WAVES AND NEAR-FIELD FLOWS DUE TO SHIPS OR OFFSHORE STRUCTURES

Francis Noblesse[1] **and Jiayi He**[2]

[1] Riverbend, 19385 Cypress Ridge Ter. Leesburg VA 20176 USA
noblfranc@gmail.com

[2] School of Ocean and Civil Engineering
Shanghai Jiao Tong University, Shanghai, China
hejiayifans@163.com

Synopsis

This book provides a solid foundation for the analysis of radiation and diffraction of water waves by large bodies such as offshore structures and ships. The book consists of two main parts. Four chapters consider *far-field waves* and wave patterns for a *general* dispersion relation associated with plane waves, with specific applications to offshore structures in waves and ships steadily advancing in calm water or through waves. Seven chapters expound a new method—that greatly differs from the usual Green-function and boundary-integral-equation method—for evaluating *near-field flows*. Specifically, two fundamental questions: what boundary-integral equation should be solved? and how can this equation be solved? are reconsidered. Main results of this reconsideration are an integral equation that is much simpler than the integro-differential equation currently solved, and a method of solution—called Fourier-Kochin (FK) method—that is simpler and more general than the usual Green-function method. Indeed, the FK method avoids major complexities associated with that usual method, and moreover is directly applicable to a wide class of plane dispersive waves, such as waves in very large floating elastic structures and ice mechanics. An optimal decomposition of the disturbance created by a general forcing function into waves and a non-oscillatory local disturbance is also given. This decomposition and the FK method, which both are directly applicable to general plane dispersive waves, and the simple integral equation given in the book lay the foundation of a new type of panel methods for computing near-field flows and far-field waves created by ships or offshore structures.

Table of contents

PART 1 : FAR-FIELD WAVES

PART 2 : NEAR-FIELD FLOWS

Preface

This book considers wave diffraction and radiation by ships and offshore structures. Realistic and practical methods that account for the dominant flow physics and are suited for applications to design and optimization are crucial. Indeed, analytical methods and related computational tools that are both realistic and practical—two critical requirements—are essential. Accordingly, the analysis expounded in the book is based on potential-flow theory, which is realistic for diffraction-radiation of water waves by large bodies such as ships and offshore structures, and the related method of Green functions and boundary-integral flow representations.

Three major classes of flows are primarily considered: diffraction and radiation of regular (time-harmonic) waves by an offshore structure (or some other stationary body such as a moored ship) in water of uniform finite depth, and flow around a ship that steadily advances in calm water or through regular waves. The general boundary-value problems associated with these three basic classes of flows are defined in chapter 1.

Far-field free waves and near-field local flow

The flow around a ship or an offshore structure is usefully decomposed into waves and a non-oscillatory local flow, which is important at the body (ship or offshore structure) and in its vicinity but decays rapidly away from the body. Although created by the body, the waves propagate with little influence from the body, and accordingly are commonly called free waves.

Both the local flow, important in the near field (at and near the body), and the free waves dominant in the far field (away from the body) are main features of flows around ships and offshore structures. Computation of the local-flow component is required to evaluate the pressure distribution at the body surface and the related hydrodynamic coefficients (added mass, wave damping), linear and nonlinear wave loads, and body motions. The free waves and the related far-field wave patterns created by ships and offshore structures are also important. Indeed, these far-field wave patterns are the most conspicuous feature of flows around ships and offshore structures.

Free waves are considered in Part 1, which consists of four chapters, and near-field flows—for which both the waves and the local-flow component are important—are considered in Part 2, which contains seven chapters.

PART 1: Free waves and wave patterns (chapters 2–5)

A radiation condition that relies on observations, e.g. a ship that steadily advances in calm water creates waves behind the ship but not ahead, is commonly invoked in the analysis of wave diffraction-radiation in ship and offshore hydrodynamics. Radiation conditions are not obvious for a ship that advances through regular waves in the regime where waves are created both behind the ship and ahead. However, radiation conditions are not necessary and indeed are not invoked in the book, which considers flows that slowly grow from rest at time $T = -\infty$ as is expressed in (1.22).

Thus, chapter 2 considers basic and modified elementary wave functions. The basic wave functions satisfy Laplace's equation and the boundary conditions at the sea bottom and at the free surface. These basic elementary waves are subsequently modified in accordance with flows that slowly grow from a state of rest at the time $T = -\infty$ and vanish in the far field. Free waves created by ships or offshore structures are then expressed in chapter 2 as a linear superposition of these generalized elementary waves. Chapter 3 presents general basic relations and far-field stationary-phase approximations that explicitly determine the group and phase velocities, as well as far-field wave patterns, in terms of the dispersion function. These relations hold for a broad class of plane dispersive waves in a general medium.

Chapters 2 and 3 include applications of the basic relations given in these two chapters for a general dispersive medium to the simple case of offshore structures in regular waves. The relations given in chapters 2 and 3 for general dispersive waves are also applied in chapters 4 and 5 to the free waves created by a ship that steadily advances in calm water or through regular waves. The application to a ship that advances through regular waves given in chapter 5 provides a vivid illustration of the notable fact that a simple dispersion relation can define multiple dispersion curves and a surprisingly rich set of wave patterns that involve widely different waves.

PART 2: Near-field local flows (chapters 6–12)

The method—commonly called Green-function and boundary-integral method—for solving boundary-value problems associated with Laplace's equation (or similar equations) and arbitrary 3D geometries is expounded in chapter 6. This general method is then applied in chapters 7–9 to the major classes of flows around ships and offshore structures considered in the book. Specifically, chapter 7 defines the Green functions associated with these classes of flows, and chapters 8 and 9 apply the classical Green identity given in chapter 6, with the Green functions defined in chapter 7, to formulate boundary-integral flow representations. Lastly, chapters 10–12

expound the method of solution called Fourier-Kochin (FK) method. Some highlights of chapters 7–12 are now noted.

Green functions (chapter 7)

The Green functions associated with diffraction-radiation of regular waves by an offshore structure in deep water or in finite water-depth, and the Green functions associated with a ship that advances at a constant speed in calm deep water or through regular waves, are considered in chapter 7.

A Green function is commonly defined as the velocity potential of the flow that is created at a flow-field point $\boldsymbol{\xi}$ by a point-source located at a source-point $\mathbf{x}$ that is submerged below the free surface. However, this common interpretation breaks down if the singularity-point $\mathbf{x}$ is located at the free-surface plane $z = 0$. In that case, the Green function must be associated with a flux through the plane $z = 0$, as is explained in section 6.7 and is explicitly stated in the fundamental relations (8.5c-d) and (9.4b-c).

A Green function can also be viewed as the velocity potential of the flow created at a flow-field point $\mathbf{x}$ by a point-source at a point $\boldsymbol{\xi}$. This symmetry however involves a subtlety—related to the boundary condition at the free surface—for a ship that steadily advances in calm water or through waves, as is explained in section 6.8 and is made explicit in the boundary conditions at the free surface in (9.3c) and (9.4b-c).

The Green functions considered in the book are associated with the Laplace equation, and accordingly are expressed in terms of two elementary solutions of the Laplace equation: the free-space singularity S, widely called Rankine source, and the basic wave function E, which are defined as

$$S \equiv 1/\sqrt{(\xi-x)^2+(\eta-y)^2+(\zeta-z)^2} \;\text{ and }\; E \equiv e^{\,k\,z\,+\,\mathrm{i}\,(\alpha\,x+\beta\,y)}$$

where α and β are Fourier variables and $k \equiv \sqrt{\alpha^2+\beta^2}$. Specifically, the Green functions, commonly denoted as G, are expressed in terms of a Fourier component G^F that is given by a Fourier superposition of elementary wave functions E and a Rankine component G^R defined in terms of Rankine sources S. The elementary solutions S and E of the Laplace equation are related via Fourier transformation, and the Rankine-Fourier decomposition $G^R + G^F$ consequently is not unique. The benefits of this non-uniqueness are exploited in chapter 7 to define *optimal* Rankine-Fourier decompositions of the Green functions associated with potential flows around offshore structures in waves and ships advancing in calm water or through waves.

Chapter 7 also includes a Green function—useful for a ship advancing through regular waves of frequency ω at a constant speed V_s in the regime $V_s\,\omega/g < 1/4$ where g is the acceleration of gravity—that agrees with the Green functions associated with the special cases $V_s = 0$ or $\omega = 0$. Specifically, expressions (7.53) provide a formal decomposition of the Green function into a component that represents a flow scaled in terms of the length

g/ω^2 and contains ring waves, and a component that is scaled with respect to V_s^2/g and contains inner and outer Kelvin-like V waves.

Boundary-integral flow representations (chapters 8 and 9)

The method of Green function and boundary-integral representation expounded in chapter 6 is applied in chapters 8 and 9 to the general boundary-value problems associated with wave diffraction and radiation by an offshore structure in regular waves (chapter 8) and a ship that steadily advances through waves (chapter 9). Specifically, Green's basic identity is applied to the classical Neumann-Kelvin linear boundary-value problem for potential flow around the hull surface of a body (ship, offshore structure) that pierces the free surface. Green's fundamental identity is also applied to an alternative linear flow model—called rigid-waterplane linear flow model—in which a free-surface-piercing ship or offshore structure is treated as a body that is closed via a rigid waterplane submerged at an infinitesimally small depth below the free surface.

Green's identity applied to the usual Neumann-Kelvin linear flow model or the rigid-waterplane flow model yields identical boundary-integral flow representations for a stationary body. However, these alternative linear flow models yield different (although consistent) flow representations for a ship that advances through waves or in calm water. The rigid-waterplane flow model—with the crucial constraint that the thin layer of water between the rigid lid that closes the submerged body and the waterplane above the lid is a 'dead-water' region—yields a remarkably simple boundary-integral flow representation. This flow representation holds for a stationary body in regular waves as well as a ship that steadily advances in calm water or through regular waves. A common feature of the alternative boundary-integral flow representations given in chapters 8 and 9 is that they are weakly singular and hence define flow potentials that are continuous at the hull surface of the ship or offshore structure.

A general method of solution (chapters 10–12)

The boundary-integral flow representations given in chapters 8 and 9 express the flow potential associated with a body (offshore structure, ship) as distributions of a Green function and its gradient over the surface of the body. The Fourier components in the Rankine-Fourier representations of the Green functions for the classes of flows considered in chapter 7 are defined by singular double Fourier integrals. The common Green-function method implemented in current panel methods involves two basic steps. The first step is the 'Fourier-integration' that is required to evaluate the Green function, and its gradient, associated with a particular class of flows. This task involves complicated mathematical analysis, reported in innumerable studies for the major classes of flows around ships and offshore structures considered in the book. The second step in the usual Green-function method

is the 'space-integration' required to integrate the Green function and its gradient over the panels that approximate the body surface. This step, while less difficult than the 'Fourier-integration' step, requires special attention because the Green functions associated with the classes of flows considered in the book involve intricate singularities. The usual Green-function method has been steadfastly applied in ship and offshore hydrodynamics (and other fields) over the past fifty years, but is not considered in the book.

A simpler and more general alternative approach, called Fourier-Kochin method, is expounded instead. The 'space-integration' over the panels that approximate the hull-surface of a body (ship, offshore structure), which is performed after the 'Fourier-integration' in the usual Green-function method, is performed first (and the 'Fourier-integration' is performed next) in the Fourier-Kochin method. Thus, the Fourier and space integrations are performed in reverse order in the Fourier-Kochin method expounded in chapter 10. An obvious benefit of this approach is that the space-integration merely consists in integrating smooth elementary functions (exponential and trigonometric functions) over the panels that approximate a body surface, whereas the usual Green-function method requires integration of intricate singularities imbedded in the Green functions associated with flows around ships or offshore structures.

Another major advantage of the Fourier-Kochin method is that it avoids the daunting mathematical analyses of Green functions that are required—for every class of flows around ships and offshore structures or every other type of dispersive waves—in the usual Green-function method. Indeed, an important benefit of the Fourier-Kochin method is its *generality*, as is now explained.

The 'Fourier integration' step, which evidently is the major task in the Fourier-Kochin method, consists in evaluating a double Fourier integral that is singular along every curve, called dispersion curve, defined (in the Fourier plane) by the dispersion relation relevant to the class of dispersive waves under consideration. This crucial fundamental task in the Fourier-Kochin method is considered in chapter 11 for a *general dispersion function*, i.e. for a broad class of dispersive plane waves, and a *general amplitude function* associated with a general distribution of singularities or forcing function. Specifically, chapter 11 presents a fundamental decomposition of the general singular double Fourier integral associated with the Fourier-Kochin method into a wave component and a non-oscillatory local disturbance. The waves in this general flow decomposition—which does not involve approximations, i.e. is exact—are defined by a single Fourier integral along every dispersion curve defined by the dispersion relation, and the local disturbance is given by a double Fourier integral that has a smooth and localized integrand.

The basic waves and local-effects decomposition given in chapter 11 for a general dispersion relation and a general forcing function is applied in

chapter 12 to the specific dispersion relations associated with an offshore structure in regular waves and a ship that advances in calm water or through regular waves. The expressions given in chapter 12 yield exact analytical representations, suited for accurate numerical evaluation, of the waves and local flows created by a general distribution of singularities for the major classes of flows around ships and offshore structures considered in the book.

Foundation of a new type of panel methods

In summary, chapters 6–12 reconsider the two most important issues associated with the evaluation of near-field potential flows around ships and offshore structures via panel methods. These two fundamental questions are: (i) What boundary-integral flow representation should be solved? and (ii) How can this flow representation be solved? The reconsideration of these two fundamental questions has led to (i) the remarkably simple boundary-integral flow representation (9.35) and (ii) an alternative, called Fourier-Kochin method, to the usual Green-function method of solution. The boundary-integral flow representation given in chapters 8–9, and the Fourier-Kochin solution method expounded in chapters 10–12 provide an alternative to the approach that has been steadfastly applied in innumerable numerical studies over the past fifty years, and are main contributions of the book. Indeed, a primary purpose of the book is to consider crucial fundamental issues rather than merely review known results and theories.

Relevance to a broad class of plane dispersive waves

As was already noted, the Fourier-Kochin approach and the associated general decomposition into waves and local-effects given in chapters 10 and 11 hold for general dispersion relations, and are then directly applicable to a broad class of plane dispersive waves; e.g. flows around bodies moving over very large floating structures or ice sheets modeled as thin elastic plates, free-surface flows dominated by surface tension, and seismic waves.

The analytical expressions, notably the expressions for the wave patterns and the group velocity, obtained in the analysis of free waves expounded in chapters 2 and 3 likewise only involve the dispersion function, and hence are applicable to a broad class of plane dispersive waves, in addition to ship waves considered in chapters 4 and 5.

The classical method of Green function and boundary-integral representation expounded in chapter 6 and its applications in chapters 7–9 to the boundary-value problems associated with flows around ships and offshore structures are relevant to similar boundary-value problems in physics and engineering. In particular, the Fourier components in the expressions for the Green functions given in chapter 7 mostly depend on the dispersion function and are then applicable—with appropriate modifications—to a wide class of plane dispersive waves.

Focus on fundamental analytical flow relations

The primary goal of the book is to expound fundamental analytical flow relations that underly the analysis of far-field flows (free waves) and near-field flows due to ships and offshore structures. Numerical implementations of these analytical flow representations can be accomplished in alternative ways, and this vast issue is beyond the scope of the book.

Some elementary material, including basic knowledge about the energy transported by elementary plane progressive waves and the decomposition of the flow around an offshore structure into a diffraction problem and six radiation problems associated with basic small-amplitude translational and rotational rigid-body motions of the structure, is not considered in the book. Analytical relations for the wave energy radiated by a ship or an offshore structure, and the related wave drag and wave damping, obtained from an analysis of the far-field waves created by the body, although elegant and interesting, are also ignored because the alternative near-field pressure-integration method is most directly related to the method of Green function and boundary-integral flow representation expounded in the book.

Target audience and requirements

The boundary-value problems and the corresponding Green functions, boundary-integral flow relations, and analytical representations of flows due to a general distribution of singularities for an offshore structure in waves or a ship that steadily advances in calm water or through waves unavoidably involve extensive mathematical developments. However, the required mathematics actually are fairly simple, and all mathematical developments are expounded in a self-contained way in the book, which therefore is suited for scientists, engineers, graduate and undergraduate students with basic knowledge of fluid mechanics and water waves, and a desire for a solid basis for the analysis of far-field waves and near-field flows in ship and offshore hydrodynamics and/or in similar dispersive media.

The book can be used as a textbook for several courses. Specifically, chapters 1-3 can be used as an introductory course on water waves and other classes of dispersive plane waves. Chapters 1-5 provide a more complete exposition that includes specific applications to the far-field wave patterns created by a ship that advances in calm water or through regular waves.

Chapters 1-3 plus chapter 6 provide an introduction to both far-field free waves and the method of Green function and boundary-integral flow relations. The addition of chapters 7–12 provides a full in-depth account of theoretical methods suited for the analysis and the analytical representation of near-field flows. The analysis of far-field waves given in chapters 2–3, the general method of Green function and boundary-integral relation introduced in chapter 6 and the Fourier-Kochin method expounded in chapters 10–11 are directly applicable to a broad class of dispersive plane waves, and can

then be used as an introduction to the analysis of such waves.

Notes

Notes, marked as **[m,n]** to identify note number **n** in chapter number **m**, are included in the text and gathered in the last chapter entitled 'Notes'.

Authors' contributions

This book, started over thirty years ago as the first author's efforts to understand difficult issues and subtleties associated with potential flows around ships and offshore structures, was written by the first author, who is also mostly responsible for the analysis given in chapters 1-10 and in sections 11.1 and 11.2. The two authors contributed roughly equally to the elucidation of the optimal wave and local-effects decomposition expounded in sections 11.3 and 11.4. The second author is primarily responsible for the analysis underlying the representation (7.53) of the Green function associated with a ship that advances through regular waves in the regime $0 \leq \tau < 1/4$, and also had a leading role in the analysis given in sections 11.5 and 11.6 and in chapter 12. Moreover, all the figures in the book are due to the second author, who made further important contributions by thoroughly checking the entire book. This thorough verification led to numerous corrections and improvements.

Acknowledgments

The first author wishes to express his gratitude to Dr. Jiayi He for his crucial contribution to the book and for many happy memories related to our close cooperation, notably on the development of the Fourier-Kochin method given in sections 11.3–6 and chapter 12. In particular, the analysis and results expounded in sections 11.3–6 grew from our discussions during our daily walks to the cafeteria, which are among my happiest memories of my stay at Shanghai Jiao Tong University (SJTU).

I am also grateful for the support of the School of Ocean and Civil Engineering at SJTU where I spent nine productive years, and had the good fortune and great pleasure of guiding the dissertations of five talented and hard-working students: Jiayi He (now co-author of the book), Huiyu Wu, Chao Ma, Yi Zhu and Chenliang Zhang. Thank you for your great work!

I also thank my wife Annie Tabarié for her sixty-year support and her wonderful smile, my good friends Zheng Yang and Profs Wei Li, Chen-Jun Yang, Ren-Chuan Zhu, Xie-Chong Gu (who was first to appreciate the interest of the Fourier-Kochin method) and Xinshu Zhang at NAOCE for their kindness, as well as Profs Chi Yang and Steve Kan at George Mason University and Jungsook Ahn for their longstanding friendship and support.

In a world ravaged by wars and widespread corruption and stupidity, a

determined search for beauty—be it in music, painting, literature or, most beautiful of all, analytical representations of fluid flows and other physical phenomena—offers a shining ray of light and arguably the best path to personal happiness. My own search for beauty and happiness has benefited from the colleagues I met in conferences and at work over the past fifty years, as they have helped me steadfastly pursue the work expounded in this book. I particularly thank the many colleagues who made the effort to understand my work in their evaluations of the studies or research proposals I submitted over the years, and showed consideration and kindness. I also thank the colleagues who made little effort and dismissed my work, as they too helped strengthen my resolve. Thus, I thank all my colleagues—some of whom became friends—for sustaining my efforts to reconsider fundamental issues related to potential flows around ships and offshore structures, and thereby uncover the beauty of their analytical representations. And what beauty that is: The extremely complicated 3D flow—which involves waves of widely different wavelengths that travel in various directions—created by a ship that advances through waves is reduced to a 2D integral equation that determines the flow via a 1D superposition of elementary plane waves and a non-oscillatory local flow given by the 2D Fourier transform of a smooth function; and this flow representation only involves smooth ordinary real functions of real variables.

Chapter 1

Basic equations and boundary-value problems

This chapter defines the general boundary-value problems associated with three main classes of flows in ship and offshore hydrodynamics:

(i) diffraction-radiation of regular waves by a large stationary body such as an offshore structure or a moored ship in water of uniform finite depth,

(ii) flow around a ship that steadily advances in calm deep water, and

(iii) wave diffraction-radiation by a ship that advances at a constant speed through regular waves in deep water.

1.1 Basic relations

The flow around a ship, of length L_s, that advances at a constant speed V_s along a straight path in calm water or through regular waves is considered in this book. The special case $V_s = 0$ that corresponds to a stationary body such as an offshore structure, of size characterized by a length L_s, is also considered. The acceleration of gravity is denoted as g, and T denotes time.

The flow due to the ship is observed from a Galilean frame of reference and a related right-handed Cartesian system of coordinates (X, Y, Z) that follows the straight path of the steadily advancing ship. The undisturbed free surface is chosen as the plane $Z = 0$ and the Z axis points upward. The X axis is taken along the track of the ship and points toward the ship bow, as is shown in Fig.1.1.

The wetted hull surface of the ship or offshore structure is denoted as Σ^H. The unit vector $\mathbf{n} \equiv (n^x, n^y, n^z)$ normal to the hull surface Σ^H points

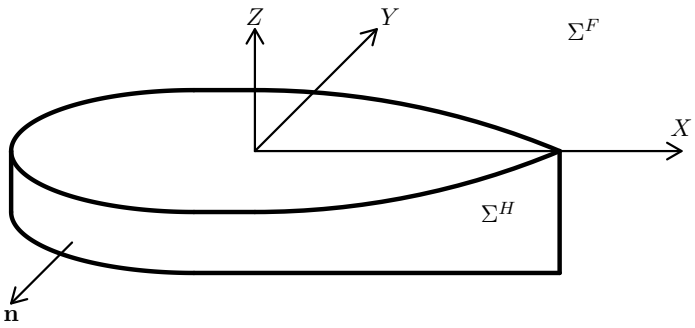

Figure 1.1: Galilean frame of reference and related Cartesian system of coordinates (X, Y, Z) used to analyze the flow around a ship that advances at a constant speed in calm water or through regular waves.

into the water, i.e. outside the ship. The free surface and the flow region outside Σ^H are denoted as Σ^F and $\mathcal{D}$, as is shown in Fig.1.1. A point within the flow domain $\mathcal{D}$ or at its boundary surface $\Sigma^F \cup \Sigma^H$ is denoted as $\mathbf{X} \equiv (X, Y, Z)$.

The flow around the ship or offshore structure is analyzed within the classical theory of incompressible inviscid flows. This theoretical framework is realistic for wave diffraction-radiation by large bodies such as ships and offshore structures of interest in the book **[1,1]**. The velocity of the flow created by the ship is then given by

$$\nabla\Phi \equiv (\Phi_X, \Phi_Y, \Phi_Z) \text{ where } \nabla \equiv (\partial_X, \partial_Y, \partial_Z)$$

and the flow potential $\Phi(\mathbf{X}, T)$ satisfies the Laplace equation

$$\nabla^2\Phi \equiv \nabla \cdot \nabla\Phi \equiv \Phi_{XX} + \Phi_{YY} + \Phi_{ZZ} = 0 \text{ in } \mathcal{D}\,. \tag{1.1}$$

At a large distance from the ship, the flow due to the ship vanishes and the far-field boundary condition

$$\Phi \to 0 \text{ as } \sqrt{X^2 + Y^2 + Z^2} \to \infty \tag{1.2}$$

holds. In water of uniform depth D, the sea-bottom boundary condition

$$\Phi_Z = 0 \text{ at } Z = -D \tag{1.3}$$

must be satisfied.

Two boundary conditions—known as the dynamic and kinematic free-surface boundary conditions—must be satisfied at the free surface, which is defined as

$$Z = Z^F(X, Y, T)\,. \tag{1.4}$$

These boundary conditions are considered in the next section. In addition, the flow-velocity component normal to the hull surface Σ^H and the normal velocity of the hull surface Σ^H are equal at Σ^H. The hull-surface boundary condition is considered in section 1.4.

In the Galilean frame of reference that follows the ship, the flow velocity is given by

$$(\Phi_X - V_s\,, \Phi_Y, \Phi_Z) \tag{1.5}$$

where $\nabla\Phi$ is the velocity of the flow created by the ship and the velocity $(-V_s, 0, 0)$ is the apparent uniform stream that opposes the forward speed of the ship.

The flow pressure $P(\mathbf{X}, T)$ is explicitly determined in terms of the flow potential Φ and the related flow velocity $\nabla\Phi$ via the Bernoulli relation

$$\frac{P}{\rho_w} + g\,Z + \Phi_T + \frac{(\Phi_X - V_s)^2 + \Phi_Y^2 + \Phi_Z^2}{2} = \frac{P_{atm}}{\rho_w} + \frac{V_s^2}{2}$$

where ρ_w denotes the density of water and P_{atm} is the atmospheric pressure. One then has

$$(P - P_{atm})/\rho_w + g\,Z = V_s\,\Phi_X - \Phi_T - (\Phi_X^2 + \Phi_Y^2 + \Phi_Z^2)/2\;. \tag{1.6}$$

Far away from the ship, i.e. in the far field, one has $\Phi_T \approx 0$ and $\nabla\Phi \approx 0$ in accordance with the far-field condition (1.2), and the Bernoulli relation (1.6) becomes

$$P - P_{atm} = -\rho_w\, g\, Z\;.$$

Motions of both the water and the air below and above the free surface Σ^F occur concurrently with the motions of Σ^F. Related variations in the air pressure about the atmospheric pressure associated with unperturbed conditions are proportional to the air density ρ_{air} in accordance with the Bernoulli equation applied to air motions above Σ^F. These variations of the air pressure above the free surface have a negligible influence on the flow of water below Σ^F because $\rho_{air} \ll \rho_w$. The air pressure can then be regarded as effectively constant at the free surface, equal to the atmospheric pressure, for the purpose of determining the flow of water; i.e. the water-flow can be analyzed independently of the air-flow. This decoupling of the flows above and below a free surface does not hold for internal waves, for instance, where the densities of the upper and lower fluids are nearly equal.

The flow pressures in the water and in the air are equal at the water-air interface, except for the jump in pressure that can be sustained due to surface tension. This pressure jump is proportional to the curvature of the free surface, and can be neglected except for small-scale free-surface deformations that have no practical effect at the scale of ships and offshore structures. Thus, surface tension is ignored hereafter.

1.2 Free-surface boundary conditions

Dynamic free-surface boundary condition

The pressure at the free surface Σ^F can differ from the atmospheric pressure P_{atm} for some types of ships, notably hovercrafts. In such a case, the pressure is given by

$$P = P_{atm} + P^F \text{ at } \Sigma^F \tag{1.7}$$

where $P^F(X, Y, T)$ represents a distribution of pressure applied at Σ^F. The Bernoulli relation (1.6) then yields

$$g\, Z^F = V_s\, \Phi_X - \Phi_T - (\Phi_X^2 + \Phi_Y^2 + \Phi_Z^2)/2 - P^F/\rho_w \text{ at } \Sigma^F \tag{1.8}$$

where Φ_T and $\nabla\Phi$ are evaluated at the free surface $Z = Z^F$. This boundary condition, called dynamic free-surface boundary condition, determines the free-surface elevation $Z^F(X, Y, T)$ in terms of the pressure $P^F(X, Y, T)$ applied at the free surface and the flow potential $\Phi(X, Y, Z = Z^F, T)$.

In the particular case $P^F = 0$ and $\Phi_T = 0$, which corresponds to steady flow around a common displacement ship that advances at a constant speed V_s in calm water, the dynamic free-surface boundary condition (1.8) yields

$$2\, g\, Z^F = V_s^2 - [\,(V_s - \Phi_X)^2 + \Phi_Y^2 + \Phi_Z^2\,] \leq V_s^2\,.$$

This expression yields the upper bound

$$g\, Z^F / V_s^2 \leq 1/2 \tag{1.9}$$

for the elevation Z^F of the free surface. The general upper bound (1.9) is important, e.g. because it determines whether a plane progressive wave, and the bow wave created by a ship that steadily advances in calm water, is steady or unsteady. **[1,2]**

Kinematic free-surface boundary condition

The kinematic free-surface boundary condition is now considered in the general case when a flux of water, denoted as $Q^F(X, Y, T)$ and defined as positive or negative if water is added or removed through the free surface, is allowed. This general case is considered because it is required further on in the formulation of boundary-integral flow representations based on Green functions. The kinematic free-surface boundary condition is

$$(\Phi_X - V_s\,, \Phi_Y, \Phi_Z) \cdot \mathbf{n} = \mathbf{V}^F \cdot \mathbf{n} - Q^F \tag{1.10}$$

where $(\Phi_X - V_s\,, \Phi_Y, \Phi_Z)$ is the flow velocity (1.5), $\mathbf{V}^F$ denotes the velocity of the free surface Σ^F, $\mathbf{n}$ is the upward-pointing unit vector normal to Σ^F, and Q^F is the flux of water through Σ^F.

Equation (1.4) can be expressed as

$$F(\mathbf{X},T) \equiv Z - Z^F(X,Y,T) = 0\ . \tag{1.11}$$

At any given instant of time T, one has both

$$F(\mathbf{X},T) = 0 \ \text{ and } \ F(\mathbf{X}+\mathbf{X}',T) = 0$$

if $\mathbf{X}$ and $\mathbf{X}+\mathbf{X}'$ are two arbitrary points of the free surface. In the limit $\mathbf{X}' \to 0$, one then has

$$0 = F(\mathbf{X}+\mathbf{X}',T) - F(\mathbf{X},T) = \mathbf{X}' \cdot \nabla F(\mathbf{X},T)\ .$$

This relation shows that the vector ∇F is normal to the surface $F = 0$, as is well known. The unit vector $\mathbf{n}$ normal to the free surface therefore is

$$\mathbf{n} = \nabla F / \|\nabla F\| = (-Z_X^F\,, -Z_Y^F\,, 1)\,/\sqrt{1+(Z_X^F)^2+(Z_Y^F)^2} \tag{1.12}$$

where (1.11) was used. The vector $\mathbf{n}$ defined by (1.12) points upward. Expression (1.12) yields

$$\mathbf{n}\cdot\nabla\Phi = (\Phi_Z - \Phi_X Z_X^F - \Phi_Y Z_Y^F)\,/\sqrt{1+(Z_X^F)^2+(Z_Y^F)^2}\ . \tag{1.13}$$

A point $\mathbf{X}$ of the free surface $F(\mathbf{X},T) = 0$ at some time T becomes the point $\mathbf{X}+\mathbf{V}^F(\mathbf{X},T)\,dT$ of the surface $F(\mathbf{X}+\mathbf{V}^F dT, T+dT) = 0$ at the time $T+dT$, where $\mathbf{V}^F(\mathbf{X},T)$ is the velocity of the free-surface point $\mathbf{X}$ at the time T. It follows that one has

$$0 = F(\mathbf{X}+\mathbf{V}^F dT, T+dT) - F(\mathbf{X},T) = (\mathbf{V}^F\cdot\nabla F + F_T)\,dT\ .$$

One then has

$$\mathbf{V}^F\cdot\nabla F = -F_T = Z_T^F$$

where (1.11) was used. This relation and (1.12) yield

$$\mathbf{V}^F\cdot\mathbf{n} = \mathbf{V}^F\cdot\nabla F/\|\nabla F\| = Z_T^F/\sqrt{1+(Z_X^F)^2+(Z_Y^F)^2}\ . \tag{1.14}$$

The relations (1.10) and (1.12)-(1.14) finally yield the kinematic free-surface boundary condition

$$\Phi_Z - Z_T^F + V_s\,Z_X^F - \Phi_X\,Z_X^F - \Phi_Y\,Z_Y^F + Q^F\sqrt{1+(Z_X^F)^2+(Z_Y^F)^2} = 0 \tag{1.15}$$

where $\nabla\Phi$ is evaluated at the free surface $Z = Z^F(X,Y,T)$.

Linearization

Both the kinematic boundary condition (1.15) and the dynamic boundary condition (1.8) involve nonlinear terms. Moreover, the location $Z = Z^F$ of the free surface, where the boundary conditions (1.8) and (1.15) hold, is unknown. An analysis of wave diffraction-radiation by ships and offshore structures based on the nonlinear free-surface boundary conditions (1.15) and (1.8) is then extremely difficult. Moreover, such an analysis might be of limited interest because wavebreaking typically occurs if nonlinearities are significant, and the potential-flow assumption underlying the boundary conditions (1.15) and (1.8) is not justified in that case.

For most practical applications in ship and offshore hydrodynamics, the nonlinear terms in the boundary conditions (1.8) and (1.15) are then either neglected or taken into account via a perturbation analysis for ambient waves of small amplitude **[1,3]**. The free-surface boundary conditions (1.8) and (1.15) are applied at the plane $Z = 0$ of the undisturbed free surface in a linear analysis, and also in a weakly nonlinear analysis.

The linear approximations to the free-surface boundary conditions (1.8) and (1.15) are

$$g\,Z^F = V_s\,\Phi_X - \Phi_T - P^F/\rho_w\ , \tag{1.16a}$$

$$\Phi_Z - Z^F_T + V_s\,Z^F_X + Q^F = 0\ . \tag{1.16b}$$

For a ship that steadily advances in calm water or through regular waves, the linear boundary conditions (1.16) are associated with the realistic and practical Kelvin-Michell assumption that the velocity $\nabla\Phi$ of the flow created by the ship is small in comparison to the ship speed V_s. The linear dynamic condition (1.16a) explicitly determines the free-surface elevation Z^F in terms of the flow potential Φ at $Z = 0$ and the pressure P^F applied at the free surface.

Substitution of expression (1.16a) for the free-surface elevation Z^F into the linear kinematic condition (1.16b) yields

$$g\,\Phi_Z + \Phi_{TT} - 2V_s\,\Phi_{XT} + V_s^2\,\Phi_{XX} = (V_s\,P^F_X - P^F_T)/\rho_w - g\,Q^F\ . \tag{1.17a}$$

This linear boundary condition can be expressed more compactly as

$$g\,\Phi_Z + (V_s\,\partial_X - \partial_T)^2\,\Phi = (V_s\,\partial_X - \partial_T)P^F/\rho_w - g\,Q^F\ . \tag{1.17b}$$

The boundary conditions (1.17) only involve the flow potential Φ and its derivatives at the plane $Z = 0$ of the undisturbed free surface. The free-surface boundary condition (1.17a) becomes

$$g\,\Phi_Z + \Phi_{TT} = -P^F_T/\rho_w - g\,Q^F \ \text{ if } \ V_s = 0\ . \tag{1.17c}$$

The Bernoulli relation (1.6) readily yields the linear approximation

$$(P - P_{atm})/\rho_w + g\,Z = V_s\,\Phi_X - \Phi_T = (V_s\,\partial_X - \partial_T)\,\Phi \tag{1.18}$$

to the dynamic flow pressure.

1.3 Steady and time-harmonic flows

A flow is not fully determined unless initial conditions are specified at some time T_0. The basic issue of defining initial conditions for time-harmonic flows associated with diffraction-radiation of regular waves by an offshore structure, and for steady and time-harmonic flows around a ship that steadily advances in calm water or through regular waves, is now considered **[1,4]**.

Ship that steadily advances in calm water

A steady flow around a ship that advances at a constant speed V_s in calm water can be assumed to slowly grow from rest at the time $T = -\infty$ in accordance with the flow potential $\widehat{\Phi}(\mathbf{X}, T)$ defined as

$$\widehat{\Phi}(\mathbf{X}, T) = \Phi(\mathbf{X})\, e^{\,\nu\, T} \;\text{ where }\; 0 < \nu\;. \tag{1.19}$$

The flow potential $\widehat{\Phi}(\mathbf{X}, T)$ satisfies the initial conditions $\widehat{\Phi} = 0$ and $\widehat{\Phi}_T = 0$ at $T = -\infty$, and steady state is obtained for $\nu = +0$. The flow potential (1.19) can be associated with a ship hull Σ^H that slowly grows from a needle-like ship, which creates no flow disturbance, and a free-surface pressure $P^F e^{\,\nu\, T}$ and flux $Q^F e^{\,\nu\, T}$ that slowly grow from $P^F = 0$ and $Q^F = 0$, at the time $T = -\infty$.

Substitution of expressions $P^F e^{\,\nu\, T}$ and $Q^F e^{\,\nu\, T}$ for the pressure and the flux applied at the free surface, and expression (1.19) for the flow potential into the Laplace equation (1.1), the far-field condition (1.2) and the sea-bottom boundary condition (1.3) yield

$$\nabla^2\,\Phi = 0 \;\text{ in }\; \mathcal{D}\;,\;\; \Phi \to 0 \;\text{ as }\; \mathbf{X} \to \infty\;,\;\; \Phi_Z = 0 \;\text{ at }\; Z = -D\;, \tag{1.20}$$

while the linearized free-surface boundary condition (1.17b) becomes

$$g\,\Phi_Z + (V_s\,\partial_X - \nu)^2\,\Phi = (V_s\,\partial_X - \nu)\,P^F/\rho_w - g\,Q^F \;\text{ at }\; \Sigma^F\;.$$

The growth parameter $\nu = +0$ in this boundary condition is crucial on the left side but is inconsequential on the right side, which is merely a forcing term that does not affect the dispersion relation as is made clear further on in the book. The free-surface boundary condition associated with the flow around a ship that steadily advances in calm water then becomes

$$g\,\Phi_Z + (V_s\,\partial_X - \nu)^2\,\Phi = V_s\,P^F_X/\rho_w - g\,Q^F \;\text{ at }\; \Sigma^F\;. \tag{1.21}$$

Offshore structure in regular waves

The time-harmonic flow around an offshore structure in ambient regular waves of frequency ω can similarly be assumed to slowly grow from rest at the time $T = -\infty$ in accordance with a flow potential

$$\widehat{\Phi}(\mathbf{X}, T) = \mathrm{Re}\, \Phi(\mathbf{X})\, e^{(\nu - \mathrm{i}\,\omega) T} \text{ where } 0 < \nu\,. \tag{1.22}$$

A time-harmonic flow is obtained for $\nu = +0$. The flow potential (1.22) can be associated with diffraction-radiation by an offshore structure in regular waves of amplitude A that slowly grows as $A\, e^{\nu T}$ and a free-surface pressure P^F and flux Q^F that similarly grow as

$$P^F e^{(\nu - \mathrm{i}\,\omega) T} \text{ and } Q^F e^{(\nu - \mathrm{i}\,\omega) T}\,. \tag{1.23}$$

Substitution of expressions (1.22) and (1.23) into the Laplace equation (1.1), the far-field condition (1.2), the sea-bottom boundary condition (1.3) and the free-surface boundary condition (1.17c) show that the potential Φ in (1.22) satisfies Laplace's equation and the boundary conditions (1.20) and the free-surface boundary condition

$$g\, \Phi_Z - (\omega + \mathrm{i}\,\nu)^2\, \Phi = \mathrm{i}\,\omega\, P^F/\rho_w - g\, Q^F \text{ at } \Sigma^F. \tag{1.24}$$

The inconsequential term $\nu = +0$ is ignored on the right side of (1.24), as in (1.21).

Ship that steadily advances through regular waves

The potential of the flow around a ship that steadily advances through regular waves can also be expressed as in (1.22), where ω now denotes the *encounter* wave frequency (the frequency observed in the Galilean frame of reference that follows the ship), associated with ambient regular waves of amplitude $A\, e^{\nu T}$ and a free-surface pressure P^F and flux Q^F that slowly grow from nil in accordance with expressions (1.23).

Substitution of these expressions into the Laplace equation (1.1), the far-field condition (1.2), the sea-bottom boundary condition (1.3) and the free-surface boundary condition (1.17b) show that the flow potential Φ in (1.22) satisfies the Laplace equation and the boundary conditions (1.20), and the free-surface boundary condition

$$g\, \Phi_Z + (V_s\, \partial_X + \mathrm{i}\,\omega - \nu)^2\, \Phi = (V_s P_X^F + \mathrm{i}\,\omega\, P^F)/\rho_w - g\, Q^F \text{ at } \Sigma^F \tag{1.25}$$

where ν is taken as $\nu = 0$ on the right side, as in (1.21) and (1.24). The free-surface boundary condition (1.25) is identical to (1.21) or (1.24) if $V_s = 0$ or $\omega = 0$.

Free-surface elevation and flow pressure

Expressions (1.16a) and (1.22) determine the free-surface elevation Z^F as

$$g\,Z^F = \mathrm{Re}\,[\,V_s\,\Phi_X + \mathrm{i}\,\omega\,\Phi - P^F/\rho_w\,]\,e^{-\mathrm{i}\,\omega\,T}\,. \tag{1.26a}$$

The dynamic component of the pressure is defined by (1.18) and (1.22) as

$$P_d\,/\rho_w \equiv (P - P_{atm})/\rho_w + g\,Z = \mathrm{Re}\,[\,V_s\,\Phi_X + \mathrm{i}\,\omega\,\Phi\,]\,e^{-\mathrm{i}\,\omega\,T}\,. \tag{1.26b}$$

The hydrostatic component $g\,Z$ does not contribute to the dynamic pressure defined in (1.26b). The inconsequential time-growth parameter $\nu = +0$ is ignored in expressions (1.26).

1.4 Hull-surface boundary condition

The boundary condition at the hull surface Σ^H of a ship or offshore structure is now considered.

Ship that steadily advances in calm water

The position of a ship that advances at a constant speed V_s in calm water is fixed (in the Galilean frame of reference that follows the ship) and the flow-velocity component normal to the ship-hull surface Σ^H is then nil. It follows from (1.5) that one has

$$\mathbf{n}\cdot\nabla\Phi = V_s\,n^x \;\text{ at }\; \Sigma^H\,. \tag{1.27}$$

The location of the hull surface Σ^H is not known precisely a priori because the flow, specifically the dynamic flow pressure distribution, around the ship (especially at the hull bottom) causes the ship to experience a hydrodynamic lift and pitch moment. As a result, the position of the ship is modified, i.e. differs from the position of the ship at rest. Specifically, the ship experiences a vertical displacement and a rotation, called sinkage and trim. **[1,5]**

Offshore structure in regular waves

For an offshore structure in ambient regular waves, one has $V_s = 0$ and the flow velocity (1.5) becomes $\nabla\Phi + \nabla\Phi^a$ where $\nabla\Phi^a$ denotes the flow velocity associated with the ambient waves. The hull boundary condition for an offshore structure that is fixed (not allowed to move) in waves is then

$$\mathbf{n}\cdot\nabla\Phi = -\mathbf{n}\cdot\nabla\Phi^a\,. \tag{1.28}$$

The flow around a *freely-floating* offshore structure Σ^H that undergoes oscillatory motions about a mean position Σ_0^H is classically decomposed into a 'diffraction problem', which corresponds to the hull boundary condition (1.28) for the offshore structure in its mean location Σ_0^H, and 6 'radiation problems' associated with canonical oscillatory motions (surge, sway, heave, roll, pitch, yaw) of Σ^H about its mean position Σ_0^H. The hull-surface boundary conditions for these radiation problems are of the form

$$\mathbf{n} \cdot \nabla \Phi = \mathbf{n} \cdot \mathbf{V}^H \text{ at } \Sigma^H \tag{1.29}$$

where $\mathbf{V}^H$ is the velocity of the hull surface Σ^H. The boundary condition (1.29) is enforced at the mean position Σ_0^H of the offshore structure. **[1,6]**

Ship that steadily advances through regular waves

The flow around a ship that steadily advances through regular waves can be expressed as the sum of a steady flow component that corresponds to the flow around the ship advancing in calm water, for which the hull boundary condition is (1.27), and a time-harmonic component that can be decomposed into a diffraction-problem and six radiation-problems for which the hull boundary conditions (applied at the mean position of the ship) are of the form (1.28) and (1.29).

1.5 Nondimensional formulation

Nondimensionalization

Nondimensional coordinates $\mathbf{x}$, time t, flow velocity $\nabla\phi$, potential ϕ and dynamic pressure p_d are defined in terms of a reference length L_r, the acceleration of gravity g and the water density ρ_w as

$$\mathbf{x} \equiv \frac{\mathbf{X}}{L_r} \,,\; t \equiv T\sqrt{\frac{g}{L_r}} \,,\; \nabla\phi \equiv \frac{\nabla\Phi}{\sqrt{gL_r}} \,,\; \phi \equiv \frac{\Phi/L_r}{\sqrt{gL_r}} \,,\; p_d \equiv \frac{P_d}{\rho_w\, g L_r} \;. \tag{1.30a}$$

Nondimensional water depth d, free-surface elevation z^F, hull velocity $\mathbf{v}^H$, and free-surface flux q^F and pressure p^F are similarly defined as

$$d \equiv \frac{D}{L_r} \,,\; z^F \equiv \frac{Z^F}{L_r} \,,\; \mathbf{v}^H \equiv \frac{\mathbf{V}^H}{\sqrt{gL_r}} \,,\; q^F \equiv \frac{Q^F}{\sqrt{gL_r}} \,,\; p^F \equiv \frac{P^F}{\rho_w\, g L_r} \;. \tag{1.30b}$$

The wavelength Λ and wavenumbers K, K^x, K^y are nondimensionalized as

$$\lambda \equiv \Lambda/L_r \text{ and } (k,\alpha,\beta) \equiv (K, K^x, K^y)\, L_r \;. \tag{1.30c}$$

In the particular case of a ship that steadily advances in calm water, the ship speed V_s is often used instead of $\sqrt{gL_r}$ as reference velocity. One has

$$\frac{\nabla\Phi}{V_s} = \frac{\nabla\phi}{F} \text{ and } \frac{\Phi}{L_r V_s} = \frac{\phi}{F} \tag{1.31}$$

where F is the Froude number defined in (1.32).

The Froude number F, the nondimensional frequency f, and the related nondimensional parameters $\tau \equiv Ff$ and $S \equiv F/f$ are defined as

$$F \equiv \frac{V_s}{\sqrt{gL_r}} \ , \ f \equiv \omega\sqrt{\frac{L_r}{g}} \ , \ \tau \equiv Ff \equiv \frac{V_s\,\omega}{g} \ , \ S \equiv \frac{F}{f} \equiv \frac{V_s}{\omega\,L_r} \tag{1.32}$$

where S is the inverse of the usual Strouhal number. The nondimensional time-growth parameter ϵ is defined as

$$\epsilon \equiv \nu\sqrt{L_r/g} \ .$$

The analysis given further on shows that the waves created by an offshore structure are conveniently analyzed in terms of the nondimensional 'frequency-scaled' coordinates and Fourier variables

$$\mathbf{x}^\omega \equiv f^2\,\mathbf{x} \equiv \frac{\omega^2\mathbf{X}}{g} \text{ and } (\alpha^\omega, \beta^\omega, k^\omega) \equiv \frac{(\alpha,\beta,k)}{f^2} \equiv \frac{g}{\omega^2}\,(K^x, K^y, K) \tag{1.33a}$$

associated with the choice of reference length $L_r \equiv g/\omega^2$.

It is also shown further on that the waves created by a ship advancing at a constant speed V_s in calm water are conveniently analyzed in terms of the nondimensional 'speed-scaled' coordinates and Fourier variables

$$\mathbf{x}^V \equiv \frac{\mathbf{x}}{F^2} \equiv \frac{g\mathbf{X}}{V_s^2} \text{ and } (\alpha^V, \beta^V, k^V) \equiv F^2(\alpha,\beta,k) \equiv \frac{V_s^2}{g}\,(K^x, K^y, K) \tag{1.33b}$$

associated with the reference length $L_r \equiv V_s^2/g$.

Lastly, the nondimensional coordinates and Fourier variables

$$\mathbf{x}^S \equiv \frac{\mathbf{x}}{S} \equiv \frac{\omega\mathbf{X}}{V_s} \text{ and } (\alpha^S, \beta^S, k^S) \equiv S(\alpha,\beta,k) \equiv \frac{V_s}{\omega}\,(K^x, K^y, K) \tag{1.33c}$$

are shown further on to be well suited to analyze the flow around a ship that steadily advances through regular waves in the regime $0.3 < \tau$. These nondimensional coordinates and Fourier variables are associated with the reference length $L_r \equiv V_s/\omega$.

The reference lengths L_r that correspond to the three alternative scalings (1.33) are related to the free waves created by a ship or an offshore structure. Accordingly, these three reference lengths are independent of the length

L_s that characterizes the size of the ship or the structure, which has no significant influence on the wavelength of far-field free waves. However, the reference length L_r in expressions (1.30)-(1.32) is commonly taken as the length L_s that characterizes the size of the ship or structure to analyze near-field flows around ships or offshore structures.

Nondimensional boundary-value problems

The nondimensional flow potential that corresponds to the flow potential (1.22) can be expressed as

$$\widehat{\phi}(\mathbf{x},t) = \mathrm{Re}\,\phi(\mathbf{x})\, e^{\,(\epsilon - \mathrm{i}\, f)\, t}\ . \tag{1.34}$$

The relations (1.20), (1.25), (1.27)-(1.29) then show that the spatial component $\phi(\mathbf{x})$ of the potential $\widehat{\phi}(\mathbf{x},t)$ in (1.34) satisfies the Laplace equation

$$\nabla^2_{\mathbf{x}}\phi \equiv \partial_x^2\phi + \partial_y^2\phi + \partial_z^2\phi = 0 \ \text{ in } \ \mathcal{D}\ , \tag{1.35a}$$

the far-field condition

$$\phi \to 0 \ \text{ as } \ \mathbf{x} \to \infty\ , \tag{1.35b}$$

the sea-bottom condition

$$\partial_z\,\phi = 0 \ \text{ at } \ z = -d\ , \tag{1.35c}$$

the free-surface boundary condition

$$\partial_z\,\phi + (F\,\partial_x + \mathrm{i}\, f - \epsilon)^2\,\phi = (F\,\partial_x + \mathrm{i}\, f)\, p^F - q^F \ \text{ at } \ \Sigma^F \tag{1.35d}$$

where $\epsilon = +0$, and the hull boundary condition

$$\nabla\phi\cdot\mathbf{n} = q^H \ \text{ at } \ \Sigma^H \ \text{ where} \tag{1.35e}$$

$$q^H \equiv \left\{ \begin{matrix} F\, n^x \\ -\,\mathbf{n}\cdot\nabla\phi^a \ \text{ or } \ \mathbf{n}\cdot\mathbf{v}^H \end{matrix} \right\} \ \text{ if } \ \left\{ \begin{matrix} f = 0 \\ f \neq 0 \end{matrix} \right\}\ . \tag{1.36}$$

The boundary-value problem defined by the Laplace equation (1.35a) and the boundary conditions (1.35b-e) is considered hereafter for a *general* but *presumed known* flux q^H in the boundary condition (1.35e) and for general, also presumed known, pressure p^F and flux q^F in the boundary condition (1.35d) at the free surface.

The three general boundary-value problems, formulated in nondimensional form in accordance with the nondimensionalization (1.30), that determine the flow potential (1.34) associated with diffraction-radiation by an offshore structure in regular waves or the flow around a ship that steadily advances in calm water or through regular waves are defined by (1.35).

The corresponding free-surface elevation and flow pressure are now considered. The free-surface elevation z^F is determined by (1.26a) as

$$z^F = \mathrm{Re}\,(F\phi_x + \mathrm{i}f\phi - p^F)\,e^{-\mathrm{i}ft} \;\text{ where }\; \mathbf{x} \in \Sigma^F \tag{1.37a}$$

and ϕ and ϕ_x are evaluated at the plane $z = 0$ of the undisturbed free surface. Expression (1.26b) for the dynamic flow pressure similarly yields

$$p_d = \mathrm{Re}\,(F\phi_x + \mathrm{i}f\phi)\,e^{-\mathrm{i}ft} \;\text{ where }\; \mathbf{x} \in \mathcal{D}\,. \tag{1.37b}$$

Expressions (1.37a-b) explicitly determine the nondimensional free-surface elevation z^F and the dynamic pressure p_d in terms of the flow potential ϕ (at the undisturbed free surface Σ^F or in the mean flow domain $\mathcal{D}$) that is given by the solution of the boundary-value problem (1.35).

Chapter 2

Basic and generalized elementary free waves

This chapter considers the boundary-value problem (1.35) that determines the spatial component $\phi(\mathbf{x})$ of the flow potential

$$\widehat{\phi}(\mathbf{x},t) = \mathrm{Re}\,\phi(\mathbf{x})\,e^{(\epsilon - \mathrm{i}\,f)t} \tag{2.1}$$

associated with an offshore structure in regular waves or a ship that advances through regular waves or (if $f = 0$) in calm water at a large distance from the ship or structure, i.e. in the far field where the flow predominantly consists of free waves that propagate with little influence from the ship or structure.

Basic elementary wave functions that satisfy the Laplace equation (1.35a) and the boundary conditions (1.35c-d) at the sea bottom and at the free surface are obtained for ϵ taken as $\epsilon = 0$ in (2.1) and (1.35d). These elementary waves are subsequently modified to satisfy the initial conditions consistent with ϵ taken as $\epsilon = +0$ in (2.1) and the far-field condition (1.35b), in addition to the Laplace equation and the boundary conditions at the sea bottom and at the free surface already satisfied by the basic elementary waves that correspond to $\epsilon = 0$. This two-step analysis, in which the cases $\epsilon = 0$ or $\epsilon = +0$ are successively considered, clearly illustrates the crucial role of the initial conditions associated with the time-growth parameter ϵ in (2.1) and (1.35d). **[2,1]**

The second step of the two-step analysis expounded in this chapter shows that far-field waves can be expressed as a linear superposition of elementary plane waves that are consistent with initial conditions associated with a flow that starts from rest and satisfies the Laplace equation (2.3a), the far-field boundary condition (2.3b), the sea-bottom boundary condition (2.3c) and

the free-surface boundary condition (2.3d) with $\epsilon = +0$.

2.1 Near-field flow and free waves

The flow created by an offshore structure in regular waves, or a ship that advances in calm water or through waves, can be decomposed into a local flow and waves. The local-flow component in this fundamental flow decomposition vanishes rapidly away from the body (ship or offshore structure). Specifically, the flow velocity $\nabla\phi^L$ that corresponds to the local-flow component decays as $1/h^3$ as $h \to \infty$, where $h \equiv \sqrt{x^2+y^2}$ is the horizontal distance from the body **[2,2]**. However, the flow velocity $\nabla\phi^W$ associated with the waves created by the body decays at a much slower rate than the local-flow velocity $\nabla\phi^L$. Specifically, basic considerations of the energy transported by the waves created by the body **[2,3]** show that $\nabla\phi^W$ vanishes as $1/\sqrt{h}$. One then has

$$\nabla\phi^W \sim 1/\sqrt{h} \text{ and } \nabla\phi^L \sim 1/h^3 \text{ as } h \equiv \sqrt{x^2+y^2} \to \infty\,. \tag{2.2}$$

At some distance from a ship or offshore structure, the local-flow velocity $\nabla\phi^L$ is then negligible in comparison to the wave component $\nabla\phi^W$, and the waves created by the body (ship or structure) propagate 'freely' under little influence from the body, which mostly determines the initial amplitude of the waves. Indeed, the near-field boundary condition at the body surface determines the initial amplitude of the waves created by the body, but has no appreciable influence—except in a small near-field region in the vicinity of the body—on the propagation of the waves away from the body that created them. Accordingly, the waves at some distance from a body are commonly called 'free waves'.

Thus, the flow potential $\phi(\mathbf{x})$ associated with far-field free waves satisfies the Laplace equation

$$\nabla^2_{\mathbf{x}}\phi \equiv (\partial_x^2 + \partial_y^2 + \partial_z^2)\,\phi = 0 \text{ in } -d < z < 0\,, \tag{2.3a}$$

the far-field condition

$$\phi \to 0 \text{ as } \mathbf{x} \to \infty\,, \tag{2.3b}$$

the sea-bottom condition

$$\partial_z\,\phi = 0 \text{ at } z = -d\,, \tag{2.3c}$$

and the free-surface boundary condition

$$\partial_z\,\phi + (F\,\partial_x + \mathrm{i}\,f - \epsilon)^2\,\phi = 0 \text{ at } z = 0 \text{ where } \epsilon = +0\,. \tag{2.3d}$$

The near-field free-surface pressure p^F and flux q^F in (1.35d) are ignored in (2.3d) because they are assumed to be nil except (eventually) in the vicinity of the body. Similarly, the hull boundary condition (1.35e) is ignored in the *far-field* analysis considered in this chapter.

2.2 Elementary waves and dispersion relations

An essential property of the incomplete boundary-value problem, called 'far-field boundary-value problem' for convenience hereafter, defined by the Laplace equation (2.3a) and the three boundary conditions (2.3b-d) is that these homogeneous equations have nontrivial solutions, i.e. eigensolutions. These eigensolutions, which correspond to elementary waves, are considered first for the special case when the time-growth parameter ϵ in the free-surface boundary condition (2.3d) is taken as $\epsilon = 0$. The case $\epsilon = +0$ is subsequently considered in sections 2.8–2.10.

Laplace's equation, sea-bottom and free-surface conditions

The far-field boundary condition (2.3b), although relevant for a far-field study, is ignored at this stage of the analysis, which considers elementary wave functions that satisfy the Laplace equation (2.3a), the sea-bottom condition (2.3c) and the free-surface condition (2.3d) with $\epsilon = 0$, i.e.

$$\nabla_{\mathbf{x}}^2 \phi \equiv (\partial_x^2 + \partial_y^2 + \partial_z^2)\,\phi = 0 \ \text{ in } \ -d < z < 0\,, \tag{2.4a}$$

$$\partial_z \phi = 0 \ \text{ at } \ z = -d\,, \tag{2.4b}$$

$$\partial_z \phi + (F\,\partial_x + \mathrm{i}\,f)^2\,\phi = 0 \ \text{ at } \ z = 0\,. \tag{2.4c}$$

Elementary wave solutions and dispersion relations

The wave function

$$W(\mathbf{x}) = e^{\,\mathrm{i}\,(\alpha\,x\,+\,\beta\,y)}\,\cosh\left[k\,(z+d)\right]/\cosh(kd) \tag{2.5}$$

satisfies the sea-bottom condition (2.4b) and the Laplace equation (2.4a) if

$$k = \sqrt{\alpha^2+\beta^2}\,. \tag{2.6}$$

The wave function (2.5) also satisfies the free-surface condition (2.4c) if

$$\Delta\,(f,\alpha,\beta\,;F,d) \equiv (f+F\alpha)^2 - k\,\tanh(kd) = 0\,. \tag{2.7}$$

The relation $\Delta = 0$ is called dispersion relation, and the related function $\Delta\,(f,\alpha,\beta\,;F,d)$ is the dispersion function, for the waves created by a ship that steadily advances through regular waves in water of uniform finite depth.

In the deep-water limit $d = \infty$, the elementary wave function (2.5) and the dispersion relation (2.7) become

$$W(\mathbf{x}) = e^{\,\mathrm{i}\,(\alpha\,x+\beta\,y)+k\,z} \text{ where } k \equiv \sqrt{\alpha^2+\beta^2} \tag{2.8}$$

$$\text{and } \Delta(f,\alpha,\beta;F) \equiv (f+F\alpha)^2 - k = 0\ . \tag{2.9}$$

The deep-water dispersion relation (2.9) is significantly simpler than the dispersion relation (2.7) for finite water-depth, which involves a hyperbolic function and the additional parameter d that defines the water-depth.

The dispersion relations (2.7) and (2.9) define curves in the Fourier plane (α,β). These curves are called dispersion curves. E.g., in the particularly simple case of diffraction-radiation of regular waves by an offshore structure, the dispersion relation (2.7) becomes

$$\Delta(f,\alpha,\beta;d) \equiv f^2 - k\tanh(k\,d) = 0\ . \tag{2.10}$$

This dispersion relation has a single root and therefore defines a single dispersion curve, a circle centered at the origin of the Fourier plane (α,β).

The dispersion function $\Delta(f,\alpha,\beta;F,d)$ and the related dispersion relation and dispersion curves $\Delta = 0$ are essential elements of potential flows around ships and offshore structures. The term $F\alpha$ in the dispersion relations (2.7) and (2.9) stems from the fact that the flow is observed from a Galilean frame of reference that advances at a (nondimensional) speed F in the direction of the positive x axis. In a 'sea-fixed' frame of reference $(x_{sea}, y_{sea}, z_{sea})$, one has $F = 0$ in (2.7), and this dispersion relation becomes

$$\Delta^{sea}(f_{sea},\alpha,\beta;d) \equiv f_{sea}^2 - k\tanh(k\,d) = 0 \tag{2.11}$$

in agreement with (2.10).

Expressions (2.1) and (2.5) define the flow potential associated with the elementary wave function $W(\mathbf{x})$ as

$$\widehat{\phi}(\mathbf{x},t) = \frac{\cosh[k\,(z+d)]}{\cosh(k\,d)}\,\cos\theta^t \text{ where } \theta^t \equiv \alpha\,x+\beta\,y-f\,t\ . \tag{2.12}$$

Notations

The notations

$$h \equiv \sqrt{x^2+y^2}\ ,\ \mathbf{h} \equiv (x,y) \equiv h\,(\cos\psi,\sin\psi)\ ,\ \nabla_{\mathbf{h}} \equiv (\partial_x,\partial_y)\ , \tag{2.13a}$$

$$k \equiv \sqrt{\alpha^2+\beta^2}\ ,\ \mathbf{k} \equiv (\alpha,\beta) \equiv k\,(\cos\gamma,\sin\gamma)\ ,\ \nabla_{\mathbf{k}} \equiv (\partial_\alpha,\partial_\beta)\ , \tag{2.13b}$$

$$\theta \equiv \alpha\,x+\beta\,y \equiv \mathbf{k}\cdot\mathbf{h} \equiv k\,h\cos(\gamma-\psi) \text{ and} \tag{2.13c}$$

$$\partial_k \equiv (\alpha/k)\,\partial_\alpha + (\beta/k)\,\partial_\beta = (\cos\gamma)\,\partial_\alpha + (\sin\gamma)\,\partial_\beta \tag{2.13d}$$

are used hereafter. The wavenumbers k, α and β are nondimensional in accordance with (1.30c). The differential operator ∂_k defined by (2.13d) denotes differentiation along the radial direction $(\alpha,\beta)/k$.

Encounter wave frequency

In a 'sea-fixed' frame of reference $(x_{sea}, y_{sea}, z_{sea})$ where

$$x_{sea} \equiv x + Ft \ , \ y_{sea} \equiv y \ \text{and} \ z_{sea} \equiv z \, , \tag{2.14}$$

the phase θ^t in expression (2.12) for the potential of an elementary wave observed from a moving frame of reference is given by

$$\begin{aligned} \theta^t_{sea} &= \alpha\, x_{sea} + \beta\, y_{sea} - f_{sea}\, t = \alpha\,(x + Ft) + \beta\, y - f_{sea}\, t \\ &= \alpha\, x + \beta\, y - (f_{sea} - F\alpha)\, t = \alpha\, x + \beta\, y - f t \end{aligned}$$

where f_{sea} denotes the wave frequency in the sea-fixed reference frame.

Thus, a wave frequency f_{sea} in the sea-fixed reference frame corresponds to the encounter frequency

$$f = f_{sea} - F\alpha = f_{sea} - Fk\cos\gamma \tag{2.15}$$

in the moving frame of reference considered in (2.12). The relation (2.15) yields $f = f_{sea}$ if $\gamma = \pm 90^\circ$ (beam seas), $f < f_{sea}$ if $-90^\circ < \gamma < 90^\circ$ (following seas) and $f_{sea} < f$ if $90^\circ < \gamma < 270^\circ$ (head seas). In the particular case of a ship that advances at a constant speed in calm water, one has $f = 0$ and expression (2.15) yields

$$f_{sea} = Fk\cos\gamma \ .$$

Phase velocity

Expression (2.12) for θ^t and the relations (2.13) yield

$$\theta^t = \mathbf{k}\cdot\mathbf{h} - ft \ \text{ and } \ d\theta^t/dt = \mathbf{k}\cdot d\mathbf{h}/dt - f \, .$$

It follows that an observer traveling at the velocity $d\mathbf{h}/dt = \mathbf{v}_p$ given by

$$\mathbf{v}_p = v_p\, \frac{\mathbf{k}}{k} = \frac{f}{k}\, \frac{\mathbf{k}}{k} = \frac{f}{k} \begin{Bmatrix} \cos\gamma \\ \sin\gamma \end{Bmatrix} \tag{2.16}$$

sees a constant value of the phase θ^t, e.g. a particular wave crest. The velocity $\mathbf{v}_p$ defined by (2.16) is then called the 'phase velocity'.

Thus, a wave crest, or more generally a constant-phase line associated with a given value of the phase θ^t, advances along the normal to the wave-crest line, i.e. in the direction

$$\nabla_{\mathbf{h}}\,\theta^t = (\partial_x\,\theta^t, \partial_y\,\theta^t) = (\alpha, \beta) \equiv k\,(\cos\gamma, \sin\gamma) \equiv \mathbf{k}\ ,$$

at a velocity

$$\mathbf{v}_p \equiv v_p\,(\cos\gamma, \sin\gamma) \equiv v_p\,\mathbf{k}/k \ \text{ with } \ v_p = f/k\ .$$

In the particular case of a ship that advances at a constant speed in calm water, one has $f = 0$ and expression (2.16) yields $\mathbf{v}_p = 0$, in accordance with the fact that the waves created by the ship appear steady (frozen) in a Galilean frame of reference that follows the ship.

In a sea-fixed frame of reference, expression (2.16) becomes

$$\mathbf{v}_p^{sea} = v_p^{sea}\,\frac{\mathbf{k}}{k} = \frac{f_{sea}}{k}\,\frac{\mathbf{k}}{k} \tag{2.17}$$

where f_{sea} and k are related via the dispersion relation (2.11).

Alternative representations of dispersion relations

The dispersion relation (2.7) means that the wave frequency f and the wavenumbers α and β of waves created by a ship that advances at a given (nondimensional) speed F in water of uniform finite depth d are related. The relationship between the frequency f and the wavenumbers α and β, the Froude number F and the water depth d can be expressed via an implicit equation

$$\Delta\,(f, \alpha, \beta\,; F, d) = 0 \ \text{ with } \ k = \sqrt{\alpha^2 + \beta^2}\ , \tag{2.18a}$$

as in (2.7). Alternatively, this dispersion relation can be used to determine the frequency f in terms of the wavenumbers α and β, the Foude number F and the water depth d via an explicit equation

$$f = f(\alpha, \beta\,; F, d) \ \text{ where } \ k = \sqrt{\alpha^2 + \beta^2}\,. \tag{2.18b}$$

The alternative 'implicit' or 'explicit' forms (2.18a) and (2.18b) of the dispersion relation yield

$$\Delta_f\,df + \Delta_\alpha\,d\alpha + \Delta_\beta\,d\beta = 0 \ \text{ or } \ df = f_\alpha\,d\alpha + f_\beta\,d\beta\ . \tag{2.19}$$

The two differential relations (2.19) yield

$$(\Delta_\alpha + \Delta_f\,f_\alpha)\,d\alpha + (\Delta_\beta + \Delta_f\,f_\beta)\,d\beta = 0\ .$$

This differential relation yields the relations

$$f_\alpha = -\Delta_\alpha/\Delta_f \ \text{ and } \ f_\beta = -\Delta_\beta/\Delta_f\ . \tag{2.20}$$

The notation

$$\nabla_{\mathbf{k}}\,\Delta \equiv (\Delta_\alpha\,,\Delta_\beta) \equiv -\|\,\nabla_{\mathbf{k}}\,\Delta\,\|\,(\cos\delta,\sin\delta) \tag{2.21a}$$

$$\text{where } \|\nabla_{\mathbf{k}}\,\Delta\| \equiv \sqrt{\Delta_\alpha^2+\Delta_\beta^2} \tag{2.21b}$$

is used further on. The vector $\nabla_{\mathbf{k}}\,\Delta$ is orthogonal to a dispersion curve $\Delta = 0$, and δ denotes the angle between the vector $-\nabla_{\mathbf{k}}\,\Delta$ and the axis $\beta = 0$ in the Fourier plane (α,β). Expressions (2.21a) and (2.13b) yield

$$\frac{|\,\Delta_k\,|}{\|\,\nabla_{\mathbf{k}}\,\Delta\,\|} \equiv \frac{|\,\alpha\,\Delta_\alpha+\beta\,\Delta_\beta\,|/k}{\sqrt{\Delta_\alpha^2+\Delta_\beta^2}} = |\,\cos(\gamma-\delta)|\;. \tag{2.22}$$

This relation is used further on.

2.3 Group velocity

The wave function W defined by (2.5), where k is given by (2.6) and the wavenumbers α and β satisfy the dispersion relation (2.7), is an elementary solution that satisfies the Laplace equation (2.4a) and the boundary conditions (2.4b) and (2.4c) at the sea bottom and the free surface. The flow potential ϕ^W given by a superposition of elementary wave functions W also satisfies the homogeneous equations (2.4). An interesting special superposition of two elementary wave potentials (2.12) is now considered.

Specifically, these two elementary waves have frequencies f and $f+\delta f$, and wavenumbers (α,β) and $(\alpha+\delta\alpha,\beta+\delta\beta)$, where the differences δf, $\delta\alpha$ and $\delta\beta$ are small. The related wavenumbers k and $k+\delta k$ are given by $k \equiv \sqrt{\alpha^2+\beta^2}$ and $\delta k \approx (\alpha\,\delta\alpha+\beta\,\delta\beta)/k$. The amplitudes of the two waves are denoted as a and a', where a' can be equal to a or can differ from a.

At the free-surface plane $z = 0$, expression (2.12) shows that the potential of these two superposed elementary waves is given by

$$a\,\mathrm{Re}\,e^{\,\mathrm{i}\,\theta^t} + a'\,\mathrm{Re}\,e^{\,\mathrm{i}\,(\theta^t+\delta\theta^t)} = a\,\mathrm{Re}\,m\,e^{\,\mathrm{i}\,\theta^t} \;\text{ where} \tag{2.23a}$$

$$m \equiv 1+(a'/a)\,e^{\,\mathrm{i}\,\delta\theta^t} \;\text{ and }\; \delta\theta^t \equiv x\,\delta\alpha + y\,\delta\beta - t\,\delta f\;. \tag{2.23b}$$

The potential (2.23a) corresponds to a wave $a\,\mathrm{Re}\,m\,e^{\,\mathrm{i}\,\theta^t}$ with a modulated complex amplitude $m\,a$. Expressions (2.23b) show that the modulation factor m is also a wave, with frequency δf and wavenumbers $(\delta\alpha,\delta\beta)$. Expressions (2.23b) and (2.19) yield

$$\frac{d\,\delta\theta^t}{dt} = \delta\alpha\,\frac{dx}{dt} + \delta\beta\,\frac{dy}{dt} - \delta f = \delta\alpha\left(\frac{dx}{dt}-\frac{\partial f}{\partial\alpha}\right) + \delta\beta\left(\frac{dy}{dt}-\frac{\partial f}{\partial\beta}\right).$$

An observer advancing at the velocity $\mathbf{v}_g = (v_g^x, v_g^y)$ where

$$v_g^x \equiv dx/dt = f_\alpha \text{ and } v_g^y \equiv dy/dt = f_\beta \tag{2.24}$$

observes a constant value of the modulation factor m, i.e. advances at the velocity—called group velocity—of the group of modulated waves defined by (2.23), and observes waves that have the same amplitude.

Since the energy transported by a wave is proportional to the square a^2 of the wave amplitude a, an observer advancing at the group velocity $\mathbf{v}_g$ observes the same wave energy, which is then transported at a velocity that is equal to the group velocity. Thus, the velocity $\mathbf{v}_e$ at which wave energy is transported is equal to the group velocity $\mathbf{v}_g$, an important basic result of the theory of water waves.

The relations (2.24), (2.13b), (2.20) and (2.21a) yield the alternative expressions

$$\mathbf{v}_g \equiv \begin{Bmatrix} v_g^x \\ v_g^y \end{Bmatrix} = \begin{Bmatrix} f_\alpha \\ f_\beta \end{Bmatrix} \equiv \nabla_{\mathbf{k}} f = \frac{-1}{\Delta_f} \begin{Bmatrix} \Delta_\alpha \\ \Delta_\beta \end{Bmatrix} \equiv \frac{\nabla_{\mathbf{k}} \Delta}{-\Delta_f} \tag{2.25a}$$

for the group velocity $\mathbf{v}_g$. The vector $\nabla_{\mathbf{k}} \Delta$ associated with a dispersion function Δ is orthogonal to a dispersion curve $\Delta = 0$. Thus, expressions (2.25a) show that the group velocity $\mathbf{v}_g$ at a point (α, β) of a dispersion curve is orthogonal to the dispersion curve. Expressions (2.25a) show that the magnitude v_g of the group velocity $\mathbf{v}_g$ is given by

$$v_g \equiv \sqrt{(v_g^x)^2 + (v_g^y)^2} = \frac{\| \nabla_{\mathbf{k}} \Delta \|}{|\Delta_f|} \equiv \frac{\sqrt{\Delta_\alpha^2 + \Delta_\beta^2}}{|\Delta_f|} \,. \tag{2.25b}$$

Expressions (2.25a-b) then yield

$$\frac{\mathbf{v}_g}{v_g} = \text{sign}(\Delta_f) \, \frac{-\nabla_{\mathbf{k}} \Delta}{\| \nabla_{\mathbf{k}} \Delta \|} \,. \tag{2.25c}$$

The relations (2.25a-c) explicitly determine the group velocity $\mathbf{v}_g$ in terms of the dispersion function Δ. Expressions (2.25c) and (2.21) also yield

$$\mathbf{v}_g \equiv \begin{Bmatrix} v_g^x \\ v_g^y \end{Bmatrix} = \text{sign}(\Delta_f) \; v_g \begin{Bmatrix} \cos\delta \\ \sin\delta \end{Bmatrix} \tag{2.25d}$$

This relation shows that the angle between the group velocity $\mathbf{v}_g$ and the axis $\beta = 0$ is δ or $\delta + \pi$ if $0 < \Delta_f$ or $\Delta_f < 0$.

In a sea-fixed frame of reference, expression (2.25a) becomes

$$\mathbf{v}_g^{sea} = \frac{\nabla_{\mathbf{k}} \Delta^{sea}}{-\Delta_f^{sea}} \tag{2.26}$$

where Δ^{sea} is the dispersion relation (2.11).

2.4 Dispersion functions

The dispersion function $\Delta(f,\alpha,\beta;F,d)$ related to the free waves created by a ship that steadily advances through regular waves in water of uniform finite depth is now considered.

The derivatives of the dispersion function $\Delta(f,\alpha,\beta;F,d)$ given by (2.7) with respect to the wave frequency f and the wavenumbers α and β are

$$\begin{aligned}\Delta_f &= 2(f+F\alpha) \\ \Delta_\alpha &= 2F(f+F\alpha) - [\tanh(kd) + kd/\cosh^2(kd)]\,\alpha/k\ , \\ \Delta_\beta &= -[\tanh(kd) + kd/\cosh^2(kd)]\,\beta/k\ .\end{aligned} \tag{2.27a}$$

The alternative expressions

$$\Delta_\alpha = 2F(f+F\alpha) - (1+s^d)\tanh(kd)\,\alpha/k \ \text{ and} \tag{2.27b}$$

$$\Delta_\beta = -(1+s^d)\tanh(kd)\,\beta/k \tag{2.27c}$$

follow from the identity

$$\tanh(kd) + (kd)/\cosh^2(kd) \equiv (1+s^d)\tanh(kd) \equiv t^d \tag{2.28a}$$

where s^d and t^d are defined as

$$s^d \equiv (2kd)/\sinh(2kd) \ \text{ and } \ t^d \equiv (1+s^d)\tanh(kd)\ . \tag{2.28b}$$

One has $0 \le t^d \le 1$ and $0 \le s^d \le 1$ as kd increases within the range $0 \le kd \le \infty$.

The derivative of the dispersion function $\Delta(f,\alpha,\beta;F,d)$ in the radial direction $(\alpha,\beta)/k$ is given by

$$\Delta_k \equiv (\alpha/k)\,\Delta_\alpha + (\beta/k)\,\Delta_\beta = \Delta_\alpha\cos\gamma + \Delta_\beta\sin\gamma \tag{2.29}$$

in accordance with (2.13d). Expressions (2.29), (2.27b-c) and (2.6) then yield

$$\Delta_k = 2F(f+F\alpha)\,\alpha/k - (1+s^d)\tanh(kd)\ . \tag{2.30}$$

Particular cases

Expressions (2.27), (2.30), (2.13b) and (2.28b) yield

$$\Delta_f = 2f \ \text{ and } \ \begin{Bmatrix}\Delta_\alpha\\ \Delta_\beta\\ \Delta_k\end{Bmatrix} = -\begin{Bmatrix}\cos\gamma\\ \sin\gamma\\ 1\end{Bmatrix} t^d \ \text{ if } F=0 \tag{2.31a}$$

i.e. for an offshore structure in regular waves,

$$\left.\begin{cases} \Delta_f = 2F\alpha = 2Fk\cos\gamma \\ \Delta_\alpha = (2F^2k - t^d)\,\alpha/k = (2F^2k - t^d)\cos\gamma \\ \Delta_\beta = -\,t^d\,\beta/k = -\,t^d\sin\gamma \\ \Delta_k = 2F^2\alpha^2/k - t^d = 2F^2k\cos^2\gamma - t^d \end{cases}\right\} \text{ if } f = 0 \qquad (2.31b)$$

i.e. for a ship that steadily advances in calm water, and

$$\left.\begin{cases} \Delta_f = 2\,(f + F\alpha) = 2\,(f + Fk\cos\gamma) \\ \Delta_\alpha = 2F(f + F\alpha) - \alpha/k = 2F(f + Fk\cos\gamma) - \cos\gamma \\ \Delta_\beta = -\beta/k = -\sin\gamma \\ \Delta_k = 2F(f + F\alpha)\,\alpha/k - 1 = 2F(f + Fk\cos\gamma)\cos\gamma - 1 \end{cases}\right\} \text{ if } d = \infty \quad (2.31c)$$

i.e. in deep water, for which expression (2.28b) yields $s^d = 0$ and $t^d = 1$.

In a sea-fixed frame of reference, it readily follows from (2.10) and (2.11) that expressions (2.31a) become

$$\Delta_f^{sea} = 2\,f_{sea} \text{ and } \begin{Bmatrix} \Delta_\alpha^{sea} \\ \Delta_\beta^{sea} \\ \Delta_k^{sea} \end{Bmatrix} = -\begin{Bmatrix} \cos\gamma \\ \sin\gamma \\ 1 \end{Bmatrix} t^d \qquad (2.32)$$

where the dispersion relation Δ^{sea} is given by (2.11).

2.5 Phase and group velocities

The expressions for the derivatives of the dispersion function $\Delta\,(f, \alpha, \beta\,; F, d)$ given in the previous section can readily be applied to determine the group velocity $\mathbf{v}_g$ and the phase velocity $\mathbf{v}_p$ of the waves created by a ship that steadily advances through regular waves in water of uniform finite depth.

Expressions (2.25a), (2.27) and (2.7) show that $\mathbf{v}_g$ is given by

$$\mathbf{v}_g \equiv \begin{Bmatrix} v_g^x \\ v_g^y \end{Bmatrix} = \text{sign}(f + F\alpha)\,\frac{1 + s^d}{2}\sqrt{\frac{\tanh(k\,d)}{k}}\begin{Bmatrix} \cos\gamma \\ \sin\gamma \end{Bmatrix} - \begin{Bmatrix} F \\ 0 \end{Bmatrix} \qquad (2.33a)$$

where $(\cos\gamma, \sin\gamma) = \mathbf{k}/k$ and s^d is given by (2.28b). The component $(-F, 0)$ on the right of (2.33a) stems from the fact that the flow is observed from a Galilean frame of reference that advances at a (nondimensional) speed F in the direction of the positive x axis. Expressions (2.16) and (2.7) yield

$$\mathbf{v}_p \equiv \begin{Bmatrix} v_p^x \\ v_p^y \end{Bmatrix} = \left(\text{sign}(f + F\alpha)\sqrt{\frac{\tanh(k\,d)}{k}} - F\cos\gamma\right)\begin{Bmatrix} \cos\gamma \\ \sin\gamma \end{Bmatrix} \qquad (2.33b)$$

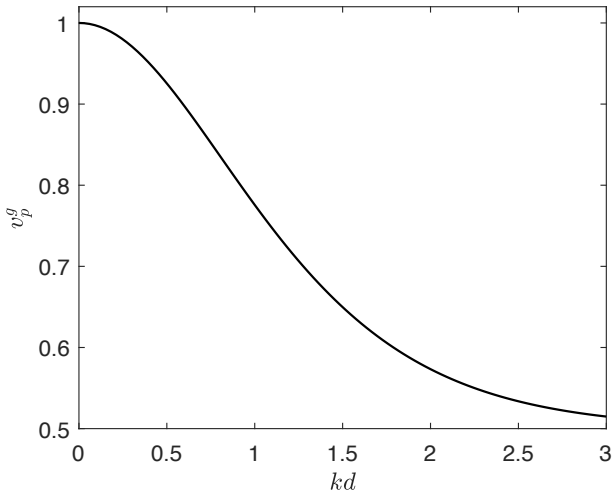

Figure 2.1: Function $v_p^g(k\,d)$ defined by (2.34b) for $0 \leq k\,d \leq 3$.

The group velocity $\mathbf{v}_g$ and the phase velocity $\mathbf{v}_p$ are not colinear except if $F = 0$, i.e. for diffraction-radiation of regular waves by an offshore structure.

In this special case, expressions (2.33) become

$$\mathbf{v}_p = \sqrt{\frac{\tanh(k\,d)}{k}} \begin{Bmatrix} \cos\gamma \\ \sin\gamma \end{Bmatrix} \text{ and } \mathbf{v}_g = v_p^g\,\mathbf{v}_p \tag{2.34a}$$

$$\text{where } v_p^g \equiv \frac{1+s^d}{2} = \frac{1}{2}\left[1+\frac{2k\,d}{\sinh(2k\,d)}\right] \tag{2.34b}$$

and (2.28b) was used. Expression (2.34b) yields

$$1/2 \leq v_p^g \leq 1 \text{ with } v_p^g \to 1/2 \text{ as } k\,d \to \infty \text{ and } v_p^g \to 1 \text{ as } k\,d \to 0\,.$$

The function v_p^g defined by (2.34b) is depicted in Fig.2.1 for $0 \leq k\,d \leq 3$. For diffraction-radiation of regular waves by offshore structures in deep water, i.e. for $F = 0$ and $d = \infty$, one has $s^d = 0$ in (2.33a) and expressions (2.34) yield

$$\mathbf{v}_p = (\cos\gamma, \sin\gamma)/\sqrt{k} \text{ and } \mathbf{v}_g = \mathbf{v}_p/2\,. \tag{2.35}$$

In a sea-fixed frame of reference, the group velocity $\mathbf{v}_g^{sea}$ and the phase velocity $\mathbf{v}_p^{sea}$ are colinear, in agreement with (2.34a). Specifically, one has

$$\mathbf{v}_p^{sea} = \text{sign}(f_{sea})\sqrt{\frac{\tanh(k\,d)}{k}}\,\frac{\mathbf{k}}{k} \text{ and } \mathbf{v}_g^{sea} = v_p^g\,\mathbf{v}_p^{sea} \tag{2.36}$$

where v_p^g is given by (2.34b).

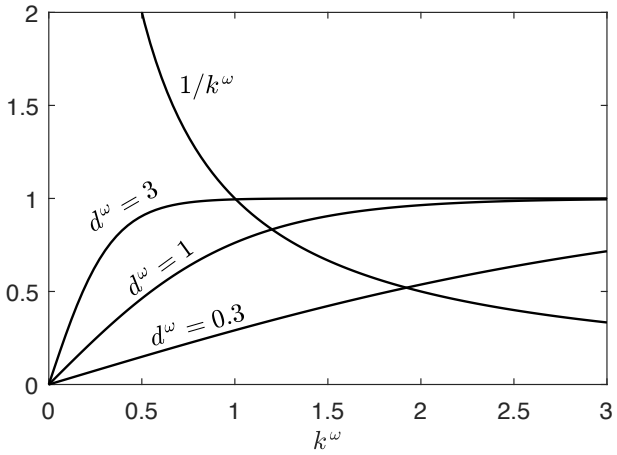

Figure 2.2: Functions $1/k^\omega$ and $\tanh(d^\omega k^\omega)$ for $d^\omega = 3$, 1 or 0.3.

In the general case $F \neq 0$, expressions (2.33a) and (2.36) show that the group velocity $\mathbf{v}_g$ can be expressed as the sum of the apparent uniform current $(-F, 0)$ associated with the moving Galilean frame of reference and the group velocity $\mathbf{v}_g^{sea}$ in a sea-fixed frame of reference, i.e. one has

$$\mathbf{v}_g^{sea} = \mathbf{v}_g + \mathbf{v}_{ship} \text{ where } \mathbf{v}_{ship} \equiv (F, 0) \tag{2.37}$$

is the ship speed. The basic relation (2.37) between velocities observed in different Galilean frames of reference does not hold for the phase velocity $\mathbf{v}_p$. Specifically, one has

$$\mathbf{v}_p^{sea} = \mathbf{v}_p + F(\cos\gamma)\,\mathbf{k}/k$$

Thus, one has $\mathbf{v}_p^{sea} \neq \mathbf{v}_p + \mathbf{v}_{ship}$ in accordance with the fact that the phase velocity is fundamentally different from a flow velocity.

2.6 Offshore structures in regular waves

Diffraction-radiation of regular waves by an offshore structure in water of uniform finite depth d is now considered. The dispersion relation (2.10) can be expressed in the 'frequency-scaled' form

$$\frac{1}{k^\omega} = \tanh(d^\omega k^\omega) \text{ where } k^\omega \equiv \frac{k}{f^2} \equiv \frac{gK}{\omega^2} \text{ and } d^\omega \equiv f^2 d \equiv \frac{\omega^2 D}{g} \tag{2.38}$$

in accordance with (1.33a).

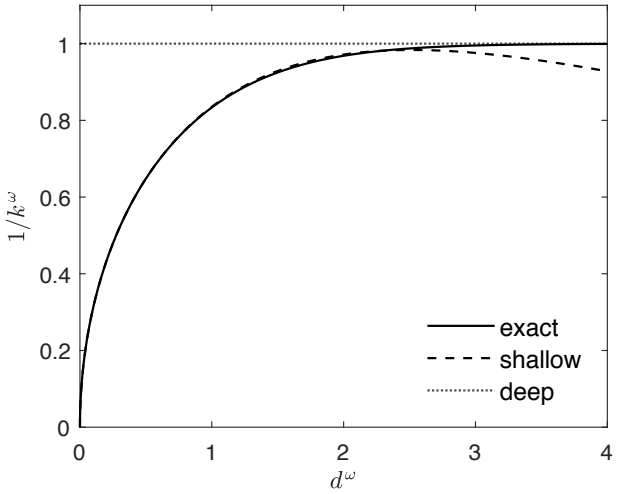

Figure 2.3: Root of the dispersion relation (2.38) and related deep-water and shallow-water approximations (2.39b) for $0 \le d^\omega \le 4$.

Fig.2.2 shows that the dispersion equation (2.38) has a single real root, denoted as $k_*^\omega(d^\omega)$, and therefore defines a single dispersion curve for every value of d^ω. This dispersion curve is the circle

$$k^\omega = k_*^\omega(d^\omega) \tag{2.39a}$$

centered at the origin of the Fourier plane. The root $k_*^\omega(d^\omega)$ of (2.38) is depicted in Fig.2.3, where the deep-water and shallow-water approximations

$$k_*^\omega \sim 1 \text{ as } d^\omega \to \infty \text{ and } k_*^\omega \sim \frac{1+(1+11\,d^\omega/60)\,d^\omega/6}{\sqrt{d^\omega}} \text{ as } d^\omega \to 0 \tag{2.39b}$$

are also shown.

The dispersion relation (2.38) yields

$$1/k_*^\omega(d^\omega) = \tanh[d^\omega k_*^\omega(d^\omega)] \le 1 \ .$$

One then has

$$1 = k_*^\omega(\infty) \le k_*^\omega(d) \ . \tag{2.40a}$$

The corresponding wavelength $\lambda^\omega \equiv 2\pi/k^\omega$ is given by

$$\lambda^\omega \equiv f^2\lambda \equiv \frac{\omega^2\Lambda}{g} = \frac{2\pi}{k_*^\omega(d)} \le \frac{2\pi}{k_*^\omega(\infty)} = \lambda_\infty^\omega = 2\pi \ . \tag{2.40b}$$

Thus, for a given wave frequency f, the wavelength λ^ω decreases as the water depth d decreases, i.e. time-harmonic waves are shorter in finite water depth

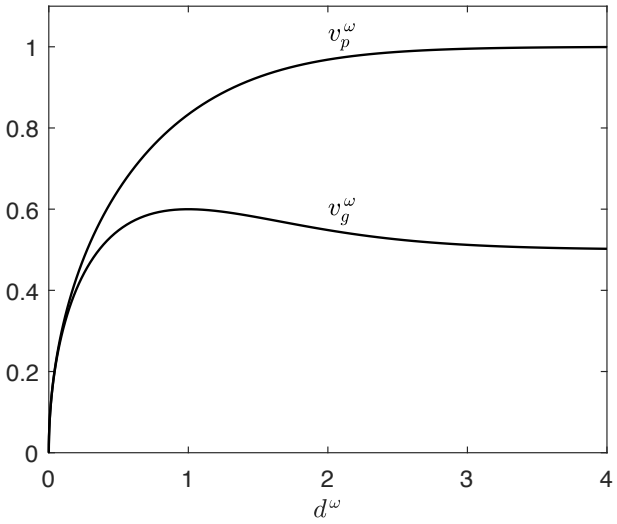

Figure 2.4: Phase and group velocities v_p^ω and v_g^ω given by (2.41) for diffraction-radiation of regular waves by an offshore structure in water of uniform depth $0 \le d^\omega \le 4$.

than in deep water. The relations (2.40b) yield

$$\Lambda \le \Lambda^{deep} \equiv 2\,\pi\,g/\omega^2\,. \tag{2.40c}$$

Expression (2.40c) for the deep-water wavelength Λ^{deep} shows that Λ^{deep} is smaller than a characteristic length L_s related to the size of an offshore structure if

$$\omega\sqrt{L_s/g} > \sqrt{2\,\pi} \approx 2.5 \;\text{ or }\; \sqrt{L_s/g}/T_\omega > 1/\sqrt{2\,\pi} \approx 0.4$$

where $T_\omega \equiv 2\,\pi/\omega$ denotes the wave period.

As was already noted, expressions (2.33) with $F = 0$ show that the phase velocity $\mathbf{v}_p$ and the group velocity $\mathbf{v}_g$ are colinear, with magnitude given by

$$v_p^\omega = \sqrt{\frac{\tanh(d^\omega\,k_*^\omega)}{k_*^\omega}} \;\text{ and }\; v_g^\omega = \frac{1}{2}\left[1 + \frac{2\,d^\omega\,k_*^\omega}{\sinh(2\,d^\omega\,k_*^\omega)}\right] v_p^\omega \tag{2.41}$$

where $v^\omega \equiv V\omega/g$ and $k_*^\omega(d^\omega)$ is the root of the dispersion relation (2.38). Expressions (2.41) yield $v_g^\omega \sim v_p^\omega/2$ in the deep-water limit $d^\omega k^\omega \to \infty$, and $v_g^\omega \sim v_p^\omega$ in the shallow-water limit $d^\omega k^\omega \to 0$, as can be observed in Fig.2.4 where the phase velocity v_p^ω and the group velocity v_g^ω given by (2.41) are depicted.

As was also noted previously, the dispersion relation (2.38) defines a single dispersion curve, a circle centered at the origin $k = 0$ of the Fourier

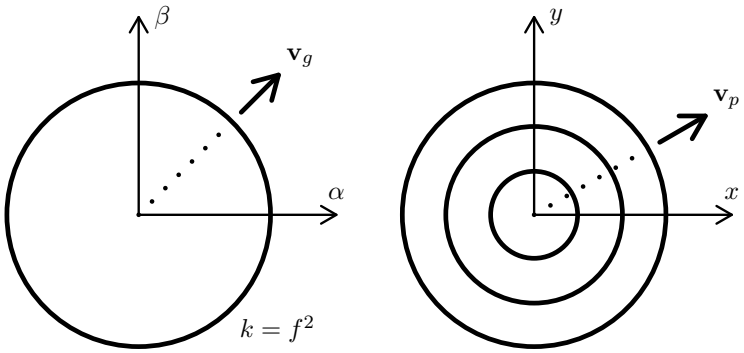

Figure 2.5: The figure illustrates—for the simplest case of diffraction-radiation of regular waves by an offshore structure in deep water—the basic properties that the group velocity $\mathbf{v}_g$ is orthogonal to the dispersion curve (the circle $k = f^2$) in the Fourier plane (α, β), and the phase velocity $\mathbf{v}_p$ is orthogonal to the wave crests (a series of concentric circles) in the free surface plane (x, y).

plane. Moreover, the corresponding waves (e.g. wave crests) are shown further on (in section 3.5) to consist of a series of concentric circles centered at the origin $h = 0$ of the (physical) free-surface plane $z = 0$. Thus, the group velocity $\mathbf{v}_g = v_g \mathbf{k}/k$ is orthogonal to the dispersion circle in the Fourier plane (α, β) and the phase velocity $\mathbf{v}_p = v_p \mathbf{h}/h$ is orthogonal to the circular waves in the free-surface plane (x, y), as is illustrated in Fig.2.5 for deep water.

2.7 Superposition of basic elementary waves

As was already noted in section 2.3, the flow potential ϕ^W associated with a superposition of elementary plane wave functions W along the dispersion curves defined by the dispersion relation $\Delta\,(f, \alpha, \beta\,; F, d) = 0$, i.e.

$$\phi^W(\mathbf{x}) = \sum_{\Delta=0} \int_{\Delta=0} ds\; a^\phi\, W(\mathbf{x}, \alpha, \beta) \;\text{ where }\; (\alpha\,, \beta) \in (\Delta = 0)\;, \qquad (2.42)$$

satisfies the Laplace equation (2.4a) and the boundary conditions (2.4b) and (2.4c) at the sea bottom and the free surface. In (2.42), the summation is performed over all the dispersion curves, the point $(\alpha\,, \beta)$ lies on a dispersion curve, and $W(\mathbf{x}, \alpha, \beta)$ is the elementary wave function (2.5). Furthermore, $ds \equiv \sqrt{(d\alpha)^2 + (d\beta)^2}$ denotes the (nondimensional) differential element of arc length of a dispersion curve and a^ϕ represents a general wave-amplitude function. Expression (2.42) assumes that the dispersion curves are defined

in terms of parametric representations in which the arc length s is taken as the parameter, although alternative parametric representations of the dispersion curves can be used.

Thus, free waves and the corresponding flow potential $\phi^W(\mathbf{x})$ in (2.1) can be represented as a one-dimensional Fourier superposition of elementary plane waves, defined by the wave function W, along the dispersion curves determined by the dispersion relation $\Delta(f, \alpha, \beta; F, d) = 0$. However, the elementary wave function W in the Fourier superposition (2.42) corresponds to $\epsilon \equiv 0$ in (2.3d). It follows that the elementary wave function W defined by (2.5), and the related Fourier superposition (2.42), do not account for the initial conditions associated with the choices $0 < \epsilon$ or $\epsilon = +0$ in (2.1).

The Fourier superposition (2.42) is not a satisfactory representation of free waves. For instance, this representation of free waves does not preclude ship waves ahead of a ship that advances in calm water. A satisfactory flow representation requires initial conditions, as in (2.1) with $\epsilon = +0$. Alternatively, ϵ could be taken as $\epsilon = 0$ in (2.1) and (2.3d) if an additional condition, commonly called 'radiation condition', is imposed **[2,4]**. A straightforward analysis associated with $\epsilon = +0$ and a flow that grows from rest at time $t = -\infty$ is used in the book, and a generalized elementary wave function that accounts for initial conditions and the far-field boundary condition (2.3b) is defined in sections 2.8−2.10.

Specifically, the spatial component $\phi(\mathbf{x})$ of the flow potential related to the far-field boundary-value problem (2.3) for an offshore structure in regular waves or a ship that steadily advances through regular waves or (if $f = 0$) in calm water with the 'time-growth' parameter ϵ in the free-surface boundary condition (2.3d) taken as $\epsilon = +0$, instead of $\epsilon \equiv 0$, is now considered. The elementary wave function given by (2.5)-(2.7) is generalized to satisfy initial conditions that correspond to a flow starting from rest at time $t = -\infty$, and the far-field condition (2.3b).

2.8 Initial conditions

Thus, elementary wave functions associated with $0 < \epsilon$ in the free-surface boundary condition (2.3d), or equivalently the 'complex frequency' $f + \mathrm{i}\,\epsilon$ in (2.1), are now considered.

These elementary waves can be determined by considering the complex wavenumbers

$$\alpha + \mathrm{i}\,\epsilon\,\alpha_1 \;\;,\;\; \beta + \mathrm{i}\,\epsilon\,\beta_1 \;\;,\;\; k + \mathrm{i}\,\epsilon\,k_1 \tag{2.43}$$

in the elementary wave function (2.5), which is then generalized as

$$e^{\,\mathrm{i}\,(\alpha\,x + \beta\,y) - \epsilon\,(\alpha_1\,x + \beta_1\,y)}\;\frac{\cosh[(k + \mathrm{i}\,\epsilon\,k_1)(z+d)]}{\cosh[(k + \mathrm{i}\,\epsilon\,k_1)\,d\,]}\;. \tag{2.44}$$

Sea-bottom boundary condition and Laplace's equation

The elementary wave function (2.44) satisfies the sea-bottom condition (2.3c), and also satisfies the Laplace equation (2.3a) if

$$(k + \mathrm{i}\,\epsilon k_1)^2 = (\alpha + \mathrm{i}\,\epsilon\alpha_1)^2 + (\beta + \mathrm{i}\,\epsilon\beta_1)^2 \,. \tag{2.45a}$$

This condition is satisfied exactly, not only for $0 < \epsilon \ll 1$ but for every value of ϵ, if

$$k^2 = \alpha^2 + \beta^2 \;,\;\; k\,k_1 = \alpha\,\alpha_1 + \beta\,\beta_1 \;\text{ and }\; k_1^2 = \alpha_1^2 + \beta_1^2 \;. \tag{2.45b}$$

The condition (2.45a) and the equivalent conditions (2.45b) are satisfied if (α_1, β_1, k_1) are proportional to (α, β, k), i.e. if

$$(\alpha_1, \beta_1, k_1) = (\alpha, \beta, k)/\mu \tag{2.45c}$$

where μ denotes a proportionality factor.

Free-surface boundary condition

Furthermore, the elementary wave function (2.44) satisfies the free-surface condition (2.3d) if

$$[f + \mathrm{i}\,\epsilon + F\alpha(1 + \mathrm{i}\,\epsilon/\mu)]^2 = k\,(1 + \mathrm{i}\,\epsilon/\mu)\tanh[k\,d(1 + \mathrm{i}\,\epsilon/\mu)] \tag{2.46}$$

where the relations $\alpha_1 = \alpha/\mu$ and $k_1 = k/\mu$ were used in accordance with (2.45c). The Taylor series of the free-surface boundary condition (2.46) about $\epsilon = 0$ yields

$$(f + F\alpha)^2 + 2\,\mathrm{i}\,\epsilon\,(f + F\alpha)(1 + F\alpha/\mu) = k\tanh(kd) + \mathrm{i}\,\epsilon\,(1 + s^d)k\tanh(kd)/\mu$$

where $O(\epsilon^2)$ terms are ignored and expression (2.28a) was used on the right side. The $O(1)$ and $O(\mathrm{i}\,\epsilon)$ terms in this expansion are

$$\begin{aligned} &(f + F\alpha)^2 = k\tanh(k\,d) \;, \\ &2\,(f + F\alpha)(1 + F\alpha/\mu) = (1 + s^d)\,k\tanh(k\,d)/\mu \;. \end{aligned} \tag{2.47}$$

The $O(1)$ relation (2.47) is the dispersion relation (2.7) previously obtained for $\epsilon \equiv 0$, and the $O(\mathrm{i}\,\epsilon)$ term determines the proportionality factor μ in (2.45c) as

$$\mu = (f + F\alpha)(1 + s^d)/2 - F\alpha \tag{2.48}$$

where (2.47) was used and s^d is given by (2.28b). Expressions (2.45c) and (2.48) determine the complex wavenumbers α_1, β_1, k_1 in (2.43).

Alternative approach

Expression (2.48) can be obtained in another way, now considered. The dispersion relation (2.46) corresponds to the limit $\epsilon \to 0$ of the dispersion relation

$$\Delta(f + \mathrm{i}\,\epsilon, \alpha + \mathrm{i}\,\epsilon\,\alpha_1, \beta + \mathrm{i}\,\epsilon\,\beta_1; F, d) = 0 \tag{2.49}$$

associated with the dispersion relation $\Delta(f, \alpha, \beta; F, d) = 0$ defined by (2.7) and the complex frequency and wavenumbers (2.43) in the related wave function (2.44). The Taylor series expansion of the dispersion relation (2.49) about $\epsilon = 0$ yields

$$\Delta(f, \alpha, \beta; F, d) + \mathrm{i}\,\epsilon\,(\Delta_f + \alpha_1\,\Delta_\alpha + \beta_1\,\Delta_\beta) + O(\epsilon^2) = 0\ . \tag{2.50}$$

The $O(1)$ relation (2.50) is the dispersion relation (2.7), already obtained for $\epsilon \equiv 0$, and the $O(\epsilon)$ term determines the proportionality factor μ in (2.45c) as

$$\mu = -(\alpha\,\Delta_\alpha + \beta\,\Delta_\beta)/\Delta_f \equiv -k\,\Delta_k/\Delta_f \tag{2.51a}$$

where Δ_k is the derivative of the dispersion function $\Delta(f, \alpha, \beta; F, d)$ in the radial direction $(\alpha, \beta)/k$, as in (2.29). Expressions (2.27a), (2.30) and (2.7) then yield

$$\mu = -k\,\Delta_k/\Delta_f = (f + F\alpha)(1 + s^d)/2 - F\alpha \tag{2.51b}$$

in agreement with (2.48). The proportionality factor μ defined by (2.51b) can be expressed as

$$\mu = \sigma^\Delta \mu' \ \text{ where } \ \mu' \equiv |\mu| = k|\Delta_k|/|\Delta_f| \ \text{ and} \tag{2.51c}$$

$$\sigma^\Delta \equiv -\mathrm{sign}(\Delta_f\,\Delta_k) \tag{2.52}$$

This expression determines the sign function σ^Δ in terms of the dispersion function Δ.

Application to ships and offshore structures

In particular, expression (2.52) yields

$$\sigma^\Delta = \mathrm{sign}\,[(f + F\alpha)(1 + s^d)/2 - F\alpha\,] \tag{2.53a}$$

for a ship that steadily advances through regular waves in finite water-depth. Expression (2.53a) becomes

$$\sigma^\Delta = 1 \text{ if } F = 0 \quad \text{and} \quad \sigma^\Delta = -\mathrm{sign}(\alpha) = -\mathrm{sign}(\cos\gamma) \text{ if } f = 0\ , \tag{2.53b}$$

i.e. for an offshore structure in regular waves or a ship that steadily advances in calm water, and

$$\sigma^\Delta = \mathrm{sign}(f - F\alpha) = \mathrm{sign}(f/F - \alpha) \ \text{ if } \ d = \infty\ , \tag{2.53c}$$

i.e. in deep water.

2.9 Far-field boundary condition

The relations (2.44), (2.45c) and (2.51c) yield the elementary wave function

$$\frac{\cosh[k\,(1+\sigma^{\Delta}\,\mathrm{i}\,\epsilon/\mu')(z+d)]}{\cosh[k\,(1+\sigma^{\Delta}\,\mathrm{i}\,\epsilon/\mu')\,d]}\,e^{\,\mathrm{i}\,(\alpha\,x+\beta\,y)\,-\,\sigma^{\Delta}\,\epsilon\,(\alpha\,x+\beta\,y)/\mu'}\,. \tag{2.54}$$

The elementary wave function (2.54) with $0<\epsilon\ll 1$ and the dispersion relation (2.7) was already shown to satisfy the Laplace equation (2.3a) and the boundary conditions (2.3c) and (2.3d) at the sea bottom and the free surface. The elementary wave function (2.54) vanishes in the far field if $0<\sigma^{\Delta}\,\mathrm{sign}(\alpha\,x\,+\,\beta\,y)\equiv\sigma^{\Delta}\,\mathrm{sign}(\theta)$ in accordance with expression (2.13c) for the phase θ.

The polar representations (2.13b) and (2.13a) for the Fourier variables α and β and the horizontal coordinates x and y then show that bounded elementary waves are obtained if $\sigma^{\theta}=\sigma^{\Delta}$, where σ^{θ} is defined as

$$\sigma^{\theta}\equiv\mathrm{sign}(\theta)\equiv\mathrm{sign}[\cos(\gamma-\psi)]\equiv\mathrm{sign}(\alpha\,x+\beta\,y)\,. \tag{2.55}$$

The condition $\sigma^{\theta}=\sigma^{\Delta}$ and expression (2.55) yield the restrictions

$$\left\{\begin{array}{l}\psi-\pi/2<\gamma<\psi+\pi/2\\ \psi+\pi/2<\gamma<\psi+3\,\pi/2\end{array}\right\}\ \text{if}\ \left\{\begin{array}{l}0<\sigma^{\Delta}\\ \sigma^{\Delta}<0\end{array}\right\}\,. \tag{2.56}$$

The condition (2.56) defines 'active' portions of the dispersion curves $\Delta=0$ in the Fourier representation (2.42) of free waves. These active portions of the dispersion curves in the Fourier plane (α,β) depend on the angle ψ determined in the physical plane (x,y) by (2.13a).

2.10 Fourier representation of far-field waves and generalized elementary waves

Alternatively, the Fourier representation (2.42) can be modified as

$$\phi^{W}(\mathbf{x})=\sum_{\Delta=0}\int_{\Delta=0}ds\;a^{\phi}\,H(\sigma^{\Delta}\sigma^{\theta})\,W(\mathbf{x},\alpha,\beta)$$
$$\text{where}\ \ (\alpha,\beta)\in(\Delta=0)\,. \tag{2.57a}$$

Moreover, σ^{Δ} and σ^{θ} are defined by (2.53a) and (2.55) as

$$\sigma^{\Delta}\equiv-\mathrm{sign}(\Delta_f\,\Delta_k)=\mathrm{sign}[(f+F\alpha)(1+s^{d})/2-F\alpha]\,, \tag{2.57b}$$
$$\sigma^{\theta}\equiv\mathrm{sign}(\theta)\equiv\mathrm{sign}[\cos(\gamma-\psi)]\equiv\mathrm{sign}(\alpha\,x+\beta\,y)\,. \tag{2.57c}$$

The summation in (2.57a) is performed over all the dispersion curves defined by the dispersion relation $\Delta = 0$ and the point $(\alpha\,,\beta)$ lies on a dispersion curve, as in (2.42). The Heaviside unit-step function $H(\sigma^{\Delta}\sigma^{\theta})$ in (2.57a) takes the values

$$H(\sigma^{\Delta}\sigma^{\theta}) = \left\{ \begin{matrix} 1 \\ 0 \end{matrix} \right\} \text{ if } \sigma^{\Delta}\sigma^{\theta} = \left\{ \begin{matrix} 1 \\ -1 \end{matrix} \right\} . \tag{2.57d}$$

The elementary wave function $W(\mathbf{x}, \alpha, \beta)$ can be expressed as

$$W(\mathbf{x}, \alpha, \beta) \equiv a^z \, e^{\,\mathrm{i}\,(\alpha\, x + \beta\, y)} \equiv a^z \, e^{\,\mathrm{i}\,\theta} \tag{2.57e}$$

where the function $a^z(k\,z, k\,d)$ is defined as

$$a^z \equiv \frac{\cosh\left[k\,(z+d)\right]}{\cosh(k\,d)} \text{ if } d < \infty \quad \text{or} \quad a^z \equiv e^{\,k\,z} \text{ if } d = \infty \tag{2.57f}$$

in accordance with (2.5) and (2.8).

The representation (2.42), where portions of the dispersion curves $\Delta = 0$ are eliminated in accordance with (2.56), and the representation (2.57a) restrict the dispersion curves in equivalent ways. The Fourier superposition (2.57a) of elementary waves satisfies the Laplace equation (2.3a), the far-field boundary condition (2.3b) and the boundary conditions (2.3c) and (2.3d) at the sea bottom and the free surface, and is consistent with the potential (2.1) for a flow that starts from rest. Expression (2.57a) therefore provides a satisfactory analytical representation of the free waves created by a body (ship, offshore structure) at some distance from the body, unlike the representation (2.42). In particular, the Fourier superposition (2.57a) can be expected to yield correct far-field wave patterns.

Application to offshore structures in deep water

For purposes of illustration, the general Fourier superposition (2.57a) of elementary free waves is now applied to diffraction-radiation of regular waves by an offshore structure, i.e. for $F = 0$, in deep water. The dispersion relation (2.10) for this particularly simple case yields a single dispersion curve: the circle $k = f^2$. Expressions (2.53b) and (2.57c) yield

$$H(\sigma^{\Delta}\sigma^{\theta}) = H(\sigma^{\theta}) = H\left[\cos(\gamma - \psi)\right] . \tag{2.58}$$

One then has $H(\sigma^{\Delta}\sigma^{\theta}) = 0$ for $\psi + \pi/2 < \gamma < \psi + 3\,\pi/2$ in agreement with (2.56). Figure 2.6 shows the 'active' half $\psi - \pi/2 < \gamma < \psi + \pi/2$ and the 'inert' half $\psi + \pi/2 < \gamma < \psi + 3\,\pi/2$ of the dispersion circle $k/f^2 = 1$ that correspond to $\psi = \pi/4$.

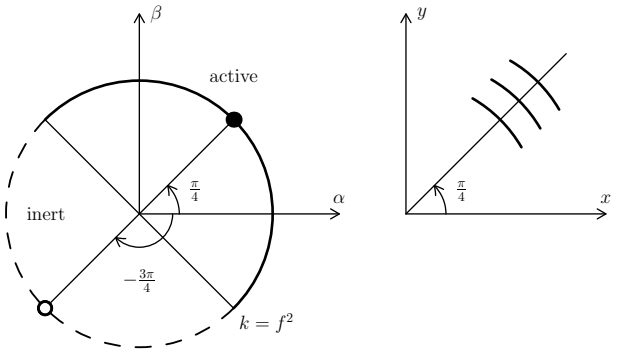

Figure 2.6: 'Active' (solid line) and 'inert' (dashed line) halves of the dispersion circle $k = f^2$ that correspond to the ray angle $\psi = \pi/4$ for wave diffraction-radiation by an offshore structure in deep water. The two points of stationary phase at $\gamma = \psi$ and $\gamma = \psi + \pi$ defined (in the next chapter) by (3.8) are also marked. The waves in the direction $\psi = \pi/4$ mostly stem from the dominant wave generator at $\gamma = \psi = \pi/4$, located at the center of the active half of the dispersion circle.

Expressions (2.57a), (2.57e-f) and (2.13a-b) show that the free-wave potential ϕ^W is given by

$$\phi^W(f^2 z, f^2 h, \psi) = e^{f^2 z}\, \varphi^W(f^2 h, \psi) \text{ where} \tag{2.59a}$$

$$\varphi^W(f^2 h, \psi) = \int_{\psi - \pi/2}^{\psi + \pi/2} d\gamma\; a^\phi(\gamma)\; e^{\,\mathrm{i}\, f^2 h \cos(\gamma - \psi)}\;. \tag{2.59b}$$

This expression provides an analytical representation of the free waves created by an offshore structure in deep water. The amplitude function $a^\phi(\gamma)$ in (2.59b), and in the general Fourier superposition (2.57a), can only be determined if the near-field boundary condition (1.35e) is considered, as was already noted. This near-field boundary condition is ignored in the analysis of free waves related to the 'far-field boundary-value problem' (2.3).

Modified elementary free waves

The basic elementary wave function $W(\mathbf{x}, \alpha, \beta)$ in (2.42) is modified as

$$W^*(\mathbf{x}, \alpha, \beta) \equiv H(\sigma^\Delta \sigma^\theta)\; a^z\, e^{\,\mathrm{i}\,\theta} \text{ where } \theta \equiv \alpha x + \beta y \tag{2.60}$$

in (2.57a) where $(\alpha, \beta) \in (\Delta = 0)$ and σ^Δ, σ^θ and a^z are given by (2.57b-c) and (2.57f). Unlike the basic elementary wave function (2.5), the modified wave function (2.60) corresponds to a flow that starts from rest and satisfies the far-field boundary condition (2.3b).

The origin $(x = 0, y = 0)$ of the horizontal coordinates $\mathbf{h} \equiv (x, y)$ in (2.13a) is arbitrary and can be chosen as $(x = \xi, y = \eta)$. The phase function θ in (2.13c), (2.57c) and (2.60) then becomes

$$\theta = \alpha\,(x-\xi) + \beta\,(y-\eta)\ . \tag{2.61}$$

A set of elementary wave functions (2.60), with θ given by (2.61), associated with a corresponding set of origins (ξ_p, η_p) taken as a set of near-field points can be considered, and provides a basis for representing the free waves generated by a ship or an offshore structure.

Thus, the free waves generated by a ship that advances (at a constant speed along a straight path) through regular (time-harmonic) ambient waves in water of uniform finite depth, can be expressed as a Fourier superposition of the generalized elementary plane waves (2.60). This Fourier superposition of elementary waves provides an analytical representation of the free waves generated by a ship, at some distance away from the ship, that satisfies the Laplace equation (2.3a), the far-field condition (2.3b) and the boundary conditions (2.3c) and (2.3d) at the sea bottom and the free surface, and is consistent with a flow that starts from rest.

Chapter 3

Dispersion curves and wave patterns

This chapter considers the Fourier superposition of modified elementary waves, given in the previous chapter by (2.57), in the far field $1 \ll h$ where $h \equiv \sqrt{x^2+y^2}$ is the horizontal distance from a ship or offshore structure. This far-field analysis of the representation (2.57) of free waves provides relationships between the dispersion curves, defined in the Fourier plane (α, β) by the dispersion relation, and the far-field waves generated by the body (ship or offshore structure) in the physical space (x, y). In particular, far-field wave patterns are determined in terms of the dispersion function via simple explicit analytical relations. These relations, and much of the analysis given in this chapter, hold not only for the waves created by a ship or an offshore structure but more generally for a broad class of plane dispersive waves.

3.1 Stationary phase and far-field waves

The general Fourier superposition (2.57) of elementary free waves is now considered in the far field $1 \ll h \equiv \sqrt{x^2+y^2}$. The Fourier integral (2.57a) is expressed as

$$\phi^W(\mathbf{x}) = \sum_{\Delta=0} \int_{\Delta=0} ds\, \widehat{a}\, e^{\,\mathrm{i}\, h\, \Theta} \tag{3.1a}$$

where $\widehat{a} \equiv \widehat{a}(s)$ and $\Theta \equiv \Theta(s)$ are functions of the arc length s along a dispersion curve $\Delta = 0$.

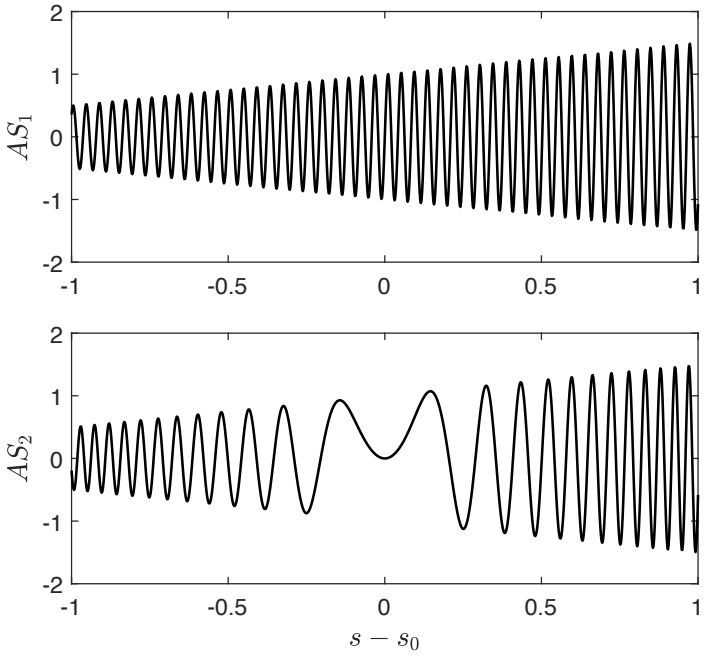

Figure 3.1: Functions AS_1 (top) and AS_2 (bottom) defined by expressions (3.3) for $-1 \leq s - s_0 \leq 1$. The function S_2 has a point of stationary phase at $s = s_0$.

The functions $\widehat{a}$ and Θ are defined as

$$\widehat{a} \equiv H(\sigma^{\Delta}\sigma^{\theta})\, a^{\phi} a^{z} \text{ and } \Theta \equiv \theta/h \equiv (\alpha x + \beta y)/h \equiv k\cos(\gamma - \psi) \quad (3.1b)$$

where θ is the phase function defined by (2.13c). The wavelength δs of the oscillations of the trigonometric function $e^{\,\mathrm{i}\,h\,\Theta}$ in the wave integral (3.1a) is determined by the relation $h\,|\,\Theta'(s)|\,\delta s = 2\,\pi$ where $\Theta' \equiv d\Theta(s)/ds$ is the derivative of the phase function $\Theta(s)$ at a point s of the dispersion curve $\Delta = 0$. One then has

$$\delta s = \frac{2\,\pi}{h\,|\,\Theta'(s)|}\ . \quad (3.2)$$

This relation shows that the wavelength δs varies along the dispersion curve $\Delta = 0$. Expression (3.2) also shows that the local wavelength δs becomes smaller, and hence the trigonometric function $e^{\,\mathrm{i}\,h\,\Theta}$ oscillates more rapidly, as h increases. The trigonometric function $e^{\,\mathrm{i}\,h\,\Theta}$ is then rapidly oscillatory in the far field $1 \ll h$, except at a point $s = s_0$ where $\Theta'(s) = 0$, i.e. where the phase Θ is stationary (does not change).

This property is illustrated in Fig.3.1, where the functions AS_1 and AS_2

defined as

$$A \equiv 1 + \frac{s - s_0}{2} \ , \ S_1 \equiv \sin[h\,(s - s_0)] \ , \ S_2 \equiv \sin\left(h\,\frac{(s - s_0)^2}{2}\right) \qquad (3.3)$$

are depicted for $-1 \leq s - s_0 \leq 1$ and $h = 150$. The trigonometric functions S_1 and S_2 respectively correspond to the phase functions

$$\Theta_1 \equiv s - s_0 \ \text{ and } \ \Theta_2 \equiv (s - s_0)^2/2$$

and the related derivatives

$$\Theta_1' = 1 \ \text{ and } \ \Theta_2' = s - s_0$$

in (3.1a) and (3.2). The amplitude function A varies slowly (linearly) within the range $1/2 \leq A \leq 3/2$ as s varies within the range $-1 \leq s - s_0 \leq 1$. The trigonometric function S_1 oscillates rapidly within the entire range $-1 \leq s - s_0 \leq 1$. The trigonometric function S_2 is also rapidly oscillatory within that range, except in the vicinity of the point $s = s_0$, where $\Theta_2' = 0$ and the phase Θ_2 of S_2 is stationary.

Fig.3.1 suggests that the rapidly oscillatory function AS_1 only yields a small contribution to the Fourier integral (3.1a) because the contributions of the positive and negative values of AS_1 largely cancel out. Fig.3.1 also suggests that the main contribution of the function AS_2 to the integral (3.1a) stems from the vicinity of the point of stationary phase $s = s_0$, and that the function AS_2 yields a larger contribution than the function AS_1 to the integral (3.1a). A mathematical verification of these intuitive expectations is given in section 3.3.

3.2 Dispersion curves and far-field waves

Expression (3.1b) for the phase function Θ shows that a point of stationary phase is defined by the equivalent relations

$$\frac{d\Theta}{ds} \equiv \frac{d\alpha}{ds}\cos\psi + \frac{d\beta}{ds}\sin\psi = 0 \ \text{ or } \ \frac{d\theta}{ds} \equiv h\,\frac{d\Theta}{ds} \equiv \frac{d\alpha}{ds}\,x + \frac{d\beta}{ds}\,y = 0\,, \quad (3.4)$$

where $ds \equiv \sqrt{(d\alpha)^2 + (d\beta)^2}$ is the differential element of arc length along a dispersion curve. The vector $(d\alpha/ds, d\beta/ds)$ is tangent to the dispersion curve. It then follows from (3.4) that, at a point $(\alpha\,, \beta)$ of a dispersion curve where $d\Theta/ds = 0$, i.e. at a point of stationary phase, the vector $\mathbf{h} \equiv (x, y)$ is normal to the dispersion curve and therefore is colinear with the vector $\nabla_{\mathbf{k}}\,\Delta$ defined by (2.21). Thus, the stationary-phase relation (3.4) shows that the relations

$$\frac{\mathbf{h}}{h} \equiv \frac{(x, y)}{\sqrt{x^2 + y^2}} = \frac{\nu\,(\Delta_\alpha, \Delta_\beta)}{\sqrt{\Delta_\alpha^2 + \Delta_\beta^2}} \equiv \frac{\nu\,\nabla_{\mathbf{k}}\,\Delta}{\|\nabla_{\mathbf{k}}\,\Delta\|} \ \text{ where } \ \nu = \pm 1 \qquad (3.5)$$

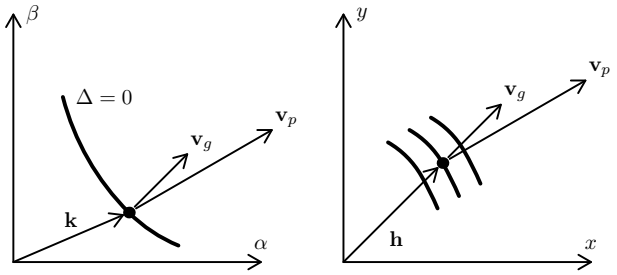

Figure 3.2: A point (α, β) of a dispersion curve (in the Fourier plane) where the stationary-phase condition $d\Theta/ds = 0$ is satisfied generates waves, in the free-surface plane (x, y), in a direction $\mathbf{h} \equiv (x, y)$ that is orthogonal to the dispersion curve and is colinear with, and oriented as, the group velocity $\mathbf{v}_g$. Thus, the group velocity $\mathbf{v}_g = v_g \mathbf{h}/h$ is aligned with the ray that originates at the origin $\mathbf{h} = 0$ (the wavemaker) of the free-surface plane (x, y) and is orthogonal to the dispersion curve $\Delta = 0$ in the Fourier plane (α, β). The phase velocity $\mathbf{v}_p = v_p \mathbf{k}/k$, aligned with the ray that originates at the origin $\mathbf{k} = 0$ of the Fourier plane (α, β), is orthogonal to the constant-phase curves (e.g. wave crests and troughs) in the free-surface plane (x, y).

hold at a point (α, β) of a dispersion curve where $d\Theta/ds = 0$.

This stationary-phase relation and expressions (2.57c) and (2.29) yield

$$\sigma^\theta \equiv \text{sign}(\alpha x + \beta y) = \nu \, \text{sign}(\alpha \Delta_\alpha + \beta \Delta_\beta) = \nu \, \text{sign}(\Delta_k) \; .$$

This relation and expression (2.57b) then yield

$$\sigma^\Delta \sigma^\theta = -\nu \, \text{sign}(\Delta_f) \; .$$

The function $H(\sigma^\Delta \sigma^\theta)$ in (2.57a) shows that a point of stationary phase only contributes to the Fourier integral (2.57a) if $0 < \sigma^\Delta \sigma^\theta$, i.e. if

$$\nu = -\text{sign}(\Delta_f) \; .$$

At such a stationary-phase point, expressions (3.5) then become

$$\frac{\mathbf{h}}{h} = \frac{(x, y)}{\sqrt{x^2 + y^2}} = -\,\text{sign}(\Delta_f) \, \frac{(\Delta_\alpha \, , \Delta_\beta)}{\sqrt{\Delta_\alpha^2 + \Delta_\beta^2}} \quad . \tag{3.6}$$

The relations (3.6) and (2.25a) show that a point (α, β) of a dispersion curve (in the Fourier plane) where $d\Theta/ds = 0$ mostly generates waves (in the physical space) in a direction $\mathbf{h} \equiv (x, y)$ that is orthogonal to the dispersion

curve and is colinear with, and oriented as, the group velocity

$$\mathbf{v}_g \equiv \begin{Bmatrix} v_g^x \\ v_g^y \end{Bmatrix} = \frac{-1}{\Delta_f} \begin{Bmatrix} \Delta_\alpha \\ \Delta_\beta \end{Bmatrix} \ . \tag{3.7}$$

Conversely, far-field waves observed in a direction $\mathbf{h}$ of the physical space predominantly stem from a point (or possibly several points) of a dispersion curve (or several dispersion curves) where the dispersion curve is orthogonal to $\mathbf{h}$. This important result, illustrated in Fig.3.2, is in agreement with the basic property that wave energy is transported along the direction of the group velocity $\mathbf{v}_g$.

The contribution of a point of a dispersion curve where the phase Θ is stationary, i.e. where $d\Theta/ds = 0$, is then non-zero if $\text{sign}(\mathbf{h}\cdot\mathbf{v}_g) = 1$, but is nil if $\text{sign}(\mathbf{h}\cdot\mathbf{v}_g) = -1$. Thus, one has $H(\sigma^\Delta\sigma^\theta) = 1$ as well as $H(\mathbf{h}\cdot\mathbf{v}_g) = 1$ at a stationary point $(\alpha\,,\beta)$ of a dispersion curve that contributes to the Fourier representation (2.57a). The Heaviside step function $H(\sigma^\Delta\sigma^\theta)$ in this Fourier representation can indeed be expressed as $H(\mathbf{h}\cdot\mathbf{v}_g)$ because only points of stationary phase create far-field waves.

For instance, in the simplest case $F = 0$ and $1 \ll d$ that corresponds to diffraction-radiation of regular waves by an offshore structure in deep water, the dispersion relation (2.10) defines a single dispersion curve; specifically, the circle $k = f^2$. Expression (2.13c) for the phase function θ becomes

$$\theta = f^2 h\,\cos(\gamma - \psi)\ .$$

The derivative $d\theta/d\gamma = -\,f^2 h\,\sin(\gamma - \psi)$ vanishes for

$$\gamma = \psi \ \text{ and } \ \gamma = \psi + \pi\ . \tag{3.8}$$

One then has two points of stationary phase along the dispersion circle $k = f^2$. These two stationary-phase points are marked in Fig.2.6 for the particular case $\psi = \pi/4$. Expressions (2.35) and (2.13a-b) yield

$$\mathbf{h}\cdot\mathbf{v}_g = h\,v_g\,\cos(\gamma - \psi)\ .$$

Thus, the point of stationary phase $\gamma = \psi$ yields a non-zero contribution to the Fourier integral (2.57a) and creates far-field waves. However, the point $\gamma = \psi + \pi$ yields a nil contribution and does not create waves.

Indeed, the point of stationary phase $\gamma = \psi + \pi$ is the center of the 'inert' half $\psi + \pi/2 < \gamma < \psi + 3\pi/2$ of the dispersion circle $k = f^2$ determined by the step function $H(\sigma^\Delta\sigma^\theta)$ in (2.57a), in accordance with (2.58) and as is illustrated in Fig.2.6 for $\psi = \pi/4$. The point of stationary phase $\gamma = \psi$ similarly is the center of the 'active' half $\psi - \pi/2 < \gamma < \psi + \pi/2$ of the dispersion circle. Thus, the far-field waves created by an offshore structure consist of a single system of waves associated with a single point of stationary phase (a single wave generator) on a single dispersion curve.

3.3 Far-field approximations to a general wave integral

The wave potential $\phi^W(\mathbf{x})$ defined by (3.1) is now considered in the far field $1 \ll h$. Specifically, the basic wave integral

$$\Psi^W \equiv \int_{-\infty}^{\infty} ds\, \widehat{a}(s)\, e^{\,\mathrm{i}\, h\, \Theta(s) - (s-s_0)^2/\ell^2} \quad \text{where } 1 \ll h \tag{3.9}$$

is analyzed. This analysis, given below, shows that the far-field behavior of the function Ψ^W defined by the integral (3.9) is greatly influenced by the phase function $\Theta(s)$. Specifically, the value of the wave integral (3.9) for $1 \ll h$ is dominated by the existence of point(s) where the derivative $\Theta' \equiv d\Theta/ds$ of the phase function $\Theta(s)$ vanishes, i.e. where the phase Θ is stationary.

The influence of the phase function Θ on the far-field value of the wave integral (3.9) is analyzed by considering the behavior of the phase function $\Theta(s)$ and of the amplitude function $\widehat{a}(s)$ in the vicinity of any given (arbitrary) point $s = s_0$. Indeed, the localizing function $\exp[-(s-s_0)^2/\ell^2]$ is introduced in (3.9) to study the influence of the phase function $\Theta(s)$ in the vicinity of a point $s = s_0$. Specifically, this localizing function is negligible outside the approximate range $s_0 - 2\,\ell < s < s_0 + 2\,\ell$ of effective width $4\,\ell$ determined by the positive real number ℓ.

Thus, the phase function $\Theta(s)$ and the amplitude function $\widehat{a}(s)$ in the wave integral (3.9) are approximated via the Taylor series

$$\Theta = \Theta_0 + (s-s_0)\,\Theta_0' + (s-s_0)^2\,\Theta_0''/2 + \dots\,, \tag{3.10a}$$

$$\widehat{a} = \widehat{a}_0 + (s-s_0)\,\widehat{a}_0' + (s-s_0)^2\,\widehat{a}_0''/2 + \dots\,, \tag{3.10b}$$

where $'_0$ and $''_0$ mean that the first or second derivatives are evaluated at the point $s = s_0$, which is arbitrary as was already noted. The integral (3.9) then becomes

$$\Psi^W = \; e^{\,\mathrm{i}\, h\, \Theta_0} \left(\widehat{a}_0\, \Psi_0^W + \widehat{a}_0'\, \Psi_1^W + \widehat{a}_0''\, \Psi_2^W/2 + \dots\right) \tag{3.11a}$$

$$\text{where } \; \Psi_n^W \equiv \int_{-\infty}^{\infty} dt\, t^n\, e^{-t^2/\ell^2 + \mathrm{i}\, h\, (\Theta_0'\, t + \Theta_0''\, t^2/2 + \dots)} \tag{3.11b}$$

and the change of variable $t = s - s_0$ was performed.

Contribution of a point where $\Theta_0' \neq 0$

The contribution of a range $s_0 - 2\,\ell < s < s_0 + 2\,\ell$ that does not contain a point of stationary phase is considered first. Thus, it is now assumed

that $\Theta_0' \neq 0$ and that the point $s = s_0$ is not in the vicinity of a point of stationary phase, i.e. is 'far from a stationary point'. Expression (3.11b) then yields

$$\Psi_0^W \approx 2\int_0^\infty dt\; e^{-t^2/\ell^2}\cos(h\,\Theta_0'\,t) = \sqrt{\pi}\,\ell\; e^{-\ell^2(\Theta_0')^2h^2/4} \;\text{ and}$$
$$\Psi_1^W \approx 2\,\mathrm{i}\int_0^\infty dt\; t\; e^{-t^2/\ell^2}\sin(h\,\Theta_0'\,t) = \frac{-\,\mathrm{i}}{\Theta_0'}\,\frac{\partial\psi_0^W}{\partial h} = \mathrm{i}\,\frac{\sqrt{\pi}}{2}\,\ell^3\,\Theta_0'\,h\,e^{-\ell^2(\Theta_0')^2h^2/4}\,.$$

The contributions of a point $s = s_0$ where $\Theta_0' \neq 0$ to the integrals Ψ_n^W in the Taylor series (3.11a) are then exponentially small in the limit $h \to \infty$.

Contribution of a point where $\Theta_0' = 0$ and $\Theta_0'' \neq 0$

The contribution of a range $s_0 - 2\,\ell < s < s_0 + 2\,\ell$ that contains a point of stationary phase is now considered. Specifically, it is now assumed that $\Theta_0' = 0$ and $\Theta_0'' \neq 0$. Expression (3.11b) then yields

$$\Psi_0^W \approx 2\int_0^\infty dt\; e^{-t^2/\ell^2}\left[\cos(h\,\Theta_0''\,t^2/2) + \mathrm{i}\,\sin(h\,\Theta_0''\,t^2/2)\right] \;\text{ and}$$
$$\Psi_1^W \approx \int_{-\infty}^\infty dt\; t\; e^{-t^2/\ell^2\,+\,\mathrm{i}\,h\,\Theta_0''\,t^2/2} = 0\;.$$

The integral Ψ_0^W is convergent (even as $\ell \to \infty$) and is given by

$$\Psi_0^W \approx \sqrt{\frac{2\,\pi}{h\,|\,\Theta_0''\,|}}\,\frac{1 + \mathrm{sign}(\Theta_0'')\,\mathrm{i}}{\sqrt{2}} = \sqrt{\frac{2\,\pi}{h\,|\,\Theta_0''\,|}}\;e^{\,\mathrm{sign}(\Theta_0'')\,\mathrm{i}\,\pi/4}$$

in the limit $\ell \to \infty$. This asymptotic approximation and the expansion (3.11a) then yield Kelvin's stationary-phase approximation **[3,1]**

$$\Psi^W \approx \widehat{a}_0\sqrt{\frac{2\,\pi}{h\,|\,\Theta_0''\,|}}\;e^{\,\mathrm{i}\,[\,h\,\Theta_0\,+\,\mathrm{sign}(\Theta_0'')\,\pi/4\,]}\;. \tag{3.12}$$

The stationary-phase approximation (3.12) is not valid if $\Theta_0'' = 0$. This case is now considered.

Contribution of a point where $\Theta_0' = 0$ and $\Theta_0'' = 0$

Specifically, the contribution of a range $s_0 - 2\,\ell < s < s_0 + 2\,\ell$ that contains a stationary-phase point $s = s_0$ where $\Theta_0' = 0$ and $\Theta_0'' = 0$ is considered. In

the limit $\ell \to \infty$, expression (3.11b) then yields

$$\Psi_0^W \approx 2\int_0^\infty dt\, \cos(h\,\Theta_0'''\,t^3/6) = \frac{6^{1/3}\,2}{(h\,\Theta_0''')^{1/3}}\int_0^\infty du\, \cos(u^3) = \frac{\Gamma(1/3)/\sqrt{3}}{(h\,\Theta_0'''/6)^{1/3}}$$

$$\Psi_1^W \approx 2\,\mathrm{i}\int_0^\infty dt\, t\, \sin(h\,\Theta_0'''\,t^3/6) = \frac{6^{2/3}\,2\,\mathrm{i}}{(h\,\Theta_0''')^{2/3}}\int_0^\infty du\, u\, \sin(u^3) = \frac{\mathrm{i}\,\Gamma(2/3)/\sqrt{3}}{(h\,\Theta_0'''/6)^{2/3}}$$

where $\Gamma(\cdot)$ is the Gamma function. This asymptotic approximation and the expansion (3.11a) then yield Havelock's stationary-phase approximation

$$\Psi^W \approx \widehat{a}_0\,\frac{\Gamma(1/3)}{\sqrt{3}}\left[\frac{6}{h\,\Theta_0'''}\right]^{1/3} e^{\,\mathrm{i}\,h\,\Theta_0} \approx 1.5467\,\widehat{a}_0\left[\frac{6}{h\,\Theta_0'''}\right]^{1/3} e^{\,\mathrm{i}\,h\,\Theta_0}\,. \quad (3.13)$$

The stationary-phase approximation (3.13) is valid if $\Theta_0' = 0$ and $\Theta_0'' = 0$, but $\Theta_0''' \neq 0$.

The asymptotic approximations (3.12) and (3.13) show that the function Ψ^W defined by the wave integral (3.9) decays like $1/h^{1/2}$ as $h \to \infty$ if $\Theta_0' = 0$ and $\Theta_0'' \neq 0$, or decays like $1/h^{1/3}$ (less rapidly) if $\Theta_0' = 0 = \Theta_0''$ and $\Theta_0''' \neq 0$.

Other far-field approximations

The Kelvin and Havelock far-field stationary-phase approximations (3.12) and (3.13) have been extended in a number of ways. Indeed, asymptotic approximations of integrals are considered and applied in a vast literature. **[3,2]**

3.4 Far-field approximation to free waves

Kelvin's stationary-phase approximation (3.12) to the wave integral (3.9), applied to the general Fourier superposition (2.57) of elementary free waves, yields the far-field approximation

$$\phi^W(\mathbf{x}) \approx \sum_{\theta_j' = 0} H(\sigma^{\Delta_j}\,\sigma^{\theta_j})\,a_j^\phi\,\sqrt{\frac{2\,\pi}{|\,\theta_j''\,|}}\;a_j^z\,e^{\,\mathrm{i}\,[\,\theta_j + \mathrm{sign}(\theta_j'')\,\pi/4\,]} \quad (3.14a)$$

where the relation $\theta = h\,\Theta$ was used. The phase function θ_j and its derivatives θ_j' and θ_j'' are given by

$$\theta_j \equiv \alpha_j\,x + \beta_j\,y\;\;,\;\;\theta_j' \equiv \alpha_j'\,x + \beta_j'\,y\;\;,\;\;\theta_j'' \equiv \alpha_j''\,x + \beta_j''\,y \quad (3.14b)$$

$$\text{where}\;\;(\alpha',\beta') \equiv d\,(\alpha,\beta)/ds\;\;,\;\;(\alpha'',\beta'') \equiv d^2(\alpha,\beta)/ds^2 \quad (3.14c)$$

and $ds \equiv \sqrt{(d\alpha)^2 + (d\beta)^2}$ is the differential element of arc length of a dispersion curve. The summation in (3.14a) is performed over all the points

(α_j, β_j) that satisfy the stationary-phase condition $\theta'_j = 0$ for every dispersion curve defined by the dispersion relation $\Delta = 0$.

Every component of the superposition of far-field waves defined by the analytical approximation (3.14a) decays as $1/\sqrt{h}$ as $h \to \infty$, i.e. one has

$$a_j^\phi \sqrt{\frac{2\pi}{|\theta''_j|}}\; a_j^z \; e^{\,\mathrm{i}\,[\,\theta_j + \mathrm{sign}\,(\theta''_j)\,\pi/4\,]} = O\!\left(\frac{1}{\sqrt{h}}\right) \text{ as } h \equiv \sqrt{x^2+y^2} \to \infty\,.$$

The waves created by an offshore structure or by a ship that advances in calm water or through regular waves therefore decay as $1/\sqrt{h}$ as $h \to \infty$, in accordance with basic considerations related to the energy transported by elementary waves. The far-field stationary-phase approximation (3.14) becomes more accurate as h increases, and evidently is not valid as $h \to 0$ or for small values of h, i.e. in the near field.

The amplitude of every wave component is given by

$$\sqrt{2\,\pi}\; a_j^\phi / \sqrt{|\,\theta''_j\,|} \text{ where } a_j^\phi \equiv a^\phi(\alpha_j, \beta_j)$$

is the value of the amplitude function at a point (α_j, β_j) of the dispersion curve that satisfies the stationary-phase condition $\theta'_j \equiv \theta'(\alpha_j, \beta_j) = 0$.

The amplitude function a^ϕ can only be determined from the near-field hull-surface boundary condition, which is ignored in the far-field boundary-value problem (2.3) considered in this chapter. However, further information about far-field free waves—notably wave patterns—created by ships and offshore structures can be gained from the far-field approximation (3.14a), i.e. without solving the near-field boundary-value problem that includes the boundary condition at the ship-hull surface. This additional analysis of far-field waves is considered further on.

The asymptotic (stationary-phase) approximation (3.14a) shows that the far-field waves due to diffration-radiation of regular waves by an offshore structure, and the far-field waves created by a ship that steadily advances in calm water or through regular waves, mostly consist of a finite (indeed small) number of dominant waves. These waves are associated with points of the dispersion curves, defined by the dispersion relation, where the phase θ is stationary, i.e. where $\theta' = 0$ as already noted.

For instance, for diffraction-radiation of regular waves by a floating body without forward speed, i.e. in the particular case $F = 0$, the dispersion relation (2.10) defines a single dispersion curve and only one point of stationary phase that satisfies the condition $0 < \sigma^\Delta \sigma^\theta$ exists for any ray angle ψ, in accordance with (2.58) and (2.56). Thus, only one wave exists at any far-field point $(x, y) = h\,(\cos\psi, \sin\psi)$ in this (particularly simple) case.

For a ship that steadily advances along a straight path in deep water, i.e. in the particular case $f = 0$ and $d = \infty$, the dispersion relation (2.7)

becomes $F^2\alpha^2 = k$. This dispersion relation defines two dispersion curves, which are symmetric about both the axis $\alpha = 0$ and the axis $\beta = 0$. It is shown in the next chapter that, in this case, one has either no (i.e. zero) point of stationary phase, or two points of stationary phase where $0 < \sigma^{\Delta}\sigma^{\theta}$, depending on the location of the point $(x, y) = h(\cos\psi, \sin\psi)$ with respect to the path of the ship.

Thus, the free surface around a ship that steadily advances in calm water can be divided into a region (notably ahead of the ship) where there are no waves, and a wake behind the ship where two waves (called 'transverse' and 'divergent' waves) are found at every point. This commonly-observed and well-known feature of the flow around a ship that steadily advances in calm water of large depth is demonstrated in the next chapter.

Alternative representations of dispersion curves

Expressions (3.14c) presume that the dispersion curves are defined in terms of parametric representations in which the arc length s is taken as the parameter. Alternative parametric representations of the dispersion curves can evidently be used. Both the elementary wave function

$$a_j^z \; e^{\,\mathrm{i}\,[\,\theta_j + \mathrm{sign}(\theta_j'')\,\pi/4\,]}$$

and the potential function $\phi^W(\mathbf{x})$ in (3.14a) are independent of the parametric representation chosen to define the dispersion curves $\Delta = 0$. The stationary-phase approximation (3.14a) is then independent of the mathematical representation of the dispersion curves.

Indeed, the amplitude functions $a^{\phi}(s)$ and $\underline{a}^{\phi}(\underline{s})$ associated with alternative parametric representations $\mathbf{k}(s)$ and $\mathbf{k}(\underline{s})$ of a dispersion curve are related as

$$\underline{a}^{\phi}(\underline{s}) = (ds/d\underline{s})\, a^{\phi}(s) \; .$$

The derivatives of the phase functions $\theta(s)$ and $\underline{\theta}(\underline{s})$ are similarly related as

$$\underline{\theta}'(\underline{s}) = (ds/d\underline{s})\, \theta'(s) \;\text{ and }\; \underline{\theta}''(\underline{s}) = (ds/d\underline{s})^2\, \theta''(s) \; .$$

One then has

$$\underline{a}^{\phi}(\underline{s}) \,/\sqrt{|\, d^2\underline{\theta}(\underline{s})/d\underline{s}^2\,|} = \mathrm{sign}(ds/d\underline{s})\, a^{\phi}(s) \,/\sqrt{|\, d^2\theta(s)/ds^2\,|} \; .$$

However, the integration limits in the integral (3.9) must be interchanged if $ds/d\underline{s} < 0$.

Application to offshore structures in deep water

For purposes of illustration, Kelvin's far-field approximation (3.12) is now applied to the wave integral $\varphi^W(f^2h, \psi)$ defined by (2.59b) in the Fourier

representation (2.59) of regular waves created by an offshore structure in deep water. The phase function θ and its derivatives θ' and θ'' with respect to γ are given by

$$\theta = f^2 h \cos(\gamma - \psi) \ , \ \theta' = -f^2 h \sin(\gamma - \psi) \ , \ \theta'' = -f^2 h \cos(\gamma - \psi) \ .$$

The integration range $\psi - \pi/2 \le \gamma \le \psi + \pi/2$ in (2.59b) contains the single point of stationary phase $\gamma = \psi$, where $\mathrm{sign}(\theta'') = -1$ and $|\theta''| = f^2 h$. The stationary-phase approximation (3.12) then yields

$$\varphi^W(f^2 h, \psi) \approx \sqrt{\frac{2\pi}{f^2 h}} \ a^{\phi}_{\gamma=\psi} \ e^{\,\mathrm{i}\,(f^2 h - \pi/4)} \tag{3.15a}$$

where $a^{\phi}_{\gamma=\psi}$ means that the function $a^{\phi}(\gamma)$ is evaluated at $\gamma = \psi$. Expressions (2.1), (2.59) and (3.15a) yield

$$\widehat{\phi}(\mathbf{x}, t) \approx \sqrt{\frac{2\pi}{f^2 h}} \ e^{f^2 z} \ \mathrm{Re} \ a^{\phi}_{\gamma=\psi} \ e^{\,\mathrm{i}\,(f^2 h - f t - \pi/4)} \ . \tag{3.15b}$$

The flow potential (3.15b) is associated with concentric circular waves with frequency f, wavenumber $k = f^2$, wavelength $\lambda = 2\pi/f^2$, and amplitude that decays as $1/\sqrt{h} \equiv 1/\sqrt{x^2 + y^2}$ as the waves propagate outward away from a wave generator (floating body) centered at $h = 0$.

3.5 Wave patterns

Additional information about important features of far-field waves created by ships and offshore structures can be obtained from the dispersion function $\Delta(f, \alpha, \beta; F, d)$ and the related dispersion curves $\Delta = 0$. In particular, the wave patterns formed by far-field waves are now considered.

The relations (3.6) and (2.13b) yield

$$\left\{ \begin{array}{c} x \\ y \end{array} \right\} = -\,\mathrm{sign}(\Delta_f) \, \frac{h}{\|\nabla_{\mathbf{k}} \Delta\|} \left\{ \begin{array}{c} \Delta_\alpha \\ \Delta_\beta \end{array} \right\} \ . \tag{3.16}$$

This relation and expression (2.29) show that the phase $\theta \equiv \alpha x + \beta y$ of the trigonometric function in (2.57c) and (2.60) is given by

$$\theta \equiv \alpha x + \beta y = -\,\mathrm{sign}(\Delta_f) \, \frac{h\,k}{\|\nabla_{\mathbf{k}} \Delta\|} \, \Delta_k \ .$$

This relation yields

$$\frac{h}{\|\nabla_{\mathbf{k}} \Delta\|} = \frac{|\theta|}{k |\Delta_k|} \ .$$

The relation (3.16) can then be expressed as

$$\begin{Bmatrix} x \\ y \end{Bmatrix} = -\operatorname{sign}(\Delta_f)\frac{|\theta|/k}{|\Delta_k|}\begin{Bmatrix} \Delta_\alpha \\ \Delta_\beta \end{Bmatrix} . \tag{3.17}$$

The relation (3.17), where the point $(\alpha\,,\beta)$ moves along a dispersion curve $\Delta = 0$, yields parametric equations that determine the coordinates x and y associated with any given value of the phase θ, e.g. a particular wave crest or trough.

If the dispersion relation $\Delta = 0$ defines several dispersion curves, different wave patterns are obtained as the point $(\alpha\,,\beta)$ in (3.17) moves along every dispersion curve, as is illustrated in chapter 5 for a ship that steadily advances through regular waves. Specifically, the dispersion relation (2.7) for deep water defines three dispersion curves if $0 \le \tau < 1/4$ or two dispersion curves if $1/4 < \tau$, and a ship that steadily advances through regular waves consequently creates three or two families of waves and corresponding distinct wave patterns in these two flow regimes.

Successive waves, e.g. a series of wave crests, are obtained if a series of phase values $|\,\theta_n\,| = 2\,n\,\pi$ with $n = 1, 2, 3, \ldots$ is considered in (3.17). Thus, far-field wave patterns can be determined from the dispersion function Δ via the parametric equations

$$\mathbf{h}_n \equiv \begin{Bmatrix} x_n \\ y_n \end{Bmatrix} = \frac{2\,n\,\pi\,\sigma^\Delta}{k\,\Delta_k}\begin{Bmatrix} \Delta_\alpha \\ \Delta_\beta \end{Bmatrix} \equiv \frac{2\,n\,\pi\,\sigma^\Delta}{k\,\Delta_k}\,\nabla_{\mathbf{k}}\,\Delta \tag{3.18}$$

where σ^Δ is given by (2.52). This relation yields

$$h_n \equiv |\,\mathbf{h}_n\,| \equiv \sqrt{x_n^2 + y_n^2} = \frac{2\,n\,\pi\,\|\,\nabla_{\mathbf{k}}\,\Delta\,\|}{k\,|\,\Delta_k\,|} \equiv n\,\lambda\,\frac{\|\,\nabla_{\mathbf{k}}\,\Delta\,\|}{|\,\Delta_k\,|} \tag{3.19a}$$

where $\lambda \equiv 2\,\pi/k$ is the wavelength. Expressions (3.19a) and (2.22) yield

$$h_n\,|\cos(\gamma - \delta)| = n\,\lambda \tag{3.19b}$$

where γ and δ are the angles associated with the phase velocity $\mathbf{v}_p$ or the group velocity $\mathbf{v}_g$ in (2.16) and (2.25d).

Wave patterns and group velocity

Expressions (3.18)-(3.19a) and (2.52) yield

$$\frac{\mathbf{h}_n}{h_n} = -\operatorname{sign}(\Delta_f)\frac{\nabla_{\mathbf{k}}\,\Delta}{\|\,\nabla_{\mathbf{k}}\,\Delta\,\|} \tag{3.20}$$

in agreement with (3.6). This relation and expression (2.25c) relate the group velocity $\mathbf{v}_g$ and the wave pattern as

$$\frac{\mathbf{h}_n}{h_n} \equiv \frac{(x_n, y_n)}{\sqrt{x_n^2 + y_n^2}} = \frac{(v_g^x, v_g^y)}{v_g} \equiv \frac{\mathbf{v}_g}{v_g}\,. \tag{3.21}$$

This relation shows that a wave observed at a far-field point $\mathbf{h}_n \equiv (x_n, y_n)$ stems from the energy that is transmitted, at the group velocity $\mathbf{v}_g$, along straight lines drawn from the origin $\mathbf{h}_0 \equiv (x_0, y_0) = (0, 0)$ of the wave pattern, as is illustrated in Fig.3.2. The origin $\mathbf{h}_0$ of the wave pattern approximates a near-field wavemaker, e.g. a ship or an offshore structure, which appears as a point to a far-field observer at a large distance from the near-field wavemaker.

The factor σ^{Δ}, given by (2.52), in the parametric equations (3.18) that determine far-field wave patterns is related to the generalized elementary waves considered in sections 2.8 and 2.9. This factor is crucial. For instance, it explains why a ship that steadily advances in calm water only creates waves behind the ship. Indeed, if the basic elementary waves given in section 2.2 are used instead of the generalized elementary waves given in sections 2.8 and 2.9, the resulting parametric equations that determine far-field wave patterns do not involve the factor σ^{Δ} and cannot predict whether steady ship waves exist behind the ship or ahead.

Wave patterns and phase velocity

The phase function

$$\theta_n \equiv \alpha\, x_n + \beta\, y_n$$

in expressions (3.14) for the stationary-phase approximation of far-field waves is constant along a wave-crest line. It follows that

$$d\theta_n/ds = (x_n\, d\alpha/ds + y_n\, d\beta/ds) + (\alpha\, dx_n/ds + \beta\, dy_n/ds) = 0\ .$$

This relation and the stationary-phase relation

$$d\theta_n/ds = x_n\, d\alpha/ds + y_n\, d\beta/ds = 0$$

yield $\alpha\, dx_n + \beta\, dy_n = 0$. This relation shows that the differential element (dx_n, dy_n) of a far-field wave-crest line is orthogonal to the wave vector $\mathbf{k} \equiv (\alpha, \beta)$ and consequently to the phase velocity $\mathbf{v}_p = v_p\, \mathbf{k}/k$ given by (2.16). The phase velocity $\mathbf{v}_p$ is then orthogonal to the constant-phase curves (e.g. wave crests and troughs) defined by (3.18), as is illustrated in Fig.3.2.

Diffraction-radiation of regular waves by offshore structures

In the particularly simple case of diffraction-radiation of regular waves by an offshore structure in finite water-depth, the parametric equations (3.18), the dispersion relation (2.10) and expressions (2.31a) and (2.53b) yield

$$f^2 \left\{ \begin{matrix} x_n \\ y_n \end{matrix} \right\} = \frac{2\,n\,\pi}{k_*/f^2} \left\{ \begin{matrix} \cos\gamma \\ \sin\gamma \end{matrix} \right\} \quad \text{where} \quad -\,\pi \le \gamma \le \pi$$

and $k_*/f^2 \equiv k_*^\omega$ is the root of the dispersion relation (2.38). These parametric equations define a series of concentric circles with radii

$$h_n^\omega \equiv H_n^\omega\, \omega^2/g = 2n\pi/k_*^\omega = 2n\pi \tanh(d^\omega k_*^\omega) \leq 2n\pi\,. \tag{3.22}$$

Furthermore, the phase velocity $\mathbf{v}_p$ and the group velocity $\mathbf{v}_g$ are colinear, and one has $\delta = \gamma$ in accordance with (2.35), (2.25d) and (2.31a).

3.6 Cusps and asymptotes of wave patterns

Inflection point of a dispersion curve

The unit vector

$$\frac{\nabla_{\mathbf{k}}\Delta}{\|\nabla_{\mathbf{k}}\Delta\|} \equiv \frac{(\Delta_\alpha\,, \Delta_\beta)}{\sqrt{\Delta_\alpha^2 + \Delta_\beta^2}}$$

is normal to a dispersion curve $\Delta(f, \alpha, \beta; F, d) = 0$. Thus, the unit vector

$$(\Delta_\beta\,, -\Delta_\alpha)/\sqrt{\Delta_\alpha^2 + \Delta_\beta^2}$$

is tangent to a dispersion curve, and the derivative d/ds in a direction tangent to a dispersion curve is given by

$$\frac{1}{\sqrt{\Delta_\alpha^2 + \Delta_\beta^2}} \begin{Bmatrix} \Delta_\beta \\ -\Delta_\alpha \end{Bmatrix} \cdot \begin{Bmatrix} \partial_\alpha \\ \partial_\beta \end{Bmatrix} = \frac{\Delta_\beta\, \partial_\alpha - \Delta_\alpha\, \partial_\beta}{\|\nabla_{\mathbf{k}}\Delta\|}\,. \tag{3.23}$$

An inflection point of a dispersion curve is a point where the angle δ between the vector $\nabla_{\mathbf{k}}\Delta \equiv (\Delta_\alpha\,, \Delta_\beta)$ normal to the dispersion curve and the α axis reaches a local maximum or minimum. Thus, inflection points are determined by the condition

$$d(\tan\delta)/ds \equiv d(\Delta_\beta/\Delta_\alpha)/ds = 0\,.$$

This relation and (3.23) yield

$$\Delta_\beta\, \partial_\alpha(\Delta_\beta/\Delta_\alpha) - \Delta_\alpha\, \partial_\beta(\Delta_\beta/\Delta_\alpha) = 0\,.$$

This condition can be verified to yield

$$\Delta_\beta^2\, \Delta_{\alpha\alpha} - 2\,\Delta_\alpha\, \Delta_\beta\, \Delta_{\alpha\beta} + \Delta_\alpha^2\, \Delta_{\beta\beta} = 0\,. \tag{3.24a}$$

Equation (3.24a) determines the inflection point(s) of a dispersion curve defined by an implicit equation $\Delta(f, \alpha, \beta; F, d) = 0$.

An inflection point of a dispersion curve defined by the parametric equations $\alpha = A(t)$ and $\beta = B(t)$ is determined by the equation

$$A'B'' - B'A'' = 0 \tag{3.24b}$$

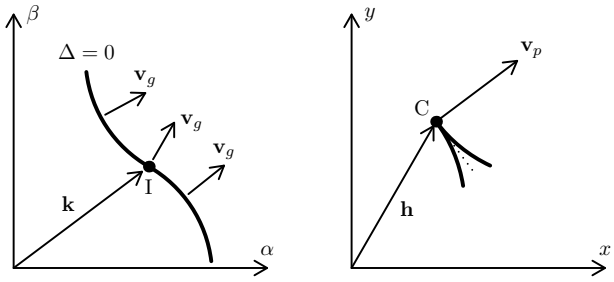

Figure 3.3: An inflection point, marked I in the figure, of a dispersion curve $\Delta = 0$ in the Fourier plane (α, β) yields a cusp, marked C, of the corresponding wave pattern in the free-surface plane (x, y).

where the superscript ' means differentiation with respect to the parameter t. For a dispersion curve defined by the polar equation $k = k_0(\gamma)$, equation (3.24b) yields

$$k_0^2 + 2\,(k_0')^2 - k_0\,k_0'' = 0 \tag{3.24c}$$

where the superscript ' means differentiation with respect to the polar angle γ. Finally, for a dispersion curve defined by the explicit equations $\beta = B(\alpha)$ or $\alpha = A(\beta)$, (3.24b) becomes

$$d^2B/d\alpha^2 = 0 \;\text{ or }\; d^2A/d\beta^2 = 0\,, \tag{3.24d}$$

respectively. The alternative equations (3.24) can be used to determine the inflection point(s) of a dispersion curve, depending on the mathematical representation of the dispersion curve.

Cusp line of a wave pattern

A dispersion curve that has an inflection point (α^i, β^i) is now considered. As the point $(\alpha\,, \beta)$ moves along the dispersion curve in the vicinity of the inflection point (α^i, β^i), the angle δ between the vector $\nabla_{\mathbf{k}}\Delta$ normal to the dispersion curve and the α axis reaches a local maximum or minimum, denoted as δ^i, at the inflection point. Accordingly, the corresponding angle ψ in the free-surface plane also reaches a local maximum or minimum ψ^i, given by $\psi^i = \delta^i$ or $\psi^i = \delta^i + \pi$, and the far-field wave pattern has a cusp at the angle ψ^i, as is illustrated in Fig.3.3.

Asymptote line of a wave pattern

The relations (3.19a) and (2.22) yield

$$\frac{h_n}{2n\pi} = \frac{\|\nabla_{\mathbf{k}}\Delta\|}{k\,|\,\Delta_k\,|} \equiv \frac{\sqrt{\Delta_\alpha^2+\Delta_\beta^2}}{|\,\alpha\,\Delta_\alpha+\beta\,\Delta_\beta\,|} \equiv \frac{1}{k\,|\cos(\gamma-\delta)|}\ .$$

One then has

$$h_n \equiv \sqrt{x_n^2+y_n^2} \to \infty \ \text{ if } \ k\,\Delta_k = 0 \tag{3.25}$$

or $\gamma-\delta = \pm\,\pi/2$ with $k<\infty$. Thus, a point $(k\,,\gamma)$ of a dispersion curve where $k\,\Delta_k$ vanishes yields an asymptote of the far-field wave pattern, at an angle ψ that is orthogonal to the angle γ at the point where $k\,\Delta_k$ vanishes. The wave patterns depicted in Fig.5.12, Fig.5.15 and Fig.5.16, created by a ship that advances at a constant speed V_s through regular waves of frequency ω in the regime $1/4 < \tau \equiv V_s\,\omega/g$ are examples of patterns that include asymptote lines.

3.7 Size and shape of wave generator, and wave interferences

The analytical representation (3.18) of wave patterns is associated with the stationary-phase approximation (3.14). This approximation is based on an asymptotic (far-field) analysis that *only* involves the *phase* θ. Specifically, this stationary-phase analysis does not involve the *amplitude* function a^ϕ in (3.14). However, the wave-amplitude function a^ϕ, related to the size and the shape of the wave generator (ship or offshore structure), can have a significant influence on the actual appearance of the far-field waves, as is well known from common observations of the waves created by various types of ships (slow or fast monohull or multihull ships, fully-submerged bodies) and is illustrated in Fig.3.4 for diffraction-radiation of regular waves by an offshore structure.

Indeed, the far-field stationary-phase approximation (3.14) and the related representation (3.18) of wave patterns consider the far-field waves created by a near-field wave generator that is located at a point, taken as the origin $\mathbf{h} = (x,y) = (0,0)$. The assumption that far-field waves originate from a point located at the centroid of a ship hull (or offshore structure) is reasonable because a ship appears as a point from far away, i.e. in the far field. However, an important limitation of this 1-point wavemaker flow model is that the relations (3.14) and (3.18) evidently cannot account for the influence of the size and the shape of the ship or structure.

In particular, a monohull ship that advances along a straight path in calm water is a slender body that creates two dominant waves at the bow

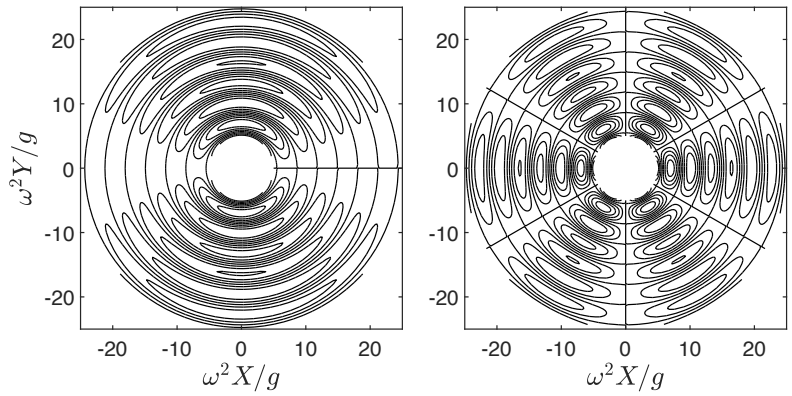

Figure 3.4: Contour plots of the real part of the potential function φ^W defined by (3.15a) where the amplitude function a^ϕ is taken as $a^\phi = \sin\gamma$ on the left side or as $a^\phi = \cos(3\gamma)$ on the right side, within the annular region $5 \leq \omega^2\sqrt{X^2+Y^2}/g \leq 25$. These wave patterns illustrate the influence of the wave-amplitude function a^ϕ, and of wave interferences, in the particular case of diffraction-radiation of regular waves by an offshore structure.

and the stern of the ship, where the hull geometry varies abruptly, and is then more realistically modeled as a 2-point wavemaker than as a 1-point wavemaker, which is a highly simplified flow model that does not involve the length of the ship or the related Froude number F. Interferences between the two dominant waves created by the bow and the stern of a ship have important consequences that cannot be explained via the representation (3.18) of wave patterns based on the stationary-phase approximation (3.14) for a 1-point wavemaker model.

Specifically, interferences between the transverse waves created (predominantly) by the bow and the stern of a ship result in oscillations (humps and hollows) in the wave drag of the ship at low Froude numbers (for F smaller than about 0.4) where transverse waves are important. Similarly, constructive interferences between the divergent waves, dominant at high Froude numbers (for F greater than about 0.6), created by the bow and the stern of a ship result in highest waves along rays that are located inside the cusps of the Kelvin wake and the appearance of a 'narrow ship wake'. **[3,3]**

The assumption that far-field waves created by a near-field wavemaker (a ship hull or an offshore structure) are generated at a single point located at the centroid of the wavemaker is then restrictive, notably for floating bodies that consist of several major elements, e.g. the four legs of a typical offshore structure or the three hulls of a trimaran. Indeed, the 1-point wavemaker model is restrictive even for a monohull ship, as is illustrated by the high-speed ship wakes narrower than the Kelvin wake noted in the

previous paragraph.

Useful additional information about far-field waves can be gained by considering the superposition of far-field waves created by major elements of a near-field wave generator, e.g. the legs of an offshore structure in regular waves, and the bow and the stern of a monohull ship or the three hulls of a trimaran that steadily advances in calm water.

The relations (3.14) and (3.18) can readily be applied to a wave generator located at a point $(x, y) = (x_m, y_m)$ by replacing (x, y) by $(x - x_m, y - y_m)$. Thus, the horizontal distance h, the polar angle ψ and the phase angle θ defined by (2.13a-c) become

$$h_m \equiv \sqrt{(x - x_m)^2 + (y - y_m)^2} \ , \ \tan \psi_m \equiv (y - y_m)/(x - x_m)$$
$$\text{and} \ \ \theta_m \equiv \alpha (x - x_m) + \beta (y - y_m) \ .$$

For instance, for wave diffraction-radiation by an offshore structure that consists of M main elements, e.g. M cylindrical legs, the far-field approximation (3.15a) yields

$$\frac{\varphi^W}{\sqrt{2\pi}} \approx \sum_{m=1}^{m=M} a^{\phi}_{\gamma=\psi_m} \, e^{\,\mathrm{i}\,(f^2 h_m - \pi/4)} / \sqrt{f^2 h_m} \tag{3.26}$$

where $a^{\phi}_{\gamma=\psi_m}$ denotes the value of the amplitude function $a^{\phi}(\gamma)$ at $\gamma = \psi_m$.

An important feature of the superposition of far-field waves created at several points (x_m, y_m) is wave interferences. These interference effects are illustrated in Fig.3.5 for regular waves created by identical (in-phase) heaving motions of three or four identical vertical circular cylinders, i.e. for $M = 3$ or $M = 4$ in (3.26) where the function a^{ϕ} is taken as $a^{\phi} = 1$. The heaving vertical cylinders are centered at the points

$$f^2 (x_m, y_m) = \rho \, (\cos \mu_m, \sin \mu_m) \ \text{ where } \ \mu_m = 2\pi (m - 1)/M \tag{3.27}$$
$$\text{and} \ \ \rho \equiv f^2 \sqrt{x_m^2 + y_m^2} = \pi \ \text{ or } \ \rho = 2\pi \, .$$

Fig.3.5 shows that wave interferences, associated with the size and the shape of a wavemaker (ship or offshore structure) and the related 'amplitude function' in the Fourier representation of far-field waves, can have a striking influence on the actual appearance of far-field wave patterns, which can then greatly differ from the wave patterns predicted via a stationary-phase analysis for a 1-point wavemaker. **[3,4]**

Nevertheless, the wave patterns predicted via a 'phase-only' analysis, in which the influence of the amplitude function related to the size and the shape of the wavemaker is ignored, provides important information about the far-field waves that correspond to a given dispersion function. These basic wave patterns are considered in chapters 4 and 5 for a ship that steadily advances in calm water or through regular waves.

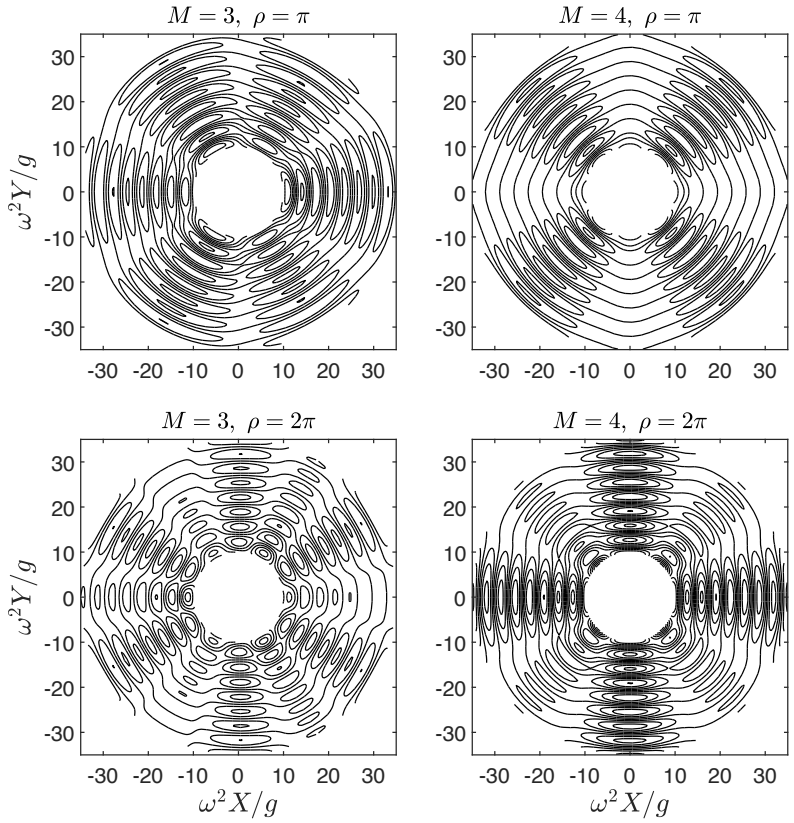

Figure 3.5: Contour plots of the real part of the potential function φ^W defined by (3.26) with $a^\phi = 1$, $M = 3$ (left side) or $M = 4$ (right) and $\rho \equiv \omega^2\sqrt{X_m^2 + Y_m^2}/g = \pi$ (top half) or $\rho = 2\pi$ (bottom) within the annular region $10 \leq \omega^2\sqrt{X^2+Y^2}/g \leq 35$. These wave patterns illustrate the effect of interferences in the particular case of radiation of regular waves by an offshore structure.

Chapter 4

Free ship waves in calm deep water

The analysis of free waves considered in the two previous chapters largely holds for a broad class of dispersive plane waves associated with a general dispersion relation. The results of this general analysis are applied in this chapter to the free waves created by a ship that advances at a constant speed in calm water of large depth and lateral extent.

4.1 Dispersion relation and dispersion curves

In the special case $f = 0$ and $d = \infty$ considered in this chapter, the dispersion function Δ defined by (2.7) or (2.9) becomes

$$\Delta(\alpha, \beta; F) \equiv F^2\alpha^2 - k \text{ where } k \equiv \sqrt{\alpha^2+\beta^2}\,. \tag{4.1}$$

The corresponding dispersion relation $\Delta(\alpha, \beta; F) = 0$ can be expressed as

$$(\alpha^V)^2 = k^V = \sqrt{(\alpha^V)^2 + (\beta^V)^2} \text{ where} \tag{4.2}$$

$$(k^V, \alpha^V, \beta^V) \equiv F^2(k, \alpha, \beta) \equiv (K, K^x, K^y)V_s^2/g \tag{4.3}$$

denote speed-scaled wavenumbers, in accordance with (1.33b).

The dispersion relation (4.2) and expressions (2.13b) yield

$$(k^V, \alpha^V, \beta^V) = (1, \cos\gamma, \sin\gamma)/\cos^2\gamma \text{ where } -\pi \le \gamma \le \pi\,.$$

One then has two dispersion curves, depicted in Fig.4.1, that correspond to $-\pi/2 < \gamma < \pi/2$ and $\pi/2 < \gamma < 3\pi/2$. These dispersion curves are

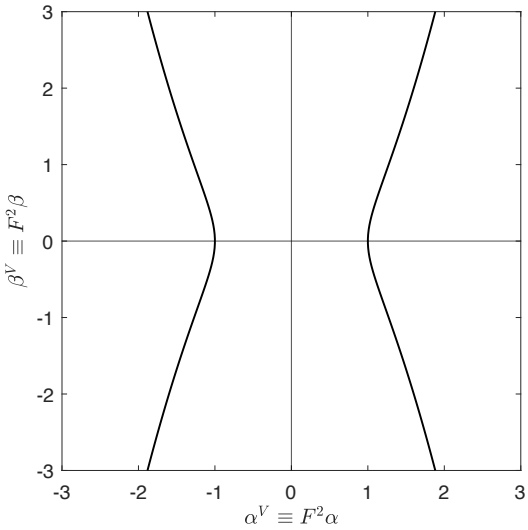

Figure 4.1: Dispersion curves associated with ship waves in calm deep water.

symmetric with respect to the axis $\alpha^V = 0$ and are also symmetric about the axis $\beta^V = 0$, and can be represented as

$$(k^V, \pm\alpha^V, \beta^V) = (1, \cos\gamma, \sin\gamma)/\cos^2\gamma \text{ where } -\pi/2 < \gamma < \pi/2 \quad (4.4a)$$

or in the alternative forms

$$\pm\,\alpha^V = \sqrt{1/2 + \sqrt{1/4 + (\beta^V)^2}} \text{ where } -\infty < \beta^V < \infty\,, \quad (4.4b)$$

$$\left(k^V, \pm\alpha^V, \beta^V\right) = \left(1+q^2, \sqrt{1+q^2}, q\sqrt{1+q^2}\right) \text{ where } -\infty < q < \infty\,. \quad (4.4c)$$

The polar equations (4.4a) determine the speed-scaled wavelength λ^V as

$$\lambda^V \equiv \frac{\lambda}{F^2} \equiv \frac{g\Lambda}{V_s^2} = \frac{2\pi}{k^V} = 2\pi\cos^2\gamma \le 2\pi \equiv \lambda^V_{max}\,. \quad (4.5a)$$

The parametric representation (4.4c) similarly yields

$$k^V = 1 + q^2 \ge 1 \text{ and } \lambda^V = \frac{2\pi}{k^V} = \frac{2\pi}{1+q^2} \le 2\pi \equiv \lambda^V_{max}\,. \quad (4.5b)$$

The parametric representation (4.5b) yields

$$\lambda^V/\lambda^V_{max} = 1, 0.5, 0.2, 0.1, 0.02 \text{ for } q = 0, 1, 2, 3, 7\,.$$

Expressions (4.5) show that a ship advancing in calm deep water at a speed V_s creates waves with wavelengths

$$\Lambda \le \Lambda^{max} \equiv 2\pi V_s^2/g\,.$$

The longest waves created by the ship, along its track as is shown further on, are shorter than the ship length L_s at 'low' Froude numbers

$$F \equiv V_s/\sqrt{gL_s} < 1/\sqrt{2\,\pi} \approx 0.4$$

but are longer than the ship length at 'high' Froude numbers $0.4 < F$; i.e.

$$\Lambda^{max} < L_s \text{ if } F < 0.4 \quad \text{and} \quad L_s < \Lambda^{max} \text{ if } 0.4 < F\,.$$

The Froude number $F \approx 0.4$ is then significant for practical applications, notably for ship design.

The Cartesian representation (4.4b) yields

$$|\alpha^V| \sim 1 + (\beta^V)^2/2 \text{ as } \beta^V \to 0 \quad \text{and} \quad |\alpha^V| \sim \sqrt{|\beta^V|} \text{ as } \beta^V \to \pm\infty\,.$$

The parametric representation (4.4c) yields

$$\begin{aligned} &\beta^V \sim q + q^3/2 \;\ll\; |\alpha^V| \sim 1 + q^2/2 \;\sim\; k^V = 1 + q^2 \text{ as } q \to 0\,, \\ &|\alpha^V| \sim q \;\ll\; |\beta^V| \sim q^2 \sim k^V \text{ as } q \to \pm\infty\,. \end{aligned}$$

The representation (4.4c) is convenient to evaluate the Fourier integral that determines the waves contained in the Green function and the related Fourier integrals associated with a distribution of singularities.

4.2 Elementary free ship waves

The dispersion relation (4.2) shows that the waves created by a ship that advances at a constant speed in calm deep water consist of a superposition of elementary free waves

$$e^{\,k^V z^V + \mathrm{i}\,\theta} \text{ where } k^V = 1/\cos^2\gamma \text{ and } \theta \equiv k^V(x^V\cos\gamma + y^V\sin\gamma)\,. \tag{4.6}$$

Moreover, x^V, y^V, z^V denote the speed-scaled coordinates

$$(x^V, y^V, z^V) \equiv (x, y, z)/F^2 \equiv (X, Y, Z)\,g/V_s^2 \tag{4.7}$$

as in (1.33b). The phase function θ in (4.6) is then given by

$$\theta = (x^V\cos\gamma + y^V\sin\gamma)/\cos^2\gamma = (x^V\cos\gamma + y^V\sin\gamma)(1 + \tan^2\gamma)\,. \tag{4.8}$$

In the far field $h^V \equiv \sqrt{(x^V)^2 + (y^V)^2} \to \infty$, dominant contributions to a superposition of the elementary waves (4.6) stem from values of γ for which the phase function θ given by (4.8) is stationary, i.e. from the roots of the 'stationary-phase equation' $d\theta/d\gamma = 0$. This equation yields

$$\tan\psi^* \equiv \frac{y^V}{-x^V} \equiv \frac{Y}{-X} = \frac{\tan\gamma}{1 + 2\tan^2\gamma} \tag{4.9}$$

where the ray angle ψ^* is measured from the negative x axis ($x < 0, y = 0$), i.e. from the track of the ship, which corresponds to $\psi = \pi$ and $\psi^* = 0$.

4.3 Kelvin's wave pattern

The far-field wave pattern due to a ship that steadily advances in calm deep water, known as Kelvin's wave pattern or Kelvin's wake, is now considered.

Analytical representation of Kelvin's ship wake

The far-field wave pattern associated with a dispersion function Δ is determined from Δ by the general parametric equations (3.18), where σ^{Δ} is given by (2.53b) in the special case of steady ship waves now considered. The pattern of far-field waves created by a ship that steadily advances in calm deep water is then defined by the parametric equations

$$\mathbf{h}_n \equiv \begin{Bmatrix} x_n \\ y_n \end{Bmatrix} = -\text{sign}(\alpha)\, \frac{2n\pi}{k\,\Delta_k} \begin{Bmatrix} \Delta_\alpha \\ \Delta_\beta \end{Bmatrix} \tag{4.10}$$

where $n = 1, 2, 3, \ldots$ and Δ is the dispersion function (4.1). The derivatives Δ_α, Δ_β and Δ_k of Δ in (4.10) are given by (2.31b), with $t^d = 1$ in deep water. One then has

$$\Delta_\alpha = (2F^2k - 1)\,\alpha/k = (2 - 1/k^V)\,\alpha^V = (1+\sin^2\gamma)/\cos\gamma\ , \tag{4.11a}$$

$$\Delta_\beta = -\beta^V\!/k^V = -\sin\gamma\ ,\ \ \Delta_k = 2k^V\cos^2\gamma - 1 = 1 \tag{4.11b}$$

where expressions (4.2), (4.3) and (4.4a) were used.

Expressions (4.7), (4.10) and (4.11) yield

$$\begin{Bmatrix} -x_n^V \\ y_n^V \end{Bmatrix} = 2n\pi \begin{Bmatrix} 1+\sin^2\gamma \\ \sin\gamma\cos\gamma \end{Bmatrix} |\cos\gamma| \ \text{ with } \ -\pi < \gamma < \pi\ . \tag{4.12}$$

The parametric equations (4.12) define the pattern of free waves created by a ship that advances at a constant speed in calm deep water. Equations (4.12) show that the dispersion curves located in the half planes $-\pi/2 < \gamma < \pi/2$ and $\pi/2 < \gamma < 3\pi/2$ yield identical waves patterns, and that these wave patterns are symmetric about the horizontal axis $y^V = 0$, i.e. the track of the ship.

The Kelvin wave pattern defined by (4.12) can then be represented as

$$\begin{Bmatrix} -x_n^V \\ y_n^V \end{Bmatrix} = 2n\pi \begin{Bmatrix} 1+\sin^2\gamma \\ \sin\gamma\cos\gamma \end{Bmatrix} \cos\gamma \ \text{ where } \ -\pi/2 \le \gamma \le \pi/2\ . \tag{4.13a}$$

These expressions yield

$$h_n^V \equiv \sqrt{(x_n^V)^2 + (y_n^V)^2} = 2n\pi\sqrt{1+3\sin^2\gamma}\,\cos\gamma \tag{4.13b}$$

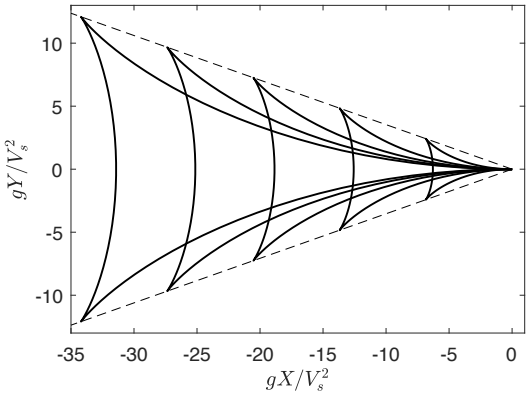

Figure 4.2: Kelvin's pattern of transverse and divergent waves created by a ship that advances at a constant speed in calm deep water.

where $-\pi/2 \le \gamma \le \pi/2$. Expressions (4.7), (4.10) and (4.11) also yield the representation

$$\frac{g}{V_s^2}\begin{Bmatrix} -X_n \\ Y_n \end{Bmatrix} = \frac{2n\pi}{k^V}\begin{Bmatrix} (2-1/k^V)\sqrt{k^V} \\ \pm\sqrt{1-1/k^V} \end{Bmatrix} \text{ where } 1 \le k^V. \tag{4.14}$$

The Kelvin wave pattern defined by the alternative parametric equations (4.13a) or (4.14) is depicted in Fig.4.2 for $n = 1, 2, \ldots, 5$.

The Kelvin wave pattern (4.12) only depends on the speed-scaled coordinates x^V and y^V defined by (4.7). Thus, Kelvin's ship wave pattern is independent of the length L_s of the ship, and only depends on the ship speed V_s and the acceleration of gravity g.

Expressions (4.12) yield $x_n < 0$, which shows that a ship that steadily advances in calm deep water only creates waves in the region $x < 0$ behind the ship **[4,1]**. These expressions also show that Kelvin's wave pattern is symmetric about the axis $y = 0$, i.e. the track of the ship, as is expected for a ship that is modeled as a one-point wavemaker.

Expressions (4.12) yield

$$\tan\psi^* \equiv \frac{y_n^V}{-x_n^V} \equiv \frac{y_n}{-x_n} \equiv \frac{Y_n}{-X_n} = \frac{\tan\gamma}{1+2\tan^2\gamma} \tag{4.15a}$$

in agreement with the stationary-phase relation (4.9). As was already noted, the angle ψ^* in (4.15a) is measured from the negative x axis ($x < 0, y = 0$), i.e. from the ship track, which corresponds to $\psi = \pi$ and $\psi^* = 0$. Expression (4.15a) determines the ray angle ψ^* of a dominant wave in terms of its

propagation angle γ. Expression (4.15a) yields

$$2\tan\psi^*\tan^2\gamma - \tan\gamma + \tan\psi^* = 0\ . \tag{4.15b}$$

Equation (4.15b) is a quadratic equation that determines $\tan\gamma$ in terms of $\tan\psi^*$, and therefore determines the wave-propagation angle γ in terms of the ray angle ψ^*.

The Kelvin wake angle ψ^K

The quadratic equation (4.15b) has two distinct real roots if $\tan^2\psi^* < 1/8$, i.e. if

$$-\psi^K < \psi^* < \psi^K \ \text{ where } \ \psi^* \equiv \arctan\left(\frac{y_n^V}{-x_n^V}\right) \ \text{ and} \tag{4.16a}$$

$$\psi^K \equiv \arctan(1/\sqrt{8}) = \arcsin(1/3) \approx 19^\circ 28' \tag{4.16b}$$

is the Kelvin wake angle. If $\psi^K < |\psi^*|$, the quadratic equation (4.15b) has no real root, and waves do not exist outside the Kelvin wedge (4.16a) that trails a ship.

The Kelvin angle (4.16b) and the wave pattern (4.13a) are independent of the Froude number, and are then identical for every ship, including fully-submerged bodies (e.g., a submarine at a low submergence depth), displacement ships (built in a wide range of lengths and speeds), hovercrafts and surface-effect-ships, fast ships and planing boats. This classical theoretical result is based on a far-field stationary-phase analysis in which a ship is modeled as a 1-point wavemaker, as is explained in section 3.7.

If $\tan^2\psi^* = 1/8$, i.e. if $\psi^* = \pm\,\psi^K$, the quadratic equation (4.15b) has a double real root, given by

$$\tan\gamma^C = \pm 1/\sqrt{2} \ \text{ i.e. } \gamma^C \approx \pm 35^\circ 16' \tag{4.17}$$

that corresponds to the cusps of the Kelvin wake. Thus, Kelvin's pattern of free waves behind a ship that steadily advances in calm deep water has two cusps along the ray angles $\psi^* \approx \pm 19^\circ 28'$, as can be observed in Fig.4.2 .

These cusps correspond to inflection points of the dispersion curves, as is shown in section 3.6. Specifically, the inflection-point condition (3.24c) for a dispersion curve defined via a polar representation yields

$$(k^V)^2 + 2\,(dk^V/d\gamma)^2 - k^V d^2k^V/d\gamma^2 = 0 \ \text{ where } \ k^V = 1/\cos^2\gamma \tag{4.18}$$

and k^V is the speed-scaled wavenumber defined by (4.3). Equation (4.18) has real roots given by $\tan\gamma = \pm 1/\sqrt{2}$, in agreement with (4.17). The corresponding cusp angles are determined by (4.15a) as

$$\tan\psi^* = \frac{\tan\gamma}{1 + 2\tan^2\gamma} = \frac{\pm 1}{2\sqrt{2}}$$

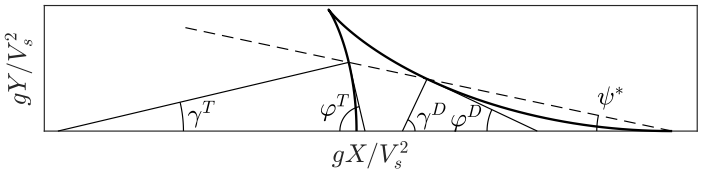

Figure 4.3: Wave-propagation angles γ^T and γ^D and related wave-crest angles φ^T and φ^D of the dominant transverse and divergent waves found at a ray angle ψ^* within Kelvin's pattern of ship waves in calm deep water.

in agreement with (4.16b).

If the parametric representation (4.4c) of the dispersion curves is used, instead of the polar representation (4.4a), inflection points of the dispersion curves are determined by the inflection-point equation (3.24b), which yields

$$2\,q^4 + q^2 - 1 = 0\ .$$

This equation has two real roots

$$q^C = \pm 1/\sqrt{2} \approx \pm\, 0.7\ . \tag{4.19}$$

Transverse and divergent waves

The two real roots of the quadratic equation (4.15b) are given by

$$\tan\gamma^T = \frac{2\tan\psi^*}{1+\sqrt{1-8\tan^2\psi^*}} \ \text{ and } \ \tan\gamma^D = \frac{1+\sqrt{1-8\tan^2\psi^*}}{4\tan\psi^*}\ . \tag{4.20a}$$

The two roots (4.20a) mean that at any point along a ray at an angle ψ^* inside the Kelvin wedge (4.16a), one has two dominant waves, which are known as transverse and divergent waves. These waves propagate at angles $\gamma = \gamma^T$ and $\gamma = \gamma^D$, as is shown in Fig.4.3. The corresponding angles of the wave pattern (e.g. crest-lines) are given by

$$\varphi^T = (\mathrm{sign}\gamma^T)\,90^\circ - \gamma^T \ \text{ and } \ \varphi^D = (\mathrm{sign}\,\gamma^D)\,90^\circ - \gamma^D\ . \tag{4.20b}$$

The wavelength $\lambda^V = 2\pi/k^V = 2\pi\cos^2\gamma = 2\pi/(1+\tan^2\gamma)$ is given by

$$\lambda_T^V/\pi = \left(1 + 4\tan^2\psi^* + \sqrt{1-8\tan^2\psi^*}\right)\cos^2\psi^* \ \text{ and} \tag{4.20c}$$

$$\lambda_D^V/\pi = 16\tan^2\psi^* \Big/ \left(1 + 4\tan^2\psi^* + \sqrt{1-8\tan^2\psi^*}\right) \tag{4.20d}$$

for the transverse and divergent waves. Expressions (4.20) determine main features—wave-propagation angles, wave-crest angles, wavelengths—of the

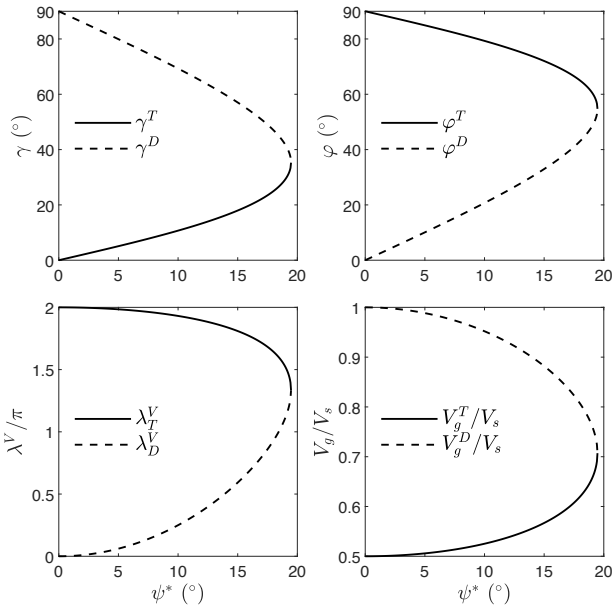

Figure 4.4: Variations of the wave-propagation angles γ^T and γ^D (top left corner), the wave-crest angles φ^T and φ^D (top right), the wavelengths λ_T^V and λ_D^V (bottom left) and the speed-scaled group velocities V_g^T/V_s and V_g^D/V_s (bottom right) related to the dominant transverse and divergent waves found at ray angles $0 \le \psi^* \le \psi^K$ within Kelvin's pattern of ship waves in deep calm water.

transverse and divergent waves found at a ray angle ψ^* within the Kelvin wake. The wave-propagation angles γ^T and γ^D, the wave-crest angles φ^T and φ^D, and the wavelengths λ_T^V and λ_D^V given by (4.20) are depicted in Fig.4.4 for ray angles ψ^* within the positive half of the Kelvin wake (4.16).

Only the ranges $0 \le \psi^* \le \psi^K$ and $0 \le \gamma \le \pi/2$ associated with the positive half $0 \le y^V$ of the Kelvin wave pattern is now considered due to symmetry about $\psi^* = 0, \gamma = 0, y^V = 0$. Expressions (4.20) and Fig.4.4 show that the wave-propagation angles γ^T and γ^D, the wave-crest angles φ^T and φ^D, the wavenumbers k_T^V and k_D^V and the corresponding wavelengths λ_T^V and λ_D^V of the transverse and divergent waves in Kelvin's ship wake vary within the ranges

$$0 \le \tan^2\gamma^T \le 1/2 \le \tan^2\gamma^D \text{ i.e. } 0 \le \gamma^T \le 35°16' \le \gamma^D \le 90° , \quad (4.21a)$$

$$0 \le \tan^2\varphi^D \le 2 \le \tan^2\varphi^T \quad \text{i.e. } 0 \le \varphi^D \le 54°44' \le \varphi^T \le 90° , \quad (4.21b)$$

$$1 \le k_T^V \le 3/2 \le k_D^V \text{ and } 0 \le \lambda_D^V \le 4\pi/3 \approx 4.2 \le \lambda_T^V \le 2\pi \approx 6.3 . \quad (4.21c)$$

Expressions (4.21) and (4.15a) show that the longest ship waves are found along the ship track $\psi^* = 0$ and correspond to $\gamma^T = 0$, $\varphi^T = 90°$ and $k_T^V = 1$.

At the cusps of the Kelvin wake, expressions (4.21) yield

$$\gamma^T = \gamma^D = \gamma^C \approx 35^\circ 16' \ , \ \ \varphi^T = \varphi^D = \varphi^C \approx 54^\circ 44' \, , \tag{4.22a}$$

$$k_T^V = k_D^V = k_C^V = 3/2 \ \text{ and } \ \lambda_T^V = \lambda_D^V = \lambda_C^V = 4\,\pi/3 \ . \tag{4.22b}$$

Thus, the wavelength of the waves (transverse and divergent) at the cusps of the Kelvin wake are equal to 2/3 of the wavelength of the longest (transverse) waves at the track of the ship.

Expressions (4.20a-b) yield the asymptotic approximations

$$\gamma^D \sim 90^\circ - 2\,\psi_\circ \ \text{ and } \ \varphi^D \sim 2\,\psi_\circ \ \text{ as } \ \psi_\circ \to 0 \tag{4.23a}$$

where $\psi_\circ \equiv 180\,\psi^*/\pi$ is expressed in degrees. These approximations show that the divergent waves near the track $\psi^* = 0$ propagate in a direction γ^D that is nearly orthogonal to the ship track.

Expressions (4.21c) also show that the divergent waves contain short waves. In particular, the wavelength λ_D^V of the divergent waves vanishes at the ship track $\psi^* = 0$. Specifically, expression (4.20d) yields

$$\lambda_D^V \equiv g\,\Lambda^D/V_s^2 \sim 8\,\pi\,(\psi^*)^2 = \pi^3 \psi_\circ^2/4050 \approx (\psi_\circ/11.4)^2 \ \text{ as } \ \psi_\circ \to 0 \ . \tag{4.23b}$$

Expressions (4.23b) and (4.22b) yield

$$\lambda_D^V/\lambda_C^V \equiv \Lambda^D/\Lambda^C < 0.1 \ \text{ if } \ \psi_\circ < 7.4^\circ. \tag{4.23c}$$

The relation (4.23c) shows that the divergent waves created by a ship that steadily advances in calm deep water are significantly shorter than the waves found along the cusps of Kelvin's ship wake within an inner wedge with angle approximately equal to 15°. This inner wake, where divergent are short, is a significant portion of the 39° angle of the Kelvin wake where waves exist.

The approximations (4.23b) mean that short divergent waves in the vicinity of the track of a ship can be influenced by surface tension, which is significant for wavelengths Λ smaller than about 7cm. Much shorter wavelengths near the ship track could also be influenced by viscosity. However, a more stringent restriction stems from nonlinear effects and wavebreaking.

Specifically, although the amplitude A of the divergent waves created by a ship vanishes at the ship track, the steepness A/Λ is unbounded at $\psi^* = 0$ because the wavelength Λ vanishes at a faster rate than the wave amplitude A as $\psi^* \to 0$. Divergent waves therefore cannot exist within an inner portion of the Kelvin wake that borders the track of a ship. Indeed, the inner region where short divergent waves are too steep to exist in reality is a significant portion of Kelvin's ship wake **[4,2]**.

If the dispersion curves are represented via the parametric representation (4.4c), expression (4.19) shows that the transverse and divergent waves in the Kelvin wake correspond to the ranges

$$0 \le |\,q^T\,| \le |\,q^C\,| \equiv 1/\sqrt{2} \approx 0.7 \le |\,q^D\,| \ . \tag{4.24}$$

4.4 Group velocity

The group velocity, i.e. the transmission-velocity of energy, is determined from the dispersion function Δ by the general expressions (2.25). In the particular case of steady ship waves, these expressions yield (2.33a), where one has $s^d = 0$ in deep water. Expression (2.33a) then yields

$$\frac{\mathbf{v}_g}{F} \equiv \frac{1}{F}\begin{Bmatrix} v_g^x \\ v_g^y \end{Bmatrix} = \frac{\text{sign}(\cos\gamma)}{2\sqrt{k^V}}\begin{Bmatrix} \cos\gamma \\ \sin\gamma \end{Bmatrix} - \begin{Bmatrix} 1 \\ 0 \end{Bmatrix} = \frac{1}{2}\begin{Bmatrix} \cos\gamma \\ \sin\gamma \end{Bmatrix}\cos\gamma - \begin{Bmatrix} 1 \\ 0 \end{Bmatrix}$$

where $k^V \equiv F^2 k$ is the speed-scaled wavenumber and the dispersion relation (4.4a) was used.

These expressions for the group velocity $\mathbf{v}_g$ yield

$$\begin{Bmatrix} -V_g^x/V_s \\ V_g^y/V_s \end{Bmatrix} = \frac{1}{2}\begin{Bmatrix} 1+\sin^2\gamma \\ \sin\gamma\,\cos\gamma \end{Bmatrix} \quad \text{where} \quad -\pi \le \gamma \le \pi \tag{4.25a}$$

and the identity $\mathbf{v}_g/F \equiv \mathbf{V}_g/V_s$ was used. Expressions (4.25a) show that the magnitude of the group velocity is given by

$$\frac{V_g}{V_s} = \frac{\sqrt{1+3\,\sin^2\gamma}}{2} = \sqrt{1-\frac{3}{4}\,\cos^2\gamma} = \sqrt{1-\frac{3/4}{1+\tan^2\gamma}}\ . \tag{4.25b}$$

Expressions (4.25) determine the transmission velocity V_g of the wave energy radiated by a ship in its wake.

At the cusps $\psi^* = \pm\psi^K$ of the ship wake, one has $\tan^2\gamma^C = 1/2$ in accordance with (4.20a), and expression (4.25b) yields $V_g/V_s = 1/\sqrt{2}$. At the track $\psi^* = 0$ of the ship, (4.20a) and (4.25b) yield $\gamma = 0$ or $\gamma = 90^\circ$ and $V_g = V_s/2$ or $V_g = V_s$ for the transverse or divergent waves, and (4.25a) yields $\mathbf{V}_g = -\mathbf{V}_s/2$ if $\gamma = 0$ (transverse waves) and $\mathbf{V}_g = -\mathbf{V}_s$ if $\gamma = 90^\circ$ (divergent waves) where $\mathbf{V}_s \equiv (V_s, 0)$ is the velocity of the ship. The relation (2.37) then shows that, in a sea-fixed frame of reference, one has

$$\mathbf{V}_g^{sea} = \mathbf{V}_s/2 \ \text{ if } \ \gamma = 0 \ \text{ and } \ \mathbf{V}_g^{sea} = 0 \ \text{ if } \ \gamma = 90^\circ\ .$$

Expressions (4.25) for the group velocity and the parametric equations (4.12) that define Kelvin's wave pattern show that one has

$$\begin{Bmatrix} -x_n^V \\ y_n^V \end{Bmatrix} = 4\,n\,\pi\begin{Bmatrix} -V_g^x/V_s \\ V_g^y/V_s \end{Bmatrix}|\cos\gamma|\ . \tag{4.26a}$$

These expressions and expressions (4.13b) and (4.25b) yield

$$(-x_n^V, y_n^V)/h_n^V = (-V_g^x, V_g^y)/V_g \tag{4.26b}$$

in agreement with the general relation (3.21). One then has $V_g^x < 0$ as well as $X_n < 0$, and the group velocity $\mathbf{V}_g$ points toward the wake that trails the ship. Expression (4.26b) illustrates how wave energy is transmitted, at the group velocity $\mathbf{v}_g$, along straight lines that radiate from the ship, which appears to be located at the origin of the wave pattern to a far-field observer located at a large distance from the ship. The relations (4.26b) and (4.9) yield

$$\frac{V_g^y}{-V_g^x} = \frac{Y_n}{-X_n} = \tan\psi^* = \frac{\tan\gamma}{1+2\tan^2\gamma} \ . \tag{4.26c}$$

The group velocities V_g^T and V_g^D that correspond to the transverse and divergent waves are given by (4.25b) where γ is taken as $\gamma = \gamma^T$ or $\gamma = \gamma^D$ and varies within the ranges (4.21a). Expressions (4.25b) and (4.20a) yield

$$V_g^T/V_s = \sqrt{\tfrac{3}{4}\,(3-\sqrt{1-8\tan^2\psi^*})\cos^2\psi^* - 1}\,/\sqrt{2} \ , \tag{4.27a}$$

$$V_g^D/V_s = \sqrt{\tfrac{3}{4}\,(3+\sqrt{1-8\tan^2\psi^*})\cos^2\psi^* - 1}\,/\sqrt{2} \ . \tag{4.27b}$$

These expressions determine the group velocities V_g^T and V_g^D of the transverse and divergent waves found at a ray angle ψ^* within the Kelvin wake. Expressions (4.27) yield

$$V_g^T = V_s/2 \ \text{ and } \ V_g^D = V_s \ \text{ at } \ \psi^* = 0 \ , \tag{4.28a}$$

$$V_g^T = V_g^D = V_g^C = V_s/\sqrt{2} \ \text{ at } \ \psi^* = \pm\psi^K \ , \tag{4.28b}$$

$$1/2 \le V_g^T/V_s \le 1/\sqrt{2} \le V_g^D/V_s \le 1 \ \text{ for } \ -\psi^K \le \psi^* \le \psi^K \ . \tag{4.28c}$$

Thus, one has $1/2 \le V_g/V_s \le 1$. The speed-scaled group velocities V_g^T/V_s and V_g^D/V_s given by (4.27) are depicted in Fig.4.4 for ray angles ψ^* within the positive half of the Kelvin wake (4.16).

Chapter 5

Free waves made by a ship that advances through regular waves

The analysis of free waves expounded in chapters 2 and 3 for a broad class of dispersive plane waves is applied in this chapter to the particular case of a ship that steadily advances through regular waves in deep water. This application provides a vivid illustration of the fact that a simple dispersion relation can define multiple dispersion curves and a surprisingly rich set of wave patterns that involve widely different waves. **[5,1]**.

5.1 Dispersion curves

The free waves created by a ship that steadily advances through deep-water regular waves are determined by the dispersion relation (2.9), i.e.

$$\Delta(f,\alpha,\beta;F) \equiv (f+F\alpha)^2 - k \equiv (f+Fk\cos\gamma)^2 - k = 0 \tag{5.1a}$$

where $k \equiv \sqrt{\alpha^2+\beta^2}$. The corresponding dispersion curves $\Delta = 0$ are symmetric about the axis $\beta = 0$, and can be expressed in the Cartesian form

$$\beta(\alpha;f,F) = \pm\sqrt{(f+F\alpha)^4 - \alpha^2}\ . \tag{5.1b}$$

The dispersion relations (5.1) yield

$$k/f^2 = 1 \ \text{ and } \ \beta/f^2 = \pm 1 \ \text{ for } \ \alpha = 0\ . \tag{5.2}$$

Thus, the dispersion curves intersect the axis $\alpha = 0$ at $\beta = \pm f^2$.

Polar representations of the dispersion curves

The dispersion curves associated with the dispersion relation (5.1a) can be expressed in the polar form

$$k = \frac{1/2 - \tau\cos\gamma \pm \sqrt{1/4 - \tau\cos\gamma}}{F^2\cos^2\gamma} = \frac{(\sqrt{1/4 - \tau\cos\gamma} \pm 1/2)^2}{F^2\cos^2\gamma} \tag{5.3}$$

where τ denotes the parameter defined by (1.32) as

$$\tau \equiv Ff = V_s\,\omega/g\ . \tag{5.4}$$

The wavenumber (5.3) is not a real number if $1/4 < \tau\cos\gamma$, i.e. if

$$-\gamma^\tau < \gamma < \gamma^\tau \ \text{ where } \ \gamma^\tau \equiv \arccos[(1/4)/\tau] \ \text{ and } \ 1/4 \le \tau\,. \tag{5.5}$$

The $\pm$ branches of the polar representation (5.3) can be expressed as

$$k^V \equiv F^2k = (\sqrt{1/4 - \tau\cos\gamma}\ + 1/2)^2/\cos^2\gamma \ \text{ and} \tag{5.6a}$$

$$k^\omega \equiv k/f^2 = 1/(\sqrt{1/4 - \tau\cos\gamma} + 1/2)^2 \tag{5.6b}$$

$$\text{where } \ k^\omega \equiv Kg/\omega^2 \equiv k/f^2 \ \text{ and } \ k^V \equiv KV_s^2/g \equiv F^2k \tag{5.7}$$

are the frequency-scaled or the speed-scaled nondimensional wavenumbers defined by (1.33a-b).

The dispersion curves defined by (5.6) intersect the axis $\beta = 0$ for $\gamma = 0$ and $\gamma = \pi$. The wavenumbers corresponding to these intersection points are

$$\left\{\begin{array}{l} F^2k_o^+ = (\sqrt{1/4 - \tau}\ + 1/2)^2 \\ F^2k_o^- = (\sqrt{1/4 + \tau}\ + 1/2)^2 \\ k_i^+/f^2 = 1/(\sqrt{1/4 - \tau}\ + 1/2)^2 \\ k_i^-/f^2 = 1/(\sqrt{1/4 + \tau}\ + 1/2)^2 \end{array}\right\} \tag{5.8}$$

where k_o^+ and k_i^+ correspond to $\gamma = 0$, and k_o^- and k_i^- correspond to $\gamma = \pi$. The intersection wavenumbers k_o^- and k_i^- are real for every value of $0 \le \tau$, but the wavenumbers k_o^+ and k_i^+ are only real if $\tau \le 1/4$. Expressions (5.8) yield

$$k_i^\pm/f^2 = 1 \ \text{ and } \ F^2k_o^\pm = 1 \quad \text{if } \tau = 0\ , \tag{5.9a}$$

$$\frac{k_i^+}{f^2} = 4 = \frac{k_o^+}{f^2}\ ,\ \frac{k_i^-}{f^2} = \frac{4}{(\sqrt{2}+1)^2} \approx 0.7\ ,\ \frac{k_o^-}{f^2} = 4(\sqrt{2}+1)^2 \approx 23$$

$$\text{if } \tau = 1/4\ . \tag{5.9b}$$

Dispersion curves for $\tau \leq 1/4$

If $\tau \leq 1/4$, the condition $\tau \cos\gamma \leq 1/4$ that ensures that the wavenumbers defined by (5.6) are real is always satisfied, and the polar representations (5.6) yield the three dispersion curves

$$k^V = (\sqrt{1/4 - \tau\cos\gamma} + 1/2)^2/\cos^2\gamma \text{ where } \pi/2 < \gamma < 3\pi/2\,, \tag{5.10a}$$

$$k^\omega = 1/(\sqrt{1/4 - \tau\cos\gamma} + 1/2)^2 \text{ where } 0 \leq \gamma \leq 2\pi\,, \tag{5.10b}$$

$$k^V = (\sqrt{1/4 - \tau\cos\gamma} + 1/2)^2/\cos^2\gamma \text{ where } -\pi/2 < \gamma < \pi/2\,. \tag{5.10c}$$

These dispersion curves are located within the three regions

$$-\infty < \alpha \leq -k_o^-\ ,\ -k_i^- \leq \alpha \leq k_i^+\ ,\ k_o^+ \leq \alpha < \infty \quad \text{if } \tau \leq 1/4\,. \tag{5.11}$$

The dispersion curve in the inner region $-k_i^- \leq \alpha \leq k_i^+$ in (5.11) is called 'inner dispersion curve' and is denoted as I hereafter. The dispersion curves in the two outer regions $-\infty < \alpha \leq -k_o^-$ and $k_o^+ \leq \alpha < \infty$ are similarly called 'outer dispersion curves' and are denoted as O^- or O^+.

In the special case $\tau = 0$, the dispersion curve defined by (5.10b) becomes

$$k^\omega \equiv k/f^2 = 1 \tag{5.12a}$$

in agreement with the dispersion circle (2.10) associated with diffraction-radiation of regular waves by an offshore structure, and the dispersion curves (5.10c) are symmetric about the axis $\alpha = 0$ and given by

$$k^V \equiv F^2 k = 1/\cos^2\gamma \text{ where } -\pi \leq \gamma \leq \pi \tag{5.12b}$$

in agreement with the dispersion curves (4.4) associated with ship waves in calm deep water.

In the special case $\tau = 1/4$, one has $k_i^+ = k_o^+ = 4f^2$ in accordance with (5.9b). The dispersion curves in the regions $-k_i^- \leq \alpha \leq k_i^+$ and $k_o^+ \leq \alpha < \infty$ are then connected at $\alpha = 4f^2$ in this special case. Thus, the dispersion curves are located in the regions

$$-\infty < \alpha \leq -k_o^- \text{ and } -k_i^- \leq \alpha < \infty \quad \text{if } \tau = 1/4\,. \tag{5.13}$$

The (closed) inner dispersion curve I defined by (5.10b) and the two (open) dispersion curves O^- and O^+ defined by (5.10a) and (5.10c) are depicted in Fig.5.1 for $\tau = 0.2$ and $\tau = 1/4$ in the Strouhal-scaled Fourier plane $(\alpha^S, \beta^S) \equiv (K^x, K^y)V_s/\omega$ associated with the representation (5.18) given further on. Fig.5.1 shows that the inner dispersion curve I and the outer dispersion curve O^+ are connected at $\alpha^S = 1$ if $\tau = 1/4$, in accordance with (5.13) and the relation $\alpha^S = \tau\alpha^\omega$. Fig.5.1 also illustrates the notable feature that the wavenumbers k_i^- and k_i^+ associated with the inner

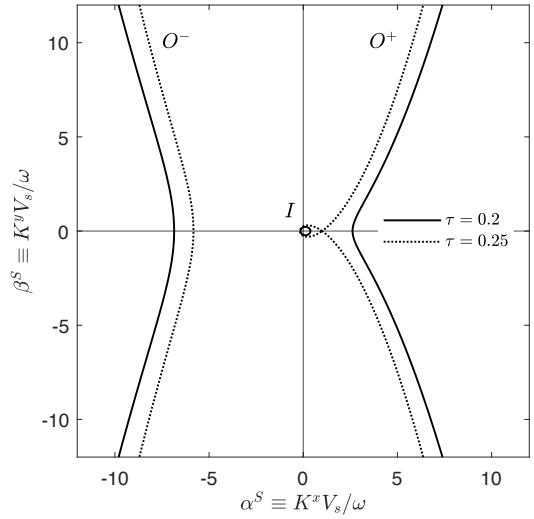

Figure 5.1: This figure depicts the closed inner dispersion curve I and the two dispersion curves O^- and O^+ defined by the dispersion relation (5.1) in the regime $\tau < 1/4$. These three dispersion curves are depicted for $\tau = 0.2$ and $\tau = 0.25$ in the Strouhal-scaled Fourier plane $(\alpha^S, \beta^S) \equiv (K^x, K^y)V_s/\omega$.

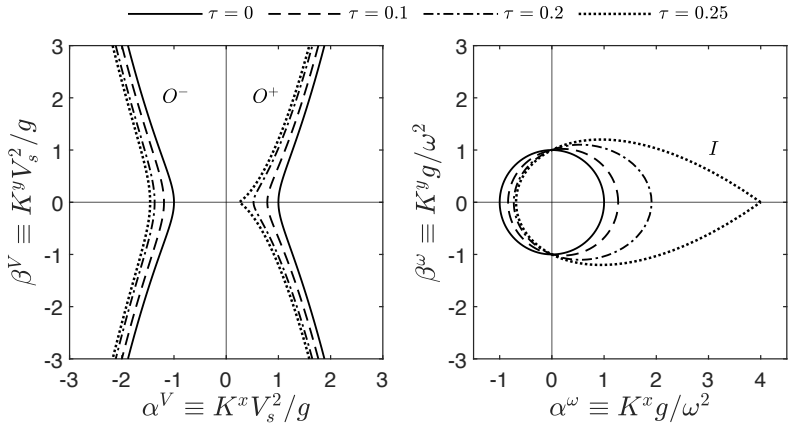

Figure 5.2: This figure depicts the dispersion curves defined by (5.10) in the regime $0 \leq \tau \leq 1/4$. The figure on the left side depicts the outer dispersion curves O^- and O^+ in the speed-scaled Fourier plane $(\alpha^V, \beta^V) \equiv (K^x, K^y)V_s^2/g$ and the figure on the right depicts the inner dispersion curve I in the frequency-scaled Fourier plane $(\alpha^\omega, \beta^\omega) \equiv (K^x, K^y)\, g/\omega^2$.

dispersion curve I are significantly smaller than the wavenumbers k_o^- and k_o^+ associated with the outer dispersion curves O^- and O^+ for $\tau < 0.2$.

The inner and outer dispersion curves defined by the dispersion relation (5.1) in the regime $\tau \leq 1/4$ are further considered in Fig.5.2. Specifically, the left half of Fig.5.2 depicts the outer dispersion curves O^- and O^+ in the speed-scaled Fourier plane $(\alpha^V, \beta^V) \equiv (K^x, K^y)V_s^2/g$ for $\tau = 0$, 0.1, 0.2 and $1/4$, and the right half of the figure depicts the inner dispersion curve I in the frequency-scaled Fourier plane $(\alpha^\omega, \beta^\omega) \equiv (K^x, K^y)\, g/\omega^2$ for the same values of τ within the range $0 \leq \tau \leq 1/4$.

The polar representations (5.10) of the inner dispersion curve I and the outer dispersion curves O^- and O^+ are well suited to represent the flow created by an arbitrary distribution of singularities (sources or dipoles) in the regime $\tau < 1/4$.

Dispersion curves for $1/4 < \tau$

For $1/4 \leq \tau$ and $-\pi/2 < \gamma < \pi/2$, the condition $\tau \cos\gamma \leq 1/4$ that ensures that the wavenumbers defined by (5.6) are real is not satisfied if (5.5) holds. The constraint (5.5) is irrelevant for the dispersion curve defined by (5.10a) but restricts the ranges of the polar angle γ in expressions (5.10b-c). Specifically, the polar representations (5.10) become

$$k^V = (\sqrt{1/4 - \tau\cos\gamma} + 1/2)^2/\cos^2\gamma \text{ where } \pi/2 < \gamma < 3\pi/2\,, \tag{5.14a}$$

$$k^\omega = 1/(\sqrt{1/4 - \tau\cos\gamma} + 1/2)^2 \text{ where } \gamma^\tau \leq \gamma \leq 2\pi - \gamma^\tau, \tag{5.14b}$$

$$k^V = (\sqrt{1/4 - \tau\cos\gamma} + 1/2)^2/\cos^2\gamma \text{ where } (-\pi/2 < \gamma \leq -\gamma^\tau) \cup (\gamma^\tau \leq \gamma < \pi/2)\,. \tag{5.14c}$$

These dispersion curves are located within the three regions

$$-\infty < \alpha \leq -k_o^-\ ,\ -k_i^- \leq \alpha \leq \alpha_{io}\ ,\ \alpha_{io} \leq \alpha < \infty \quad \text{if } 1/4 \leq \tau \tag{5.15a}$$

where α_{io} and the corresponding values of β and k are given by

$$\alpha_{io} = f^2/\tau = f/F\ ,\ \beta_{io} = \pm f^2\sqrt{16 - 1/\tau^2}\ ,\ k_{io} = 4f^2\,. \tag{5.15b}$$

The two regions $-k_i^- \leq \alpha \leq \alpha_{io}$ and $\alpha_{io} \leq \alpha < \infty$ are contiguous. The inner dispersion curve I located in the region $-k_i^- \leq \alpha \leq \alpha_{io}$ and the outer dispersion curve O^+ located in the region $\alpha_{io} \leq \alpha < \infty$ are then two portions of the continuous dispersion curve $I \cup O^+$, denoted as IO^+ hereafter, that is located in the region $-k_i^- \leq \alpha < \infty$. One then has only two dispersion curves O^- and IO^+ located in the regions

$$-\infty < \alpha \leq -k_o^- \text{ and } -k_i^- \leq \alpha < \infty \quad \text{if } 1/4 \leq \tau\,. \tag{5.15c}$$

The point $(\alpha_{io}, \beta_{io})$ that separates the connected dispersion curves I and O^+ in the two contiguous regions $-k_i^- \leq \alpha \leq \alpha_{io}$ and $\alpha_{io} \leq \alpha < \infty$ in

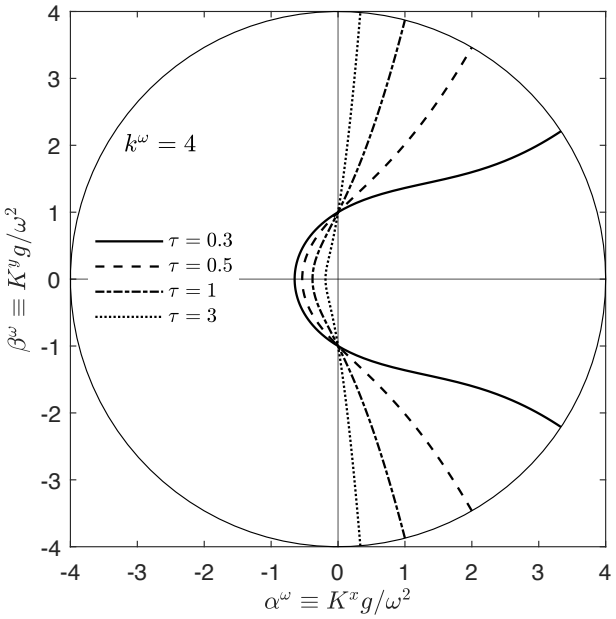

Figure 5.3: This figure depicts the inner dispersion curves I located in the region $-k_i^- \leq \alpha \leq \alpha_{io}$ in (5.15a) and defined by (5.14b) in the frequency-scaled Fourier plane $(\alpha^\omega, \beta^\omega) \equiv (K^x, K^y)\, g/\omega^2$ for $\tau = 0.3$, 0.5, 1 and 3. The circle $k^\omega = 4$ that separates the inner dispersion curve I and the outer dispersion curve O^+ in the three regions in (5.15a) associated with the regime $1/4 \leq \tau$ is also depicted.

(5.15a) is located on the circle $k = 4f^2$. One has

$$(\alpha_{io}^\omega, \beta_{io}^\omega) = (4, 0) \text{ if } \tau = 1/4 \quad \text{and} \quad (\alpha_{io}^\omega, \beta_{io}^\omega) \to (0, \pm 4) \text{ as } \tau \to \infty$$

where $(\alpha^\omega, \beta^\omega) \equiv (\alpha, \beta)/f^2$. The circle $k^\omega = 4$ is depicted in Fig.5.3, where the dispersion curve I associated with the inner region $-k_i^- \leq \alpha \leq \alpha_{io}$ in (5.15a) and defined by (5.14b) is also depicted for several values of $1/4 < \tau$. Expressions (5.15b) and (5.8) show that one has $k_{io} = k_o^-$ if $\tau = 3/4$.

The polar representations (5.10) of the dispersion curves for $\tau \leq 1/4$ are identical to the polar representations (5.14) for $1/4 \leq \tau$ if γ^τ in (5.14) is taken as $\gamma^\tau = 0$. Thus, the representations (5.14) can be used for every value of τ if γ^τ is defined as

$$\gamma^\tau \equiv 0 \text{ if } \tau \leq 1/4 \quad \text{or} \quad \gamma^\tau \equiv \arccos[(1/4)/\tau] \text{ if } 1/4 \leq \tau \,. \tag{5.16}$$

The polar representations (5.14) can also be expressed in terms of the Strouhal-scaled wavenumber k^S defined by (1.33c) as

$$k^S \equiv K V_s/\omega \,. \tag{5.17}$$

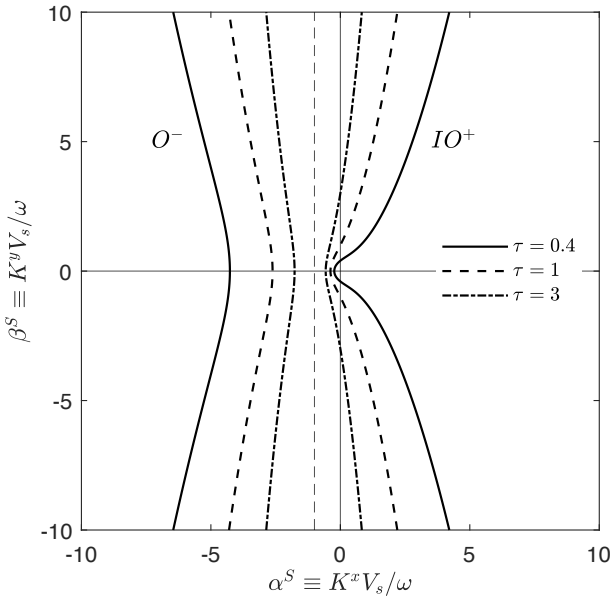

Figure 5.4: This figure depicts the two dispersion curves O^- (left side) and IO^+ (right side) defined by the dispersion relation (5.1) for $\tau = 0.4, 1, 3$ in the Strouhal-scaled Fourier plane $(\alpha^S, \beta^S) \equiv (K^x, K^y)V_s/\omega$. The vertical line $\alpha^S = -1$ is also shown.

Specifically, the relations $F^2 k = \tau k^S$ and $k/f^2 = k^S/\tau$ and expressions (5.14) define $k^S(\gamma;\tau)$ via the polar representations

$$k^S = (\sqrt{1/4 - \tau\cos\gamma} + 1/2)^2/(\tau\cos^2\gamma) \text{ where } \pi/2 < \gamma < 3\pi/2\,, \quad (5.18a)$$

$$k^S = \tau/(\sqrt{1/4 - \tau\cos\gamma} + 1/2)^2 \text{ where } \gamma^\tau \le \gamma \le 2\pi - \gamma^\tau\,, \quad (5.18b)$$

$$k^S = (\sqrt{1/4 - \tau\cos\gamma} + 1/2)^2/(\tau\cos^2\gamma) \text{ where } (-\pi/2 < \gamma \le -\gamma^\tau) \cup (\gamma^\tau \le \gamma < \pi/2)\,. \quad (5.18c)$$

As was already noted and is illustrated in Fig.5.1, the wavenumbers k_i^- and k_i^+ associated with the inner dispersion curve I are significantly smaller than the wavenumbers k_o^- and k_o^+ that correspond to the outer dispersion curves O^- and O^+ for small values of τ, i.e. in the regime $\tau \le \tau^\ell$ where $\tau^\ell \approx 0.2$. Indeed, the frequency-scaling $k^\omega \equiv Kg/\omega^2$ and the speed-scaling $k^V \equiv K V_s^2/g$ are well suited to represent the inner dispersion curve I or the outer dispersion curves O^- and O^+ in the regime $\tau \le 1/4$, and these two alternative scalings are used in Fig.5.2.

The Strouhal-scaling is well suited to represent the dispersion curves in the regime $0.25 < \tau$, as is illustrated in Fig.5.4, and is particularly well adapted for very large values of τ as is illustrated in Fig.5.5. Indeed, the

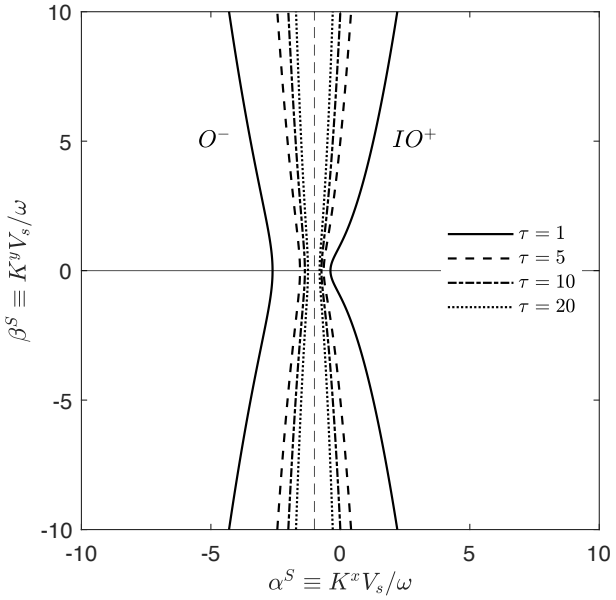

Figure 5.5: Dispersion curves that correspond to $\tau = 1$, 5, 10 and 20 in the Strouhal-scaled Fourier plane $(\alpha^S, \beta^S) \equiv (K^x, K^y)V_s/\omega$. The vertical line $\alpha^S = -1$ is also shown.

Strouhal-scaling is preferable to the frequency-scaling or the speed-scaling for large values of $\tau \geq \tau^L$ with $\tau^L \approx 0.4$.

Regime $0.25 < \tau \leq \sqrt{2/27} \approx 0.272$

If $\tau \leq 1/4$, Fig.5.1 and Fig.5.2 show that a constant-β line intersects the outer dispersion curve O^- at a single point, and also intersects the outer dispersion curve O^+ at a single point. If $1/4 \leq \tau$, Fig.5.4 and Fig.5.5 show that a constant-β line also intersects the outer dispersion curve O^- at a single point. However, a constant-β line can intersect the dispersion curve IO^+ at a single point or at three points, as can be observed in Fig.5.6 and is now shown.

A constant-β line is tangent to the dispersion curve IO^+ at a point where $\Delta = 0$ and $\Delta_\alpha = 0$. Expression (5.1a), where $0 < f + F\alpha$ for the dispersion curve IO^+, and expression (2.31c) for the derivative Δ_α of the dispersion function Δ then yield

$$\cos\gamma = (\sqrt{k} - f)/(Fk) = 2\tau/(1 - 2F^2 k)$$

at a point where a constant-β line is tangent to the dispersion curve IO^+.

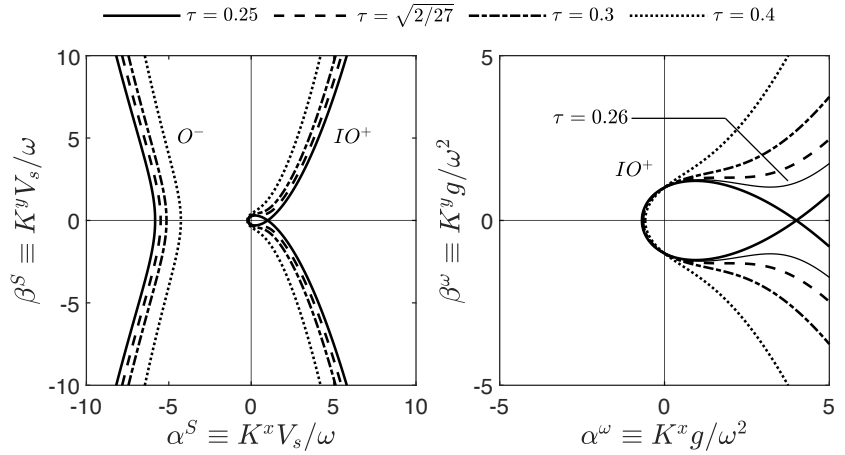

Figure 5.6: The figure on the left depicts the dispersion curves O^- and IO^+, located in the regions $-\infty < \alpha \le -k_o^-$ and $-k_i^- \le \alpha < \infty$ in (5.15c), in the Strouhal-scaled Fourier plane $(\alpha^S, \beta^S) \equiv (K^x, K^y)V_s/\omega$ for $0.25 \le \tau \le 0.4$. The figure on the right depicts the dispersion curve IO^+ in the vicinity of the origin of the frequency-scaled Fourier plane $(\alpha^\omega, \beta^\omega) \equiv (K^x, K^y)g/\omega^2$ for five values of τ in the range $0.25 \le \tau \le 0.4$.

It follows that such a point corresponds to a root of the equation

$$\tau^4 (k^\omega)^3 - \tau^2 (k^\omega)^2 + k^\omega/4 - 1/4 = 0 \ \text{ where } \ k^\omega \equiv k/f^2 \tag{5.19}$$

is the frequency-scaled wavenumber. The discriminant of the cubic equation (5.19) is given by $D = (2 - 27\tau^2)\tau^6/16$. This cubic equation has three real roots if $0 < D$, i.e. if

$$\tau < \sqrt{2/27} \approx 0.272 \ . \tag{5.20}$$

Two of the three real roots correspond to two points where $\Delta = 0$ and $\Delta_\alpha = 0$. Thus, a constant-β line intersects the dispersion curve IO^+ at a single point if $\sqrt{2/27} < \tau$ or at three points if $1/4 < \tau < \sqrt{2/27}$ as is illustrated in the figure on the right half of Fig.5.6.

Cartesian representation of the two outer dispersion curves for $0 \le \tau < 1/4$

The closed dispersion curve in the inner region $-k_i^- \le \alpha \le k_i^+$ is conveniently represented in the polar form (5.10b). The two open dispersion curves in the outer regions $-\infty < \alpha \le -k_o^-$ and $k_o^+ \le \alpha < \infty$ can also be represented in the polar form (5.10a) and (5.10c). However, in the special case $f = 0$,

these dispersion curves are conveniently expressed in the Cartesian form

$$F^2\alpha = \pm\sqrt{1/2+\sqrt{1/4+(F^2\beta)^2}} \text{ where } -\infty < \beta < \infty\,. \tag{5.21}$$

This Cartesian representation of the outer dispersion curves $O^{\pm}$ is now extended to the more general case $0 \le \tau < 1/4$.

Expression (5.1a) for the dispersion function Δ shows that the dispersion curves $\Delta = 0$ are roots of the quartic equation

$$s^4 - s^2 + 2\tau s - t^2 = 0 \text{ where} \tag{5.22a}$$

$$s \equiv F^2\alpha + \tau\ ,\ t^2 \equiv \tau^2 + v^2 \text{ and } v \equiv F^2\beta \tag{5.22b}$$

Addition and subtraction of the term $b\,s^2 + b^2/4$ in (5.22a) yields

$$(s^2 + b/2)^2 - (\sqrt{b+1}\,s - \sqrt{b^2/4+t^2}\,)^2 = 0 \tag{5.23}$$

if b satisfies the equation

$$b^3 + b^2 + 4\,t^2 b + 4\,v^2 = 0\,. \tag{5.24}$$

The three roots of the cubic equation (5.24) are given by

$$b_1 = -1/3 - (S+T) \tag{5.25a}$$

$$b_2 = -1/3 + (S+T)/2 - \mathrm{i}\,(S-T)\sqrt{3}/2 \tag{5.25b}$$

$$b_3 = -1/3 + (S+T)/2 + \mathrm{i}\,(S-T)\sqrt{3}/2 \text{ where}$$

$$S = (\sqrt{D} - R)^{1/3} \text{ and } T = -Q/S \text{ with } D = Q^3 + R^2 \tag{5.25c}$$

$$Q = \frac{4\tau^2 + (2F^2\beta)^2 - 1/3}{3} \text{ and } R = \frac{2\tau^2 - (2F^2\beta)^2 - 1/9}{3}\ . \tag{5.25d}$$

The root b_1 is real and the roots b_2 and b_3 are complex conjugates if $D > 0$ and $\sqrt{D} - R \ge 0$. The root b_2 is real and the roots b_1 and b_3 are complex conjugates if $D > 0$ and $\sqrt{D} - R < 0$. The three roots are real if $D \le 0$. The root b defined as

$$b = \begin{cases} b_2 & \text{if } Q^3 + R^2 > 0 \text{ and } \sqrt{Q^3+R^2} - R < 0 \\ b_1 & \text{otherwise} \end{cases} \tag{5.26}$$

is then real and is chosen. It can be verified that $-1 \le b \le 0$.

Expression (5.23) shows that the roots of (5.22) are given by the roots of the two quadratic equations

$$s^2 + \sqrt{b+1}\,s + \left(b/2 - \sqrt{b^2/4+t^2}\right) = 0 \tag{5.27a}$$

$$s^2 - \sqrt{b+1}\,s + \left(b/2 + \sqrt{b^2/4+t^2}\right) = 0 \tag{5.27b}$$

where $t^2 = v^2 + \tau^2$ in accordance with (5.22b). The quadratic equation (5.27a) has two roots

$$s^{\pm} = \pm\sqrt{\delta}/2 - \sqrt{1+b}/2 \ \text{ where} \tag{5.28a}$$

$$\delta = 1 - b + 4\sqrt{b^2/4 + \tau^2 + (F^2\beta)^2} \tag{5.28b}$$

The two roots (5.28a) are real and correspond to the two outer dispersion curves O^+ and O^- for $\tau < 1/4$.

Expressions (5.22b) and (5.28) then determine the two outer dispersion curves $O^{\pm}$ as

$$F^2\alpha^{\pm} = \pm\sqrt{\frac{1-b}{4} + \sqrt{b^2/4 + \tau^2 + (F^2\beta)^2}} - \frac{\sqrt{1+b}}{2} - \tau \tag{5.29}$$

where b is given by (5.26) with (5.25). The Cartesian representation (5.29) of the dispersion curves in the regions $-\infty < \alpha \le -k_o^-$ and $k_o^+ \le \alpha < \infty$ agrees with the representation (5.21) in the limit $f = 0$, as is required to obtain consistent representations of flows around ships steadily advancing through regular waves or in calm water.

Cartesian representation of the dispersion curves for $\tau^L \approx 0.3 \le \tau$

In the regime $\sqrt{2/27} < \tau^L \le \tau$, a constant-$\beta$ line intersects the dispersion curve O^- at a single point and similarly intersects the dispersion curve IO^+ at a single point, as was just shown and is illustrated in Fig.5.4, Fig.5.5 and Fig.5.6. The dispersion curves O^- and IO^+ can then be represented as

$$\alpha^S = \alpha_-^S(\beta^S;\tau) \ \text{ or } \ \alpha^S = \alpha_+^S(\beta^S;\tau) \tag{5.30}$$

where the Strouhal-scaling (1.33c) is used.

In the regime $\tau^L \approx 0.3 \le \tau$ now considered, expressions (5.25d) yield

$$Q^3 + R^2 > 0 \ \text{ and } \ \sqrt{Q^3+R^2} - R > 0 \ .$$

The real root b of the cubic equation (5.24) is then given by $b = b_1$ in accordance with (5.26). Specifically, this root is defined by (5.25a) and (5.25c) as

$$b = -1/3 + (\sqrt{Q^3+R^2} + R)^{1/3} - (\sqrt{Q^3+R^2} - R)^{1/3} \tag{5.31a}$$

where Q and R are defined by (5.25d). The functions $\alpha^S = \alpha_{\pm}^S(\beta^S)$ in (5.30) are given by equation (5.29), which can be expressed as

$$\alpha_{\pm}^S = \pm\sqrt{\frac{1-b}{4\tau^2} + \sqrt{b^2/(2\tau)^2 + 1 + (\beta^S)^2}/\tau} - \frac{\sqrt{1+b}}{2\tau} - 1 \ . \tag{5.31b}$$

Expressions (5.30) and (5.31) provide Cartesian representations of the dispersion curves O^- and IO^+ for $\tau^L \le \tau$ with $\tau^L \approx 0.3$.

5.2 Fundamental wavenumbers

The wavenumber k that corresponds to points (α, β) of the outer dispersion curve O^- in (5.11) and (5.15a) varies within the range

$$k_o^- \leq k < \infty \text{ for } 0 \leq \tau < \infty \,. \tag{5.32a}$$

Similarly, the wavenumber k associated with the inner dispersion curve I in (5.11) and (5.15a) varies within the ranges

$$k_i^- \leq k < k_i^+ \text{ for } 0 \leq \tau < 1/4 \,, \tag{5.32b}$$

$$k_i^- \leq k \leq k_{io} \text{ for } 1/4 \leq \tau < \infty \,, \tag{5.32c}$$

Finally, the wavenumber associated with the outer dispersion curves O^+ in (5.11) and (5.15a) varies within the ranges

$$k_o^+ \leq k < \infty \text{ for } 0 \leq \tau < 1/4 \,, \tag{5.32d}$$

$$k_{io} \leq k \leq \infty \text{ for } 1/4 \leq \tau < \infty \,. \tag{5.32e}$$

The five wavenumbers $k_o^-, k_i^-, k_i^+, k_o^+$ and α_{io} are reference wavenumbers for the inner and outer dispersion curves located in the regions (5.11) and (5.15a). These five basic wavenumbers are now considered. Expressions (5.8), (5.15b) and the relation $kF/f = k^S$ yield

$$k_{io}^S = 4\tau \text{ and } \left\{ \begin{array}{l} (k^S)_o^- = (\sqrt{1/4+\tau} + 1/2)^2/\tau \\ (k^S)_o^+ = (\sqrt{1/4-\tau} + 1/2)^2/\tau \\ (k^S)_i^- = \tau/(\sqrt{1/4+\tau} + 1/2)^2 \\ (k^S)_i^+ = \tau/(\sqrt{1/4-\tau} + 1/2)^2 \end{array} \right\} . \tag{5.33}$$

Expressions (5.33) yield

$$\left\{ \begin{array}{l} (k^S)_i^+ = 1 = (k^S)_o^+ \\ (k^S)_i^- = 1/(\sqrt{2}+1)^2 \approx 0.17 \\ (k^S)_o^- = (\sqrt{2}+1)^2 \approx 5.83 \end{array} \right\} \text{ if } \tau = 1/4 \,, \tag{5.34a}$$

$$(k^S)_i^- = 1/3 \text{ and } (k^S)_o^- = 3 \text{ if } \tau = 3/4 \,. \tag{5.34b}$$

Expressions (5.33) also show that one has

$$(k^S)_i^\pm \sim \tau \text{ and } (k^S)_o^\pm \sim 1/\tau \text{ as } \tau \to 0 \,, \tag{5.35a}$$

$$(k^S)_o^- \sim 1 \sim (k^S)_i^- \text{ as } \tau \to \infty \,. \tag{5.35b}$$

The approximations (5.35a) yield $k_i^- \sim k_i^+$ and $k_o^- \sim k_o^+$ as $\tau \to 0$, and

$$k_i^\pm / k_o^\pm \sim \tau^2 \text{ as } \tau \to 0 \,. \tag{5.36}$$

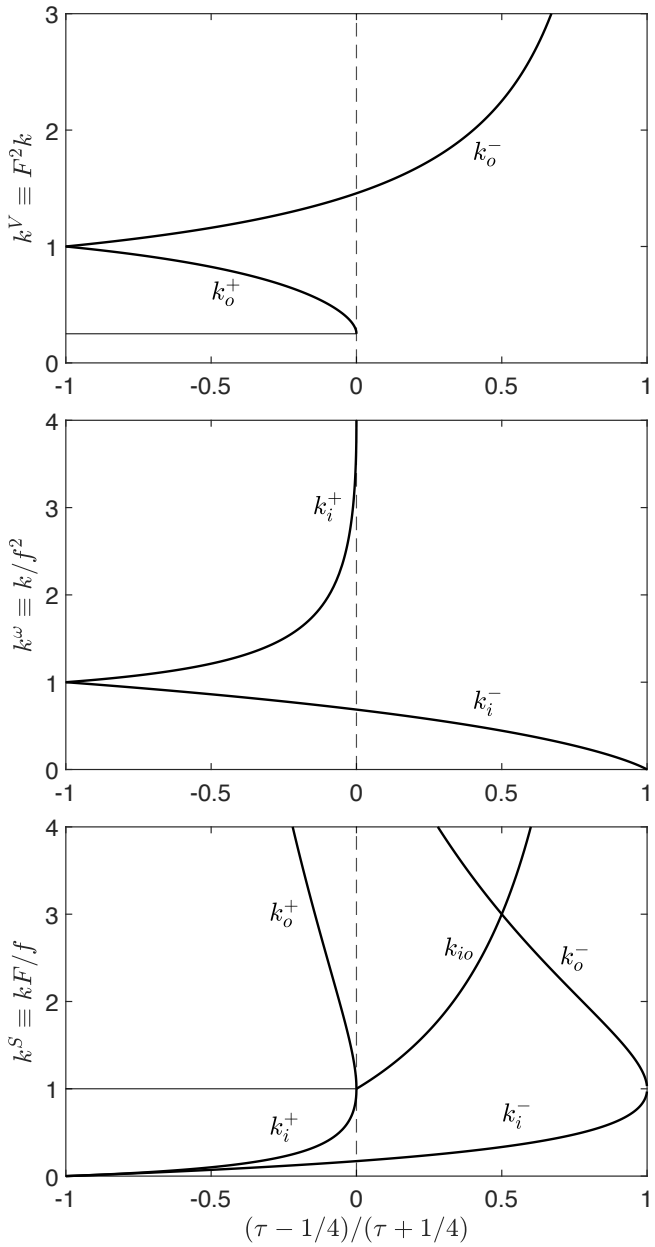

Figure 5.7: This figure depicts the speed-scaled wavenumbers $F^2 k_o^-$ and $F^2 k_o^+$ (top), the frequency-scaled wavenumbers k_i^-/f^2 and k_i^+/f^2 (center), and the Strouhal-scaled wavenumbers $k_i^\pm F/f$, $k_o^\pm F/f$ and $k_{io} F/f = 4\tau$ (bottom).

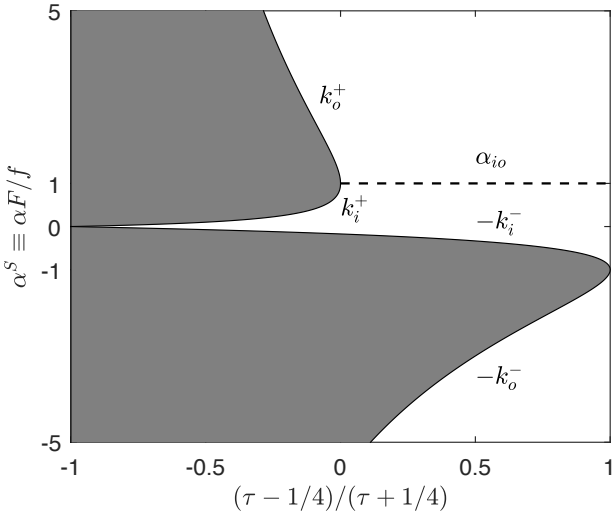

Figure 5.8: This figure depicts the Strouhal-scaled wavenumbers α^S that correspond to the boundaries $\alpha = -k_o^-,\ -k_i^-,\ k_i^+,\ k_o^+,\ \alpha_{io}$ of the regions that contain the dispersion curves associated with a ship steadily advancing through regular waves in deep water.

Thus, the inner wavenumbers k_i^- and k_i^+ are much smaller than the outer wavenumbers k_o^- and k_o^+ for small values of τ.

The basic wavenumbers $k_i^-,\ k_i^+,\ k_o^-,\ k_o^+$ given by (5.33) are depicted in Fig.5.7 for $0 \le \tau \le 1/4$. This figure also depicts the wavenumbers $k_i^-,\ k_o^-$ and k_{io} for $1/4 \le \tau < \infty$.

Fig.5.7 shows that a ship that advances through regular waves creates waves of widely different lengths, notably for $\tau < 0.2$. Indeed, the wavenumbers $k_i^\pm$ and $k_o^\pm$ (and the corresponding wavelengths $\lambda = 2\pi/k$) can differ significantly from the wavenumbers $k/f^2 = 1$ or $F^2 k = 1$ that correspond to the limit $F = 0$ or the limit $f = 0$. The wavenumbers $(k^S)_o^+$ and $(k^S)_o^-$ decrease, but $(k^S)_i^+$ and $(k^S)_i^-$ increase, as τ increases from 0 to 1/4.

Fig.5.7 also shows that k_i^- is the smallest wavenumber. Thus, a ship that advances through waves creates waves with wavenumbers $k_i^- \le k$ and wavelengths $\lambda \le 2\pi/k_i^-$.

Moreover, Fig.5.7 shows that one has

$$\left\{ \begin{array}{l} k_i^- < k_i^+ \le k_o^+ < k_o^- \\ k_i^- < k_{io} \le k_o^- \\ k_i^- < k_o^- \le k_{io} \end{array} \right\} \text{ for } \left\{ \begin{array}{l} 0 \le \tau \le 1/4 \\ 1/4 \le \tau \le 3/4 \\ 3/4 \le \tau < \infty \end{array} \right\} . \tag{5.37}$$

The dispersion curves are contained within the regions defined by (5.11)

and (5.15a) as

$$-\infty < \alpha \le -k_o^- \ , \ -k_i^- \le \alpha \le k_i^+ \ , \ k_o^+ \le \alpha < \infty \quad \text{if } \tau \le 1/4$$
$$-\infty < \alpha \le -k_o^- \ , \ -k_i^- \le \alpha \le \alpha_{io} \ , \ \alpha_{io} \le \alpha < \infty \quad \text{if } 1/4 \le \tau$$

where $k_o^\pm$ and $k_i^\pm$ are given by (5.8) and α_{io} is defined by (5.15b). The Strouhal-scaled wavenumbers α^S that correspond to $\alpha = -k_o^-$, $-k_i^-$, k_i^+, k_o^+ and α_{io} are depicted in Fig.5.8 for $0 \le \tau < \infty$.

5.3 Limits $\tau \to 0$ or $\tau \to \infty$

The dispersion curves associated with ship motions in regular waves and the related fundamental wavenumbers are now further considered in the limit $\tau \to 0$ and the limit $\tau \to \infty$.

Limit $\tau \to 0$

Expressions (5.8) yield the asymptotic approximations

$$F^2 k_o^+ \sim 1 - 2\tau - \tau^2 \ \text{ and } \ F^2 k_o^- \sim 1 + 2\tau - \tau^2 \ \text{ as } \ \tau \to 0 \ , \tag{5.38a}$$
$$k_i^+/f^2 \sim 1 + 2\tau + 5\tau^2 \ \text{ and } \ k_i^-/f^2 \sim 1 - 2\tau + 5\tau^2 \ \text{ as } \ \tau \to 0 \ . \tag{5.38b}$$

These approximations yield $k_i^\pm \sim \tau^2 k_o^\pm$ as $\tau \to 0$ in agreement with (5.36). Moreover, as is noted in (5.12), expressions (5.10a) and (5.10c) both become $F^2 k = 1/\cos^2\gamma$ and expression (5.10b) becomes $k/f^2 = 1$ in the limit $\tau = 0$, in agreement with the dispersion relations (2.10) and (4.4) associated with wave diffraction-radiation by offshore structures and steady ship waves.

Indeed, for $0 \le \tau \le 0.1$, the dispersion curve associated with the inner region $-k_i^- \le \alpha \le k_i^+$ in (5.11) does not differ greatly from the dispersion circle $k = f^2$ that corresponds to the special case $F = 0$ and offshore structures in regular waves, as can be observed in Fig.5.2. Similarly, for $0 \le \tau \le 0.1$, the dispersion curves associated with the two outer regions $\alpha \le -k_o^-$ and $k_o^+ \le \alpha$ in (5.11) do not differ greatly from the dispersion curves associated with the special case $f = 0$ and steady ship waves, as can also be observed in Fig.5.2.

The dispersion curve in the inner region $-k_i^- \le \alpha \le k_i^+$ in (5.11) corresponds to the limit $F \ll 1$ with $f = O(1)$ that is associated with a ship that advances through regular waves at low speed or an offshore structure in a uniform current, for which the ship creates short waves with $O(F^2)$ wavelengths. The dispersion curves in the outer regions $\alpha \le -k_o^-$ and $k_o^+ \le \alpha$ correspond to the limit $f \ll 1$ with $F = O(1)$ associated with a ship that advances through long (low-frequency) waves.

Thus, the inner and outer dispersion curves in (5.11) are associated with a decomposition of the limit $fF \to 0$ into the two limits

$$F \to 0 \text{ with } f = O(1) \quad \text{and} \quad f \to 0 \text{ with } F = O(1) \,.$$

The dispersion relation (5.1a) can be expressed in the alternative forms

$$(1 + \tau\, k^{\omega} \cos\gamma)^2 = k^{\omega} \text{ where } k^{\omega} \equiv k/f^2 \,, \tag{5.39a}$$

$$(k^{V} \cos\gamma + \tau)^2 = k^{V} \text{ where } k^{V} \equiv F^2 k \,, \tag{5.39b}$$

associated with the frequency-scaled or speed-scaled wavenumbers k^{ω} or k^{V} that are appropriate for an offshore structure in regular waves or a ship steadily advancing in calm water, and are related to the dispersion curves defined by (5.6a) and (5.6b).

The dispersion relations (5.39) can be expressed as

$$\kappa - 1 - 2\tau\,\kappa \cos\gamma - \tau^2 \kappa^2 \cos^2\gamma = 0 \text{ where } \kappa \equiv k/f^2 \,, \tag{5.40a}$$

$$\kappa - \kappa^2 \cos^2\gamma - 2\tau\,\kappa \cos\gamma - \tau^2 = 0 \text{ where } \kappa \equiv F^2 k \,, \tag{5.40b}$$

respectively. The dispersion curves defined by these dispersion relations can be studied in the limit $\tau \to 0$ via the asymptotic expansion

$$\kappa \sim \kappa_0 + \tau\,\kappa_1 + \tau^2 \kappa_2 + \tau^3 \kappa_3 + \cdots$$

By substituting this expansion into the dispersion relations (5.40) and grouping the expressions that are $O(1)\,, O(\tau), O(\tau^2), \ldots$ one obtains

$$k/f^2 \sim 1 + 2\,\mu + 5\,\mu^2 + 14\,\mu^3 + 42\,\mu^4 + 132\,\mu^5 + \cdots \tag{5.41a}$$

$$F^2 k \cos^2\gamma \sim 1 - 2\,\mu - \mu^2 - 2\,\mu^3 - 5\,\mu^4 - 14\,\mu^5 + \cdots \tag{5.41b}$$

$$\text{as } \mu \equiv \tau \cos\gamma \to 0 \,.$$

The asymptotic approximation (5.41a), where $-\pi \le \gamma \le \pi$, defines the inner dispersion curve associated with the limit $F \to 0$ with $f = O(1)$ that corresponds to wave diffraction-radiation at low forward speed. The approximation (5.41b) defines the outer dispersion curves corresponding to diffraction-radiation of long waves and the limit $f \to 0$ with $F = O(1)$. The ranges $-\pi/2 < \gamma < \pi/2$ and $\pi/2 < \gamma < 3\pi/2$ in (5.41b) define two distinct dispersion curves.

Limit $\tau \to \infty$

The asymptotic approximations (5.35b) show that Strouhal scaling of the Fourier plane is appropriate for large values of τ associated with diffraction-radiation of regular waves in the high-frequency and/or high-speed regimes. Indeed, expressions (5.33) yield

$$(k^S)_i^- \sim 1 - \frac{1}{\sqrt{\tau}} + \frac{1}{2\tau} \text{ and } (k^S)_o^- \sim 1 + \frac{1}{\sqrt{\tau}} + \frac{1}{2\tau} \text{ as } \tau \to \infty \,. \tag{5.42}$$

The dispersion relation (5.1a) can be expressed as

$$(1+\alpha^S)^2 \equiv (1+k^S\cos\gamma)^2 = k^S/\tau \ . \tag{5.43}$$

This dispersion relation yields the dispersion curves $\alpha^S = -1$ in the limit $\tau \to \infty$. The dispersion curves defined by (5.43) are depicted in Fig.5.5 for several large values of τ in the Strouhal-scaled Fourier plane appropriate in the high-speed and/or high-frequency regime.

5.4 Wave patterns

The far-field wave patterns associated with the dispersion curves analyzed in the previous section are now considered.

Analytical representation of wave patterns

The far-field wave pattern that corresponds to a dispersion function Δ is determined from Δ via the general parametric equations (3.18), where σ^Δ is given by (2.53c) for the dispersive waves considered in this chapter. The patterns of far-field waves created by a ship that steadily advances through regular waves are then determined by the parametric equations

$$\mathbf{h}_n \equiv \left\{ \begin{matrix} x_n \\ y_n \end{matrix} \right\} = \frac{2\,n\,\pi\,\sigma^\Delta}{k\,\Delta_k} \left\{ \begin{matrix} \Delta_\alpha \\ \Delta_\beta \end{matrix} \right\} \text{ where } \sigma^\Delta = \text{sign}(\alpha_{io} - \alpha) \ , \tag{5.44a}$$

expression (5.15b) for α_{io} was used and Δ is the dispersion function (2.9). The derivatives Δ_α, Δ_β and Δ_k of Δ in (5.44a) are given by (2.31c) as

$$\left\{ \begin{matrix} \Delta_\alpha = 2F(f + Fk\cos\gamma) - \cos\gamma \\ \Delta_\beta = -\sin\gamma \\ \Delta_k = 2F(f + Fk\cos\gamma)\cos\gamma - 1 \end{matrix} \right\} \tag{5.44b}$$

where the wavenumber k is defined in terms of the wave-propagation angle γ via the dispersion relation (5.1a).

The three regions (5.11) and (5.15a) associated with the inner and outer dispersion curves for $\tau \le 1/4$ or $1/4 \le \tau$ and Fig.5.8 show that the sign-function σ^Δ in (5.44a) is given by

$$\sigma^\Delta = 1 \ \text{ in } \ -\infty < \alpha \le -k_o^- \ \text{ for all values of } \tau \ , \tag{5.45a}$$

$$\sigma^\Delta = 1 \ \text{ in } \left\{ \begin{matrix} -k_i^- \le \alpha \le k_i^+ \ \text{ for } \ \tau \le 1/4 \\ -k_i^- \le \alpha < \alpha_{io} \ \text{ for } \ 1/4 \le \tau \end{matrix} \right\} , \tag{5.45b}$$

$$\sigma^\Delta = -1 \ \text{ in } \left\{ \begin{matrix} k_o^+ \le \alpha < \infty \ \text{ for } \ \tau \le 1/4 \\ \alpha_{io} \le \alpha < \infty \ \text{ for } \ 1/4 \le \tau \end{matrix} \right\} . \tag{5.45c}$$

The parametric representation (5.44) of the wave patterns yields the alternative representations

$$\left\{\begin{matrix} x_n^\omega \\ y_n^\omega \end{matrix}\right\} = \frac{2\,n\,\pi\,\sigma^\Delta/k^\omega}{1-2\,\tau\,(1+\tau\,k^\omega\cos\gamma)\cos\gamma} \left\{\begin{matrix} \cos\gamma - 2\,\tau(1+\tau\,k^\omega\cos\gamma) \\ \sin\gamma \end{matrix}\right\}, \tag{5.46a}$$

$$\left\{\begin{matrix} x_n^V \\ y_n^V \end{matrix}\right\} = \frac{2\,n\,\pi\,\sigma^\Delta/k^V}{2\,(\tau+k^V\cos\gamma)\cos\gamma - 1} \left\{\begin{matrix} 2\,(\tau+k^V\cos\gamma) - \cos\gamma \\ -\sin\gamma \end{matrix}\right\}, \tag{5.46b}$$

$$\left\{\begin{matrix} x_n^S \\ y_n^S \end{matrix}\right\} = \frac{2\,n\,\pi\,\sigma^\Delta/k^S}{2\,\tau\,(1+k^S\cos\gamma)\cos\gamma - 1} \left\{\begin{matrix} 2\,\tau(1+k^S\cos\gamma) - \cos\gamma \\ -\sin\gamma \end{matrix}\right\} \tag{5.46c}$$

in terms of the frequency-scaling, the speed-scaling or the Strouhal-scaling defined by (1.33).

The wave patterns that correspond to the inner and outer dispersion curves located in the regions (5.11) and (5.15a) are then determined by the alternative parametric equations (5.46) with expressions (5.45) for the sign function σ^Δ and the corresponding alternative polar representations (5.10), (5.14), (5.18) of the dispersion curves. These alternative representations of the dispersion curves and the related wave patterns correspond to the alternative scalings defined by (1.33) associated with the alternative choices

$$L_r = g/\omega^2\ ,\ \ L_r = V_s^2/g\ ,\ \ L_r = V_s/\omega \tag{5.47}$$

of reference length L_r.

Wave patterns for $\tau \leq 1/4$

The frequency-scaled parametric representation (5.46a) is best suited to represent the waves associated with the dispersion curve I defined by (5.10b) and located in the inner region $-k_i^- \leq \alpha \leq k_i^+$ in (5.11) for $\tau \leq 1/4$. These waves, depicted in Fig.5.9 for several values of τ within the range $0 \leq \tau \leq 1/4$, form a set of roughly circular waves, called 'ring waves' hereafter. These ring waves are concentric circular waves in the limit $\tau = 0$.

The speed-scaled parametric representation (5.46b) is best suited to represent the waves associated with the outer dispersion curves O^- and O^+ that are defined by (5.10a) and (5.10c) and are located in the two outer regions $-\infty < \alpha \leq -k_o^-$ and $k_o^+ \leq \alpha < \infty$ in (5.11) for $\tau \leq 1/4$. These two wave patterns are depicted in Fig.5.10 for several values of τ within the range $0 \leq \tau \leq 1/4$.

The wave patterns depicted in Fig.5.10 are qualitatively similar to the Kelvin wake of a ship advancing in calm water considered in chapter 4. In fact, these waves contain transverse and divergent waves inside the wedges formed by cusps of the wave patterns. The cusp angles of the two wave

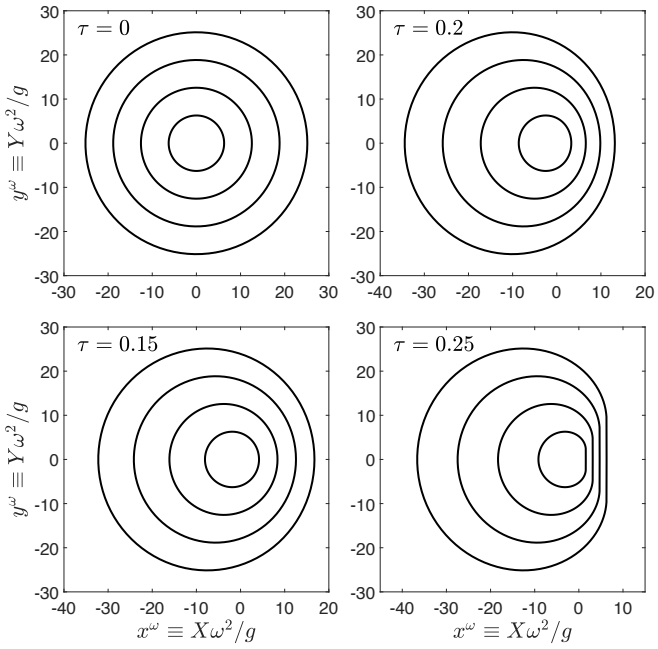

Figure 5.9: Frequency-scaled ring waves associated with the inner dispersion curve I in the region $-k_i^- \leq \alpha \leq k_i^+$ for $\tau = 0$, 0.15, 0.2 and 0.25.

patterns, called 'inner V waves' and 'outer V waves' hereafter, depicted in Fig.5.10 vary with τ, as is considered further on. These inner and outer V waves are associated with the dispersion curves O^- or O^+ located in the outer regions $-\infty < \alpha \leq -k_o^-$ or $k_o^+ \leq \alpha < \infty$, respectively, in (5.11).

Wave patterns for $1/4 \leq \tau$

The inner V waves associated with the outer dispersion curve O^- and the region $-\infty < \alpha \leq -k_o^-$ in (5.11) and (5.15a) exist in the regime $\tau \leq 1/4$ considered in Fig.5.10 and also exist in the regime $1/4 \leq \tau$. The patterns of inner V waves are depicted in Fig.5.11 for several values of τ within the range $0 \leq \tau \leq 1$. This figure shows that the inner V waves are qualitatively similar for $1/4 \leq \tau$ and $\tau < 1/4$. Fig.5.11 also shows that the cusp angle, denoted as ψ_i^V, of the inner V waves decreases as τ increases and is smaller than the Kelvin angle $\psi^K \approx 19°28'$, which corresponds to the limit $\tau = 0$.

In addition to the inner V waves associated with the outer dispersion curve O^- and the region $-\infty < \alpha \leq -k_o^-$ in (5.15a), a ship that advances through regular waves at $1/4 < \tau$ creates two sets of waves that correspond to the inner dispersion curve I and the outer dispersion curve O^+ associated

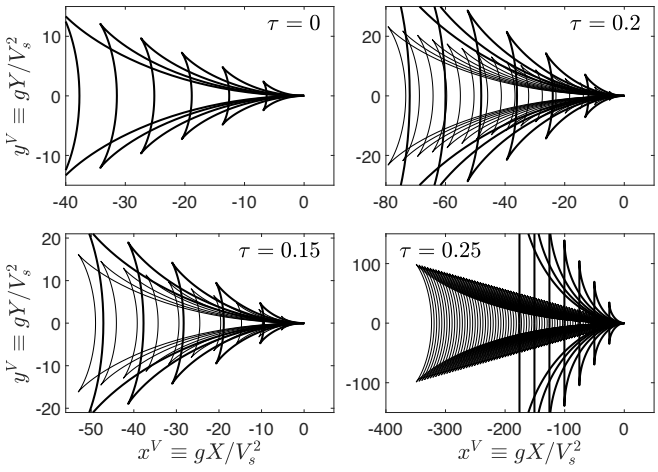

Figure 5.10: Speed-scaled inner and outer V waves associated with the outer dispersion curves O^- and O^+ in the two regions $-\infty < \alpha \leq -k_o^-$ and $k_o^+ \leq \alpha < \infty$ for $\tau = 0$, 0.15, 0.2 and 0.25.

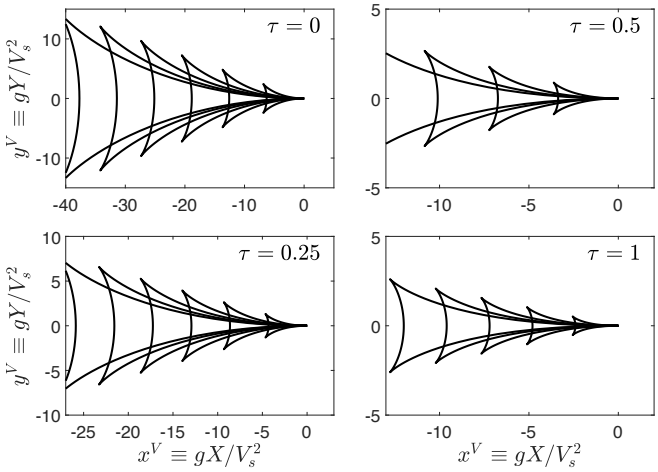

Figure 5.11: Speed-scaled inner V waves associated with the outer dispersion curve O^- in the region $-\infty < \alpha \leq -k_o^-$ for $\tau = 0$, 0.25, 0.5 and 1.

with the contiguous regions $-k_i^- \leq \alpha \leq \alpha_{io}$ and $\alpha_{io} \leq \alpha < \infty$ in (5.15a). The waves associated with the dispersion curves I and O^+ in the regime $1/4 \leq \tau$ form a pattern of partial (incomplete) rings and fan-like waves, called 'ring-fan waves' hereafter, that are connected by cusps. These ring-fan waves are depicted in Fig.5.12 for several values of $1/4 \leq \tau$.

More precisely, the waves that correspond to the inner dispersion curve I associated with the region $-k_i^- \leq \alpha \leq \alpha_{io}$ in (5.15a) form a set of 'partial-

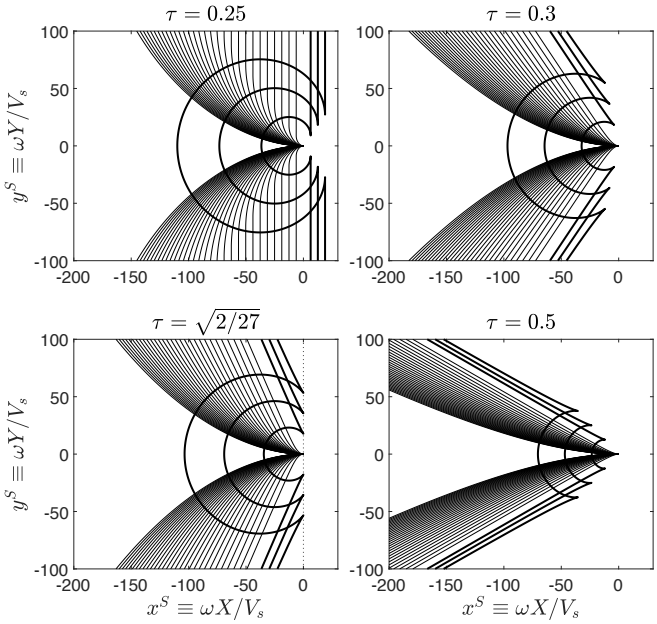

Figure 5.12: Strouhal-scaled partial-ring and fan waves associated with the dispersion curve IO^+ in the two contiguous regions $-k_i^- \leq \alpha \leq \alpha_{io}$ and $\alpha_{io} \leq \alpha < \infty$ for $\tau = 0.25$, $\sqrt{2/27} \approx 0.272$, 0.3 and 0.5.

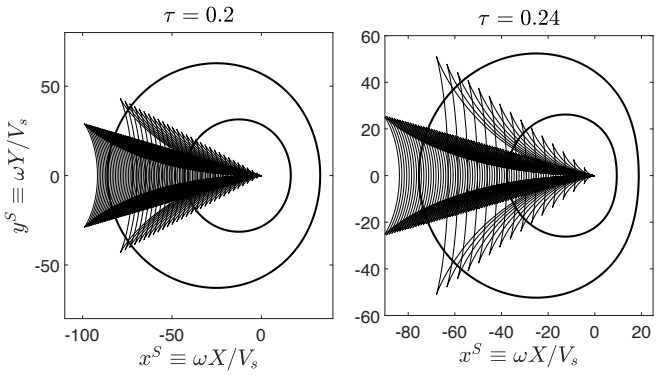

Figure 5.13: This figure depicts all the (Strouhal-scaled) wave patterns for two values of τ within the regime $\tau < 0.25$, for which three families of waves—inner and outer V waves, and ring waves—exist. The inner and outer V waves are much shorter than the ring waves and only exist behind the ship, whereas the ring waves exist ahead and behind the ship.

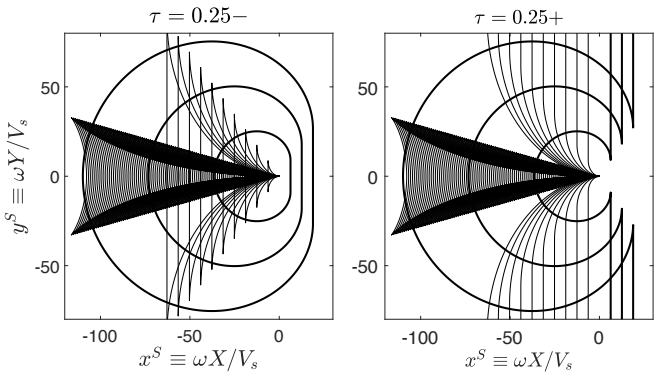

Figure 5.14: This figure depicts all the (Strouhal-scaled) wave patterns for $\tau = 0.25^-$ and $\tau = 0.25^+$.

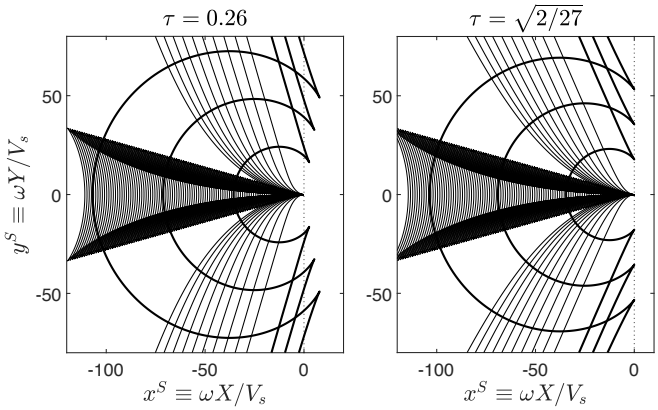

Figure 5.15: This figure depicts all the (Strouhal-scaled) wave patterns for two values of τ within the range $0.25 < \tau \leq \sqrt{2/27} \approx 0.272$, for which three families of waves—inner V waves, partial ring waves, and (inner and outer) fan waves—exist. The inner V waves and the inner fan waves only exist behind the ship, whereas the partial ring and the outer fan waves exist ahead and behind the ship in the regime $0.25 < \tau < \sqrt{2/27}$.

ring waves' and 'outer-fan waves' that are connected at cusps. The waves that correspond to the outer dispersion curve O^+ associated with the region $\alpha_{io} \leq \alpha < \infty$ in (5.15a) form a system of fan waves, called 'inner-fan waves'. The line that separates the 'outer-fan waves' and the 'inner-fan waves' corresponds to the boundary $\alpha = \alpha_{io}$ between the inner region I and the outer region O^+ in (5.15a). This separation line is considered further on.

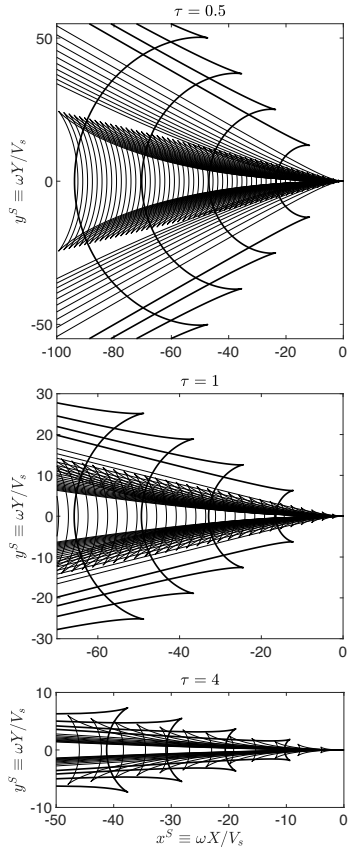

Figure 5.16: This figure depicts all the (Strouhal-scaled) wave patterns for three values of τ within the regime $\sqrt{2/27} \approx 0.272 < \tau$, for which no waves exist ahead of the ship and three families of waves—inner V waves, partial ring waves, and (inner and outer) fan waves—exist behind the ship.

Complete wave patterns for $0 \leq \tau$

The complete wave patterns that correspond to the inner dispersion curve I and the outer dispersion curves O^- and O^+ or IO^+ are depicted in Figs 5.13-5.16. Specifically, Fig.5.13 depicts all the wave patterns created by a ship that steadily advances through regular waves at two values of τ in the regime $\tau < 0.25$. Fig.5.14 similarly depicts all the wave patterns for $\tau = 0.25^-$ and $\tau = 0.25^+$. The wave patterns for two values of τ in the regime $0.25 < \tau \leq \sqrt{2/27} \approx 0.272$ are depicted in Fig.5.15. Finally, Fig.5.16 depicts the wave patterns for three values of τ in the regime $\sqrt{2/27} < \tau$, for which no waves exist ahead of the ship.

Figs 5.13-5.16 show that a ship that advances through regular waves creates a rich set of diverse waves of widely different lengths, in accordance with Fig.5.7. These four figures also show that the wave patterns vary rapidly for values of τ in the vicinity of $\tau = 1/4$.

5.5 Main features of wave patterns

The speed-scaled form of the dispersion relation (5.1b) yields

$$\beta^V = \sqrt{(\alpha^V + \tau)^4 - (\alpha^V)^2} \text{ and } k^V = (\alpha^V + \tau)^2 \tag{5.48a}$$

where only the upper half $\beta^V \geq 0$ is considered due to symmetry. The relations $\cos\gamma \equiv \alpha^V/k^V$ and $\sin\gamma \equiv \beta^V/k^V$ and expression (5.46b) then yield

$$\tan\psi^* \equiv \frac{y_n^V}{-x_n^V} = \frac{\sqrt{(\alpha^V + \tau)^4 - (\alpha^V)^2}}{2(\alpha^V + \tau)^3 - \alpha^V} = \frac{\sqrt{\tau^2(\alpha^S + 1)^4 - (\alpha^S)^2}}{2\tau^2(\alpha^S + 1)^3 - \alpha^S} \tag{5.48b}$$

where ψ^* is measured from the negative x axis ($x < 0, y = 0$) i.e. from the ship track, which corresponds to $\psi = \pi$ and $\psi^* = 0$. The relations (5.48) are used further on in section 5.5.

Basic components of wave patterns

The inner V waves depicted in Fig.5.11 consist of transverse and divergent waves located inside a wedge formed by the cusps of the wave pattern. These divergent / transverse waves are associated with the contiguous portions

$$\text{Divergent inner V waves:} \quad -\infty < \alpha \leq -a_{iV}^c \tag{5.49a}$$

$$\text{Transverse inner V waves:} \quad -a_{iV}^c \leq \alpha \leq -k_o^- \tag{5.49b}$$

of the outer dispersion curve O^- located in the region $-\infty < \alpha \leq -k_o^-$ in (5.11) and (5.15a). The wavenumber $\alpha = -a_{iV}^c$ that separates the divergent and transverse inner V waves and corresponds to the cusps of the pattern of inner V waves is given further on.

The outer V waves, which exist if $\tau \leq 1/4$ and are depicted in Fig.5.10, similarly consist of transverse and divergent waves, which are associated with the contiguous portions

$$\text{Transverse outer V waves:} \quad k_o^+ \leq \alpha \leq a_{oV}^c \tag{5.50a}$$

$$\text{Divergent outer V waves:} \quad a_{oV}^c \leq \alpha < \infty \tag{5.50b}$$

of the outer dispersion curve O^+ located in the region $k_0^+ \leq \alpha < \infty$ in (5.11). The wavenumber $\alpha = a_{oV}^c$ that separates the transverse and divergent outer

V waves and corresponds to the cusps of the pattern of outer V waves is given further on.

Finally, the ring-fan waves, which exist if $1/4 \leq \tau$ and are depicted in Fig.5.12, consist of partial-ring waves and outer and inner fan-like waves. These waves, located inside a wedge formed by the cusps of the pattern of ring-fan and outer-fan waves, are associated with the contiguous portions

$$\text{Partial ring waves}: \; -k_i^- \leq \alpha \leq a_{rf}^c \tag{5.51a}$$

$$\text{Outer fan waves}: \; a_{rf}^c \leq \alpha \leq \alpha_{io} \tag{5.51b}$$

$$\text{Inner fan waves}: \; \alpha_{io} \leq \alpha < \infty \tag{5.51c}$$

of the dispersion curve IO^+ located in the region $-k_i^- \leq \alpha < \infty$ in (5.15c).

Fan-waves angle ψ_f^* and asymptote lines

The inner and outer fan waves in (5.51) are separated by a straight line that corresponds to $\alpha = \alpha_{io}$, i.e. $\alpha^V = \tau$. Expression (5.48b) then shows that the angle, denoted as ψ_f^*, of the line that divides the inner and outer fan waves is given by

$$\tan\psi_f^* = 1/\sqrt{16\tau^2 - 1} \;\text{ where }\; 1/4 \leq \tau\,. \tag{5.52a}$$

This expression yields

$$90^\circ \geq \psi_f^* > 0 \;\text{ as }\; 1/4 \leq \tau < \infty \tag{5.52b}$$

and shows that the angle of the fan waves decreases as τ increases, as is illustrated in Fig.5.12 and Fig.5.16. These figures and Fig.5.15 show that the lines $\psi = \pm\psi_f^*$ are asymptote lines of the wave patterns, in accordance with the analysis given in section 3.6. Specifically, expressions (5.44b) and (5.15b) show that one has $k\,\Delta_k = 0$ if $\alpha = \alpha_{io}$ and $k = k_{io}$.

Cusps of wave patterns

The cusps of the wave patterns depicted in Figs.5.10–5.16 stem from inflection points of the dispersion curves defined by (5.48a). These inflection points are determined by the inflection-point condition $d^2\beta^V/d(\alpha^V)^2 = 0$, in accordance with (3.24d). The dispersion relations (5.48a) then yield the equivalent alternative quartic equations

$$2\,(\alpha^V + \tau)^4 - 3\,(\alpha^V)^2 + 2\,\tau\,\alpha^V - \tau^2 = 0\;, \tag{5.53a}$$

$$2\,\tau^2\,(\alpha^S + 1)^4 - 3\,(\alpha^S + 1)^2 + 8\,(\alpha^S + 1) - 6 = 0\;, \tag{5.53b}$$

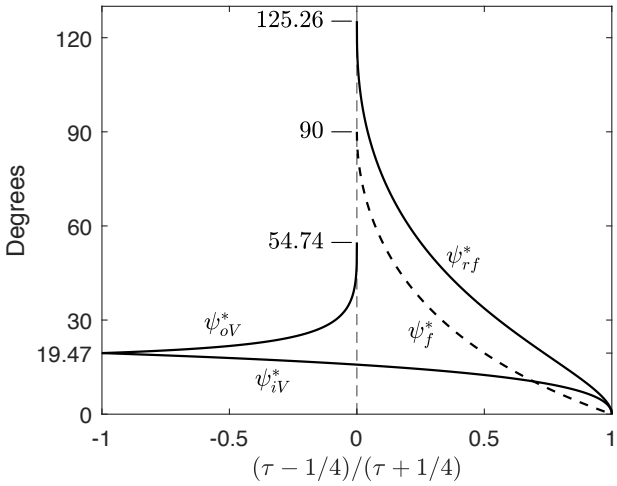

Figure 5.17: This figure depicts the angle ψ^*_f of the fan waves and the cusp angles ψ^*_{iV}, ψ^*_{oV} and ψ^*_{rf} of the inner V waves, the outer V waves and the ring-fan waves.

in accordance with the relation $\alpha^V = \tau\alpha^S$. The cusps of the wave patterns created by a ship that advances through regular waves are then determined by (5.48b) where α^V are roots of the quartic equation (5.53).

The angle, denoted as ψ^*_{iV}, of the cusps of the inner V waves corresponds to the root α^V of (5.53) that is located in the region $-\infty < \alpha \leq -k_o^-$ in (5.11) if $\tau \leq 1/4$ or (5.15a) if $1/4 \leq \tau$. Similarly, the angle ψ^*_{oV} of the cusps of the outer V waves, which exist if $\tau \leq 1/4$, corresponds to the root α^V of equation (5.53) that is located within the region $k_o^+ < \alpha < \infty$ in (5.11). Finally, the angle ψ^*_{rf} of the cusps of the ring-fan waves, which exist if $1/4 \leq \tau$, corresponds to the root α^V of equation (5.53) that is located within the region $-k_i^- \leq \alpha \leq \alpha_{io}$ in (5.15a).

Limits $\tau = 0$ and $\tau \to \infty$

In the special case $\tau = 0$, equation (5.53) yields the roots $\alpha^V = \pm\sqrt{3/2}$. Expressions (5.48) then yield $k^V = 3/2$, $\beta^V = \sqrt{3}/2$, $\tan\gamma = \pm 1/\sqrt{2}$ and $\tan\psi^* = \pm 1/\sqrt{8}$, in agreement with expressions (4.22b), (4.17), and (4.16b) obtained in chapter 4 for ship waves in calm deep water. Thus, the cusp angles ψ^*_{iV} and ψ^*_{oV} of the inner and outer V waves are identical to the Kelvin angle ψ^K in the limit $\tau \to 0$, i.e. one has

$$\psi^*_{iV} \to \psi^K \text{ and } \psi^*_{oV} \to \psi^K \text{ as } \tau \to 0\,. \tag{5.54}$$

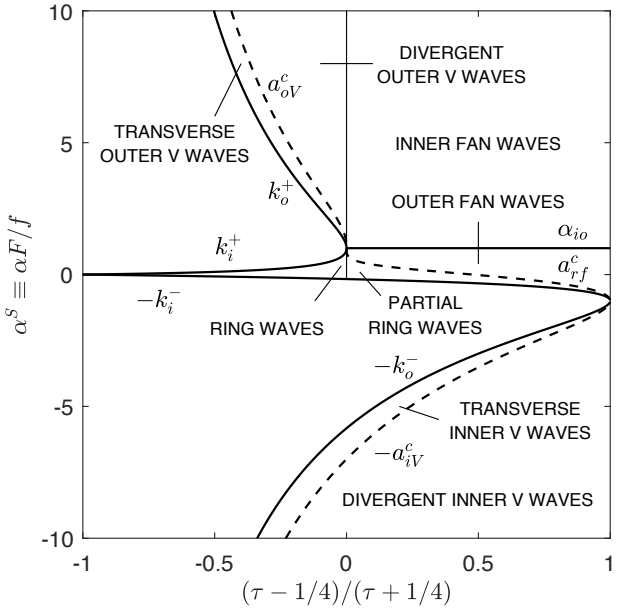

Figure 5.18: This figure depicts the Strouhal-scaled values of α^S that are associated with the regions where ring waves, inner and outer V waves, partial-ring waves, and outer and inner fan waves exist.

Equation (5.53b) yields the root

$$(\alpha^S + 1)^2 \sim \sqrt{3}/\tau \ \text{ as } \ \tau \to \infty \, . \tag{5.55a}$$

This asymptotic approximation and expressions (5.48a) and (5.48b) yield

$$\alpha^S \to -1 \ , \ \ \beta^S \to \sqrt{2} \ , \ \ k^S \to \sqrt{3} \ , \ \ \psi^* \to 0 \ \text{ as } \ \tau \to \infty \, . \tag{5.55b}$$

Thus, the cusp angles ψ^*_{iV} and ψ^*_{rf} of the inner V waves and the ring-fan waves vanish in the limit $\tau \to \infty$, i.e. one has

$$\psi^*_{iV} \to 0 \text{ and } \psi^*_{rf} \to 0 \text{ as } \tau \to \infty \, . \tag{5.56}$$

No waves ahead of a ship if $\tau > \sqrt{2/27} \approx 0.272$

Expression (5.48b) shows that one has $x_n = 0$ if

$$2\,(\alpha^V + \tau)^3 = \alpha^V . \tag{5.57}$$

This relation and the inflection-point condition (5.53a) are satisfied if

$$\tau = \sqrt{2/27} \approx 0.272 \ \text{ and } \ \alpha^S = 1/2 \, . \tag{5.58}$$

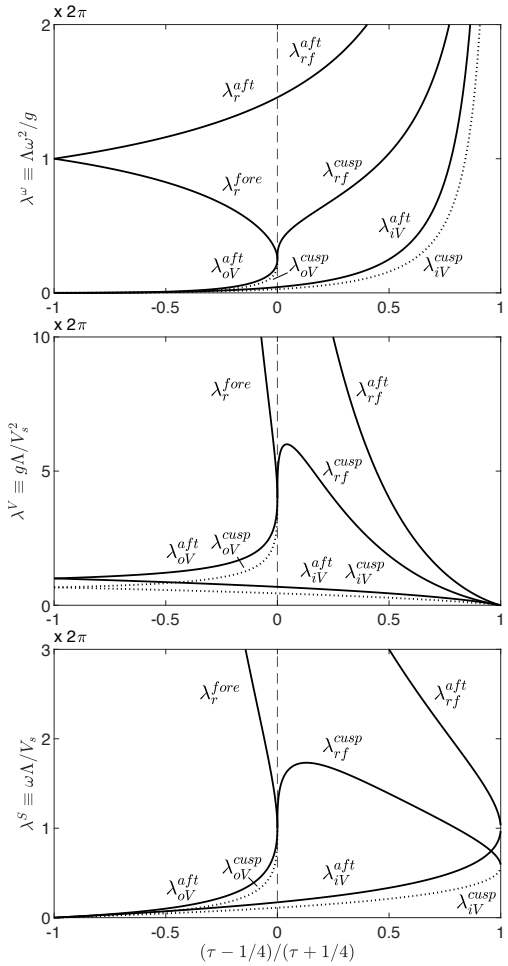

Figure 5.19: These figures depict the wavelengths $\lambda_r^{aft}(\tau)$ and $\lambda_r^{fore}(\tau)$ of the ring waves aft or fore of a ship that steadily advances through regular waves at $\tau < 1/4$, and also depict the wavelength $\lambda_{oV}^{aft}(\tau)$ of the transverse outer V waves aft of the ship and the corresponding wavelength $\lambda_{oV}^{cusp}(\tau)$ at the cusps for $\tau < 1/4$. Moreover, the figures depict the wavelength $\lambda_{iV}^{aft}(\tau)$ of the transverse inner V waves aft of the ship and the wavelength $\lambda_{iV}^{cusp}(\tau)$ at the cusps of the pattern of inner V waves, which exist for $0 \leq \tau$. Finally, the figures depict the wavelength $\lambda_{rf}^{aft}(\tau)$ of the transverse ring-fan waves aft of the ship and the corresponding wavelength $\lambda_{rf}^{cusp}(\tau)$ at the cusps of the pattern of ring-fan waves for $1/4 < \tau$. The top, middle, bottom figures depict frequency-scaled wavenumbers $\lambda^{\omega} = \Lambda\omega^2/V_s$, speed-scaled wavenumbers $\lambda^V = \Lambda g/V_s^2$ or Strouhal-scaled wavenumbers $\lambda^S = \Lambda\omega/V_s^2$.

The foregoing analysis shows that a ship that advances through regular waves does not create waves ahead of the ship if $\tau > \sqrt{2/27} \approx 0.272$, as can be observed in Figs.5.12 and 5.15.

Special case $\tau = 1/4$

The relations (5.57) and (5.53a) are also satisfied if

$$\tau = 1/4 \text{ and } \alpha^S = 1 \, .$$

However, Figs.5.12 and 5.14 show that waves exist ahead of a ship in this case, for which one has both $x_n = 0$ and $y_n = 0$ in (5.48b).

In the special case $\tau = 1/4$, the quartic equation (5.53) has two roots $\alpha^V = -7/4$ and $\alpha^V = 1/4$. The root $\alpha^V = -7/4$ corresponds to the cusps of the inner V waves for $\tau = 0.25$, and the root $\alpha^V = 1/4$ corresponds to the cusps of the outer V waves for $\tau = 0.25^-$ or the cusps of the ring-fan waves for $\tau = 0.25^+$. One then has

$$F^2 a^c_{iV} = 7/4 \text{ and } F^2 a^c_{oV} = 1/4 = F^2 a^c_{rf} \text{ if } \tau = 1/4 \tag{5.59}$$

in (5.49), (5.50) and (5.51). Expressions (5.59) and (5.48a) then yield

$$(\alpha^c_{iV}, \beta^c_{iV}, k^c_{iV}) = (-7, 4\sqrt{2}, 9) f/F \text{ and} \tag{5.60a}$$

$$(\alpha^c_{oV}, \beta^c_{oV}, k^c_{oV}) = (1, 0, 1) f/F = (\alpha^c_{rf}, \beta^c_{rf}, k^c_{rf}) \tag{5.60b}$$

in the special case $\tau = 1/4$. Expressions (5.60a) and (5.48b) show that the cusp angle ψ^*_{iV} of the inner V waves is given by

$$\psi^*_{iV} = \arctan(\sqrt{2}/5) \approx 15°48' \text{ if } \tau = 1/4 \, . \tag{5.61}$$

The numerator and the denominator of expression (5.48b) both vanish if $\tau = 1/4$ and $\alpha^V = 1/4$. Expression (5.53b) yields

$$(16\,\tau^2 - 1) A^4 = 3 - 8A + 6A^2 - A^4 \text{ where } 2A \equiv \alpha^S + 1 \, .$$

This equation shows that one has $A = 1$ if $\tau = 1/4$ and

$$A \sim 1 - (4\tau - 1)^{1/3} / 2^{1/3} \text{ as } \tau \to 1/4$$

as can be verified via substitution. One then has

$$\alpha^S \sim 1 - 2^{2/3} (4\,\tau - 1)^{1/3} \text{ as } \tau \to 1/4 \, . \tag{5.62}$$

Thus, one has $\alpha^S \to 1 \mp 0$ as $\tau \to 1/4 \pm 0$. The asymptotic approximation (5.62) and expression (5.48b) finally yield $\tan\psi^* \to \mp\sqrt{2}$ as $\tau \to 1/4 \pm 0$. One then has

$$\tan\psi^*_{oV} = \sqrt{2} \text{ and } \psi^*_{oV} \approx 54°44' \text{ if } \tau = 1/4 \, , \tag{5.63a}$$

$$\tan\psi^*_{rf} = -\sqrt{2} \text{ and } \psi^*_{rf} \approx 125°16' \text{ if } \tau = 1/4 \, . \tag{5.63b}$$

Moreover, one has

$$\psi^K \approx 19^\circ 28' \leq \psi^*_{oV} \leq 54^\circ 44' \text{ as } 0 \leq \tau \leq 1/4 \,, \tag{5.64a}$$

$$125^\circ 16' \geq \psi^*_{rf} > 0 \text{ as } 1/4 \leq \tau < \infty \,. \tag{5.64b}$$

Thus, the angle ψ^*_{oV} of the wedge that contains the outer V waves increases as τ increases within the range $0 \leq \tau \leq 1/4$ for which outer V waves exist, and the angle ψ^*_{rf} of the wedge that contains the ring-fan waves decreases as τ increases within the range $1/4 \leq \tau$ for which these waves exist.

Cusp angles for all values of $0 \leq \tau$

The roots of the quartic equation (5.53) are given by

$$\alpha^V = -\left(\sqrt{1+c} \pm \sqrt{2 - c + \sqrt{(1-2c)^2 + 48\tau^2}}\right)/2 - \tau$$

$$\text{where } c \equiv (16\tau^2 - 1)^{1/3} \left[(1+4\tau)^{1/3} + (1-4\tau)^{1/3}\right]/2 \,. \tag{5.65}$$

In the special case $\tau = 1/4$, one has $c = 0$ and the roots (5.65) become $\alpha^V = -7/4$ and $\alpha^V = 1/4$ in accordance with (5.59). The wavenumbers a^c_{iV}, a^c_{oV} and a^c_{rf} in (5.49), (5.50) and (5.51) are then given by

$$2F^2 a^c_{iV} = \sqrt{2 - c + \sqrt{(1-2c)^2 + 48\tau^2}} + \sqrt{1+c} + 2\tau \text{ if } 0 \leq \tau \,, \tag{5.66a}$$

$$2F^2 a^c_{oV} = \sqrt{2 - c + \sqrt{(1-2c)^2 + 48\tau^2}} - \sqrt{1+c} - 2\tau \text{ if } \tau \leq 1/4 \,, \tag{5.66b}$$

$$2F^2 a^c_{rf} = \sqrt{2 - c + \sqrt{(1-2c)^2 + 48\tau^2}} - \sqrt{1+c} - 2\tau \text{ if } 1/4 \leq \tau \,. \tag{5.66c}$$

The corresponding wavenumbers $F^2 k = (F^2\alpha + \tau)^2$ are then given by

$$2F\sqrt{k^c_{iV}} = \sqrt{2 - c + \sqrt{(1-2c)^2 + 48\tau^2}} + \sqrt{1+c} \text{ if } 0 \leq \tau \,, \tag{5.67a}$$

$$2F\sqrt{k^c_{oV}} = \sqrt{2 - c + \sqrt{(1-2c)^2 + 48\tau^2}} - \sqrt{1+c} \text{ if } \tau \leq 1/4 \,, \tag{5.67b}$$

$$2F\sqrt{k^c_{rf}} = \sqrt{2 - c + \sqrt{(1-2c)^2 + 48\tau^2}} - \sqrt{1+c} \text{ if } 1/4 \leq \tau \,. \tag{5.67c}$$

These expressions yield $F^2 k^c_{iV} = 9/4$ and $F^2 k^c_{oV} = 1/4 = F^2 k^c_{rf}$ in the special case $\tau = 1/4$, in agreement with (5.60).

The cusp angles $\psi^*_{iV}(\tau)$, $\psi^*_{oV}(\tau)$ and $\psi^*_{rf}(\tau)$ of the inner V waves, the outer V waves or the ring-fan waves determined by expressions (5.48b) and (5.65) are depicted in Fig.5.17, where the angle $\psi^*_f(\tau)$ of the fan waves defined by expression (5.52a) is also shown.

Fig.5.18 depicts the functions $\alpha(\tau)$ associated with the values of

$$\alpha = (-a^c_{iV}\,, -k^-_o\,, -k^-_i\,, k^+_i\,, k^+_o\,, a^c_{oV}\,, a^c_{rf}\,, \alpha_{io}) \tag{5.68}$$

that determine the boundaries of the regions where inner V waves, outer V waves, partial-ring waves, outer fan waves and inner fan waves created by a ship that steadily advances through deep-water regular waves exist.

Basic wavelengths

The wavelengths $\lambda = 2\pi/k$ that correspond to the three wavenumbers k^c_{iV}, k^c_{oV} and k^c_{rf} given by (5.67) and the four wavenumbers $k^\pm_o$ and $k^\pm_i$ are important reference wavelengths for the waves created by a ship that advances through regular waves.

The wavelengths $\lambda^{aft}_r \equiv 2\pi/k^-_i$ and $\lambda^{fore}_r \equiv 2\pi/k^+_i$ are the wavelengths of the longest or shortest waves along the path of a ship, aft or fore of the ship, in the set of ring waves created if $0 \le \tau \le 1/4$.

The wavelength $\lambda^{aft}_{iV} \equiv 2\pi/k^-_o$ corresponds to the longest transverse waves in the set of inner V waves created aft of a ship (for every value of τ) and $\lambda^{cusp}_{iV} \equiv 2\pi/k^c_{iV}$ is the wavelength at the cusps $\psi^* = \pm\psi^*_{iV}$ of the pattern of inner V waves.

Similarly, $\lambda^{aft}_{oV} \equiv 2\pi/k^+_o$ is the wavelength of the longest transverse waves in the set of outer V waves created aft of a ship in the regime $0 \le \tau \le 1/4$ and $\lambda^{cusp}_{oV} \equiv 2\pi/k^c_{oV}$ is the wavelength at the cusps $\psi^* = \pm\psi^*_{oV}$ of the pattern of outer V waves.

Finally, $\lambda^{aft}_{rf} \equiv 2\pi/k^-_i$ is the wavelength of the longest transverse waves, aft of the ship, in the set of ring-fan waves that exist in the regime $1/4 < \tau$ and $\lambda^{cusp}_{rf} \equiv 2\pi/k^c_{rf}$ is the wavelength at the cusps $\psi^* = \pm\psi^*_{rf}$ of the ring-fan waves.

The wavelengths

$$\lambda^{aft}_r(\tau),\, \lambda^{fore}_r(\tau),\, \lambda^{aft}_{iV}(\tau),\, \lambda^{cusp}_{iV}(\tau),\, \lambda^{aft}_{oV}(\tau),\, \lambda^{cusp}_{oV}(\tau),\, \lambda^{aft}_{rf}(\tau),\, \lambda^{cusp}_{rf}(\tau)$$

are depicted in Fig.5.19, where the alternative scalings

$$\lambda^\omega \equiv f^2\lambda \equiv \frac{\Lambda\omega^2}{g}\ \ ,\ \ \lambda^V \equiv \frac{\lambda}{F^2} \equiv \frac{\Lambda g}{V_s^2}\ \ ,\ \ \lambda^S = \frac{\lambda}{S} \equiv \alpha_{io}\,\lambda \equiv \frac{\Lambda\omega}{V_s}$$

are used.

Inconsequential short waves

The divergent inner and outer V waves associated with the regions

$$-\infty < \alpha \le -a^c_{iV} \ \text{ or } \ a^c_{oV} \le \alpha < \infty \tag{5.69a}$$

in (5.49a) or (5.50b) contain short waves that may be influenced by nonlinearities or surface tension, and thus are unrealistic, or are too short to have a significant influence on flow features (hydrodynamic coefficients, ship motions and wave loads) of practical interest and are then inconsequential. These inconsequential or unrealistic short waves correspond to subregions

$$-\infty < \alpha \le -a_{iV}^{\infty} \text{ or } a_{oV}^{\infty} \le \alpha < \infty \tag{5.69b}$$

of the regions (5.69a). The dispersion relation (5.48a) determines the wavenumbers that correspond to $\alpha = -a_{iV}^{\infty}$ and $\alpha = a_{oV}^{\infty}$ as

$$F^2 k_{iV}^{\infty} = (-F^2 a_{iV}^{\infty} + \tau)^2 \text{ and } F^2 k_{oV}^{\infty} = (F^2 a_{oV}^{\infty} + \tau)^2 \,. \tag{5.70a}$$

Divergent waves that are significantly shorter than the waves at the cusps of the inner and outer V waves are eliminated if the wavenumbers k_{iV}^{∞} and k_{oV}^{∞} defined by (5.70a) are chosen as

$$k_{iV}^{\infty} = C\, k_{iV}^{c} \text{ and } k_{oV}^{\infty} = C\, k_{oV}^{c} \tag{5.70b}$$

where k_{iV}^{c} and k_{oV}^{c} are the wavenumbers of the waves at the cusps of the inner or outer V waves and $1 \le C$ denotes a proportionality factor. Expressions (5.70) yield

$$F^2 a_{iV}^{\infty} = \sqrt{C\, F^2 k_{iV}^{c}} + \tau \text{ and } F^2 a_{oV}^{\infty} = \sqrt{C\, F^2 k_{oV}^{c}} - \tau \,. \tag{5.71a}$$

These expressions and expressions (5.66a) and (5.66b) yield the ranges

$$-a_{iV}^{\infty} \le \alpha \le -a_{iV}^{c} \text{ or } a_{oV}^{c} \le \alpha \le a_{oV}^{\infty} \tag{5.71b}$$

where divergent inner and outer V waves are meaningful. The choice $C = 10$ eliminates divergent waves that are 10 times shorter than the waves at the cusps $\psi^* = \pm\, \psi_{iV}^*$ and $\psi^* = \pm\, \psi_{oV}^*$ of the inner or outer V waves.

Similarly, the range

$$a_{rf}^{c} \le \alpha \le a_{rf}^{\infty} \text{ where } F^2 a_{rf}^{\infty} = \sqrt{C F^2 k_{rf}^{c}} - \tau \tag{5.72}$$

and $C = 10$ eliminates inner fan waves that are 10 times shorter than the waves at the cusps $\psi^* = \pm\, \psi_{rf}^*$ of the ring-fan waves.

Chapter 6

Green functions and boundary-integral flow representations

Chapters 2-5 consider far-field (free) waves and wave patterns for general dispersion relations (in chapters 2 and 3) and for three specific dispersion relations associated with diffraction-radiation of regular waves by offshore structures in water of uniform finite depth (chapters 2 and 3) and waves created by a ship that steadily advances in deep calm water (chapter 4) or through regular waves (chapter 5). Near-field flows around ships and offshore structures, determined by the near-field boundary-value problem (1.35) stated in chapter 1, are considered hereafter in the book.

The boundary-value problem (1.35) can easily be solved, via the method of Fourier transformation, to determine the flow created by a distribution of pressure $p^F(\xi, \eta)$ and/or flux $q^F(\xi, \eta)$ applied at the free surface plane $\zeta = 0$ if no ship or offshore structure is present and the body boundary condition (1.35e) is therefore irrelevant. The method of Fourier transformation can also be applied for a vessel modeled via a distribution of sources (or dipoles) over a plane, as was done by Michell in 1898 in his classical theory of the wave drag of a ship that steadily advances in calm water **[6,1]**. Analytical solutions to the boundary-value problem (1.35) can also be obtained for simple special body geometries. In particular, analytical solutions exist for diffraction-radiation of regular waves by a circular cylinder, a sphere and an ellipsoid. Analytical solutions have also been obtained for flows around submerged spheroids that steadily advance in calm water or through regular waves **[6,2]**.

However, these analytical methods cannot be applied to general body shapes. A method of solution that is useful for bodies of arbitrary shape, required for practical applications, is expounded hereafter. This general method of solution, invented by Green in 1828 **[6,3]**, is known as the Green-function and boundary-integral method or, more precisely, as the method of Green function and boundary-integral representation. Green's method is introduced in this chapter, and is applied in chapters 7-9 to the boundary-value problem (1.35).

6.1 Basic mathematical identities

Green functions are associated with a classical identity, due to Green, that is related to the fundamental 'divergence theorem'. These two basic identities are now considered.

The divergence theorem

$$\int_{\mathcal{D}} dv(\boldsymbol{\xi})\, \nabla_{\boldsymbol{\xi}} \cdot \mathbf{V}(\boldsymbol{\xi}) = \int_{\Sigma} da(\boldsymbol{\xi})\, \mathbf{m}(\boldsymbol{\xi}) \cdot \mathbf{V}(\boldsymbol{\xi}) \;\text{ where }\; \nabla_{\boldsymbol{\xi}} \equiv (\partial_\xi, \partial_\eta, \partial_\zeta) \quad (6.1)$$

states that the flux $\mathbf{m} \cdot \mathbf{V}$ of a differentiable vector field $\mathbf{V} \equiv (V^\xi, V^\eta, V^\zeta)$ through a surface Σ that encloses a finite three-dimensional region $\mathcal{D}$ is equal to the integral of the divergence $\nabla_{\boldsymbol{\xi}} \cdot \mathbf{V}$ of the vector $\mathbf{V}$ over the region $\mathcal{D}$ inside the boundary surface Σ. The unit vector $\mathbf{m} \equiv (m^\xi, m^\eta, m^\zeta)$ normal to the boundary surface Σ points outside the region $\mathcal{D}$, and $dv(\boldsymbol{\xi})$ and $da(\boldsymbol{\xi})$ denote the differential elements of volume or area at points $\boldsymbol{\xi} \in \mathcal{D}$ or $\boldsymbol{\xi} \in \Sigma$.

Green's classical identity is obtained if the divergence theorem (6.1) is applied to the particular vector field

$$\mathbf{V}(\boldsymbol{\xi}) \equiv \varphi(\boldsymbol{\xi})\, \nabla_{\boldsymbol{\xi}} \psi(\boldsymbol{\xi}) - \psi(\boldsymbol{\xi})\, \nabla_{\boldsymbol{\xi}} \varphi(\boldsymbol{\xi}) \quad (6.2)$$

where $\varphi(\boldsymbol{\xi})$ and $\psi(\boldsymbol{\xi})$ are differentiable scalar functions of $\boldsymbol{\xi} \in (\mathcal{D} \cup \Sigma)$. The relations (6.1) and (6.2) yield

$$\int_{\mathcal{D}} dv\, (\varphi\, \nabla^2_{\boldsymbol{\xi}} \psi - \psi\, \nabla^2_{\boldsymbol{\xi}} \varphi) = \int_{\Sigma} da\, \mathbf{m} \cdot (\varphi\, \nabla_{\boldsymbol{\xi}} \psi - \psi\, \nabla_{\boldsymbol{\xi}} \varphi) \quad (6.3)$$

where $\nabla^2_{\boldsymbol{\xi}} \equiv \nabla_{\boldsymbol{\xi}} \cdot \nabla_{\boldsymbol{\xi}} \equiv \partial^2_\xi + \partial^2_\eta + \partial^2_\zeta$ is the Laplacian operator.

The functions φ and ψ in Green's identity (6.3) are general differentiable functions. The special case when the function φ satisfies Laplace's equation

$$\nabla^2_{\boldsymbol{\xi}} \varphi = 0 \;\text{ for }\; \boldsymbol{\xi} \in \mathcal{D} \quad (6.4)$$

is considered hereafter. In this special case, Green's identity (6.3) becomes

$$\int_{\mathcal{D}} dv\; \varphi\, \nabla^2_{\boldsymbol{\xi}} \psi = \int_{\Sigma} da\; \mathbf{m} \cdot (\varphi\, \nabla_{\boldsymbol{\xi}} \psi - \psi\, \nabla_{\boldsymbol{\xi}} \varphi)\;. \quad (6.5)$$

An important identity is obtained if the function $\psi(\boldsymbol{\xi})$ in (6.5) is chosen as a function that is singular, in the particular way defined further on, at a point $\boldsymbol{\xi} = \mathbf{x}$. To this end, a short mathematical detour is necessary to briefly consider a useful special function, called the Dirac 'delta' function.

6.2 The Dirac delta function

Functions are ordinarily defined via a 'point-wise relation' in which function values $\eta \equiv f(\xi)$ are associated with corresponding values of ξ. This ordinary definition of a function, based on a $\xi \to \eta \equiv f(\xi)$ relation, is useful even for a function $f(\xi)$ that is unbounded at a singular value x of ξ if the singularity of $f(\xi)$ at $\xi = x$ is specified, e.g. if $f(\xi) \sim 1/\sqrt{\xi - x}$ or $f(\xi) \sim 1/(\xi - x)^2$.

However, this ordinary definition of a function is less useful for a more general indeterminate singularity, as is the case for the delta function $\delta(\xi - x)$ now considered. An alternative framework based on a class of functions, called generalized functions **[6,4]**, can be used to define singular functions like $\delta(\xi - x)$. A generalized function is defined in an 'integrated sense', i.e. via an integration process, rather than via a 'point-wise relation' $\xi \to \eta \equiv f(\xi)$ as for ordinary functions.

Specifically, the singularity of the Dirac function $\delta(\xi - x)$ is defined via the relation

$$\int_a^b d\xi \; \delta(\xi - x)\, f(\xi) = \left\{ \begin{matrix} f(x) \\ 0 \end{matrix} \right\} \text{ if } \left\{ \begin{matrix} a < x < b \\ x < a \text{ or } b < x \end{matrix} \right\} \tag{6.6}$$

where $f(\xi)$ denotes an arbitrary continuous function.

The definition (6.6) can be extended to higher dimensions. For a three-dimensional region $\mathcal{D}$ bounded by a surface Σ, Dirac's relation (6.6) yields

$$\int_{\mathcal{D}} dv \; \delta(\xi - x)\, \delta(\eta - y)\, \delta(\zeta - z)\, f(\boldsymbol{\xi}) = \left\{ \begin{matrix} f(\mathbf{x}) \\ 0 \\ f(\mathbf{x})/2 \end{matrix} \right\} \text{ if } \left\{ \begin{matrix} \mathbf{x} \in \mathcal{D} \\ \mathbf{x} \notin (\mathcal{D} \cup \Sigma) \\ \mathbf{x} \in \Sigma \end{matrix} \right\} \tag{6.7}$$

where $dv \equiv d\xi\, d\eta\, d\zeta$, $f(\boldsymbol{\xi}) \equiv f(\xi, \eta, \zeta)$ and $f(\mathbf{x}) \equiv f(x, y, z)$. The identity (6.7) for the case when the point $\mathbf{x}$ is at the boundary surface Σ of the region $\mathcal{D}$ assumes that the surface Σ is smooth at the point $\mathbf{x}$.

In the special case $f(\boldsymbol{\xi}) \equiv 1$, the identities (6.7) become

$$\int_{\mathcal{D}} d\xi\, d\eta\, d\zeta \; \delta(\xi - x)\, \delta(\eta - y)\, \delta(\zeta - z) = \left\{ \begin{matrix} 1 \\ 0 \\ 1/2 \end{matrix} \right\} \text{ if } \left\{ \begin{matrix} \mathbf{x} \in \mathcal{D} \\ \mathbf{x} \notin (\mathcal{D} \cup \Sigma) \\ \mathbf{x} \in \Sigma \end{matrix} \right\}. \tag{6.8}$$

These important identities are used further on.

6.3 Basic boundary-integral relations

The arbitrary function $\psi(\boldsymbol{\xi})$ in the relation (6.5) is now taken as a function

$$\psi(\boldsymbol{\xi}) = G(\boldsymbol{\xi}, \mathbf{x})$$

that satisfies the Poisson equation

$$\nabla^2_{\boldsymbol{\xi}} G(\boldsymbol{\xi}, \mathbf{x}) = \delta(\xi - x)\, \delta(\eta - y)\, \delta(\zeta - z) \tag{6.9}$$

related to the Laplace equation (6.4). The Dirac relations (6.7) and Green's identity (6.5) yield the three complementary relations

$$\int_\Sigma da\, (\varphi\, \mathbf{m}\cdot\nabla_{\boldsymbol{\xi}} G - G\, \mathbf{m}\cdot\nabla_{\boldsymbol{\xi}} \varphi) = \varphi(\mathbf{x}) \text{ if } \mathbf{x}\in\mathcal{D}\,, \tag{6.10a}$$

$$\int_\Sigma da\, (\varphi\, \mathbf{m}\cdot\nabla_{\boldsymbol{\xi}} G - G\, \mathbf{m}\cdot\nabla_{\boldsymbol{\xi}} \varphi) = \varphi(\mathbf{x})/2 \text{ if } \mathbf{x}\in\Sigma\,, \tag{6.10b}$$

$$\int_\Sigma da\, (\varphi\, \mathbf{m}\cdot\nabla_{\boldsymbol{\xi}} G - G\, \mathbf{m}\cdot\nabla_{\boldsymbol{\xi}} \varphi) = 0 \text{ if } \mathbf{x}\notin(\mathcal{D}\cup\Sigma)\,. \tag{6.10c}$$

The notation $\phi \equiv \varphi(\mathbf{x})$ is used further on for shortness.

Expression (6.10a) explicitly determines the function $\phi \equiv \varphi(\mathbf{x})$ at a point $\mathbf{x}$ within the three-dimensional region $\mathcal{D}$ in terms of the values of the function $\varphi \equiv \varphi(\boldsymbol{\xi})$ and its normal derivative $\mathbf{m}\cdot\nabla_{\boldsymbol{\xi}}\varphi$ at the boundary surface Σ. This relation therefore provides a boundary-integral representation of the function $\phi \equiv \varphi(\mathbf{x})$. The identity (6.10b) only involves the function φ and its normal derivative $\mathbf{m}\cdot\nabla_{\boldsymbol{\xi}}\varphi$ at the surface Σ, and therefore provides a boundary-integral equation that determines φ at Σ if $\mathbf{m}\cdot\nabla_{\boldsymbol{\xi}}\varphi$ is specified (known) at the boundary surface Σ.

The boundary-integral relations (6.10a) and (6.10b) yield a space reduction from a three-dimensional region $\mathcal{D}$ to the two-dimensional boundary surface Σ that encloses $\mathcal{D}$. This

$$\text{3D region } \mathcal{D} \Longrightarrow \text{2D boundary surface } \Sigma$$

reduction is made possible by the relation (6.9) satisfied by the function G, which is called a Green function. The boundary surface Σ in Green's boundary-integral relations (6.10) is general. The general relations (6.10) and the related Green function G can then be used to solve 3D boundary-value problems for general geometries, notably for the hull surfaces Σ^H of offshore structures and ships that are of primary interest in this book.

6.4 Free-space and general Green functions

Free-space Green function

The divergence theorem (6.1) can be applied to the vector field $\nabla_{\boldsymbol{\xi}} G$ and the region Δ inside an arbitrary boundary surface Σ. The divergence theorem (6.1), the Poisson equation (6.9) and the Dirac relations (6.8) yield

$$\int_\Sigma da\ \mathbf{m}\cdot\nabla_{\boldsymbol{\xi}} G = \int_\Delta dv\ \nabla_{\boldsymbol{\xi}}\cdot\nabla_{\boldsymbol{\xi}} G \equiv \int_\Delta dv\ \nabla^2_{\boldsymbol{\xi}} G$$
$$= \left\{\begin{matrix}1\\0\end{matrix}\right\} \text{ if } \left\{\begin{matrix}\mathbf{x}\in\Delta\\ \mathbf{x}\notin(\Delta\cup\Sigma)\end{matrix}\right\} . \tag{6.11}$$

The unit vector $\mathbf{m}$ normal to the surface Σ that encloses the region Δ points outside Δ in (6.11). The identities (6.11) show that the integral over the surface Σ of the normal flux $\mathbf{m}\cdot\nabla_{\boldsymbol{\xi}} G$ is equal to 1 for every point $\mathbf{x}$ inside the closed surface Σ, but is nil if $\mathbf{x}$ is outside Σ.

In particular, the arbitrary surface Σ can be taken as a sphere centered at $\mathbf{x}$. If r is the radius of the sphere, its surface area is $4\pi r^2$. The identity that involves the integral over the surface Σ in (6.11) then shows that the flux of $\mathbf{m}\cdot\nabla_{\boldsymbol{\xi}} G \equiv dG/dr$ through the surface Σ of the sphere is given by $dG/dr = 1/(4\pi r^2)$ if G only depends on r. This relation yields

$$4\pi G(\boldsymbol{\xi},\mathbf{x}) = -1/r \text{ where} \tag{6.12}$$
$$r \equiv \sqrt{(\xi-x)^2+(\eta-y)^2+(\zeta-z)^2} \tag{6.13}$$

is the distance between the points $\boldsymbol{\xi}\equiv(\xi,\eta,\zeta)$ and $\mathbf{x}\equiv(x,y,z)$.

The gradient of (6.12) is

$$4\pi\nabla_{\boldsymbol{\xi}} G = (\xi-x,\eta-y,\zeta-z)/r^3 = (\boldsymbol{\xi}-\mathbf{x})/r^3 . \tag{6.14}$$

It follows that $4\pi\partial^2 G/\partial\xi^2 = 1/r^3 - 3(\xi-x)^2/r^5$. Analogous expressions for the derivatives $\partial^2 G/\partial\eta^2$ and $\partial^2 G/\partial\zeta^2$ show that G satisfies the Laplace equation

$$\nabla^2_{\boldsymbol{\xi}} G = 0 \text{ if } 0<r \tag{6.15}$$

in agreement with (6.9).

Thus, the function (6.12) satisfies the 3D Poisson equation (6.9), i.e.

$$\nabla^2_{\boldsymbol{\xi}}\left(\frac{-1/r}{4\pi}\right) = \delta(\xi-x)\,\delta(\eta-y)\,\delta(\zeta-z) . \tag{6.16}$$

The Green function (6.12) is known by several names, including the free-space or unbounded-space Green function, the fundamental singularity, and the Rankine source potential.

Physical interpretation

The function $G \equiv G(\boldsymbol{\xi}, \mathbf{x})$ and its gradient $\nabla_{\boldsymbol{\xi}} G$ can be associated with a flow potential and the corresponding flow velocity in an unbounded fluid. Specifically, the Green function (6.12) represents the velocity potential of the flow created at a point $\boldsymbol{\xi}$ by a unit source located at a point $\mathbf{x}$ or, alternatively, as the flow created at a point $\mathbf{x}$ by a unit source located at a point $\boldsymbol{\xi}$. Indeed, the fundamental Green function (6.12) satisfies the Poisson equation (6.9) as well as the Poisson equation

$$\nabla^2_{\mathbf{x}} G \equiv (\,\partial_x^2 + \partial_y^2 + \partial_z^2\,) G = \delta(x-\xi)\,\delta(y-\eta)\,\delta(z-\zeta)\ . \tag{6.17}$$

It is shown further on that this symmetry between the points $\mathbf{x}$ and $\boldsymbol{\xi}$ and the related definition of a flow-field point and a source point in $G(\boldsymbol{\xi}, \mathbf{x})$ are not as obvious for more general Green functions, notably the Green functions associated with the flow around a ship that steadily advances in calm water or through regular waves of primary interest in the book.

The boundary-integral representations (6.10a-b) determine a harmonic function $\phi \equiv \varphi(\mathbf{x})$ at a point $\mathbf{x}$ located inside a region $\mathcal{D}$ or at its boundary surface Σ in terms of a distribution of sources and dipoles, with densities equal to the normal flux $\mathbf{m}\cdot\nabla_{\boldsymbol{\xi}}\varphi$ or the function φ, associated with a Green function G and its normal derivative $\mathbf{m}\cdot\nabla_{\boldsymbol{\xi}} G$, respectively. Moreover, a harmonic function $\phi \equiv \varphi(\mathbf{x})$ is fully determined at every point $\mathbf{x}$ of the finite region inside a closed boundary surface Σ by means of the boundary-integral representation (6.10a) if φ and its normal derivative $\mathbf{m}\cdot\nabla_{\boldsymbol{\xi}}\varphi$ are known at Σ.

General Green function

Expression (6.16) shows that the general solution of (6.9) is given by

$$4\pi G = -1/r + H \ \text{ where } \ \nabla^2_{\boldsymbol{\xi}} H = 0 \ \text{ for } \ \boldsymbol{\xi} \in \mathcal{D}\,. \tag{6.18}$$

Thus, Green functions $G(\boldsymbol{\xi}, \mathbf{x})$ associated with the Laplace equation in the three-dimensional space satisfy the Poisson equation (6.9) and are given by the sum of the fundamental singularity (6.12) and a function H that is harmonic (satisfies the Laplace equation) in $\mathcal{D}$, or more generally in a larger region that contains $\mathcal{D}$.

Green functions are not unique because the harmonic function H in the general solution (6.18) can be chosen in alternative ways, as is illustrated in the next section. However, every Green function associated with the three-dimensional Laplace equation is of the form (6.18).

The basic boundary-integral representation (6.10a) and the relations

(6.10b) and (6.10c) have been applied, with the general Green function (6.18), to numerous boundary-value problems in engineering and physics.

6.5 Alternative Green functions

Green's fundamental relations (6.10) are now considered for the boundary-value problem that determines the velocity potential

$$\widehat{\varphi}(\boldsymbol{\xi}, t) = \mathrm{Re}\, \varphi(\boldsymbol{\xi})\, e^{(\epsilon - \mathrm{i} f)\, t} \tag{6.19}$$

associated with the flow around a ship that advances at a constant speed along a straight path through regular waves in water of finite uniform depth. This boundary-value problem is stated by (1.34) and (1.35) where $\phi(\mathbf{x})$ is now replaced by $\varphi(\boldsymbol{\xi})$.

Boundary-value problem

Specifically, the spatial component $\varphi(\boldsymbol{\xi})$ of the flow potential $\widehat{\varphi}(\boldsymbol{\xi}, t)$ satisfies the Laplace equation

$$\nabla^2_{\boldsymbol{\xi}}\, \varphi \equiv (\partial^2_\xi + \partial^2_\eta + \partial^2_\zeta)\, \varphi = 0 \ \text{ in } \ \mathcal{D} \tag{6.20a}$$

and the boundary conditions

$$\varphi \approx 0 \ \text{ at } \ \Sigma^\infty, \tag{6.20b}$$

$$\partial_\zeta\, \varphi = 0 \ \text{ at } \ \Sigma^B, \tag{6.20c}$$

$$[\, \partial_\zeta + (F\, \partial_\xi + \mathrm{i} f - \epsilon)^2\,]\, \varphi = F p^F_\xi + \mathrm{i} f\, p^F - q^F \ \text{ at } \ \Sigma^F, \tag{6.20d}$$

$$\mathbf{n} \cdot \nabla_{\boldsymbol{\xi}}\, \varphi = q^H \ \text{ at } \ \Sigma^H. \tag{6.20e}$$

One has $\epsilon = +0$ in the free-surface boundary condition (6.20d) where the Froude number F and the non-dimensional (encounter) frequency f are defined by (1.32). Moreover, every flow variable is non-dimensional as in (1.30a-b). The unit vector $\mathbf{n}$ normal to the hull surface Σ^H points outside the ship (into the water). The hull flux q^H in the boundary condition (6.20e) at the ship-hull surface Σ^H and the pressure p^F and the flux q^F in the boundary condition (6.20d) at the free surface Σ^F are *presumed known* in the general boundary-value problem (6.20).

The boundary surface Σ in (6.10) is given by

$$\Sigma \equiv \Sigma^\infty \cup \Sigma^B \cup \Sigma^F \cup \Sigma^H \tag{6.21}$$

where Σ^∞ is an infinitely large surface that encloses the flow region $\mathcal{D}$, Σ^B is the part of the sea-bottom plane $\zeta = -d$ that is inside Σ^∞, and Σ^F is

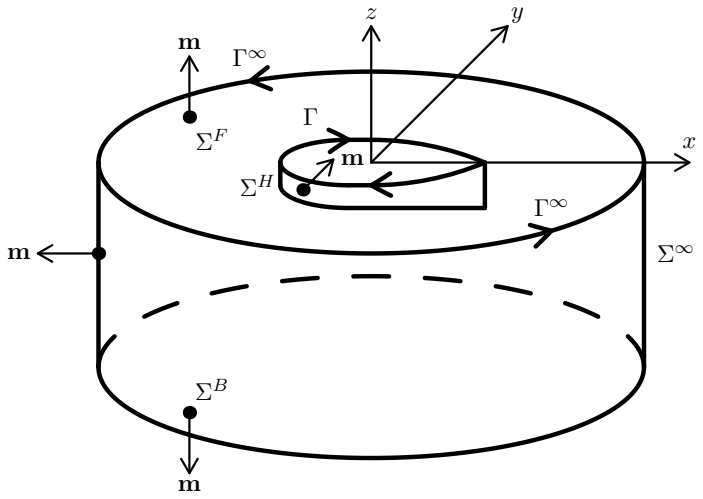

Figure 6.1: Closed boundary surface $\Sigma \equiv \Sigma^\infty \cup \Sigma^B \cup \Sigma^F \cup \Sigma^H$ associated with the boundary-value problem that corresponds to the flow around a ship that steadily advances through regular waves in water of uniform finite depth. The unit vector $\mathbf{m}$ normal to the boundary surface Σ points outside the flow region enclosed by Σ. The unit vector $\mathbf{n} = -\mathbf{m}$ normal to the hull surface Σ^H points outside the ship (into the water).

the part of the undisturbed free-surface plane $\zeta = 0$ that is inside Σ^∞ and outside the mean wetted ship-hull surface Σ^H, as is shown in Fig.6.1.

Green functions $G(\boldsymbol{\xi}, \mathbf{x})$ associated with the Laplace equation in a three-dimensional region $\mathcal{D}$ satisfy the Poisson equation (6.9), and are expressed in (6.18) as the sum of the fundamental free-space singularity (6.12) and a function H that satisfies the Laplace equation, i.e. is harmonic, in $\mathcal{D}$. As was already noted, the harmonic function H in the general expression (6.18) for the Green function G associated with the 3D Laplace equation is not uniquely defined and indeed can largely be chosen at will. Thus, Green functions are not uniquely defined and alternative Green functions can be used, as is illustrated in the remainder of this section.

In particular, Green functions can be—and usually are—defined in a region $\mathcal{D}_G$ that is larger than the flow region $\mathcal{D}$ and contains $\mathcal{D}$. Specifically, the flow region $\mathcal{D}$ for the boundary-value problem (6.20) is bounded by the surface Σ defined by (6.21), whereas the Green function G is usually defined within the entire lower half space $\zeta \leq 0$ (in deep water), which includes the flow region $\mathcal{D}$ as well as the region $\mathcal{D}_i$ inside the ship-hull surface Σ^H.

Far-field contribution

A particularly simple choice of the general harmonic function H in (6.18) is $H = 0$. The Green function that corresponds to this simplest choice is the free-space Green function (6.12). The Rankine source potential (6.12) vanishes as $r \to \infty$. This property and the far-field boundary condition (6.20b) ensure that the contribution of the far-field surface Σ^∞ in the boundary-integral relations (6.10) is negligible if Σ^∞ is sufficiently large. This result holds for more general Green functions G, notably all the Green functions considered in the book, as can be shown via an analysis of the behaviors of G and the flow potential φ in the far-field limit $r \to \infty$.

Contribution of the sea bottom

The contribution of the sea-bottom surface Σ^B, where $\mathbf{m} \equiv (0, 0, -1)$ and the boundary condition (6.20c) holds, in (6.10) is given by

$$-\int_{\Sigma^B} d\xi \, d\eta \; \varphi \; \partial_\zeta G \;\text{ where }\; \zeta = -d \; .$$

This contribution is nil if the harmonic function H is chosen so that the Green function G satisfies the boundary condition

$$\partial_\zeta G = 0 \;\text{ at }\; \zeta = -d \; . \tag{6.22}$$

The boundary condition (6.22) applied to the Green function G is identical to the boundary condition (6.20c) satisfied by φ.

The boundary condition (6.22) is satisfied if H is chosen as

$$H = -1/r_d \;\text{ where} \tag{6.23a}$$

$$r_d \equiv \sqrt{(\xi - x)^2 + (\eta - y)^2 + (\zeta + z + 2\,d)^2} \tag{6.23b}$$

denotes the distance between the point $\boldsymbol{\xi} \equiv (\xi, \eta, \zeta)$ and the mirror image $\mathbf{x}^d \equiv (x, y, -z - 2\,d)$ of the point $\mathbf{x} \equiv (x, y, z)$ with respect to the sea-bottom plane $\zeta = -d$. Expressions (6.18) and (6.23a) yield

$$4\,\pi\,G = -1/r - 1/r_d \; . \tag{6.23c}$$

Thus, the contribution of the sea bottom Σ^B in (6.10) is eliminated via the simple choice of Green function given by (6.23c).

Contribution of the free surface in the special case $F = 0$

The contribution of the free surface Σ^F, where $\mathbf{m} \equiv (0, 0, 1)$, in (6.10) is given by

$$\int_{\Sigma^F} d\xi \, d\eta \; (\varphi \; \partial_\zeta G - G \; \partial_\zeta \varphi) \; . \tag{6.24a}$$

The free-surface boundary condition (6.20d) is now considered in the special case $F = 0$ associated with diffraction-radiation of regular waves by an offshore structure, and for the common case $p^F = 0$ and $q^F = 0$. In this particular case, the free-surface condition (6.20d) becomes

$$[\,\partial_\zeta - (f + \mathrm{i}\,\epsilon)^2\,]\,\varphi = 0 \;\text{ at }\; \Sigma^F. \tag{6.24b}$$

The integrand of (6.24a) is nil, and the contribution of the free surface Σ^F in (6.10) is eliminated, if one chooses a Green function G that satisfies the free-surface boundary condition

$$[\,\partial_\zeta - (f + \mathrm{i}\,\epsilon)^2\,]\,G = 0 \;\text{ at }\; \zeta = 0\,. \tag{6.24c}$$

This boundary condition is identical to the free-surface condition (6.24b) satisfied by the flow potential φ.

Contribution of the free surface in the general case $Ff \neq 0$

The general case $Ff \neq 0$ associated with the free-surface boundary condition (6.20d) is now considered in the common case $p^F = 0$ and $q^F = 0$. Thus, the potential φ satisfies the condition

$$[\,\partial_\zeta + (\mathrm{i}f - \epsilon + F\partial_\xi)^2\,]\,\varphi = 0 \;\text{ at }\; \Sigma^F. \tag{6.25a}$$

If one chooses a Green function G that satisfies the free-surface boundary condition

$$[\,\partial_\zeta + (\mathrm{i}f - \epsilon - F\partial_\xi)^2\,]\,G = 0 \;\text{ at }\; \zeta = 0\,, \tag{6.25b}$$

the contribution (6.24a) of the free surface Σ^F in (6.10) is given by

$$\begin{aligned}\int_{\Sigma^F} d\xi\, d\eta\,(\varphi\,\partial_\zeta G - G\,\partial_\zeta\varphi)\\ = \int_{\Sigma^F} d\xi\, d\eta\,[\,2F(\mathrm{i}f - \epsilon)\,\partial_\xi(G\,\varphi) + F^2\partial_\xi(G\,\partial_\xi\varphi - \varphi\,\partial_\xi G)\,]\;.\end{aligned} \tag{6.26}$$

Stokes' theorem

$$\int_{\mathcal{R}} d\xi\, d\eta\,(\partial Q/\partial\xi - \partial P/\partial\eta) = \int_{\mathcal{C}} (P\,d\xi + Q\,d\eta) \tag{6.27}$$

where $P(\xi,\eta)$ and $Q(\xi,\eta)$ are differentiable functions defined within a finite region $\mathcal{R}$ inside a closed curve $\mathcal{C}$ in the two-dimensional space (ξ,η), is now applied to the free-surface integral (6.26). Specifically, the curve $\mathcal{C}$ in (6.27) is taken as the waterline $\Gamma^\infty \cup \Gamma$, where Γ^∞ and Γ are the intersection curves between the free surface and the far-field surface Σ^∞ or the ship-hull surface Σ^H, and the region $\mathcal{R}$ in (6.27) is the portion Σ^F of the free surface inside

Γ^∞ and outside Γ. The waterlines Γ^∞ and Γ are oriented as in Fig.6.1. Stokes' theorem then yields

$$\begin{aligned}&\int_{\Sigma^F} d\xi\, d\eta\, [2F(\mathrm{i}f-\epsilon)\,\partial_\xi(G\,\varphi)+F^2\partial_\xi\,(G\,\partial_\xi\varphi-\varphi\,\partial_\xi G)]\\&\quad=\int_\Gamma d\eta\,[2F(\mathrm{i}f-\epsilon)\,G\,\varphi+F^2(G\,\partial_\xi\varphi-\varphi\,\partial_\xi G)]\end{aligned}\tag{6.28}$$

where the contribution of the waterline Γ^∞, negligible for a sufficiently large surface Σ^∞, is ignored.

Expressions (6.26) and (6.28) then yield

$$\begin{aligned}&\int_{\Sigma^F} d\xi\, d\eta\,(\varphi\;\partial_\zeta G-G\,\partial_\zeta\varphi)\\&\quad=\int_\Gamma d\eta\,[2F(\mathrm{i}f-\epsilon)\,G\,\varphi+F^2(G\,\partial_\xi\varphi-\varphi\;\partial_\xi G)]\,.\end{aligned}\tag{6.29}$$

The relation (6.29) shows that the contribution of the free surface Σ^F is *not* eliminated if $F\neq 0$. However, the surface integral (6.24a) over the unbounded free surface Σ^F is reduced to a line integral around the ship waterline Γ.

The sign difference between the term $+F\partial_\xi$ that appears in the free-surface boundary condition (6.25a) satisfied by the potential $\varphi(\boldsymbol{\xi})$ and the term $-F\partial_\xi$ in the free-surface boundary condition (6.25b) satisfied by the Green function $G(\boldsymbol{\xi},\mathbf{x})$ is essential in the transformation (6.29). This sign difference is considered in section 6.8.

Contribution of the ship-hull surface

The contribution

$$\int_{\Sigma^H} da\,(\varphi\;\mathbf{m}\cdot\nabla_{\boldsymbol{\xi}}\,G-G\;\mathbf{m}\cdot\nabla_{\boldsymbol{\xi}}\,\varphi)\tag{6.30a}$$

of the ship-hull surface Σ^H in (6.10) is now considered. The hull boundary condition (6.20e) specifies the flux $\mathbf{n}\cdot\nabla_{\boldsymbol{\xi}}\,\varphi$ at Σ^H, where $\mathbf{n}=-\mathbf{m}$. The contribution (6.30a) then becomes

$$\int_{\Sigma^H} da\;G\;q^H\tag{6.30b}$$

if a Green function that satisfies the boundary condition

$$\mathbf{n}\cdot\nabla_{\boldsymbol{\xi}}\,G=0\;\text{ at }\;\Sigma^H\tag{6.30c}$$

is chosen. This homogeneous boundary condition corresponds to the non-homogeneous boundary condition (6.20e) satisfied by the potential φ. The

contribution (6.30b) of the ship-hull surface Σ^H is then determined in terms of the hull flux q^H, which is presumed to be known in the boundary-value problem (6.20), and the Green function G that satisfies the ship-hull surface boundary condition (6.30c).

A Green function that satisfies the boundary condition (6.22) at the sea bottom $\zeta = -d$ and the boundary condition (6.25b) at the free surface $\zeta = 0$ can be applied to a *general* ship-hull surface Σ^H. However, a Green function that satisfies the hull boundary condition (6.30c) is associated with a specific ship-hull surface Σ^H, and a different Green function is therefore required for every ship. Furthermore, Green functions that satisfy the boundary condition (6.30c) are complicated and difficult to determine, even for special simple geometrical surfaces Σ^H such as a sphere or an ellipsoid.

Green functions that satisfy the sea-bottom boundary condition (6.22), the free-surface boundary condition (6.25b) and the hull-surface boundary condition (6.30c) are therefore not commonly used, and Green functions that satisfy the sea-bottom boundary condition (6.22) and the free-surface boundary condition (6.25b) are mostly used in practice.

6.6 Rankine-Fourier decomposition

The harmonic function H in the general Green function (6.18) can easily be chosen so that the sea-bottom boundary condition (6.22) is satisfied; indeed, the harmonic function H is given by the simple image Rankine source (6.23a). However, the function H in expression (6.18) for the Green function $G(\boldsymbol{\xi}, \mathbf{x})$ that satisfies the free-surface boundary condition (6.25b) associated with a ship that steadily advances through regular waves in finite water-depth is considerably more complicated than expression (6.23a).

This Green function is now considered in the simpler special case of deep water. The Green function $G(\boldsymbol{\xi}, \mathbf{x})$ satisfies the Poisson equation (6.9) in the lower half space $\zeta < 0$ and the far-field boundary condition $G \to 0$ as $r \to \infty$, in accordance with the far-field condition (6.20b) and the boundary condition (6.20c) in the deep-water limit $d = \infty$. Thus, the Green function $G(\boldsymbol{\xi}, \mathbf{x})$ is the solution of the boundary-value problem defined by the Poisson equation

$$\nabla^2_{\boldsymbol{\xi}} G = \delta(\xi - x)\, \delta(\eta - y)\, \delta(\zeta - z) \;\text{ in }\; \zeta < 0 \;, \tag{6.31a}$$

the far-field condition

$$G \to 0 \;\text{ as }\; r \to \infty \;, \tag{6.31b}$$

and the free-surface boundary condition

$$[\, \partial_\zeta + (\mathrm{i}f - \epsilon - F\partial_\xi)^2 \,]\, G = 0 \;\text{ at }\; \zeta = 0 \tag{6.31c}$$

in accordance with (6.25b).

The general solution of the Poisson equation (6.31a) can be expressed as

$$4\pi G = -1/r + 1/r' + H^F/\pi \text{ where} \tag{6.32}$$

$$r' \equiv \sqrt{(\xi - x)^2 + (\eta - y)^2 + (\zeta + z)^2} \tag{6.33}$$

denotes the distance between the point $\boldsymbol{\xi} \equiv (\xi, \eta, \zeta)$ and the mirror image $\mathbf{x}' \equiv (x, y, -z)$ of the point $\mathbf{x} \equiv (x, y, z)$ with respect to the free-surface plane $\zeta = 0$. The Rankine potential $1/r'$ in (6.32) satisfies the Laplace equation (is harmonic) in the lower half space $\zeta < 0$, in accordance with (6.15), (6.16) and (6.31a). The solution (6.32) corresponds to the general solution (6.18) with the harmonic function H chosen as $H = 1/r' + H^F/\pi$.

The function H^F in (6.32) satisfies the Laplace equation

$$\nabla^2_{\boldsymbol{\xi}} H^F = 0 \text{ in } \zeta < 0 \tag{6.34a}$$

and the boundary conditions

$$H^F \to 0 \text{ as } r \to \infty \ , \tag{6.34b}$$

$$[\,\partial_\zeta + (\mathrm{i}f - \epsilon - F\,\partial_\xi)^2\,]\,H^F = -2\pi\,\partial_\zeta(1/r') \text{ at } \zeta = 0 \ . \tag{6.34c}$$

The boundary condition (6.34c) follows from the boundary condition (6.31c) and expressions (6.32), (6.13) and (6.33).

Expression (6.32) defines the Green function in terms of the basic free-space singularity $-1/r$ and two components that account for free-surface effects. The component $1/r'$ corresponds to the case when the boundary condition at the free surface is simplified as $G = 0$, which corresponds to the free-surface boundary condition (6.31c) in the limits $f \to \infty$ or $F \to \infty$ and effectively negligible gravity. The component H^F in (6.32) accounts for free-surface effects and finite values of f and F in the boundary condition (6.31c). The solution H^F of the boundary-value problem (6.34) can be obtained using a double Fourier transform with respect to the two horizontal coordinates ξ and η, and can be expressed as a Fourier superposition of elementary wave functions, as is shown further on.

6.7 Submerged source or free-surface flux

The Poisson equation (6.31a) and the free-surface boundary condition (6.31c) are associated with the flow created by a unit source located at a point $\mathbf{x} = (x, y, z < 0)$ below the free-surface plane $\zeta = 0$. In the limit $z = 0$, the Green function $G(\boldsymbol{\xi}, \mathbf{x})$ corresponds to the flow created by a unit flux

$$q^F = \delta(\xi - x)\,\delta(\eta - y)$$

through the free-surface plane $z = 0$ at the point $\mathbf{x} = (x, y, z = 0)$, and the Poisson (nonhomogeneous Laplace) equation (6.31a) and the (homogeneous) free-surface condition (6.31c) are replaced by the Laplace equation

$$\nabla^2_{\boldsymbol{\xi}} G = 0 \text{ in } \zeta < 0 \tag{6.35a}$$

and the nonhomogeneous free-surface boundary condition

$$[\,\partial_\zeta + (\mathrm{i}f - \epsilon - F\partial_\xi)^2\,]\,G = -\delta(\xi - x)\,\delta(\eta - y) \text{ at } \zeta = 0\ . \tag{6.35b}$$

Thus, the Green function $G(\boldsymbol{\xi}, \mathbf{x})$ represents the velocity potential of the flow created by a unit source located at a point $(x, y, z < 0)$ below the free-surface plane $z = 0$, or a unit flux through the free surface at a point $(x, y, z = 0)$ of the free surface.

In the limit $z = 0$, expressions (6.13) and (6.33) yield $r = r'$ and (6.32) becomes

$$4\pi G = H^F/\pi\ . \tag{6.36}$$

The Laplace equation (6.35a), the far-field condition (6.31b) and the free-surface condition (6.35b) then yield

$$\nabla^2_{\boldsymbol{\xi}} H^F = 0 \text{ in } \zeta < 0\ , \tag{6.37a}$$

$$H^F \to 0 \text{ as } r \to \infty\ , \tag{6.37b}$$

$$[\,\partial_\zeta + (\mathrm{i}f - \epsilon - F\partial_\xi)^2\,]\,H^F = -4\pi^2\,\delta(\xi - x)\,\delta(\eta - y) \text{ at } \zeta = 0\ . \tag{6.37c}$$

The relations (6.37a-b) and (6.34a-b) are identical. The relations (6.37c) and (6.34c) are also identical, as is now shown. Expression (6.33) yields

$$\partial_\zeta(1/r') = -z/(h^2 + z^2)^{3/2} \text{ at } \zeta = 0 \text{ where } h \equiv \sqrt{(\xi - x)^2 + (\eta - y)^2}\,.$$

The function $\partial_\zeta(1/r')$ at $\zeta = 0$ is nil at $z = 0$ except if $h = 0$, i.e. at the point $(\xi, \eta) = (x, y)$ where $\partial_\zeta(1/r')$ is unbounded. Moreover, one has

$$\int_{-\infty}^{\infty} d\eta \int_{-\infty}^{\infty} d\xi\ \partial_\zeta(1/r') = -2\pi z \int_0^{\infty} dh\, h/(h^2 + z^2)^{3/2} = 2\pi\ , \text{ i.e.}$$
$$\frac{1}{2\pi}\int_{-\infty}^{\infty} d\eta \int_{-\infty}^{\infty} d\xi\ \partial_\zeta(1/r') = 1 = \int_{-\infty}^{\infty} d\eta\ \delta(\eta - y) \int_{-\infty}^{\infty} d\xi\ \delta(\xi - x)$$

where the integral on the right side follows from Dirac's relation (6.6) and the integral on the left side represents the flux through the free-surface plane $\zeta = 0$ due to a unit sink located at $(x, y, 0)$. Thus, the function H^F determined by the boundary-value problem (6.34) if $z < 0$ or the boundary-value problem (6.37) if $z = 0$, and the related Green function (6.32), are consistent.

6.8 Flow-field point and source point

The Laplace equation (6.37a), the far-field condition (6.37b) and the free-surface boundary condition (6.37c) that determine the harmonic function H^F suggest that this function can be expressed as a Fourier superposition of elementary wave functions

$$e^{\,k\,(\zeta+z)\,+\,\mathrm{i}\,[\,\alpha\,(\xi-x)\,+\,\beta\,(\eta-y)\,]}\ ,$$

as is verified further on. Thus, the harmonic function H^F is a function of the three coordinates $\xi - x$, $\eta - y$ and $\zeta + z$. It follows that the free-surface boundary condition (6.31c) can be expressed in the form

$$[\,\partial_z + (\,\mathrm{i}\,f - \epsilon + F\,\partial_x)^2\,]\,G = 0 \ \text{ at } \ z = 0\ . \tag{6.38}$$

The sign difference between the terms $+F\,\partial_x$ in (6.38) and $-F\,\partial_\xi$ in (6.31c) is evidently associated with differentiations with respect to the coordinates of the flow-field point $\boldsymbol{\xi}$ in (6.31c) or the source point $\mathbf{x}$ in (6.38).

The boundary condition (6.38) involves the term $+F\,\partial_x$ in accordance with the term $+F\,\partial_\xi$ in the free-surface boundary condition (6.25a) satisfied by the flow potential φ, instead of the term $-F\,\partial_\xi$ that appears in (6.31c). Indeed, the Poisson equation (6.17) and the boundary conditions (1.35b) and (1.35d) show that the velocity potential $\phi(\mathbf{x};\boldsymbol{\xi})$ of the flow created at a flow-field point $\mathbf{x}$ by a unit source located at a point $\boldsymbol{\xi}$ below the free surface $z = 0$ is determined by the boundary-value problem

$$(\partial_x^2 + \partial_y^2 + \partial_z^2)\,\phi = \delta(x-\xi)\,\delta(y-\eta)\,\delta(z-\zeta) \ \text{ in } \ z < 0\ , \tag{6.39a}$$

$$\phi \to 0 \ \text{ as } \ r \to \infty \ \text{ and} \tag{6.39b}$$

$$[\,\partial_z + (\,\mathrm{i}\,f - \epsilon + F\,\partial_x)^2\,]\,\phi = 0 \ \text{ at } \ z = 0\ . \tag{6.39c}$$

Thus, the Poisson equation (6.39a) and the free-surface boundary condition (6.39c) are associated with the velocity potential of the flow created at a point $\mathbf{x}$ by a unit source located at a point $\boldsymbol{\xi}$ that steadily advances in the direction of the positive x axis at a (nondimensional) speed F.

In the special case $F = 0$, i.e. for diffraction-radiation of regular waves by an offshore structure, the Green function $G(\boldsymbol{\xi},\mathbf{x})$ represents the velocity potential of the flow created at a point $\boldsymbol{\xi}$ by a unit source located at a point $\mathbf{x}$, as well as the velocity potential of the flow created at $\mathbf{x}$ by a unit source located at $\boldsymbol{\xi}$.

However, if $F \neq 0$, the Green function G represents the velocity potential of the flow created at a point $\mathbf{x}$ by a unit source located at a point $\boldsymbol{\xi}$ that advances in the direction of the positive x axis, or the velocity potential of the flow created at a point $\boldsymbol{\xi}$ by a unit source located at a point $\mathbf{x}$ that advances in the direction of the negative x axis. These alternative physical

interpretations are easily understood in the particular case of a ship that steadily advances in calm water along the x axis. In that special case, a source at a point $\boldsymbol{\xi}$ that advances in the direction of the positive x axis creates waves behind the source, i.e. in the region $x < \xi$. Likewise, a source at a point $\mathbf{x}$ that advances in the direction of the negative x axis creates waves behind the source, i.e. in the region $x < \xi$.

The interpretation in which the Green function $G(\boldsymbol{\xi},\mathbf{x})$ represents the velocity potential of the flow created by a source at a point $\mathbf{x} \equiv (x, y, z < 0)$ or by a flux through the free surface at a point $\mathbf{x} \equiv (x, y, z = 0)$, and the singularity point $\mathbf{x}$ advances at a nondimensional speed $-F$ along the x axis, is the physical interpretation that is used in the definition of the Green functions given in chapter 7 and in the formulation of boundary-integral flow representations, based on Green's basic identities (6.10), considered in chapters 8 and 9. This interpretation is in accordance with the Poisson equation (6.9) and the free-surface boundary condition (6.25b), which is shown to be crucial in section 6.5.

6.9 Fourier transformation

Fourier transforms are now briefly defined because they are required in the next chapter to determine the Green functions associated with the free-surface boundary conditions relevant to the classes of flows considered in the book. Fourier transforms also provide valuable basic insight into waves created by a ship and their mathematical representation.

The Fourier transform $f_*(\alpha)$ of a function $f(\xi)$ that vanishes as $\xi \to \pm\infty$ is defined in this book as

$$f_*(\alpha) = \frac{1}{\sqrt{2\,\pi}} \int_{-\infty}^{\infty} d\xi \; e^{-\mathrm{i}\,\alpha\,\xi} f(\xi) \; . \tag{6.40a}$$

The inverse Fourier transform is given by

$$f(\xi) = \frac{1}{\sqrt{2\,\pi}} \int_{-\infty}^{\infty} d\alpha \; e^{\,\mathrm{i}\,\alpha\,\xi} f_*(\alpha) \; . \tag{6.40b}$$

The definition (6.40a) shows that the Fourier transform of the derivative $f'(\xi) \equiv df(\xi)/d\xi$ of the function $f(\xi)$ is

$$f'_*(\alpha) = \frac{1}{\sqrt{2\,\pi}} \int_{-\infty}^{\infty} d\xi \; e^{-\mathrm{i}\,\alpha\,\xi} f'(\xi) \; .$$

Integration by parts yields the classical simple rule

$$f'_*(\alpha) = \mathrm{i}\,\alpha\, f_*(\alpha) \; . \tag{6.40c}$$

Thus, the Fourier transform $f'_*(\alpha)$ of the derivative $f'(\xi)$ of a function $f(\xi)$ that vanishes as $\xi \to \pm\infty$ is immediately obtained by multiplying the Fourier transform $f_*(\alpha)$ of the function $f(\xi)$ by $\mathrm{i}\,\alpha$.

Fourier transformation can be defined in more than one dimension. In particular, a double Fourier transformation with respect to two horizontal coordinates $-\infty < \xi < \infty$ and $-\infty < \eta < \infty$ is used further on. The double Fourier transform $f_*(\alpha, \beta)$ of a function $f(\xi, \eta)$ is defined as

$$f_*(\alpha, \beta) = \frac{1}{2\pi} \int_{-\infty}^{\infty} d\eta \int_{-\infty}^{\infty} d\xi \; e^{-\mathrm{i}\,(\alpha\,\xi + \beta\,\eta)} \; f(\xi, \eta) \; . \tag{6.41a}$$

The function $f(\xi, \eta)$ is related to its Fourier transform $f_*(\alpha, \beta)$ by means of the inverse transformation

$$f(\xi, \eta) = \frac{1}{2\pi} \int_{-\infty}^{\infty} d\beta \int_{-\infty}^{\infty} d\alpha \; e^{\mathrm{i}\,(\alpha\,\xi + \beta\,\eta)} \; f_*(\alpha, \beta) \; . \tag{6.41b}$$

The definitions (6.40a) and (6.6) of the Fourier transform and the Dirac delta function yield

$$\delta_*(\alpha; x) = \frac{1}{\sqrt{2\pi}} \int_{-\infty}^{\infty} d\xi \; e^{-\mathrm{i}\,\alpha\,\xi} \; \delta(\xi - x) = \frac{1}{\sqrt{2\pi}} \; e^{-\mathrm{i}\,\alpha\,x} \; .$$

Thus, the functions

$$\delta(\xi - x) \quad \text{and} \quad e^{-\mathrm{i}\,\alpha\,x}/\sqrt{2\pi}$$

are Fourier transforms. Similarly, (6.41a) shows that the functions

$$\delta(\xi - x)\,\delta(\eta - y) \quad \text{and} \quad e^{-\mathrm{i}\,(\alpha\,x + \beta\,y)}/(2\pi) \tag{6.42}$$

are Fourier transforms. This important result provides basic insight into the far-field waves created by a near-field singularity such as a Green function.

6.10 Two related fundamental solutions

Two fundamental elementary solutions of the Laplace equation have already been encountered. These basic solutions are

$$1/r \equiv 1/\sqrt{(\xi - x)^2 + (\eta - y)^2 + (\zeta - z)^2} \;\; \text{with} \;\; 0 < r \tag{6.43a}$$

$$\text{and} \;\; e^{\,k\,\zeta + \mathrm{i}\,(\alpha\,\xi + \beta\,\eta)} \;\; \text{where} \;\; k = \sqrt{\alpha^2 + \beta^2} \; . \tag{6.43b}$$

These two fundamental solutions, which correspond to the fundamental free-space Green function (6.12) and an elementary wave function, are related via the Fourier transformation defined in the previous section.

The connection between the elementary solutions (6.43a) and (6.43b) can be considered via the double Fourier transform of the fundamental Green function (6.12). Moreover, this Fourier transform is used in chapter 7 to determine the Green functions that satisfy the free-surface boundary conditions associated with the classes of flows considered in the book. The Fourier transform $(1/r)_*$ can be determined by evaluating the integral

$$\left(\frac{1}{r}\right)_* = \frac{1}{2\pi}\int_{-\infty}^{\infty} d\eta \int_{-\infty}^{\infty} d\xi \; \frac{e^{-\mathrm{i}\,(\alpha\,\xi+\beta\,\eta)}}{r}$$

in accordance with (6.41a).

However, it is simpler to determine $(1/r)_*$ by starting from the Poisson equation (6.16), i.e.

$$(\partial_\xi^2 + \partial_\eta^2 + \partial_\zeta^2)(1/r) = -\,4\,\pi\,\delta(\xi - x)\,\delta(\eta - y)\,\delta(\zeta - z) \;.$$

Expressions (6.41a), (6.40c) and (6.6) show that the double Fourier transformation of this equation with respect to the two horizontal coordinates ξ and η yields

$$d^2(1/r)_*/d\zeta^2 - k^2\,(1/r)_* = -2\;e^{-\mathrm{i}\,(\alpha\,x+\beta\,y)}\;\delta(\zeta - z) \tag{6.44}$$

where $k^2 \equiv \alpha^2 + \beta^2$. One then has

$$d^2(1/r)_*/d\zeta^2 - k^2(1/r)_* = 0 \;\text{ for }\; \zeta < z \;\text{ and }\; z < \zeta \;.$$

The general solution of this differential equation is

$$(1/r)_* = A^+\,e^{k\,\zeta} + A^-\,e^{-k\,\zeta}$$

where A^+ and A^- are unspecified. This general solution can be restricted because the function $1/r$ and (consequently) its Fourier transform $(1/r)_*$ are even function of $\zeta - z$ that vanish as $\zeta - z \to \pm\infty$. The function $(1/r)_*$ is then given by

$$(1/r)_* = A\;e^{-k\,|\,\zeta - z\,|} \tag{6.45}$$

where A is unspecified.

The function $(1/r)_*$ defined by (6.45) is continuous, equal to A, for $\zeta = z$. However, its derivative is discontinuous at $\zeta = z$. Specifically, the derivative $d(1/r)_*/d\zeta$ is given by

$$k\,A\,e^{k\,(\zeta - z)} \;\text{ for }\; \zeta < z \quad \text{or} \quad -\,k\,A\,e^{-k\,(\zeta - z)} \;\text{ for }\; z < \zeta \;.$$

It follows that one has

$$d(1/r)_*/d\zeta = \left\{ \begin{matrix} -\,k\,A \;\text{ for }\; \zeta = z + 0 \\ \;\;\,k\,A \;\text{ for }\; \zeta = z - 0 \end{matrix} \right\} \;. \tag{6.46}$$

Integration of the differential equation (6.44) with respect to ζ within the range $[\,z-0,\,z+0\,]$ yields

$$[\,d\,(1/r)_*/d\zeta\,]_{\,\zeta\,=\,z\,-\,0}^{\,\zeta\,=\,z\,+\,0} - k^2\int_{z\,-\,0}^{z\,+\,0} d\zeta\,(1/r)_* = -2\,e^{-\,\mathrm{i}\,(\alpha\,x\,+\,\beta\,y)}\ .$$

This relation and expressions (6.46) yield $-2\,k\,A\,=\,-2\,e^{-\,\mathrm{i}\,(\alpha\,x\,+\,\beta\,y)}$. The unspecified factor A in (6.45) is then given by

$$A = e^{-\,\mathrm{i}\,(\alpha\,x\,+\,\beta\,y)}/k\ .$$

This expression and expression (6.45) finally yield

$$(1/r)_* = e^{-\,k\,|\,z-\zeta\,|\,-\,\mathrm{i}\,(\alpha\,x\,+\,\beta\,y)}/k\ . \tag{6.47a}$$

Expressions (6.41b) and (6.47a) then yield the integral representation

$$\frac{1}{r} = \frac{1}{2\,\pi}\int_{-\infty}^{\infty} d\beta \int_{-\infty}^{\infty} d\alpha\ \frac{1}{k}\ e^{-\,k\,|\,\zeta\,-\,z\,|\,+\,\mathrm{i}\,[\,\alpha\,(\xi\,-\,x)\,+\,\beta\,(\eta\,-\,y)\,]} \tag{6.47b}$$

of the free-space Green function $1/r$. The changes of variables $\alpha \rightarrow -\alpha$ and $\beta \rightarrow -\beta$ in (6.47b) yield the equivalent expression

$$\frac{1}{r} = \frac{1}{2\,\pi}\int_{-\infty}^{\infty} d\beta \int_{-\infty}^{\infty} d\alpha\ \frac{1}{k}\ e^{-\,k\,|\,z\,-\,\zeta\,|\,+\,\mathrm{i}\,[\,\alpha\,(x\,-\,\xi)\,+\,\beta\,(y\,-\,\eta)\,]}\ . \tag{6.47c}$$

The integral representation (6.47b) relates the two fundamental solutions

$$1/r \ \text{ and } \ e^{-\sqrt{\alpha^2\,+\,\beta^2}\,|\,z\,-\,\zeta\,|\,+\,\mathrm{i}\,[\,\alpha\,(x\,-\,\xi)\,+\,\beta\,(y\,-\,\eta)\,]} \tag{6.47d}$$

of the Laplace equation.

The solution $1/r$ associated with the fundamental Green function (6.12) is well suited for representing near-field local flows. The other solution corresponds to an elementary plane wave, and is well suited to represent far-field waves. Expressions (6.47) show that the two complementary near-field and far-field solutions (6.47d) are related via Fourier transformation. This property is analogous to the property (6.42).

The notation

$$h \equiv \sqrt{(x-\xi)^2 + (y-\eta)^2} \tag{6.48}$$

is used hereafter.

The relations (6.47a) and (6.47c) can be generalized as

$$(1/\sqrt{h^2+c^2}\,)_* = e^{-\,k\,|\,c\,|\,-\,\mathrm{i}\,(\alpha\,x\,+\,\beta\,y)}/k \ \text{ and} \tag{6.49a}$$

$$\frac{1}{\sqrt{h^2+c^2}} = \frac{1}{2\,\pi}\int_{-\infty}^{\infty} d\beta \int_{-\infty}^{\infty} d\alpha\ \frac{1}{k}\ e^{-\,k\,|\,c\,|\,+\,\mathrm{i}\,[\,\alpha\,(x\,-\,\xi)\,+\,\beta\,(y\,-\,\eta)\,]} \tag{6.49b}$$

$$= \frac{1}{2\,\pi}\int_{0}^{\infty} dk \int_{-\pi}^{\pi} d\gamma\ e^{-\,k\,|\,c\,|\,+\,\mathrm{i}\,k\,[\,(x\,-\,\xi)\,\cos\gamma\,+\,(y\,-\,\eta)\,\sin\gamma\,]} \tag{6.49c}$$

where c is real.

The particular choice $c = z + \zeta$ yields

$$(1/r')_* = e^{k(z+\zeta) - \mathrm{i}(\alpha x + \beta y)}/k \text{ and} \tag{6.50a}$$

$$\frac{1}{r'} = \frac{1}{2\pi}\int_{-\infty}^{\infty} d\beta \int_{-\infty}^{\infty} d\alpha \; \frac{1}{k}\, e^{k(z+\zeta) + \mathrm{i}[\alpha(x-\xi) + \beta(y-\eta)]} \tag{6.50b}$$

where r' is defined by (6.33) as $r' \equiv \sqrt{h^2 + (z+\zeta)^2}$ with h given by (6.48), and one has $z \leq 0$ and $\zeta \leq 0$.

The choice $c = z + \zeta + 2\,d$ in (6.49) yields

$$(1/r_d)_* = e^{-k(z+\zeta+2\,d) - \mathrm{i}(\alpha x + \beta y)}/k \text{ and} \tag{6.51a}$$

$$\frac{1}{r_d} = \frac{1}{2\pi}\int_{-\infty}^{\infty} d\beta \int_{-\infty}^{\infty} d\alpha \; \frac{1}{k}\, e^{-k(z+\zeta+2\,d) + \mathrm{i}[\alpha(x-\xi) + \beta(y-\eta)]} \tag{6.51b}$$

where r_d is defined by (6.23b) as $r_d \equiv \sqrt{h^2 + (z+\zeta+2\,d)^2}$ with h given by (6.48), and one has $-d \leq z \leq 0$ and $-d \leq \zeta \leq 0$. Expressions (6.47)-(6.51) are used in chapter 7.

6.11 Image singularities

The mirror image of the fundamental Rankine source $-1/r$ in (6.12)-(6.13) with respect to the mean free-surface plane $\zeta = 0$ is used in expression (6.32) for the Green function that satisfies the free-surface boundary condition (6.31c). The distance r' between the point $\boldsymbol{\xi} \equiv (\xi, \eta, \zeta)$ and the mirror image $\mathbf{x}' \equiv (x, y, -z)$ of the point $\mathbf{x} \equiv (x, y, z)$ with respect to the plane $z = 0$ is given by (6.33).

An illustrative application of expressions (6.47b) and (6.51b) is now given. For $\zeta < z$, expression (6.47b) yields

$$\frac{1}{r} = \frac{1}{2\pi}\int_{-\infty}^{\infty} d\beta \int_{-\infty}^{\infty} d\alpha \; \frac{1}{k}\, e^{k(\zeta - z) + \mathrm{i}[\alpha(x-\xi) + \beta(y-\eta)]} \; . \tag{6.52}$$

Expression (6.51b) and (6.52) then yield

$$\partial_\zeta \left(\frac{1}{r} + \frac{1}{r_d}\right) = \frac{1}{2\pi}\int_{-\infty}^{\infty} d\beta \int_{-\infty}^{\infty} d\alpha \; A^d\, e^{\mathrm{i}[\alpha(x-\xi) + \beta(y-\eta)]} \text{ where}$$

$$A^d \equiv e^{k(\zeta - z)} - e^{-k(\zeta + z + 2\,d)} = e^{-k(z+d)}\left(e^{k(\zeta+d)} - e^{-k(\zeta+d)}\right)$$

$$= 2\sinh[k(\zeta + d)]\, e^{-k(z+d)} \; .$$

This expression is nil for $\zeta = -d$. The sea-bottom boundary condition

$$\partial_\zeta (1/r + 1/r_d) = 0 \text{ at } \zeta = -d \tag{6.53}$$

is then satisfied, in agreement with (6.23c) and (6.22).

Chapter 7

Green functions associated with flows due to ships or offshore structures

This chapter considers the Green functions that satisfy the free-surface boundary conditions associated with a ship that advances, in deep water, at a constant speed through regular waves or in calm water. The Green function that is appropriate for diffraction and radiation of regular waves by an offshore structure or a moored ship (or other stationary bodies) is also considered for deep water and in water of uniform finite depth.

7.1 Ship steadily advancing through regular waves

The Green function $G(\boldsymbol{\xi},\mathbf{x})$ that satisfies the free-surface condition (6.31c) associated with a ship that steadily advances through regular waves is now considered for deep water. This Green function is given by (6.32) where the harmonic function H^F is defined by the boundary-value problem (6.34). Thus, the function H^F satisfies the Laplace equation

$$(\partial_\xi^2 + \partial_\eta^2 + \partial_\zeta^2) H^F = 0 \text{ in } \zeta < 0 \tag{7.1a}$$

and the boundary conditions

$$H^F \to 0 \text{ as } r \to \infty \text{ and} \tag{7.1b}$$

$$[\,\partial_\zeta + (\,\mathrm{i} f - \epsilon - F\,\partial_\xi)^2\,]\, H^F = -2\pi\,\partial_\zeta(1/r') \text{ at } \zeta = 0\ . \tag{7.1c}$$

This boundary-value problem is solved via double Fourier transformation with respect to the two horizontal coordinates ξ and η. Specifically, the Fourier transform $H_*^F(\alpha,\beta,\zeta;\mathbf{x})$ of the function $H^F(\xi,\eta,\zeta;\mathbf{x})$ is

$$H_*^F(\alpha,\beta,\zeta;\mathbf{x}) = \frac{1}{2\pi}\int_{-\infty}^{\infty} d\eta \int_{-\infty}^{\infty} d\xi \; e^{-\mathrm{i}\,(\alpha\,\xi+\beta\,\eta)}\; H^F(\xi,\eta,\zeta;\mathbf{x}) \tag{7.2a}$$

and the function H^F is related to its Fourier transform H_*^F via the inverse Fourier transform

$$H^F(\xi,\eta,\zeta;\mathbf{x}) = \frac{1}{2\pi}\int_{-\infty}^{\infty} d\beta \int_{-\infty}^{\infty} d\alpha \; e^{\mathrm{i}\,(\alpha\,\xi+\beta\,\eta)}\; H_*^F(\alpha,\beta,\zeta;\mathbf{x}) \tag{7.2b}$$

in accordance with (6.41).

Expression (6.40c), the identity $k^2 \equiv \alpha^2+\beta^2$, and the Fourier transform (6.50a) of $1/r'$ show that Fourier transformation of the Laplace equation (7.1a) and the boundary conditions (7.1b) and (7.1c) yields

$$d^2H_*^F/d\zeta^2 - k^2 H_*^F = 0 \;\text{ in }\; -\infty < \zeta < 0 \;, \tag{7.3a}$$

$$H_*^F \to 0 \;\text{ as }\; \zeta \to -\infty \;\text{ and} \tag{7.3b}$$

$$\begin{aligned} &dH_*^F/d\zeta - [\,(f-F\alpha)^2 + 2\,\mathrm{i}\,\epsilon\,(f-F\alpha) - \epsilon^2\,]\,H_*^F \\ &\qquad = -2\,\pi\, e^{\,k\,z\,-\,\mathrm{i}\,(\alpha\,x+\beta\,y)} \;\text{ at }\; \zeta = 0 \;. \end{aligned} \tag{7.3c}$$

The general solution of the differential equation (7.3a) is

$$H_*^F = A^+\, e^{\,k\,\zeta} + A^-\, e^{-k\,\zeta}$$

where A^+ and A^- are unspecified. The boundary condition (7.3b) implies $A^- = 0$.

The boundary condition (7.3c) then yields the solution

$$H_*^F = 2\,\pi\; e^{\,k\,(\zeta+z)\,-\,\mathrm{i}\,(\alpha\,x+\beta\,y)}/(\Delta + \mathrm{i}\,\epsilon\,\Delta_f - \epsilon^2) \tag{7.4a}$$

where the functions Δ and Δ_f are defined as

$$\Delta \equiv (f-F\alpha)^2 - k \;\text{ and }\; \Delta_f \equiv 2\,(f-F\alpha) \;\text{ with }\; k \equiv \sqrt{\alpha^2+\beta^2}\;. \tag{7.4b}$$

The inverse Fourier transform (7.2b) of the function (7.4a) is given by

$$H^F = \int_{-\infty}^{\infty} d\beta \int_{-\infty}^{\infty} d\alpha \; \frac{e^{\,k\,(\zeta+z)\,+\,\mathrm{i}\,[\,\alpha\,(\xi-x)\,+\,\beta\,(\eta-y)\,]}}{\Delta + \mathrm{i}\,\epsilon\,\Delta_f - \epsilon^2} \;. \tag{7.4c}$$

The changes of variables $\alpha \to -\alpha$ and $\beta \to -\beta$ in the double Fourier integral (7.4c) yield the equivalent expression

$$H^F = \int_{-\infty}^{\infty} d\beta \int_{-\infty}^{\infty} d\alpha \; \frac{e^{\,k\,(z+\zeta)\,+\,\mathrm{i}\,[\,\alpha\,(x-\xi)\,+\,\beta\,(y-\eta)\,]}}{\Delta + \mathrm{i}\,\epsilon\,\Delta_f - \epsilon^2} \tag{7.5a}$$

where the dispersion functions Δ and Δ_f are now defined as

$$\Delta \equiv (f+F\alpha)^2 - k \;\text{ and }\; \Delta_f \equiv 2\,(f+F\alpha) \;\text{ with }\; k \equiv \sqrt{\alpha^2+\beta^2}\;. \tag{7.5b}$$

These dispersion functions agree with the dispersion function Δ associated with the analysis, considered in chapters 2 and 5, of free waves created by a ship that advances through regular waves in deep water.

Expressions (7.5), where ϵ^2 in the denominator of the double Fourier integral (7.5a) is inconsequential and can be ignored, and expression (6.32) show that the Green function $G(\boldsymbol{\xi},\mathbf{x})$ associated with a ship that steadily advances through regular waves in deep water can finally be expressed as

$$4\pi G = G^R + G^F \;\text{ where }\; G^R = -1/r + 1/r' \;\text{ i.e.} \tag{7.6a}$$

$$G^R = -1/\sqrt{h^2+(z-\zeta)^2} + 1/\sqrt{h^2+(z+\zeta)^2} \;\text{ and} \tag{7.6b}$$

$$G^F = \frac{1}{\pi}\int_{-\pi}^{\pi} d\gamma \int_0^{\infty} dk\; \frac{e^{\,k\,(z+\zeta)\,+\,\mathrm{i}\,[\,\alpha\,(x-\xi)\,+\,\beta\,(y-\eta)\,]}}{(f+F\alpha)^2/k - 1 + 2\,\mathrm{i}\,\epsilon\,(f+F\alpha)/k} \tag{7.6c}$$

$$\text{with }\; (\alpha,\beta) = k\,(\cos\gamma, \sin\gamma)\;. \tag{7.6d}$$

Moreover, h in (7.6b) is given by (6.48). Expression (7.6c) shows that the Fourier component G^F in the basic Rankine-Fourier decomposition (7.6a) of G is given by a Fourier superposition of elementary wave functions.

7.2 Nonuniqueness of decomposition into Rankine and Fourier components

The Rankine-Fourier decomposition (7.6) is not unique. In particular, the Fourier representations (6.47c) and (6.50b) of the Rankine components $1/r$ and $1/r'$ can be used to express G^R as

$$G^R = \frac{-1}{2\pi}\int_{-\infty}^{\infty} d\beta \int_{-\infty}^{\infty} d\alpha\; \frac{1}{k}\Big[\,e^{-k\,|\,z-\zeta\,|} - e^{\,k\,(z+\zeta)}\Big]\, e^{\,\mathrm{i}\,[\,\alpha\,(x-\xi)\,+\,\beta\,(y-\eta)\,]}\;.$$

This Fourier representation of the Rankine component G^R can be combined with expression (7.6c) for the Fourier component G^F. Thus, the Green function G defined by (7.6) can be expressed as

$$4\pi G = \frac{1}{\pi}\int_{-\infty}^{\infty} d\beta \int_{-\infty}^{\infty} d\alpha\; A^z A^{\zeta}\; \frac{e^{\,\mathrm{i}\,[\,\alpha\,(x-\xi)\,+\,\beta\,(y-\eta)\,]}}{\Delta + \mathrm{i}\,\epsilon\,\Delta_f} \;\text{ where} \tag{7.7a}$$

$$A^z A^{\zeta} \equiv e^{\,k\,(z+\zeta)} + \frac{(f+F\alpha)^2 - k}{2\,k}\Big[\,e^{\,k\,(\zeta+z)} - e^{-k\,|\,\zeta-z\,|}\Big] \;\text{ i.e.}$$

$$A^z = e^{\,k\,z} \;\text{ and }\; A^{\zeta} = e^{\,k\,\zeta} + \frac{\Delta}{2\,k}\big[\,e^{\,k\,\zeta} - e^{-k\,\zeta}\,\big] \;\text{ if } z < \zeta \;\text{ or} \tag{7.7b}$$

$$A^z = e^{\,k\,z} + \frac{\Delta}{2\,k}\big[\,e^{\,k\,z} - e^{-k\,z}\,\big] \;\text{ and }\; A^{\zeta} = e^{\,k\,\zeta} \;\text{ if } \zeta < z\;. \tag{7.7c}$$

The representation (7.7) of the Green function G does not involve Rankine singularities and expresses G as a double Fourier integral. The different expressions (7.7b) and (7.7c) for the functions A^z and A^ζ in (7.7a) are cumbersome, and the representation (7.7) is not useful for practical applications.

Inversely, the general expressions (6.49) associated with the Fourier transform of a Rankine source can be applied to extract Rankine sources from the Fourier integral representation of the component G^F, notably for the useful purpose of ensuring that the amplitude function $A^z A^\zeta$ in the Fourier integral (7.7a) vanishes rapidly in the limits $k \to 0$ and $k \to \infty$. Thus, the general relation (6.49) can be applied to define alternative and *optimal Rankine-Fourier decompositions* of Green functions. **[7,1]**

7.3 Ship steadily advancing in deep calm water

In the special case $f = 0$, i.e. for steady flow around a ship that advances at a constant speed in calm deep water, expressions (7.6) yield

$$4\pi G = \frac{-1}{r} + \frac{1}{r'} + \frac{1}{\pi}\int_{-\infty}^{\infty} d\beta \int_{-\infty}^{\infty} d\alpha \, \frac{e^{k(z+\zeta)+\mathrm{i}[\alpha(x-\xi)+\beta(y-\eta)]}}{F^2\alpha^2 - k + 2\,\mathrm{i}\,\epsilon F\alpha} \quad . \tag{7.8}$$

This representation of the Green function expresses G in terms of the free-space Rankine sources $1/r$ and $1/r'$ and a double Fourier superposition of elementary wave functions. Alternative Rankine-Fourier decompositions can be obtained via the Fourier representation (6.50b) that expresses the Rankine source $1/r'$ as a Fourier superposition of elementary wave functions, in the manner now explained.

Alternative Rankine-Fourier decompositions

Thus, alternative forms of (7.8) are now considered. Expression (6.50b) can be used to express (7.8) in the two alternative forms

$$4\pi G = \frac{-1}{r} + \frac{1}{\pi}\int_{-\infty}^{\infty} d\beta \int_{-\infty}^{\infty} d\alpha \, \frac{F^2\alpha^2 + k}{2k} \, \frac{e^{k(z+\zeta)+\mathrm{i}[\alpha(x-\xi)+\beta(y-\eta)]}}{F^2\alpha^2 - k + 2\,\mathrm{i}\,\epsilon F\alpha} \tag{7.9a}$$

$$4\pi G = \frac{-1}{r} - \frac{1}{r'} + \frac{1}{\pi}\int_{-\infty}^{\infty} d\beta \int_{-\infty}^{\infty} d\alpha \, \frac{F^2\alpha^2}{k} \, \frac{e^{k(z+\zeta)+\mathrm{i}[\alpha(x-\xi)+\beta(y-\eta)]}}{F^2\alpha^2 - k + 2\,\mathrm{i}\,\epsilon F\alpha} \tag{7.9b}$$

where the inconsequential term $2\,\mathrm{i}\,\epsilon F\alpha$ is ignored in the numerators of the Fourier integrals.

Limits $k \to 0$ and $k \to \infty$

The integrands of the double Fourier integrals in the three alternative representations (7.8) and (7.9) involve the functions

$$A^+ \equiv 1 \ , \ A \equiv (F^2\alpha^2/k + 1)/2 \ \text{ or } \ A^- \equiv F^2\alpha^2/k \ . \tag{7.10a}$$

In the small-wavenumber limit $k \to 0$, these expressions yield

$$A^+ \sim 1 \ , \ A \sim 1/2 \ , \ A^- \sim 0 \ . \tag{7.10b}$$

The asymptotic approximations (7.10b) show that the double Fourier integral in the representation (7.9b) is preferable to the corresponding Fourier integrals in the representations (7.8) and (7.9a) in the limit $k \to 0$. In the large-wavenumber limit $k \to \infty$, expressions (7.10a) yield

$$\left\{ \begin{matrix} A^+ \sim 1 \\ A \sim F^2\alpha^2/(2k) \\ A^- \sim F^2\alpha^2/k \end{matrix} \right\} \text{ if } 1 \ll \frac{F^2\alpha^2}{k} \ \text{ or } \ \left\{ \begin{matrix} A^+ \sim 1 \\ A \sim 1/2 \\ A^- \ll 1 \end{matrix} \right\} \text{ if } \frac{F^2\alpha^2}{k} \ll 1 \ . \tag{7.10c}$$

The asymptotic approximations (7.10c) show that the functions A and A^- are $O(k)$ as $k \to \infty$ if $\alpha \neq 0$, and that the double Fourier integral in the representation (7.8) is preferable to the corresponding Fourier integrals in the representations (7.9) in the limit $k \to \infty$, except in the special case $F^2\alpha^2/k \ll 1$ for which (7.9b) is best.

Thus, the representations (7.8) and (7.9b) are best suited in the limits $k \to \infty$ or $k \to 0$, respectively. This conclusion, based on the behavior of the double Fourier integrals in the alternative expressions (7.8) and (7.9) in the limits $k \to \infty$ or $k \to 0$, can also be justified by considering the near-field and far-field behaviors of the free-surface boundary condition (6.31c) in the special case $f = 0$ now considered. This complementary 'physical-space' analysis of the alternative representations (7.8) and (7.9b) is given in section 7.7.

Optimal Rankine-Fourier decomposition

The foregoing analysis suggests the consideration of the representation

$$4\pi G = -1/r + 1/r' - 2/r^F + \widetilde{H}/\pi \tag{7.11}$$

$$\text{where } \ r^F \equiv \sqrt{h^2 + (z + \zeta - F^2)^2} \tag{7.12}$$

is the distance between the points $\boldsymbol{\xi}$ and $\mathbf{x}^F \equiv (x, y, -z + F^2)$. Expressions (7.12) and (6.33) yield

$$\frac{-1}{r} + \frac{1}{r'} - \frac{2}{r^F} \sim \frac{-1}{r} + \frac{1}{r'} \ \text{ as } \ \frac{r'}{F^2} \to 0 \ , \tag{7.13a}$$

$$\frac{-1}{r} + \frac{1}{r'} - \frac{2}{r^F} \sim \frac{-1}{r} - \frac{1}{r'} \ \text{ as } \ \frac{r'}{F^2} \to \infty \ . \tag{7.13b}$$

Expression (6.49b) with $c = z + \zeta - F^2$ yields

$$\frac{2}{r^F} = \frac{1}{\pi}\int_{-\infty}^{\infty} d\beta \int_{-\infty}^{\infty} d\alpha \; \frac{1}{k} \; e^{\,k\,(z+\zeta-F^2)\,+\,\mathrm{i}\,[\,\alpha\,(x-\xi)\,+\,\beta\,(y-\eta)\,]} \;\; . \tag{7.14}$$

This relation and expression (7.8) show that the representation (7.11) is given by

$$4\pi G = -1/r + 1/r' - 2/r^F + \frac{1}{\pi}\int_{-\infty}^{\infty} d\beta \int_{-\infty}^{\infty} d\alpha \; a^F \; \frac{e^{\,k\,(z+\zeta)\,+\,\mathrm{i}\,[\,\alpha\,(x-\xi)\,+\,\beta\,(y-\eta)\,]}}{F^2\alpha^2 - k + 2\,\mathrm{i}\,\epsilon F \alpha} \tag{7.15a}$$

$$\text{where } \; a^F \equiv 1 + (F^2\alpha^2/k - 1)\, e^{-F^2 k} \; . \tag{7.15b}$$

One has $a^F = 1$ at the dispersion curves, defined by the equivalent relations $F^2\alpha^2 = k$ or $F^2 k = 1/\cos^2\gamma$, and

$$a^F \sim F^2 k\,(1 + \cos^2\gamma) \text{ as } k \to 0 \quad \text{and} \quad a^F \sim 1 \text{ as } k \to \infty \; . \tag{7.15c}$$

These asymptotic approximations show that the Fourier integral in (7.15) is similar to the Fourier integrals in (7.9b) or (7.8) in the limits $k \to 0$ or $k \to \infty$, respectively, and the Rankine-Fourier decomposition associated with expressions (7.15a-b) is then optimal in this respect.

The Green function that satisfies the free-surface boundary condition for a ship that steadily advances in calm deep water is finally expressed as

$$4\pi G = G^R + G^F \;\; \text{where} \;\; G^R = -1/r + 1/r' - 2/r^F \;\; \text{i.e.} \tag{7.16a}$$

$$G^R = -1/\sqrt{h^2 + (z-\zeta)^2} + 1/\sqrt{h^2 + (z+\zeta)^2} - 2/\sqrt{h^2 + (z+\zeta-F^2)^2} \; ,$$

$$G^F = \frac{1}{\pi}\int_{-\pi}^{\pi} d\gamma \int_0^{\infty} dk \; a^F \; \frac{e^{\,k\,(z+\zeta)\,+\,\mathrm{i}\,[\,\alpha\,(x-\xi)\,+\,\beta\,(y-\eta)\,]}}{F^2\alpha^2/k - 1 + 2\,\mathrm{i}\,\epsilon F \alpha/k} \tag{7.16b}$$

$$\text{with} \;\; a^F = 1 + e^{-F^2 k}\,(F^2\alpha^2/k - 1) \; . \tag{7.16c}$$

Moreover, h in (7.16b) is given by (6.48).

7.4 Diffraction-radiation of regular waves by offshore structures in deep water

In the special case of diffraction-radiation of time-harmonic waves by a stationary body in deep water, expressions (7.6) with $F = 0$ yield

$$4\pi G = \frac{-1}{r} + \frac{1}{r'} + \frac{1}{\pi}\int_{-\pi}^{\pi} d\gamma \int_0^{\infty} dk \; k \; \frac{e^{\,k\,(z+\zeta)\,+\,\mathrm{i}\,[\,\alpha\,(x-\xi)\,+\,\beta\,(y-\eta)\,]}}{f^2 - k + 2\,\mathrm{i}\,\epsilon F} \;\; . \tag{7.17}$$

The representation (6.50b) of the Rankine source $1/r'$ as a Fourier superposition of elementary wave functions can again be used to obtain alternative Rankine-Fourier decompositions and an optimal decomposition.

Alternative Rankine-Fourier decompositions

Expression (6.50b) can be used to express (7.17) in the alternative forms

$$4\pi G = \frac{-1}{r} + \frac{1}{\pi}\int_{-\pi}^{\pi} d\gamma \int_0^\infty dk\, \frac{f^2+k}{2}\, \frac{e^{k\,(z+\zeta)\,+\,\mathrm{i}\,[\,\alpha\,(x-\xi)\,+\,\beta\,(y-\eta)\,]}}{f^2-k+2\,\mathrm{i}\,\epsilon F}\ , \quad (7.18a)$$

$$4\pi G = \frac{-1}{r} - \frac{1}{r'} + \frac{f^2}{\pi}\int_{-\pi}^{\pi} d\gamma \int_0^\infty dk\, \frac{e^{k\,(z+\zeta)\,+\,\mathrm{i}\,[\,\alpha\,(x-\xi)\,+\,\beta\,(y-\eta)\,]}}{f^2-k+2\,\mathrm{i}\,\epsilon F} \quad (7.18b)$$

where the inconsequential term $2\,\mathrm{i}\,\epsilon F$ is ignored in the numerators of the integrands of the Fourier integrals.

Limits $k \to \infty$ and $k \to 0$

The double Fourier integrals in the alternative representations (7.17) and (7.18a-b) involve the functions

$$A^+ \equiv k\ ,\ A \equiv (f^2+k)/2 \ \text{ or } \ A^- \equiv f^2\ .$$

These expressions yield

$$\left\{\begin{matrix} A^+ \sim k \\ A \sim k/2 \\ A^- \sim f^2 \end{matrix}\right\} \text{ as } k \to \infty \quad \text{and} \quad \left\{\begin{matrix} A^+ \to 0 \\ A \to f^2/2 \\ A^- \to f^2 \end{matrix}\right\} \text{ as } k \to 0\ . \quad (7.19)$$

The approximations (7.19) show that the double Fourier integrals in the representations (7.18b) or (7.17) are preferable to the Fourier integrals in the alternative representations in the limits $k \to \infty$ or $k \to 0$, respectively.

This conclusion, based on the behavior of the double Fourier integrals in the alternative expressions (7.17) and (7.18) in the limits $k \to \infty$ or $k \to 0$, can be further justified by considering the near-field and far-field behaviors of the free-surface boundary condition (6.31c) in the special case $F = 0$ now considered. This complementary 'physical-space' analysis of the alternative representations (7.17) and (7.18b) is given in section 7.7.

Optimal Rankine-Fourier decomposition

The foregoing analysis suggests the consideration of the representation

$$4\pi G = -1/r - 1/r' + 2/r^f + \widetilde{H}/\pi \quad (7.20)$$

$$\text{where } r^f \equiv \sqrt{h^2 + (z+\zeta-1/f^2)^2} \quad (7.21)$$

is the distance between the points $\boldsymbol{\xi}$ and $\mathbf{x}^f \equiv (x, y, -z+1/f^2)$. Expressions (7.21) and (6.33) yield

$$\frac{-1}{r} - \frac{1}{r'} + \frac{2}{rf} \sim \frac{-1}{r} - \frac{1}{r'} \text{ as } f^2 r' \to 0 \ , \tag{7.22a}$$

$$\frac{-1}{r} - \frac{1}{r'} + \frac{2}{rf} \sim \frac{-1}{r} + \frac{1}{r'} \text{ as } f^2 r' \to \infty \ . \tag{7.22b}$$

Expression (6.49b) with $c = z + \zeta - 1/f^2$ yields

$$\frac{2}{r^f} = \frac{1}{\pi} \int_{-\infty}^{\infty} d\beta \int_{-\infty}^{\infty} d\alpha \ \frac{1}{k} \ e^{\,k\,(z+\zeta-1/f^2)\,+\,\mathrm{i}\,[\,\alpha\,(x-\xi)\,+\,\beta\,(y-\eta)\,]} \ . \tag{7.23}$$

Expressions (7.20), (7.23) and (7.18b) yield

$$4\pi G = -1/r - 1/r' + 2/r^f + \frac{f^2}{\pi} \int_{-\pi}^{\pi} d\gamma \int_0^{\infty} dk \ a^F \ \frac{e^{\,k\,(z+\zeta)\,+\,\mathrm{i}\,[\,\alpha\,(x-\xi)\,+\,\beta\,(y-\eta)\,]}}{f^2 - k + 2\,\mathrm{i}\,\epsilon F} \tag{7.24a}$$

$$\text{where } a^F \equiv 1 + (k/f^2 - 1)\, e^{-k/f^2} \ . \tag{7.24b}$$

One has $a^F = 1$ at the dispersion circle $k/f^2 = 1$, and

$$a^F \sim 1 \text{ as } k/f^2 \to \infty \quad \text{and} \quad a^F \to 0 \text{ as } k/f^2 \to 0 \ . \tag{7.24c}$$

These asymptotic approximations and the asymptotic approximations (7.19) show that the double Fourier integral in the representation (7.24) is similar to the corresponding Fourier integrals in the representations (7.18b) or (7.17) in the limits $k \to \infty$ or $k \to 0$, respectively. The Rankine-Fourier decomposition (7.24) is in this respect optimal, and is used hereafter.

The Green function that satisfies the free-surface boundary condition related to diffraction-radiation of regular waves by an offshore structure in deep water is finally expressed as

$$4\pi G = G^R + G^F \text{ where } G^R = -1/r - 1/r' + 2/r^f \text{ i.e.} \tag{7.25a}$$

$$G^R = -1/\sqrt{h^2 + (z-\zeta)^2} - 1/\sqrt{h^2 + (z+\zeta)^2} + 2/\sqrt{h^2 + (z+\zeta-1/f^2)^2} \ ,$$

$$G^F = \frac{1}{\pi} \int_{-\pi}^{\pi} d\gamma \int_0^{\infty} dk \ a^F \ \frac{e^{\,k\,(z+\zeta)\,+\,\mathrm{i}\,[\,\alpha\,(x-\xi)\,+\,\beta\,(y-\eta)\,]}}{1 - k/f^2 + 2\,\mathrm{i}\,\epsilon/f} \tag{7.25b}$$

$$\text{with } a^F = 1 + e^{-k/f^2}(k/f^2 - 1) \ . \tag{7.25c}$$

The double integral Fourier representation (7.24) can be expressed as a single Fourier integral via the relation

$$\frac{1}{\pi} \int_{-\pi}^{\pi} d\gamma \ e^{\,\mathrm{i}\,[\,\alpha\,(x-\xi)\,+\,\beta\,(y-\eta)\,]} = 2\, J_0(k\,h) \tag{7.26}$$

where $J_0(\cdot)$ denotes the Bessel function of the first kind. One then obtains the alternative expression

$$4\pi G = \frac{-1}{r} - \frac{1}{r'} + \frac{2}{r^f} + 2 \int_0^{\infty} dk \ \frac{a^F e^{\,k\,(z+\zeta)}\, J_0(k\,h)}{1 - k/f^2 + 2\,\mathrm{i}\,\epsilon/f} \ . \tag{7.27}$$

7.5 Diffraction-radiation of regular waves by offshore structures in finite water-depth

The Green function $G(\boldsymbol{\xi},\mathbf{x})$ associated with diffraction-radiation of regular waves by offshore structures in water of uniform depth d is now considered. Equations (6.31) and (6.22) show that this Green function is the solution of the boundary-value problem

$$\nabla^2_{\boldsymbol{\xi}} G = \delta(\xi - x)\,\delta(\eta - y)\,\delta(\zeta - z) \ \text{ in } \ -d < \zeta < 0 \ , \tag{7.28a}$$

$$\partial_\zeta G = 0 \ \text{ at } \ \zeta = -d \ , \tag{7.28b}$$

$$[\,\partial_\zeta - (f + \mathrm{i}\,\epsilon)^2\,]\,G = 0 \ \text{ at } \ \zeta = 0 \ , \tag{7.28c}$$

$$G \to 0 \ \text{ as } \ h \equiv \sqrt{(\xi - x)^2 + (\eta - y)^2} \to \infty \tag{7.28d}$$

with $-d \le \zeta \le 0$ and $-d < z < 0$.

Basic Rankine-Fourier decomposition

The general solution of the Poisson equation (7.28a) is now expressed as

$$4\,\pi\,G = G^R_b + G^F_b \ \text{ where } \ G^R_b = -1/r - 1/r_d \ \text{ with} \tag{7.29a}$$

$$r \equiv \sqrt{h^2 + (z - \zeta)^2} \ \text{ and } \ r_d \equiv \sqrt{h^2 + (z + \zeta + 2\,d)^2} \ . \tag{7.29b}$$

In (7.29), r_d denotes the distance between the point $\boldsymbol{\xi} \equiv (\xi, \eta, \zeta)$ and the mirror image $\mathbf{x}^d \equiv (x, y, -z - 2\,d)$ of the point $\mathbf{x} \equiv (x, y, z)$ with respect to the sea-bottom plane $z = -d$ as is shown in Fig.7.1. The function $G^F_b(\boldsymbol{\xi},\mathbf{x})$ in (7.29a) satisfies the equations

$$\nabla^2_{\boldsymbol{\xi}} G^F_b = 0 \ \text{ in } \ -d < \zeta < 0 \ , \tag{7.30a}$$

$$\partial_\zeta\, G^F_b = 0 \ \text{ at } \ \zeta = -d \ , \tag{7.30b}$$

$$[\,\partial_\zeta - (f + \mathrm{i}\,\epsilon)^2\,]\,G^F_b = (\partial_\zeta - f^2)(1/r + 1/r_d) \ \text{ at } \ \zeta = 0 \ . \tag{7.30c}$$

Expressions (6.47b) and (6.51b) yield

$$\frac{1}{r} + \frac{1}{r_d} = \frac{1}{2\,\pi}\int_{-\infty}^{\infty} d\beta \int_{-\infty}^{\infty} d\alpha\, \frac{1}{k}\Big[e^{\,k\,(z\,-\,\zeta\,)} + e^{\,-\,k\,(z\,+\,\zeta\,+\,2\,d)}\Big]\, e^{\,\mathrm{i}\,[\,\alpha\,(x\,-\,\xi)\,+\,\beta\,(y\,-\,\eta)\,]}$$

if $0 < \zeta - z$. This expression and the identity

$$\begin{aligned} e^{\,k\,(z\,-\,\zeta\,)} + e^{\,-\,k\,(z\,+\,\zeta\,+\,2\,d)} &= \Big[e^{\,k\,(z\,+\,d\,)} + e^{\,-\,k\,(z\,+\,d\,)}\Big]\, e^{\,-\,k\,(\zeta\,+\,d\,)} \\ &= 2\,\cosh[\,k\,(z + d)\,]\, e^{\,-\,k\,(\zeta\,+\,d\,)} \ \text{ yield} \end{aligned}$$

$$\begin{aligned} &\pi\,(\partial_\zeta - f^2)(1/r + 1/r_d) = \\ &-\int_{-\infty}^{\infty} d\beta \int_{-\infty}^{\infty} d\alpha \left(\frac{f^2}{k} + 1\right) \cosh[\,k\,(z + d)\,]\, e^{\,-\,k\,(\zeta\,+\,d\,)}\, e^{\,\mathrm{i}\,[\,\alpha\,(x\,-\,\xi)\,+\,\beta\,(y\,-\,\eta)\,]} \end{aligned}$$

if $0 < \zeta - z$.

The function

$$G_b^F = \int_{-\infty}^{\infty} d\beta \int_{-\infty}^{\infty} d\alpha \, A \cosh[k(z+d)] \cosh[k(\zeta+d)] \, e^{\mathrm{i}[\alpha(x-\xi)+\beta(y-\eta)]}$$

satisfies the Laplace equation (7.30a) and the boundary condition (7.30b) at the sea bottom, and also satisfies the free-surface boundary condition (7.30c) if

$$\pi A \left[f^2 - k \tanh(kd) + 2\,\mathrm{i}\,\epsilon F \right] \cosh(kd) = (f^2/k)(1 + k/f^2)/e^{k\,d} \; .$$

One then has

$$G_b^F = \frac{1}{\pi} \int_{-\pi}^{\pi} d\gamma \int_0^{\infty} dk \; a_b^F \; \frac{\cosh[k(z+d)] \cosh[k(\zeta+d)] \, e^{\mathrm{i}[\alpha(x-\xi)+\beta(y-\eta)]}}{\cosh(kd) \, e^{k\,d} \left[1 - (k/f^2) \tanh(kd) + 2\,\mathrm{i}\,\epsilon/f \right]}$$

$$\text{where } \; a_b^F = 1 + k/f^2 \; . \tag{7.31}$$

Optimal Rankine-Fourier decomposition

The optimal deep-water Rankine-Fourier decomposition (7.25) is now extended to finite water-depth. Specifically, the Rankine-Fourier decomposition (7.29a) is modified as

$$4\pi G = G^R + G^F \text{ where} \tag{7.32a}$$

$$G^R = -1/r - 1/r_d - 1/r' - 1/r'_d + 2/r^f + 2/r^f_d \text{ with} \tag{7.32b}$$

$$r' \equiv \sqrt{h^2 + (z+\zeta)^2} \;\; , \;\; r'_d \equiv \sqrt{h^2 + (z - \zeta - 2d)^2} \tag{7.32c}$$

$$r^f \equiv \sqrt{h^2 + (z + \zeta - 1/f^2)^2} \;\; , \;\; r^f_d \equiv \sqrt{h^2 + (z - \zeta - 1/f^2 - 2d)^2} \tag{7.32d}$$

and r and r_d are given by (7.29b). In (7.32c), r' is the distance between the point $\boldsymbol{\xi}$ and the mirror image $\mathbf{x}' \equiv (x, y, -z)$ of the point $\mathbf{x}$ with respect to the free-surface plane $\zeta = 0$, and r'_d is the distance between the point $\boldsymbol{\xi}$ and the mirror image $\mathbf{x}'_d \equiv (x, y, z - 2d)$ of $\mathbf{x}'$ with respect to the sea-bottom plane $\zeta = -d$. Similarly in (7.32d), r^f is the distance between the points $\boldsymbol{\xi}$ and $\mathbf{x}^f \equiv (x, y, -z + 1/f^2)$ and r^f_d is the distance between the point $\boldsymbol{\xi}$ and the mirror image $\mathbf{x}^f_d \equiv (x, y, z - 1/f^2 - 2d)$ of $\mathbf{x}^f$ with respect to the sea bottom $z = -d$. The flow-field point $\boldsymbol{\xi}$, the source point $\mathbf{x}$ and the related image points $\mathbf{x}_d$, $\mathbf{x}'$, $\mathbf{x}'_d$, $\mathbf{x}^f$, $\mathbf{x}^f_d$ are shown in Fig.7.1.

Expressions (6.50b) and (7.23) and the general expression (6.49b) yield

$$1/r' + 1/r'_d - 2/r^f - 2/r^f_d =$$

$$\frac{1}{\pi} \int_{-\infty}^{\infty} d\beta \int_{-\infty}^{\infty} d\alpha \; \frac{1 - 2\,e^{-k/f^2}}{k} \; \frac{\cosh[k(\zeta+d)]}{e^{k\,d}} \; e^{k\,z + \mathrm{i}[\alpha(x-\xi)+\beta(y-\eta)]} \; .$$

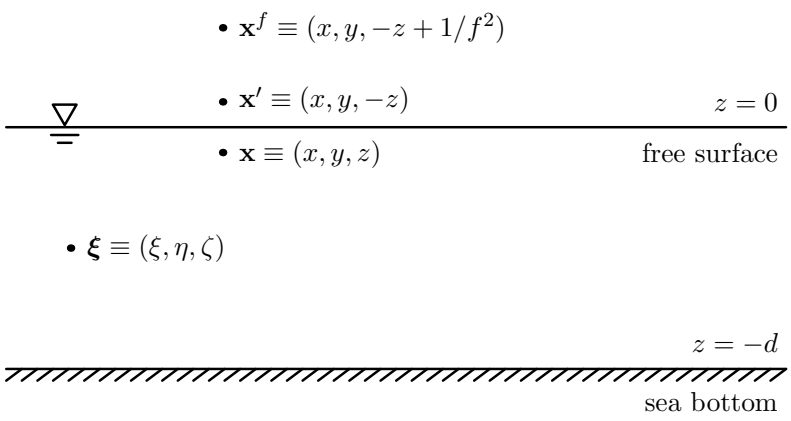

Figure 7.1: Flow-field point $\boldsymbol{\xi}$, source point $\mathbf{x}$ and image source points $\mathbf{x}_d$, $\mathbf{x}'$, $\mathbf{x}'_d$, $\mathbf{x}^f$, $\mathbf{x}^f_d$.

This expression and expressions (7.29a) and (7.31) show that the Green function associated with diffraction-radiation of regular waves by an offshore structure in water of uniform finite depth is given by (7.32a) where the Rankine component G^R is given by (7.32b-d) and (7.29b), and the Fourier component G^F can finally be expressed as

$$G^F = \frac{1}{\pi}\int_{-\pi}^{\pi} d\gamma \int_0^{\infty} dk \, \frac{A^z A^\zeta \, e^{\,\mathrm{i}\,[\,\alpha\,(x-\xi)+\beta\,(y-\eta)\,]}}{1-(k/f^2)\tanh(k\,d)+2\,\mathrm{i}\,\epsilon/f} \quad \text{where} \tag{7.33a}$$

$$A^\zeta \equiv 2\cosh[k(\zeta+d)]/e^{k\,d} \ \text{ and} \tag{7.33b}$$

$$A^z \equiv \left[1+\frac{k}{f^2}\right]\frac{\cosh[k(z+d)]}{2\cosh(k\,d)} + \left[\frac{1}{2}-e^{-k/f^2}\right]\left[1-\frac{k}{f^2}\tanh(kd)\right]e^{k\,z}\,. \tag{7.33c}$$

In the deep-water limit $d \to \infty$, expressions (7.33b) and (7.33c) yield

$$A^\zeta = e^{\,k\,\zeta} \ \text{ and } \ A^z = a^F e^{\,k\,z} \tag{7.34}$$

where a^F is defined by (7.25c). Expressions (7.32) and (7.33) for the Green

function in finite water-depth d agree with the deep-water Green function (7.25) in the limit $d \to \infty$ as expected.

Expressions (7.33b-c) for the amplitude function $A^{z\,\zeta} \equiv A^z A^\zeta$ yield

$$A^{z\,\zeta} \to 1 \text{ as } k \to \infty \text{ if } z + \zeta = 0 \text{ and } A^{z\,\zeta} \to 0 \text{ as } k \to 0 \ , \tag{7.35}$$

whereas the amplitude function

$$A_b^{z\,\zeta} \equiv \left[1 + \frac{k}{f^2}\right] \frac{\cosh[k\,(z+d)]\cosh[k\,(\zeta+d)]}{\cosh(k\,d)\,e^{\,k\,d}}$$

associated with the Fourier component G_b^F given by (7.31) is unbounded as $k \to \infty$ if $z + \zeta = 0$ and is equal to 1 at $k = 0$. The Rankine-Fourier decomposition (7.32) and (7.33) is then preferable to the basic Rankine-Fourier decomposition (7.29) and (7.31) and better suited to evaluate flows due to distributions of singularities. Expressions (7.33b-c) yield $A^{z\zeta} = A_b^{z\zeta}$ at the dispersion curve defined by the dispersion relation $\Delta = 0$ where $\Delta \equiv f^2 - k\tanh(k\,d)$.

Alternative representation of the Fourier component G^F

The function $A^{z\,\zeta} = A^z A^\zeta$ given by (7.33b-c) can be expressed as

$$\begin{aligned} A^{z\,\zeta} = &\left[1 + \frac{k}{f^2}\right] \frac{\cosh[k\,(z+\zeta+2\,d)] + \cosh[k\,(z-\zeta)]}{2\,e^{\,k\,d}\cosh(k\,d)} \\ &+ \frac{\Delta}{f^2}\left[\frac{1}{2} - e^{-k/f^2}\right] \frac{e^{\,k\,(z+\zeta+2\,d)} + e^{\,k\,(z-\zeta)}}{e^{\,2\,k\,d}} \end{aligned}$$

where $\Delta = f^2 - k\tanh(k\,d)$. The Fourier component G^F in the expression for the Green function associated with diffraction-radiation of regular waves by offshore structures in finite water depth can then be expressed as

$$G^F = \frac{1}{\pi}\int_{-\pi}^{\pi} d\gamma \int_0^\infty dk \ \frac{(A_+^{z\,\zeta} + A_-^{z\,\zeta})\,e^{\,\mathrm{i}\,[\alpha\,(x-\xi)+\beta\,(y-\eta)]}}{1 - (k/f^2)\tanh(k\,d) + 2\,\mathrm{i}\,\epsilon/f} \tag{7.36a}$$

$$= 2\int_0^\infty dk \ \frac{(A_+^{z\,\zeta} + A_-^{z\,\zeta})\,J_0(k\,h)}{1 - (k/f^2)\tanh(k\,d) + 2\,\mathrm{i}\,\epsilon/f} \quad \text{where} \tag{7.36b}$$

$$A_\pm^{z\,\zeta} \equiv \left[1 + \frac{k}{f^2}\right] \frac{\cosh(k\,z^\pm)}{2\,e^{\,k\,d}\cosh(k\,d)} + \frac{\Delta}{f^2}\left[\frac{1}{2} - e^{-k/f^2}\right] \frac{e^{\,k\,z^\pm}}{e^{\,2\,k\,d}} \tag{7.36c}$$

$$\text{with } z^+ \equiv z + \zeta + 2\,d \text{ and } z^- \equiv z - \zeta \ . \tag{7.36d}$$

The relation (7.26) was used in (7.36b). The functions $A_\pm^{z\,\zeta}$ defined by (7.36c) are functions of k/f^2, $f^2\,d$ and $f^2\,z^\pm$, and (7.36) expresses the Fourier component G^F as the sum of two components G_+^F and G_-^F. The components

$G^F_\pm$ are functions of the nondimensional water depth $f^2 d$, the horizontal distance $f^2 h \equiv f^2\sqrt{(x-\xi)^2+(y-\eta)^2}$ and the vertical distance $f^2 z^+$ or $f^2 z^-$. Thus, G^F is expressed as the sum of two components G^F_+ and G^F_- that are functions of three variables, whereas the Fourier component G^F defined by (7.33) is a function of the four variables $f^2 d$, $f^2 h$, $f^2 z$ and $f^2 \zeta$.

7.6 Physical-space analysis

The alternative representations (7.16) and (7.25) of the deep-water Green functions associated with the two particular cases $f = 0$ or $F = 0$ express G as the sum of a Rankine component defined in terms of elementary Rankine sources and a Fourier component given by a double Fourier integral. The Rankine components in these alternative representations are asymptotically equivalent to the Green functions G^+ or G^- defined as

$$4\pi G^+ \equiv -1/r + 1/r' \;\text{ and }\; 4\pi G^- \equiv -1/r - 1/r' \tag{7.37}$$

in the near field $r' \to 0$ or the far field $r' \to \infty$, as is shown in (7.13) and (7.22).

The Green functions G^+ and G^- satisfy the boundary conditions

$$G^+ = 0 \;\text{ or }\; \partial G^-/\partial\zeta = 0 \;\text{ at }\; \zeta = 0 \tag{7.38}$$

that correspond to the free-surface boundary condition (6.31c) in the 'zero-gravity' limit $g = 0$, $F = \infty$, $f = \infty$ or the 'infinite-gravity' limit $g = \infty$, $F = 0$, $f = 0$.

The limits $k \to \infty$ or $k \to 0$ in the 'Fourier-space analysis' considered in the previous sections correspond to the near-field or far-field limits $r' \to 0$ or $r' \to \infty$ in a 'physical-space analysis' of the near-field and far-field approximations to the free-surface boundary condition. This complementary physical-space analysis is now considered. **[7,1]**

Offshore structure in regular waves

In the case $F = 0$, the free-surface boundary condition (6.31c) becomes

$$G_\zeta - (f + \mathrm{i}\,\epsilon)^2 G = 0 \;\text{ at }\; \zeta = 0 \tag{7.39a}$$

where ϵ can be taken as $\epsilon = 0$ in this 'physical-space' analysis. The Green function G that satisfies the free-surface boundary condition (7.39a) is a function of the frequency-scaled variable $\mathbf{x}^f \equiv f^2\mathbf{x}$. The behaviors of the Green function G in the near-field limit $f^2 r' \to 0$ and in the far-field limit

$f^2 r' \to \infty$ are determined by the highest-order derivative G_ζ or the lowest-order derivative G in the free-surface condition (7.39a). This analysis and the boundary conditions (7.38) then yield

$$G \sim G^- \text{ for } f^2 r' \ll 1 \text{ and } G \sim G^+ \text{ for } 1 \ll f^2 r' \,. \tag{7.39b}$$

The alternative representations (7.18b) and (7.17) are then best suited in the near-field or far-field limits $f^2 r' \to 0$ or $f^2 r' \to \infty$ in the physical space, and in the limits $k \to \infty$ or $k \to 0$ in the Fourier space, respectively. The optimal representation (7.25) is equivalent to the representations (7.18b) and (7.17) in these limits in the physical and Fourier spaces.

Ship steadily advancing in calm water

In the case $f = 0$, the free-surface boundary condition (6.31c) becomes

$$G_\zeta + F^2 G_{\xi\xi} + 2\,\epsilon\, F\, G_\xi = 0 \text{ at } \zeta = 0 \tag{7.40a}$$

where ϵ can again be taken as $\epsilon = 0$. The Green function that satisfies the free-surface boundary condition (7.40a) is a function of the speed-scaled variable $\mathbf{x}^F \equiv \mathbf{x}/F^2$. The behaviors of the Green function G in the near-field limit $r'/F^2 \to 0$ and the far-field limit $r'/F^2 \to \infty$ are determined by the highest-order derivative $G_{\xi\xi}$ or the lowest-order derivative G_ζ of G in the free-surface condition (7.40a). This analysis and the boundary conditions (7.38) then yield

$$G \sim G^+ \text{ for } r'/F^2 \ll 1 \text{ and } G \sim G^- \text{ for } 1 \ll r'/F^2. \tag{7.40b}$$

The alternative representations (7.8) and (7.9b) are then best suited in the near-field or far-field limits $r'/F^2 \to 0$ or $r'/F^2 \to \infty$ in the physical space, and in the limits $k \to \infty$ or $k \to 0$ in the Fourier space, respectively. The optimal representation (7.15) is equivalent to the representations (7.8) and (7.9b) in these limits in the physical and Fourier spaces.

Ship steadily advancing through regular waves

The free-surface boundary condition (6.31c) associated with the general case $Ff \neq 0$ and a ship steadily advancing through regular waves is now considered. The highest-order and lowest-order derivatives in (6.31c) are $G_{\xi\xi}$ and G. This consideration and (7.38) then yield

$$G \sim G^+ \text{ as } r' \to 0 \text{ and as } r' \to \infty \,. \tag{7.41}$$

The representation (7.6) is then optimal in both the near-field and far-field limits $r' \to 0$ and $r' \to \infty$ in the physical space, and the limits $k \to 0$ and $k \to \infty$ in the Fourier plane.

7.7 Green functions for $Ff \neq 0$ and the limits $F = 0$ or $f = 0$

The Rankine component

$$G^R = -1/\sqrt{h^2+(z-\zeta)^2} + 1/\sqrt{h^2+(z+\zeta)^2} \tag{7.42a}$$

in expression (7.6b) associated with a ship that advances through regular waves does not agree with the Rankine components

$$G^R = \frac{-1}{\sqrt{h^2+(z-\zeta)^2}} + \frac{1}{\sqrt{h^2+(z+\zeta)^2}} - \frac{2}{\sqrt{h^2+(z+\zeta-F^2)^2}} \ , \tag{7.42b}$$

$$G^R = \frac{-1}{\sqrt{h^2+(z-\zeta)^2}} - \frac{1}{\sqrt{h^2+(z+\zeta)^2}} + \frac{2}{\sqrt{h^2+(z+\zeta-1/f^2)^2}} \tag{7.42c}$$

in expressions (7.16a) or (7.25a) associated with the particular cases $f = 0$ or $F = 0$ and a ship that steadily advances in calm water or an offshore structure in regular waves.

Modified Rankine component G^R

The Rankine component (7.42a) can be modified to be consistent with the Rankine components (7.42b) and (7.42c) if $f = 0$ or $F = 0$. In particular, the expression

$$G^R = -1/r + 1/r' - 2/r^F + 2/r^{Ff} \ \text{ where} \tag{7.43a}$$

$$r \equiv \sqrt{h^2+(z-\zeta)^2} \ , \ \ r' \equiv \sqrt{h^2+(z+\zeta)^2} \ , \tag{7.43b}$$

$$r^F \equiv \sqrt{h^2+(z+\zeta-F^2)^2} \ , \ \ r^{Ff} \equiv \sqrt{h^2+(z+\zeta-F^2-1/f^2)^2} \tag{7.43c}$$

$$\text{yields} \ \ G^R \sim -1/r + 1/r' - 2/r^F \ \text{ as } f \to 0 \ , \tag{7.43d}$$

$$G^R \sim -1/r - 1/r' + 2/r^f \ \text{ as } F \to 0 \ , \tag{7.43e}$$

$$G^R \sim -1/r + 1/r' \ \text{ as } f \to \infty \ \text{ or } \ F \to \infty \ . \tag{7.43f}$$

The approximations (7.43d) and (7.43e) are consistent with expressions (7.42b) and (7.42c), and the approximation (7.43f) is consistent with the limits $f \to \infty$ or $F \to \infty$ of the free-surface boundary conditions associated with wave diffraction-radiation by offshore structures and flows around ships steadily advancing in calm water or through regular waves.

Expressions (7.6) and (7.43a) then show that the Green function that satisfies the free-surface boundary condition for a ship that steadily advances through regular waves can be expressed as

$$4\pi G = G^R + G^F \tag{7.44}$$

where the Rankine component G^R is given by (7.43a-c) and the free-surface component G^F is defined as

$$G^F \equiv \frac{2}{r^F} - \frac{2}{r^{Ff}} + \frac{1}{\pi}\int_{-\infty}^{\infty} d\beta \int_{-\infty}^{\infty} d\alpha \, \frac{e^{\,k\,(z+\zeta)\,+\,\mathrm{i}\,[\,\alpha\,(x-\xi)\,+\,\beta\,(y-\eta)\,]}}{\Delta \,+\, \mathrm{i}\,\epsilon\,\Delta_f} \ . \qquad (7.45)$$

Expressions (6.49b) and (7.43c) yield

$$\frac{2}{r^F} - \frac{2}{r^{Ff}} = \frac{1}{\pi}\int_{-\infty}^{\infty} d\beta \int_{-\infty}^{\infty} d\alpha \, \frac{1-e^{-k/f^2}}{k} \, e^{-F^2 k} \, e^{\,k\,(z+\zeta)\,+\,\mathrm{i}\,[\,\alpha\,(x-\xi)\,+\,\beta\,(y-\eta)\,]} \ .$$

This expression and expressions (7.45) and (7.5b) yield

$$G^F = \frac{1}{\pi}\int_{-\pi}^{\pi} d\gamma \int_{0}^{\infty} dk \, \frac{a^F \, e^{\,k\,(z+\zeta)\,+\,\mathrm{i}\,[\,\alpha\,(x-\xi)\,+\,\beta\,(y-\eta)\,]}}{(f+F\alpha)^2/k - 1 + 2\,\mathrm{i}\,\epsilon\,(f+F\alpha)/k} \qquad (7.46a)$$

$$\text{where } \ a^F \equiv 1 + e^{-F^2 k}\,(1-e^{-k/f^2})\,[\,(f+F\alpha)^2/k - 1\,] \ . \qquad (7.46b)$$

Expression (7.46b) yields $a^F = 1$ at the dispersion curves defined by the dispersion relation $\Delta \equiv (f+F\alpha)^2 - k = 0$. Expression (7.46b) also yields

$$\begin{aligned} &a^F \to 2 \ \text{ as } \ k \to 0 \quad \text{and} \\ &a^F \to 1 \ \text{ as } \ k \to \infty \ \text{ if } \ F \neq 0 \quad \text{or} \\ &a^F \sim f^2/k \ \text{ as } \ k \to \infty \ \text{ if } \ F = 0 \ . \end{aligned}$$

The Rankine-Fourier representation (7.44), (7.43), (7.46) is consistent with the Rankine-Fourier representations (7.16) and (7.25) in the special cases $f = 0$ or $F = 0$.

Decomposition of the Fourier component G^F

The dispersion function Δ defined by (7.5b) yields

$$\begin{aligned} &\Delta + \mathrm{i}\,\epsilon\,\Delta_f - \epsilon^2 = (f + Fk\cos\gamma + \mathrm{i}\,\epsilon)^2 - k \\ &= F^2 k^2 \cos^2\gamma - k\,[\,1 - 2F(f+\mathrm{i}\,\epsilon)\cos\gamma\,] + (f+\mathrm{i}\,\epsilon)^2 \ . \end{aligned} \qquad (7.47)$$

The classical representation of the quadratic function $A\,x^2 - B\,x + C$ as

$$A\,x^2 - B\,x + C = A\,(x-x^+)(x-x^-) \ \text{ where } \ x^{\pm} \equiv \frac{B \pm \sqrt{B^2 - 4\,A\,C}}{2\,A}$$

applied to (7.47) yields

$$\Delta + \mathrm{i}\,\epsilon\,\Delta_f - \epsilon^2 = (k - k_\epsilon^+)\,(k - k_\epsilon^-)\,F^2\cos^2\gamma \ \text{ where } \qquad (7.48)$$

$$k_\epsilon^{\pm} \equiv \Big[\,1 - 2\,(f+\mathrm{i}\,\epsilon)\,F\cos\gamma \pm \sqrt{1 - 4\,(f+\mathrm{i}\,\epsilon)\,F\cos\gamma}\,\Big]/(2\,F^2\cos^2\gamma) \ .$$

The relation (7.48) finally yields

$$\Delta + \mathrm{i}\,\epsilon\,\Delta_f - \epsilon^2 = (k - k_\epsilon^i)\,(k - k_\epsilon^o)\,F^2\cos^2\gamma \tag{7.49a}$$

where $k_\epsilon^o \equiv k_\epsilon^+$ and $k_\epsilon^i \equiv k_\epsilon^-$ are defined as

$$F^2 k_\epsilon^o \equiv \left[\sqrt{1/4 - (f + \mathrm{i}\,\epsilon)\,F\cos\gamma} + 1/2\right]^2 / \cos^2\gamma \text{ and} \tag{7.49b}$$

$$k_\epsilon^i / f^2 \equiv (1 + \mathrm{i}\,\epsilon/f)^2 / \left[\sqrt{1/4 - (f + \mathrm{i}\,\epsilon)\,F\cos\gamma} + 1/2\right]^2 . \tag{7.49c}$$

In the limit $\epsilon = 0$, the functions $k_\epsilon^i(\gamma)$ and $k_\epsilon^o(\gamma)$ defined by (7.49b-c) become

$$k^i/f^2 = 1/(\sqrt{1/4 - \tau\cos\gamma} + 1/2)^2 = 1/(\delta + 1/2)^2 \tag{7.50a}$$

$$F^2 k^o = (\sqrt{1/4 - \tau\cos\gamma} + 1/2)^2 / \cos^2\gamma = (\delta + 1/2)^2 / \cos^2\gamma \tag{7.50b}$$

$$\text{where } \delta \equiv \sqrt{1/4 - \tau\cos\gamma} \text{ and } \tau\cos\gamma = (1/2 + \delta)(1/2 - \delta)\,. \tag{7.50c}$$

Expressions (7.50a-b) agree with expressions (5.6) for the dispersion curves determined by the dispersion relation $\Delta = 0$ associated with a ship that steadily advances through regular waves.

One has

$$\left[\sqrt{1/4 - (f + \mathrm{i}\,\epsilon)\,F\cos\gamma} + 1/2\right]^2 = (\delta + 1/2)^2 \left[1 - \frac{\mathrm{i}\,\epsilon\,F\cos\gamma}{\delta\,(\delta + 1/2)}\right] + O(\epsilon^2)\,.$$

This approximation and expressions (7.49b-c) and (7.50) then yield

$$k_\epsilon^i = k^i + \mathrm{i}\,\epsilon\,\delta^i f + O(\epsilon^2) \text{ and } k_\epsilon^o = k^o - \mathrm{i}\,\epsilon\,\delta^o/F + O(\epsilon^2) \tag{7.51a}$$

$$\text{where } \delta^i \equiv 1/[\,\delta\,(\delta + 1/2)\,] \text{ and } \delta^o \equiv (\delta + 1/2)/(\delta\cos\gamma)\,. \tag{7.51b}$$

Expressions (7.49a) and (7.51a) finally yield

$$\begin{aligned}\frac{1}{\Delta + \mathrm{i}\,\epsilon\,\Delta_f} &= \frac{1}{F^2\cos^2\gamma}\;\frac{1}{k_\epsilon^o - k_\epsilon^i}\left(\frac{1}{k - k_\epsilon^o} - \frac{1}{k - k_\epsilon^i}\right) \\ &= \frac{1}{2\,\delta}\left(\frac{1}{k - k^o + \mathrm{i}\,\epsilon\,\delta^o/F} - \frac{1}{k - k^i - \mathrm{i}\,\epsilon\,\delta^i f}\right)\,. \end{aligned} \tag{7.52}$$

where k^i, k^o, δ^i, δ^o and δ are given by (7.50) and (7.51b).

Expressions (7.46a) and (7.52) yield the decomposition

$$G^F = G_i^F + G_o^F \text{ where} \tag{7.53a}$$

$$G_i^F = \frac{1}{\pi}\int_{-\pi}^{\pi} d\gamma \int_0^\infty dk\;\frac{a^F k}{\sqrt{1 - 4\,\tau\cos\gamma}}\;\frac{e^{\,k\,(z+\zeta) + \mathrm{i}\,[\,\alpha\,(x-\xi) + \beta\,(y-\eta)\,]}}{k^i - k + \mathrm{i}\,\epsilon\,\delta^i f} \tag{7.53b}$$

$$G_o^F = \frac{1}{\pi}\int_{-\pi}^{\pi} d\gamma \int_0^\infty dk\;\frac{a^F k}{\sqrt{1 - 4\,\tau\cos\gamma}}\;\frac{e^{\,k\,(z+\zeta) + \mathrm{i}\,[\,\alpha\,(x-\xi) + \beta\,(y-\eta)\,]}}{k - k^o + \mathrm{i}\,\epsilon\,\delta^o/F}\,. \tag{7.53c}$$

The functions $a^F(k,\gamma)$, $k^i(\gamma)$ and $k^o(\gamma)$ in this decomposition are given by (7.46b) and (7.50a-b). The relations (7.51b) show that one has

$$0 < \delta^i \text{ and } \text{sign}(\delta^o) = \text{sign}(\cos\gamma) \, . \tag{7.53d}$$

Thus, the term $\delta^i f$ may be taken as 1 in (7.53b), and δ^o/F can be taken as $\text{sign}(\cos\gamma)$ in (7.53c). Expressions (7.53) provide a formal decomposition of the function G^F into two components G_i^F and G_o^F. **[7,2]**

The component G_i^F represents a flow that is scaled in terms of the length g/ω^2 and contains ring waves, associated with the dispersion curve I in the inner region $-k_i^- \leq \alpha \leq k_i^+$ in (5.11), and a related local flow. The flow defined by the component G_o^F is scaled with respect to V_s^2/g and consists of inner and outer V waves, associated with the two dispersion curves O^- and O^+ in the outer regions $-\infty < \alpha \leq -k_o^-$ and $k_o^+ \leq \alpha < \infty$ in (5.11).

7.8 Alternative representations of Green functions

The Rankine-Fourier representations (7.6) and (7.16) of the Green functions associated with a ship that steadily advances through regular waves or in calm water, and the representations (7.25) and (7.32-7.33) of the Green functions for an offshore structure in deep water or in finite water-depth express these Green functions in terms of Rankine components G^R that involve elementary Rankine sources and Fourier components G^F given by double Fourier integrals, which are singular at the dispersion curves $\Delta = 0$.

The Green functions defined by (7.6), (7.16), (7.25) and (7.32), (7.33) have been extensively considered. In particular, alternative representations of these Green functions in terms of single integrals exist. Near-field and far-field analytical approximations also exist for the simplest cases, notably in deep water and for $F = 0$ or $f = 0$. Alternative methods for evaluating the Green functions defined in this chapter, including analytical methods based on complementary analytical approximations and numerical methods based on table interpolation or polynomial approximations within contiguous regions, have also been developed.

The numerous single-integral representations, analytical approximations, and numerical approximations that have been obtained for the particular Green functions considered in this chapter for a ship that steadily advances through regular waves **[7,3]** or in calm water **[7,4]** and for offshore structures in deep water **[7,5]** or in finite water-depth **[7,6]** are reported in a vast literature. These analytical relations and numerical methods, applicable to *specific* classes of Green functions, are not considered in the book. Instead, chapters 10-12 expound an alternative general approach—called

Fourier-Kochin method—in which the flow created by a *general distribution of singularities*, rather than a unit source, is directly evaluated. This alternative method is applicable to a broad class of dispersive plane waves associated with *general dispersion functions* Δ and Δ_1.

7.9 Rankine component $(G^R)^\zeta$

The alternative boundary-integral representations of potential flow around a ship or an offshore structure (body) given in chapters 8 and 9 include flow representations that involve a distribution over the mean wetted waterline of the body, i.e. the intersection curve between the body and the free-surface plane $\zeta = 0$, of the functions

$$4\pi\,(\partial_\xi, \partial_\eta) G^\zeta = (\partial_\xi, \partial_\eta)(G^R)^\zeta + (\partial_\xi, \partial_\eta)(G^F)^\zeta \tag{7.54}$$

where G^R and G^F are the Rankine and Fourier components in the basic Rankine-Fourier decomposition $4\pi G = G^R + G^F$ defined in this chapter and $^\zeta$ means integration with respect to ζ. The contribution of the Fourier component $(G^F)^\zeta$ to the velocity potential of the flow around a body can be evaluated via the Fourier-Kochin method expounded in chapters 10–12. The Rankine component $(G^R)^\zeta$ in (7.54) is now considered.

Expressions (7.43b) and (6.48) yield

$$r \equiv \sqrt{h^2 + (z-\zeta)^2} \;\text{ and }\; r' \equiv \sqrt{h^2 + (z+\zeta)^2} \tag{7.55a}$$

$$\text{where }\; h \equiv \sqrt{(x-\xi)^2 + (y-\eta)^2}\;. \tag{7.55b}$$

At the free-surface plane $\zeta = 0$, one then has

$$(-1/r)_\zeta = (1/r')_\zeta \;\text{ and }\; (-1/r)^\zeta = (1/r')^\zeta\;.$$

It follows that one has

$$(-1/r - 1/r')^\zeta = 0 \;\text{ and }\; (-1/r + 1/r')^\zeta = (2/r')^\zeta \;\text{ at }\; \zeta = 0\;. \tag{7.56a}$$

Moreover, one has

$$\begin{Bmatrix} \partial_\xi^\zeta \\ \partial_\eta^\zeta \end{Bmatrix} \frac{1}{r'} = \frac{1/r'}{r' - (\zeta + z)} \begin{Bmatrix} x-\xi \\ y-\eta \end{Bmatrix}\;. \tag{7.56b}$$

More generally, one has

$$\begin{Bmatrix} \partial_\xi^\zeta \\ \partial_\eta^\zeta \end{Bmatrix} \frac{1}{r_c} = \frac{1/r_c}{r_c - (\zeta + c)} \begin{Bmatrix} x-\xi \\ y-\eta \end{Bmatrix} \;\text{ where}$$

$$r_c \equiv \sqrt{h^2 + (\zeta + c)^2} \;\text{ and }\; \zeta + c \le 0\;. \tag{7.56c}$$

Expressions (7.56) can be used in the boundary-integral flow representations given in chapters 8 and 9 for wave diffraction-radiation by an offshore structure in deep water or in finite water-depth and for a ship that steadily advances in calm water or through waves.

Chapter 8

Boundary-integral flow relations for an offshore structure in regular waves

The method of Green function and boundary-integral flow representation introduced in chapter 6 is now applied to diffraction-radiation of regular waves by a large stationary body (offshore structure, moored ship) in water of uniform finite depth. The body can be fixed (for wave diffraction) or it can undergo small-amplitude oscillatory motions about a mean position (for wave radiation). In the latter case, the flow around the body in its mean position is considered, in accordance with the classical analysis of diffraction-radiation of regular waves by stationary floating bodies, and as is briefly explained in chapter 1. **[1,6]**

Green's fundamental boundary-integral relation (6.3) is applied to the boundary-value problem and the Green function associated with the usual linear flow model, called 'free-waterplane flow model' in this chapter, of wave diffraction-radiation by a stationary body. Green's identity is also applied to an alternative linear flow model, called 'rigid-waterplane flow model'. Green's basic identity (6.3) applied to the usual free-waterplane flow model in sections 8.1–8.3, or to the alternative rigid-waterplane flow model in sections 8.4 and 8.5, yield identical boundary-integral flow representations. Specifically this flow representation is given by (8.36), which is the main result of this chapter. **[8,1]**

The rigid-waterplane flow model provides a simple basis for preventing spurious solutions for special wave frequencies, called irregular frequencies, that are ultimately related to the fact that the Green function for diffraction-

radiation of regular water waves is defined within the flow region outside the body as well as inside the body, and thus contains waves that propagate inside the body. **[8,2]**

8.1 General boundary-value problem and basic free-waterplane linear flow model

The boundary-value problem associated with diffraction-radiation of regular (time-harmonic) water waves of frequency ω by a stationary rigid body such as an offshore structure or a moored ship is defined in chapters 1 and 6. This boundary-value problem is now restated for ease of reference. The flow around the body is observed from a Cartesian system of coordinates, denoted as $\boldsymbol{\xi} \equiv (\xi, \eta, \zeta)$ or $\mathbf{x} \equiv (x, y, z)$. The coordinates $\boldsymbol{\xi}$ and $\mathbf{x}$, the corresponding flow potentials

$$\varphi \equiv \varphi(\boldsymbol{\xi}) \text{ and } \phi \equiv \varphi(\mathbf{x})$$

and all other flow variables are nondimensional in terms of a reference length L_r, commonly chosen as a characteristic dimension of the body, the acceleration of gravity g and (for the flow pressure) the water density ρ_w as in section 1.5.

The flow potential associated with diffraction-radiation of regular waves, with nondimensional frequency f defined by (1.32) as $f \equiv \omega\sqrt{L_r/g}$, by a stationary body is expressed as

$$\widehat{\varphi}(\boldsymbol{\xi}, t) = \text{Re}\, \varphi(\boldsymbol{\xi})\, e^{(\epsilon - \mathrm{i} f)t} = \text{Re}\, \varphi(\boldsymbol{\xi})\, e^{-\mathrm{i} f_\epsilon t} \tag{8.1a}$$

$$\text{where } f_\epsilon \equiv f + \mathrm{i}\,\epsilon \text{ with } \epsilon = +0 \tag{8.1b}$$

in accordance with (6.19). The corresponding (nondimensional) free-surface elevation and dynamic flow pressure are given by (1.37) as

$$z^F(\xi, \eta, t) = \text{Re}\,[\,\mathrm{i} f\, \varphi(\xi, \eta, 0) - p^F(\xi, \eta)\,]\, e^{-\mathrm{i} f t} \text{ where } \boldsymbol{\xi} \in \Sigma^F \tag{8.2a}$$

$$\text{and } p_d(\boldsymbol{\xi}, t) = \text{Re}\, \mathrm{i} f\, \varphi(\boldsymbol{\xi})\, e^{-\mathrm{i} f t} \text{ where } \boldsymbol{\xi} \in \mathcal{D}\ . \tag{8.2b}$$

The elevation of the free surface Σ^F and the dynamic pressure in the flow region $\mathcal{D}$ are then directly determined in terms of the flow potential φ.

The classical free-waterplane linear flow model and the related boundary-integral flow relations are associated with the 3D region $\mathcal{D}$ inside the closed boundary surface

$$\Sigma \equiv \Sigma^B \cup \Sigma^\infty \cup \Sigma^F \cup \Sigma^H \tag{8.3}$$

defined in Fig.8.1. Specifically, Σ^∞ denotes an infinitely large surface, Σ^B is the portion of the horizontal sea-bottom plane $\zeta = -d$ that is inside Σ^∞,

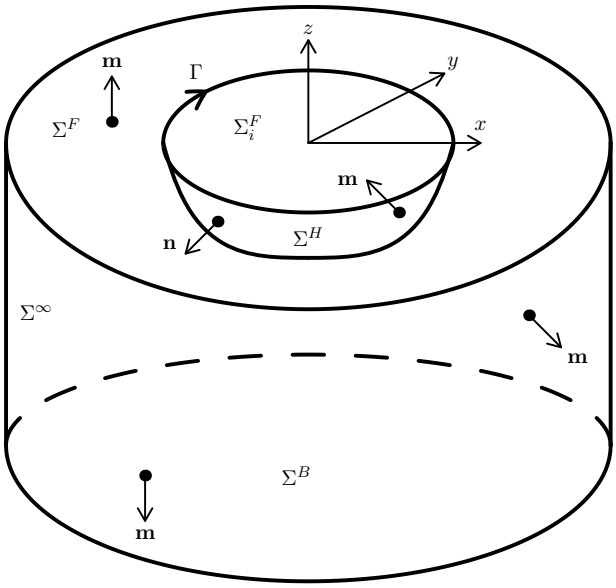

Figure 8.1: Boundary surface $\Sigma \equiv \Sigma^B \cup \Sigma^\infty \cup \Sigma^F \cup \Sigma^H$ related to the basic free waterplane boundary-value problem (8.4) for diffraction-radiation of regular waves by an offshore structure in water of uniform finite depth.

Σ^H denotes the mean wetted body surface and Σ^F is the portion of the plane $\zeta = 0$ of the undisturbed free surface that is inside Σ^∞ and outside Σ^H. The portion of the plane $\zeta = 0$ that is inside Σ^H, called waterplane hereafter, is denoted as Σ_i^F and the intersection curve between the body surface Σ^H and the plane $\zeta = 0$ is denoted as Γ, as is shown in Fig.8.1. The unit vector $\mathbf{m}$ normal to the closed boundary surface Σ points outside Σ and the region $\mathcal{D}$, as in Fig.8.1. The unit vector $\mathbf{n} = -\mathbf{m}$ normal to the body surface Σ^H points outside the body.

As is stated in (1.34-1.35) and (6.20), the spacial component $\varphi(\boldsymbol{\xi})$ of the velocity potential (8.1a) satisfies the Laplace equation

$$\nabla^2_{\boldsymbol{\xi}} \varphi \equiv \partial^2_\xi \varphi + \partial^2_\eta \varphi + \partial^2_\zeta \varphi = 0 \ \text{ in } \ \mathcal{D} \ , \tag{8.4a}$$

the far-field condition

$$\varphi \to 0 \ \text{ as } \ \sqrt{\xi^2 + \eta^2} \to \infty \tag{8.4b}$$

applied at an infinitely large surface Σ^∞, the sea-bottom boundary condition

$$\varphi_\zeta = 0 \ \text{ at } \ \Sigma^B \ , \tag{8.4c}$$

the free-surface boundary condition

$$\varphi_\zeta - f_\epsilon^2 \, \varphi = \mathrm{i} f p^F - q^F \ \text{ at } \ \Sigma^F \tag{8.4d}$$

and the body-surface boundary condition

$$\mathbf{n} \cdot \nabla_{\boldsymbol{\xi}} \varphi = q^H \text{ at } \Sigma^H \ . \tag{8.4e}$$

The flux $q^H(\boldsymbol{\xi})$ in (8.4e) is presumed to be known at every point $\boldsymbol{\xi}$ of the mean wetted body surface Σ^H in this chapter. In particular, the body-surface flux q^H that corresponds to the diffraction problem and the six radiation problems associated with a linear analysis of diffraction-radiation of regular waves of small amplitude is given by classical expressions **[1,6]**. The pressure $p^F(\xi, \eta)$ and the flux $q^F(\xi, \eta)$ in the free-surface boundary condition (8.4d) likewise are presumed to be specified at every point $(\xi, \eta, 0)$ of the undisturbed free surface Σ^F. A free-surface pressure $p^F(\xi, \eta)$ occurs within a perturbation analysis of the influence of weak nonlinearities in the free-surface boundary condition **[1,3]**. The free-surface flux q^F, where $0 < q^F$ means that water is injected through the free surface, is used in the free-surface boundary condition (8.5d).

8.2 Green function for wave diffraction and radiation by stationary bodies

In accordance with the method of Green function and boundary-integral flow representation introduced in chapter 6, a Green function $G(\boldsymbol{\xi}, \mathbf{x})$ that is associated with the boundary-value problem (8.4) is defined. Specifically, this Green function satisfies the far-field condition

$$G \to 0 \text{ as } h \equiv \sqrt{(\xi - x)^2 + (\eta - y)^2} \to \infty \ , \tag{8.5a}$$

the sea-bottom boundary condition

$$G_\zeta = 0 \text{ at } \zeta = -d \tag{8.5b}$$

and the complementary equations

$$\left\{ \begin{array}{l} \nabla^2_{\boldsymbol{\xi}} G = \delta(\xi - x)\, \delta(\eta - y)\, \delta(\zeta - z) \text{ in } \zeta < 0 \\ G_\zeta - f_\epsilon^2 G = 0 \text{ at } \zeta = 0 \end{array} \right\} \text{ if } z < 0 \tag{8.5c}$$

$$\text{or} \quad \left\{ \begin{array}{l} \nabla^2_{\boldsymbol{\xi}} G = 0 \text{ in } \zeta < 0 \\ G_\zeta - f_\epsilon^2 G = -\delta(\xi - x)\, \delta(\eta - y) \text{ at } \zeta = 0 \end{array} \right\} \text{ if } z = 0 \ . \tag{8.5d}$$

Equations (8.5c-d) show that the Green function $G(\boldsymbol{\xi}, \mathbf{x})$ represents the velocity potential of the flow created by a (pulsating) source located at the point $(x, y, z < 0)$ or a flux across the free surface at the point $(x, y, z = 0)$. These equations correspond to equations (7.28), (6.31) and (6.35).

8.3 Free-waterplane boundary-integral flow relations

Green's fundamental relation (6.3) is now applied, in the flow region bounded by the surface Σ defined by (8.3) and Fig.8.1, to the boundary-value problem (8.4) associated with the free-waterplane linear flow model and the related Green function $G(\boldsymbol{\xi},\mathbf{x})$ determined by (8.5).

Three complementary boundary-integral relations

Green's identity (6.3) with $\psi(\boldsymbol{\xi}) = G(\boldsymbol{\xi},\mathbf{x})$, the Laplace equation (8.4a), the far-field conditions (8.4b) and (8.5a), the sea-bottom conditions (8.4c) and (8.5b), and the body-surface condition (8.4e) yield

$$\int_{\mathcal{D}} dv\, \varphi\, \nabla^2_{\boldsymbol{\xi}} G = \int_{\Sigma^F} d\xi\, d\eta\, (\varphi\, G_\zeta - G\, \varphi_\zeta) + \int_{\Sigma^H} da\, (G\, q^H - \varphi\, \mathbf{n}\cdot\nabla_{\boldsymbol{\xi}} G) \qquad (8.6)$$

where $G \equiv G(\boldsymbol{\xi},\mathbf{x})$ and $\varphi \equiv \varphi(\boldsymbol{\xi})$. Furthermore, $da \equiv da(\boldsymbol{\xi})$ and $q^H \equiv q^H(\boldsymbol{\xi})$ denote the differential element of area or the flux at a point $\boldsymbol{\xi}$ of the body surface Σ^H, and $dv \equiv dv(\boldsymbol{\xi})$ is the differential element of volume at a point $\boldsymbol{\xi}$ of the 3D flow region $\mathcal{D}$. The unit vector $\mathbf{n} \equiv \mathbf{n}(\boldsymbol{\xi})$ normal to Σ^H points into the water, as was already noted and is shown in Fig.8.1.

Use of the identity

$$\varphi\, G_\zeta - G\, \varphi_\zeta = \varphi\, (G_\zeta - f_\epsilon^2 G) - G\, (\varphi_\zeta - f_\epsilon^2 \varphi) \qquad (8.7)$$

and the free-surface boundary condition (8.4d) in the surface integral over the undisturbed free surface Σ^F in (8.6) yields

$$\begin{aligned} &\int_{\mathcal{D}} dv\, \varphi\, \nabla^2_{\boldsymbol{\xi}} G - \int_{\Sigma^F} d\xi\, d\eta\, \varphi\, (G_\zeta - f_\epsilon^2 G) = \\ &\int_{\Sigma^H} da\, (G\, q^H - \varphi\, \mathbf{n}\cdot\nabla_{\boldsymbol{\xi}} G) + \int_{\Sigma^F} d\xi\, d\eta\, G\, (q^F - \mathrm{i} f p^F) \end{aligned} \qquad (8.8)$$

where q^H, p^F and q^F are *presumed known* as was already noted. The flow potential $\varphi \equiv \varphi(\boldsymbol{\xi})$ in the integrals over $\mathcal{D}$ and Σ^F in (8.8) can be expressed as $\varphi = (\varphi - \phi) + \phi$ where

$$\phi \equiv \varphi(\mathbf{x})$$

is the flow potential at the singularity-point (submerged source or free-surface flux) $\mathbf{x}$ in the Green function $G(\boldsymbol{\xi},\mathbf{x})$. The relations

$$\int_{\mathcal{D}} dv\, (\varphi - \phi)\, \nabla^2_{\boldsymbol{\xi}} G = 0 \;\text{ and }\; \int_{\Sigma^F} d\xi\, d\eta\, (\varphi - \phi)(G_\zeta - f_\epsilon^2 G) = 0\ , \qquad (8.9)$$

which follow from the identity $\varphi - \phi = 0$ if $\boldsymbol{\xi} = \mathbf{x}$ and the relations (8.5c-d) and (6.6), yield

$$\int_{\mathcal{D}} dv\ \varphi\, \nabla^2_{\boldsymbol{\xi}} G - \int_{\Sigma^F} d\xi\, d\eta\ \varphi\, (G_\zeta - f_\epsilon^2 G) = \phi\, C(\mathbf{x}) \tag{8.10a}$$

$$\text{where } C(\mathbf{x}) \equiv \int_{\mathcal{D}} dv\, \nabla^2_{\boldsymbol{\xi}} G - \int_{\Sigma^F} d\xi\, d\eta\, (G_\zeta - f_\epsilon^2 G)\ . \tag{8.10b}$$

Equations (8.5c-d) then yield

$$C(\mathbf{x}) = \left\{ \begin{array}{c} 1 \\ 0 \\ 1/2 \end{array} \right\} \text{ if } \mathbf{x} \in \left\{ \begin{array}{c} \mathcal{D} \cup \Sigma^F \\ \mathcal{D}_i \cup \Sigma_i^F \\ \Sigma^H \cup \Gamma \end{array} \right\} \tag{8.11a}$$

where $\mathcal{D} \cup \Sigma^F$ and $\mathcal{D}_i \cup \Sigma_i^F$ denote the 3D regions that are strictly outside or inside the body surface $\Sigma^H \cup \Gamma$. The relations (8.8) and (8.10a) yield the basic boundary-integral relation

$$C(\mathbf{x})\, \phi = \int_{\Sigma^H} da\, (G\, q^H - \varphi\, \mathbf{n} \cdot \nabla_{\boldsymbol{\xi}} G) + \phi^{\Sigma^F} \tag{8.11b}$$

$$\text{where } \phi^{\Sigma^F}(\mathbf{x}) \equiv \int_{\Sigma^F} d\xi\, d\eta\ G\, (q^F - \mathrm{i} f p^F)\ . \tag{8.12}$$

In the special case when no body surface Σ^H exists, the relations (8.10b) and (8.11a) yield $C = 1$ in the entire flow region $z \leq 0$, and the boundary-integral relation (8.11b) with ϕ^{Σ^F} given by (8.12) *explicitly* determines the velocity potential of the flow created by a prescribed distribution of pressure $p^F(\xi, \eta)$ and/or flux $q^F(\xi, \eta)$ at the free surface Σ^F as

$$\phi = \int_{\Sigma^F} d\xi\, d\eta\ G\, (q^F - \mathrm{i} f p^F) = \phi^{\Sigma^F}\,,$$

in agreement with the expression that can be directly obtained via Fourier transformation of the reduced boundary-value problem defined by (8.4a-d).

The relation (8.11b) with $C(\mathbf{x})$ given by expressions (8.11a) yield the three complementary boundary-integral relations

$$\phi = \int_{\Sigma^H} da\, (G\, q^H - \varphi\, \mathbf{n} \cdot \nabla_{\boldsymbol{\xi}} G) + \phi^{\Sigma^F} \text{ if } \mathbf{x} \in (\mathcal{D} \cup \Sigma^F)\ , \tag{8.13a}$$

$$\frac{\phi}{2} = \int_{\Sigma^H} da\, (G\, q^H - \varphi\, \mathbf{n} \cdot \nabla_{\boldsymbol{\xi}} G) + \phi^{\Sigma^F} \text{ if } \mathbf{x} \in (\Sigma^H \cup \Gamma)\ , \tag{8.13b}$$

$$0 = \int_{\Sigma^H} da\, (G\, q^H - \varphi\, \mathbf{n} \cdot \nabla_{\boldsymbol{\xi}} G) + \phi^{\Sigma^F} \text{ if } \mathbf{x} \in (\mathcal{D}_i \cup \Sigma_i^F)\ . \tag{8.13c}$$

The pressure p^F and the flux q^F at the free surface Σ^F in the potential ϕ^{Σ^F} defined by (8.12) and the flux $q^H \equiv \mathbf{n} \cdot \nabla_{\boldsymbol{\xi}} \varphi$ at the body surface Σ^H are presumed known in the boundary-integral relations (8.13), as in (8.4d-e).

The relation (8.13b) only involves $\varphi \equiv \varphi(\boldsymbol{\xi})$ and $\phi \equiv \varphi(\mathbf{x})$ at points $\boldsymbol{\xi}$ and $\mathbf{x}$ of the body surface Σ^H. Thus, (8.13b) yields an integral equation that determines the unknown flow potential $\phi \equiv \varphi(\mathbf{x})$ at $\mathbf{x} \in \Sigma^H$. The relation (8.13a) can be used subsequently to determine the flow potential $\varphi(\mathbf{x})$ at points $\mathbf{x}$ in the flow region $\mathcal{D} \cup \Sigma^F$ outside the body surface.

However, the relation (8.13c) does not determine ϕ inside the body. Indeed, expressions (8.11a) yield $C(\mathbf{x}) = 0$ at points $\mathbf{x}$ inside the body, which means that $\phi \equiv \varphi(\mathbf{x})$ is undetermined at such points. This result is in accordance with the fact that the relations (8.11) and (8.13), obtained from Green's fundamental relation (6.3) applied in the flow region $\mathcal{D}$ outside the body, cannot determine the flow in the region $\mathcal{D}_i$ inside the body. Thus, the basic boundary-integral relations (8.13) associated with the free-waterplane flow model do not preclude the occurrence of spurious solutions for special (irregular) frequencies because the Green function G exists in the region $\mathcal{D}_i$ inside the body surface Σ^H as well as in the flow region $\mathcal{D}$.

The boundary-integral relations (8.13a-b) involve the Green function G and its normal derivative $\mathbf{n} \cdot \nabla_{\boldsymbol{\xi}} G$. Specifically, the relations (8.13a-b) involve the distributions of $G\, q^H$ and $G(q^F - \mathrm{i} f p^F)$ over Σ^H or Σ^F and the distribution of dipoles $\varphi\, \mathbf{n} \cdot \nabla_{\boldsymbol{\xi}} G$ over Σ^H. The Green function G is $O(1/r)$ but the normal derivative $\mathbf{n} \cdot \nabla_{\boldsymbol{\xi}} G$ is $O(1/r^2)$ as $r \to 0$. Thus, G is weakly singular (and easily integrable) as $r \to 0$, but $\mathbf{n} \cdot \nabla_{\boldsymbol{\xi}} G$ is more strongly singular (although integrable).

Equivalent single weakly-singular boundary-integral relation

Both the term $C(\mathbf{x})$ on the left side of (8.11b) and the potential

$$\phi^\delta(\mathbf{x}) \equiv \int_{\Sigma^H} da\ \varphi\, \mathbf{n} \cdot \nabla_{\boldsymbol{\xi}} G \tag{8.14}$$

on the right side of (8.11b) are discontinuous across the body surface Σ^H. However, these two discontinuities exactly cancel out, and the flow potential $\phi \equiv \varphi(\mathbf{x})$ defined by the boundary-integral relation (8.11b) is continuous at Σ^H. A modified boundary-integral relation that avoids the discontinuities in the values of $C(\mathbf{x})$ and $\phi^\delta(\mathbf{x})$ in (8.11b), and holds at the body surface Σ^H as well as inside and outside Σ^H, i.e. everywhere in the lower half space $z \leq 0$, is now obtained.

In accordance with expression (8.10b), the complementary function

$$C_i(\mathbf{x}) \equiv \int_{\mathcal{D}_i} dv\ \nabla^2_{\boldsymbol{\xi}} G - \int_{\Sigma_i^F} d\xi\, d\eta\, (G_\zeta - f_\epsilon^2 G) \tag{8.15a}$$

is defined. Equations (8.5c-d) yield

$$C_i(\mathbf{x}) = \left\{ \begin{array}{c} 0 \\ 1 \\ 1/2 \end{array} \right\} \text{ if } \mathbf{x} \in \left\{ \begin{array}{c} \mathcal{D} \cup \Sigma^F \\ \mathcal{D}_i \cup \Sigma_i^F \\ \Sigma^H \cup \Gamma \end{array} \right\} . \tag{8.15b}$$

The relations (8.11a) and (8.15b) then show that one has

$$C(\mathbf{x}) + C_i(\mathbf{x}) = 1 \tag{8.16}$$

at every point $\mathbf{x}$ in the lower half space $z \leq 0$. The divergence theorem applied in expression (8.15a) yields the alternative expression

$$C_i(\mathbf{x}) = \int_{\Sigma^H} da\ \mathbf{n} \cdot \nabla_{\boldsymbol{\xi}} G + f_\epsilon^2 \int_{\Sigma_i^F} d\xi\, d\eta\ G \tag{8.17}$$

where f_ϵ can be replaced by f.

Addition of the term $C_i\, \phi$ on the left and right sides of (8.11b), with expressions (8.16) or (8.17) used on the left or right sides, yields

$$(1 - C^\Gamma)\, \phi = \int_{\Sigma^H} da\, [\, G\, q^H + (\phi - \varphi)\, \mathbf{n} \cdot \nabla_{\boldsymbol{\xi}} G\,] + \phi^{\Sigma^F} \tag{8.18a}$$

$$\text{where } C^\Gamma(\mathbf{x}) \equiv f^2 \int_{\Sigma_i^F} d\xi\, d\eta\ G(\xi, \eta, 0, \mathbf{x}) \tag{8.18b}$$

and ϕ^{Σ^F} is given by (8.12). The boundary-integral flow relation (8.18a) holds at every point $(x, y, z \leq 0)$ and is equivalent to the three complementary boundary-integral relations (8.13) for points $\mathbf{x}$ in the flow region $\mathcal{D} \cup \Sigma^F$, at the body surface $\Sigma^H \cup \Gamma$ or in the region $\mathcal{D}_i \cup \Sigma_i^F$ inside the body.

The term $\phi - \varphi \equiv \varphi(\mathbf{x}) - \varphi(\boldsymbol{\xi})$ in (8.18a) vanishes at points $\boldsymbol{\xi} = \mathbf{x}$ in the Green function $G(\boldsymbol{\xi}, \mathbf{x})$. The singularity in the integrand of the integral

$$\phi_*^\delta(\mathbf{x}) \equiv \int_{\Sigma^H} da\, (\phi - \varphi)\, \mathbf{n} \cdot \nabla_{\boldsymbol{\xi}} G \tag{8.19}$$

is then weaker than the singularity in the integrand of the integral (8.14). Specifically, the Green function G and the dipole term $(\phi - \varphi)\, \mathbf{n} \cdot \nabla_{\boldsymbol{\xi}} G$ in (8.18) both are $O(1/r)$ as $r \to 0$ and are then weakly singular. As a result, the flow potential ϕ_*^δ defined by the weak dipole distribution (8.19) is continuous at the body surface Σ^H, whereas the potential ϕ^δ defined by (8.14) is not, and every component of the weakly singular boundary-integral relation (8.18) is continuous at the body surface Σ^H.

The weakly singular boundary-integral relation (8.18) applied at points $\mathbf{x} \in \Sigma^H$ only involves $\varphi(\boldsymbol{\xi})$ at $\boldsymbol{\xi} \in \Sigma^H$ and $\varphi(\mathbf{x})$ at $\mathbf{x} \in \Sigma^H$. This boundary-integral relation therefore yields an integral equation that determines the flow potential $\varphi(\mathbf{x})$ at points $\mathbf{x}$ of the body surface, like the boundary-integral relation (8.13b).

8.4 Rigid-waterplane flow model and boundary-value problem

A complementary analysis of diffraction-radiation of regular waves by a stationary body that pierces the free surface is now considered. This analysis is based on an alternative linear flow model, called rigid-waterplane flow model hereafter, to the basic free-waterplane flow model associated with Fig.8.1 and considered in sections 8.1–8.3. In the rigid-waterplane flow model, a body that pierces the free surface is treated as the limit of a body that is closed via a rigid inner waterplane submerged at an infinitesimally small depth, as is shown in Fig.8.2 and is now explained.

The main feature of this flow model is that a thin band $-\delta \leq z \leq 0$ with $0 < \delta \ll 1$ is removed from the upper part of the body surface Σ^H, which is closed by a rigid horizontal lid denoted as Σ_i^H. The open body surface Σ^H in Fig.8.1 associated with the classical free-waterplane flow model then becomes the extended closed body surface $\Sigma_-^H \cup \Sigma_i^H$, where Σ_-^H denotes the body surface Σ^H from which the thin band $-\delta \leq z \leq 0$ has been removed. The rigid lid Σ_i^H that closes the open body surface Σ_-^H is located in the plane $z = -\delta$, as is shown in Fig.8.2. The portion of the free-surface plane $z = 0$ located inside the body surface Σ^H (above the lid Σ_i^H) is denoted as Σ_i^F, and the free surface outside Σ^H but inside Σ^∞ is denoted as Σ^F.

Thus, as is illustrated in Fig.8.2, the rigid-waterplane linear flow model and the related boundary-value problem are associated with the flow region $\mathcal{D}$ inside the closed boundary surface

$$\Sigma \equiv \Sigma^B \cup \Sigma^\infty \cup \Sigma^F \cup \Sigma_i^F \cup \Sigma_i^H \cup \Sigma_-^H \tag{8.20}$$

where Σ^∞ is an infinitely large surface, Σ^B and $\Sigma^F \cup \Sigma_i^F$ denote the portions of the sea bottom $\zeta = -d$ or the free surface $\zeta = 0$ inside Σ^∞, and $\Sigma_-^H \cup \Sigma_i^H$ is the extended body surface obtained by closing the truncated body surface Σ_-^H with a rigid horizontal lid Σ_i^H as was already explained. The unit vector $\mathbf{m}$ normal to the boundary surface Σ, notably at the rigid lid Σ_i^H and at the waterplane Σ_i^F, points outside the flow region $\mathcal{D}$, whereas the vector $\mathbf{n} = -\mathbf{m}$ normal to the body surface Σ_-^H points into the water.

In accordance with the boundary surface Σ associated with the rigid-waterplane flow model, the free-surface boundary condition is applied at the entire free-surface plane $\Sigma^F \cup \Sigma_i^F$ and the body-surface condition is applied at the extended body surface $\Sigma_-^H \cup \Sigma_i^H$ defined in Fig.8.2, rather than at the intersecting surfaces Σ^F or Σ^H shown in Fig.8.1. The limit $\delta \to 0$ is ultimately considered and compatibility between the free-surface boundary condition at the waterplane Σ_i^F and the body-boundary condition at the rigid lid Σ_i^H is imposed in that limit.

The horizontal lid Σ_i^H that closes the body surface Σ_-^H is a rigid surface,

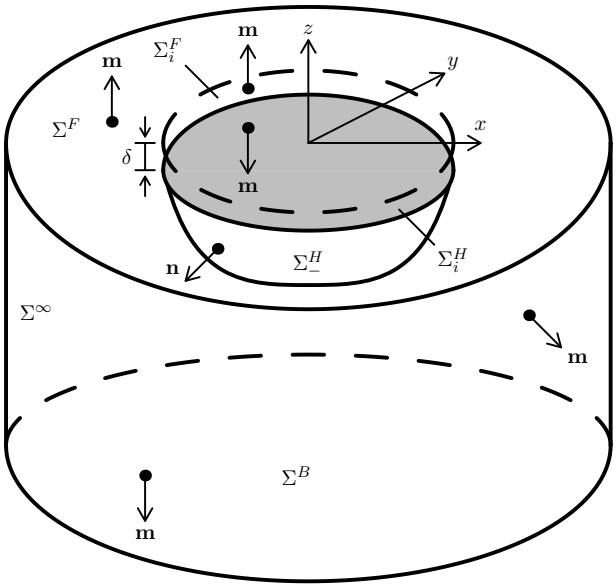

Figure 8.2: Boundary surface $\Sigma \equiv \Sigma^B \cup \Sigma^\infty \cup \Sigma^F \cup \Sigma_i^F \cup \Sigma_i^H \cup \Sigma_-^H$ associated with the rigid waterplane boundary-value problem defined by (8.21) for diffraction-radiation of regular waves by an offshore structure in water of uniform finite depth. The unit vector $\mathbf{m}$ normal to the closed boundary surface Σ points outside Σ and the flow region. The unit vector $\mathbf{n} = -\mathbf{m}$ normal to the body surface Σ_-^H points outside the body.

as was already noted. Section 2.6 shows that only very short time-harmonic waves can exist in the shallow layer of water $-\delta < z < 0$ between the lid Σ_i^H and the free surface Σ_i^F. Specifically, expression (2.39b) shows that the wavelength $\lambda^\omega = 2\pi/k^\omega$ of elementary waves in water of depth d^ω is given by $\lambda^\omega \sim 2\pi\sqrt{d^\omega}$ as $d^\omega \to 0$. Thus, only very short waves can exist in the thin layer of water above the lid Σ_i^H if $\delta \ll 1$.

The boundary-value problem associated with the rigid-waterplane linear flow model consists of the Laplace equation

$$\nabla_{\boldsymbol{\xi}}^2 \varphi \equiv \partial_\xi^2 \varphi + \partial_\eta^2 \varphi + \partial_\zeta^2 \varphi = 0 \ \text{ in } \ \mathcal{D} \tag{8.21a}$$

where $\mathcal{D}$ denotes the flow region inside the closed boundary surface Σ defined by (8.20) and Fig.8.2, the far-field boundary condition

$$\varphi \to 0 \ \text{ as } \ \sqrt{\xi^2 + \eta^2} \to \infty \tag{8.21b}$$

applied at Σ^∞, the sea-bottom boundary condition

$$\varphi_\zeta = 0 \ \text{ at } \ \Sigma^B \ , \tag{8.21c}$$

the free-surface boundary conditions

$$\varphi_\varsigma - f_\epsilon^2 \varphi = \left\{ \begin{array}{c} \mathrm{i} f p^F - q^F \\ 0 \end{array} \right\} \text{ at } \left\{ \begin{array}{c} \Sigma^F \\ \Sigma_i^F \end{array} \right\} \tag{8.21d}$$

and the body-surface boundary conditions

$$\left\{ \begin{array}{c} \mathbf{n} \cdot \nabla_{\boldsymbol{\xi}} \varphi = q^H \\ \varphi_\varsigma = 0 \end{array} \right\} \text{ at } \left\{ \begin{array}{c} \Sigma_-^H \\ \Sigma_i^H \end{array} \right\} . \tag{8.21e}$$

8.5 Rigid-waterplane boundary-integral flow relations

Green's fundamental identity (6.3) is now applied, in the flow region bounded by the surface Σ defined by (8.20) and Fig.8.2, to the Green function $G(\boldsymbol{\xi},\mathbf{x})$ determined by (8.5) and the flow potential $\varphi(\boldsymbol{\xi})$ determined by the boundary-value problem (8.21) associated with the rigid-waterplane linear flow model.

Three complementary boundary-integral relations

Green's relation (6.3) with $\psi(\boldsymbol{\xi}) \equiv G(\boldsymbol{\xi},\mathbf{x})$, the Laplace equation (8.21a), the far-field boundary conditions (8.21b) and (8.5a), the sea-bottom boundary conditions (8.21c) and (8.5b), and the body-surface boundary conditions (8.21e) yield

$$\begin{aligned} \int_{\mathcal{D}} dv\, \varphi\, \nabla_{\boldsymbol{\xi}}^2 G = & \int_{\Sigma^F \cup\, \Sigma_i^F} d\xi\, d\eta\, (\varphi\, G_\varsigma - G\, \varphi_\varsigma) - \int_{\Sigma_i^H} d\xi\, d\eta\, \varphi\, G_\varsigma \\ & + \int_{\Sigma_-^H} da\, (G\, q^H - \varphi\, \mathbf{n} \cdot \nabla_{\boldsymbol{\xi}} G) \end{aligned} \tag{8.22}$$

where $G \equiv G(\boldsymbol{\xi},\mathbf{x})$ and $\varphi \equiv \varphi(\boldsymbol{\xi})$ as was already noted. The unit vector $\mathbf{n} \equiv \mathbf{n}(\boldsymbol{\xi})$ normal to Σ_-^H points into the water, as is shown in Fig.8.2.

The identity (8.7) and the free-surface boundary conditions (8.21d) can be used in the surface integral over the undisturbed free surface $\Sigma^F \cup \Sigma_i^F$ in (8.22). One then obtains

$$\begin{aligned} & \int_{\mathcal{D}} dv\, \varphi\, \nabla_{\boldsymbol{\xi}}^2 G - \int_{\Sigma^F \cup\, \Sigma_i^F} d\xi\, d\eta\, \varphi\, (G_\varsigma - f_\epsilon^2 G) = \\ & \int_{\Sigma_-^H} da\, (G\, q^H - \varphi\, \mathbf{n} \cdot \nabla_{\boldsymbol{\xi}} G) - \int_{\Sigma_i^H} d\xi\, d\eta\, \varphi\, G_\varsigma + \phi^{\Sigma^F} \end{aligned} \tag{8.23}$$

where ϕ^{Σ^F} is given by (8.12). The flow potential $\varphi \equiv \varphi(\boldsymbol{\xi})$ in the integrals over $\mathcal{D}$ and $\Sigma^F \cup \Sigma_i^F$ in (8.23) is now expressed as $\varphi = (\varphi - \phi) + \phi$ where $\phi \equiv \varphi(\mathbf{x})$ is the flow potential at the point $\mathbf{x}$ in the Green function $G(\boldsymbol{\xi}, \mathbf{x})$. The relations (8.9) yield

$$\int_{\mathcal{D}} dv\ \varphi\, \nabla^2_{\boldsymbol{\xi}} G - \int_{\Sigma^F \cup \Sigma_i^F} d\xi\, d\eta\ \varphi\, (G_\zeta - f_\epsilon^2 G) = \phi\ C(\mathbf{x}) \tag{8.24a}$$

$$\text{where } C(\mathbf{x}) \equiv \int_{\mathcal{D}} dv\ \nabla^2_{\boldsymbol{\xi}} G - \int_{\Sigma^F \cup \Sigma_i^F} d\xi\, d\eta\, (G_\zeta - f_\epsilon^2 G)\ . \tag{8.24b}$$

Equations (8.5c-d) then yield

$$C(\mathbf{x}) = \left\{ \begin{array}{c} 1 \\ 0 \\ 1/2 \end{array} \right\} \text{ if } \mathbf{x} \in \left\{ \begin{array}{c} \mathcal{D} \cup \Sigma^F \cup \Sigma_i^F \\ \mathcal{D}_i \\ \Sigma_-^H \cup \Sigma_i^H \end{array} \right\} \tag{8.25a}$$

where $\mathcal{D} \cup \Sigma^F \cup \Sigma_i^F$ and $\mathcal{D}_i$ denote the 3D regions located strictly outside or inside the closed extended body surface $\Sigma_-^H \cup \Sigma_i^H$. The relations (8.23) and (8.24a) yield

$$C(\mathbf{x})\ \phi = \int_{\Sigma_-^H} da\, (G\, q^H - \varphi\ \mathbf{n} \cdot \nabla_{\boldsymbol{\xi}} G) - \int_{\Sigma_i^H} d\xi\, d\eta\ \varphi\ G_\zeta + \phi^{\Sigma^F}. \tag{8.25b}$$

The relation (8.25b) and expressions (8.25a) yield the three boundary-integral relations

$$\phi = \int_{\Sigma_-^H} da\, (G\, q^H - \varphi\ \mathbf{n} \cdot \nabla_{\boldsymbol{\xi}} G) - \int_{\Sigma_i^H} d\xi\, d\eta\ \varphi\ G_\zeta + \phi^{\Sigma^F}$$
$$\text{if } \mathbf{x} \in (\mathcal{D} \cup \Sigma^F \cup \Sigma_i^F)\ , \tag{8.26a}$$

$$\frac{\phi}{2} = \int_{\Sigma_-^H} da\, (G\, q^H - \varphi\ \mathbf{n} \cdot \nabla_{\boldsymbol{\xi}} G) - \int_{\Sigma_i^H} d\xi\, d\eta\ \varphi\ G_\zeta + \phi^{\Sigma^F}$$
$$\text{if } \mathbf{x} \in (\Sigma_-^H \cup \Sigma_i^H)\ , \tag{8.26b}$$

$$0 = \int_{\Sigma_-^H} da\, (G\, q^H - \varphi\ \mathbf{n} \cdot \nabla_{\boldsymbol{\xi}} G) - \int_{\Sigma_i^H} d\xi\, d\eta\ \varphi\ G_\zeta + \phi^{\Sigma^F}$$
$$\text{if } \mathbf{x} \in \mathcal{D}_i\ . \tag{8.26c}$$

The three complementary boundary-integral relations (8.26) include the distributions of dipoles $\varphi\ \mathbf{n} \cdot \nabla_{\boldsymbol{\xi}} G$ and $\varphi\, G_\zeta$ over the surface $\Sigma_-^H \cup \Sigma_i^H$, which create a discontinuous flow potential at $\Sigma_-^H \cup \Sigma_i^H$ as is explained in section 8.3. A boundary-integral relation that holds everywhere in the lower half space $z \leq 0$ and is equivalent to the three relations (8.26) is now obtained.

Equivalent single weakly-singular boundary-integral relation

In accordance with expression (8.24b), the complementary function

$$C_i(\mathbf{x}) \equiv \int_{\mathcal{D}_i} dv\, \nabla^2_{\boldsymbol{\xi}} G \tag{8.27a}$$

is defined. Equations (8.5c-d) yield

$$C_i(\mathbf{x}) = \left\{ \begin{array}{c} 0 \\ 1 \\ 1/2 \end{array} \right\} \text{ if } \mathbf{x} \in \left\{ \begin{array}{c} \mathcal{D} \cup \Sigma^F \cup \Sigma^F_i \\ \mathcal{D}_i \\ \Sigma^H_- \cup \Sigma^H_i \end{array} \right\} . \tag{8.27b}$$

The relations (8.25a) and (8.27b) show that one has

$$C(\mathbf{x}) + C_i(\mathbf{x}) = 1 \tag{8.28}$$

for every point $\mathbf{x}$ in the lower half space $z \leq 0$. The divergence theorem applied in (8.27a) yields the alternative expression

$$C_i(\mathbf{x}) = \int_{\Sigma^H_-} da\, \mathbf{n} \cdot \nabla_{\boldsymbol{\xi}} G + \int_{\Sigma^H_i} d\xi\, d\eta\, G_\zeta \ . \tag{8.29}$$

Addition of the term $C_i\, \phi$ on the left and right sides of (8.25b), with (8.28) or (8.29) used on the left or right sides, yields the boundary-integral relation

$$\phi = \int_{\Sigma^H_-} da\, [\, G\, q^H + (\phi - \varphi)\, \mathbf{n} \cdot \nabla_{\boldsymbol{\xi}} G\,] + \int_{\Sigma^H_i} d\xi\, d\eta\, (\phi - \varphi)\, G_\zeta + \phi^{\Sigma^F} \tag{8.30}$$

where ϕ^{Σ^F} is given by (8.12). The boundary-integral relation (8.30) holds at every point $\mathbf{x}$ and is equivalent to the three complementary relations (8.26).

Limit $\delta \to 0$

The boundary-integral relation (8.30), which holds for a closed body surface $\Sigma^H_- \cup \Sigma^H_i$ that is submerged at a depth $0 < \delta$ below the free-surface plane $\zeta = 0$, is now considered in the limit $\delta \to 0$. In this limit, one has $\Sigma^H_- \to \Sigma^H$ and $\Sigma^H_i \to \Sigma^F_i$, and (8.30) becomes

$$\phi = \int_{\Sigma^H} da\, [\, G\, q^H + (\phi - \varphi)\, \mathbf{n} \cdot \nabla_{\boldsymbol{\xi}} G\,] + \phi^F_i + \phi^{\Sigma^F} \tag{8.31a}$$

$$\text{where } \phi^F_i \equiv \int_{\Sigma^F_i} d\xi\, d\eta\, (\phi - \varphi)\, G_\zeta \ . \tag{8.31b}$$

The identity

$$(\phi-\varphi)\,G_\zeta=(\phi-\varphi)\,(G_\zeta-f_\epsilon^2 G)+f_\epsilon^2\,G\,(\phi-\varphi)$$

and the free-surface boundary conditions in (8.5c-d) yield the alternative expression

$$\phi_i^F=f_\epsilon^2\!\int_{\Sigma_i^F}\!d\xi\,d\eta\,(\phi-\varphi)\,G \tag{8.31c}$$

where f_ϵ can be replaced by f.

The boundary conditions (8.21d-e) at the waterplane Σ_i^F and at the rigid lid Σ_i^H are compatible if one has

$$\varphi(\boldsymbol{\xi})=0\ \text{ for }\ \boldsymbol{\xi}\in\Sigma_i^F\ \text{ as }\ \delta\to 0\ . \tag{8.32}$$

This compatibility condition and expressions (8.31b-c) yield

$$\phi_i^F=C^\Gamma\phi\ \text{ where }\ C^\Gamma\equiv\!\int_{\Sigma_i^F}\!d\xi\,d\eta\,G_\zeta=f^2\!\int_{\Sigma_i^F}\!d\xi\,d\eta\,G\ . \tag{8.33}$$

The boundary-integral flow relation (8.31a) with $\phi_i^F=C^\Gamma\phi$ and C^Γ given by the second expression in (8.33) is identical to the boundary-integral relation (8.18) associated with the free-waterplane boundary-value problem.

Representation of the function $C^\Gamma(\mathbf{x})$ as a waterline integral

The function $C^\Gamma(\mathbf{x})$ defined by the waterplane integral

$$C^\Gamma(\mathbf{x})=\!\int_{\Sigma_i^F}\!d\xi\,d\eta\,G_\zeta \tag{8.34a}$$

$$=\!\int_{\Sigma_i^F}\!d\xi\,d\eta\Big[\,\nabla^2_{\boldsymbol{\xi}}G^\zeta-(\partial_\xi^2+\partial_\eta^2)\,G^\zeta\Big]\ , \tag{8.34b}$$

where $^\zeta$ means integration with respect to ζ, can be expressed as a line integral around the waterline Γ. For points $\mathbf{x}\notin\Sigma_i^F$, the Laplace equation in (8.5d) if $z=0$ or the Poisson equation in (8.5c) if $z<0$ show that one has $\nabla^2_{\boldsymbol{\xi}}G^\zeta=0$ in (8.34b), which then becomes

$$C^\Gamma=-\!\int_{\Sigma_i^F}\!d\xi\,d\eta\,(G^\zeta_{\xi\xi}+G^\zeta_{\eta\eta})=-\!\int_{\Sigma_i^F}\!d\xi\,d\eta\,\widetilde{\nabla}_{\boldsymbol{\xi}}\cdot\nabla_{\boldsymbol{\xi}}\,G^\zeta$$

where $\widetilde{\nabla}_{\boldsymbol{\xi}}\equiv(\partial_\xi,\partial_\eta,0)$. The 2D divergence theorem finally yields

$$C^\Gamma(\mathbf{x})=-\!\int_\Gamma\!d\ell\ \boldsymbol{\nu}\cdot\nabla_{\boldsymbol{\xi}}\,G^\zeta=f^2\!\int_{\Sigma_i^F}\!d\xi\,d\eta\,G \tag{8.35}$$

where the unit vector $\boldsymbol{\nu} \equiv (\nu^x, \nu^y, 0)$ is normal to the waterline Γ and points into the water, like the unit vector $\mathbf{n}$, and the second expression for the function C^Γ in (8.33) was used. The function $C^\Gamma(\mathbf{x})$ defined by the alternative expressions (8.35) are continuous in the entire lower half space $z \leq 0$. However, the waterplane-integral representation (8.34a) is discontinuous across the waterplane Σ_i^F.

8.6 Conclusion

Final boundary-integral relations

Expressions (8.31a), (8.33) and (8.35) finally yield

$$(1 - C^\Gamma)\,\phi = \phi^H + \phi^{\Sigma^F} \quad \text{where} \tag{8.36a}$$

$$C^\Gamma \equiv -\int_\Gamma d\ell\ \boldsymbol{\nu} \cdot \nabla_{\boldsymbol{\xi}} G^\zeta = f^2 \int_{\Sigma_i^F} d\xi\, d\eta\ G\ , \tag{8.36b}$$

$$\phi^H \equiv \int_{\Sigma^H} da \left[q^H G + (\phi - \varphi)\, \mathbf{n} \cdot \nabla_{\boldsymbol{\xi}} G \right]\ , \tag{8.36c}$$

$$\phi^{\Sigma^F} \equiv \int_{\Sigma^F} d\xi\, d\eta\ \left(q^F - \mathrm{i}\, f p^F \right) G \tag{8.36d}$$

with $\varphi \equiv \varphi(\boldsymbol{\xi})$ and $\phi \equiv \varphi(\mathbf{x})$. The weakly-singular boundary-integral flow representation (8.36) holds in the entire lower half-space $z \leq 0$ and yields an integral equation that determines the unknown flow potential at the hull surface of a body in regular waves **[8,2]**. The function $C^\Gamma(\mathbf{x})$ in (8.36a) is explicitly defined via the alternative expressions (8.36b) as a line integral around the waterline Γ of the body or as an integral over the waterplane Σ_i^F inside the body surface Σ^H.

Removal of irregular frequencies

As was already noted, the Green function $G(\boldsymbol{\xi}, \mathbf{x})$ associated with diffraction and radiation of regular water waves is defined within the region $-d \leq \zeta \leq 0$ and therefore creates waves outside as well as inside the body, which can result in spurious solutions for some special wave frequencies called irregular frequencies **[8,3]**. These spurious solutions can be prevented by imposing that ϕ is nil at the waterplane Σ_i^F, which yields

$$\phi^H + \phi^{\Sigma^F} = \left\{ \begin{array}{c} (1 - C^\Gamma)\,\phi \\ 0 \end{array} \right\} \text{ if } \mathbf{x} \in \left\{ \begin{array}{c} \Sigma^H \\ \Sigma_i^F \end{array} \right\} \tag{8.37}$$

where $\phi \equiv \varphi(\mathbf{x})$. The pair of boundary-integral relations (8.37) applied at $\mathbf{x} \in \Sigma^H$ or at $\mathbf{x} \in \Sigma_i^F$ only involves the potential $\varphi(\boldsymbol{\xi})$ at points $\boldsymbol{\xi} \in \Sigma^H$ and

therefore yields an overdetermined system of equations. The flow potential $\varphi(\mathbf{x})$ defined by the pair of integral equations (8.37) is free from irregular frequencies [**8,4**].

Free-waterplane and rigid-waterplane linear flow models

In the limit $\delta = 0$, the flow region defined in Fig.8.2 associated with the rigid-waterplane linear flow model is identical to the flow region associated with the free-waterplane linear flow model and depicted in Fig.8.1. Thus, the flow potentials φ that correspond to Fig.8.2 with $\delta = 0$ or to Fig.8.1 satisfy the Laplace equation in identical flow regions and satisfy identical boundary conditions at identical boundary surfaces Σ^B, Σ^F and Σ^H.

In the free-waterplane linear flow model, Green's identity is applied in the flow region that is defined in the limit $\delta = 0$ of the rigid-waterplane model. However, in the rigid-waterplane model, Green's identity is applied in the flow region defined for $0 < \delta$, and the limit $\delta \to 0$ of the boundary-integral flow representation is considered subsequently. Thus, the order of the two processes 'apply Green's identity in a flow region' and 'consider the limit $\delta \to 0$' is interchanged in the free-waterplane and rigid-waterplane linear flow models.

The agreement between the boundary-integral relations associated with the classical free-waterplane linear flow model (in which Green's identity is applied to the flow region that corresponds to $\delta = 0$) or the rigid-waterplane flow model (in which Green's identity is applied to the flow region that corresponds to $0 < \delta \ll 1$ and the limit $\delta = 0$ of the resulting boundary-integral flow representation is then considered) shows that these linear flow models are consistent for diffraction and radiation of regular waves by a stationary body, and that the rigid waterplane Σ_i^H has no influence on the velocity potential of the flow around the body surface Σ^H outside the body or at Σ^H in that case.

Chapter 9

Boundary-integral flow relations for a ship that advances through waves

The applications of Green's fundamental boundary-integral relation (6.3) to diffraction and radiation of regular waves by a stationary body (offshore structure, moored ship) given in the previous chapter are now extended to the more general, and more complicated, case of a ship that advances through regular waves at a constant speed along a straight path. Both the free-waterplane linear flow model, commonly called Neumann-Kelvin model, and the rigid-waterplane flow model defined in chapter 8 are considered again. Specifically, Green's basic identity is applied to the usual Neumann-Kelvin (NK) flow model in sections 9.1–9.3, and three variants of the rigid-waterplane (RW) flow model are considered in sections 9.4–9.6. Thus, four alternative linear flow models, and five related alternative boundary-integral flow representations, are analyzed in sections 9.1–9.6. These alternative flow models and flow representations are compared in section 9.7. In the special case of a ship that steadily advances in calm water, an additional linear flow model, called Neumann-Michell (NM) model, is defined in section 9.8. **[9,1]**

9.1 Neumann-Kelvin boundary-value problem and related Green function

The flow created by a ship that advances, at a constant speed along a straight path, through regular waves in deep water is considered in this

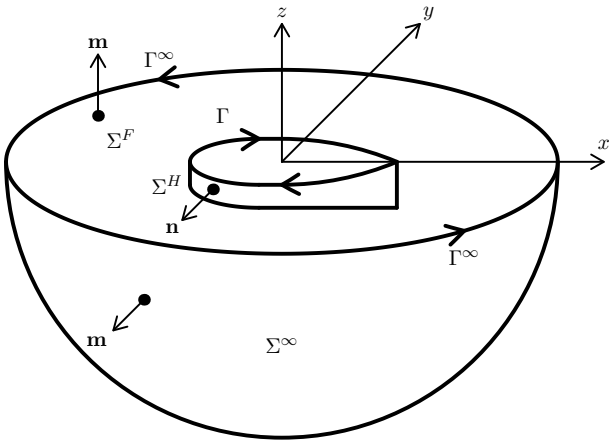

Figure 9.1: Galilean system of Cartesian coordinates (x, y, z) and boundary surface $\Sigma \equiv \Sigma^\infty \cup \Sigma^F \cup \Sigma^H$ associated with the basic Neumann-Kelvin boundary-value problem for a ship that steadily advances through regular waves in deep water.

chapter. As in chapters 1 and 6, the flow is observed from a Galilean frame of reference that follows the ship, and a related system of Cartesian coordinates $\mathbf{x} \equiv (x, y, z)$ and $\boldsymbol{\xi} \equiv (\xi, \eta, \zeta)$ is defined. The z/ζ axis is vertical and points upward, and the x/ξ axis is taken along the path of the ship and points toward the ship bow, as in chapters 1 and 6. The coordinates $\boldsymbol{\xi}$ and $\mathbf{x}$, the corresponding flow potentials

$$\varphi \equiv \varphi(\boldsymbol{\xi}) \quad \text{and} \quad \phi \equiv \varphi(\mathbf{x}) \ ,$$

and all other flow variables are nondimensional in terms of a reference length L_r, usually chosen as the length L_s of the ship, the acceleration of gravity g and (for the pressure) the water density ρ_w, as in section 1.5.

As in (1.34) and (6.19), the velocity potential of the flow created by the ship is expressed as

$$\widehat{\varphi}(\boldsymbol{\xi}, t) = \operatorname{Re} \varphi(\boldsymbol{\xi})\, e^{(\epsilon - \mathrm{i} f)\, t} = \operatorname{Re} \varphi(\boldsymbol{\xi})\, e^{-\mathrm{i} f_\epsilon t} \tag{9.1a}$$

$$\text{where } f_\epsilon \equiv f + \mathrm{i}\,\epsilon \text{ with } \epsilon = +0 \ . \tag{9.1b}$$

The spatial component $\varphi(\boldsymbol{\xi})$ in (9.1a) is determined by a classical boundary-value problem that is associated with the linear flow model called free-waterplane flow model in chapter 8. For ships advancing in calm water or through waves, this classical boundary-value problem is widely called

Neumann-Kelvin (NK) problem, and this common name is used hereafter. The classical NK linear flow model and boundary-value problem are associated with the closed boundary surface

$$\Sigma \equiv \Sigma^\infty \cup \Sigma^F \cup \Sigma^H \tag{9.2}$$

where Σ^∞ is an infinitely large surface that encloses the flow region $\mathcal{D}$, and Σ^F is the portion of the free-surface plane $z = 0$ that is inside Σ^∞ but outside the mean wetted ship-hull surface Σ^H, as is shown in Fig.9.1. The intersection curves between the free-surface plane $z = 0$ and the surfaces Σ^∞ and Σ^H are denoted as Γ^∞ or Γ, which are oriented as in Fig.9.1. The portion of the plane $z = 0$ located inside the ship-hull surface Σ^H is denoted as Σ_i^F and called 'ship waterplane'. The unit vector $\mathbf{m}$ normal to the boundary surface Σ that encloses the flow region $\mathcal{D}$ points outside $\mathcal{D}$, whereas the unit vector $\mathbf{n} = -\mathbf{m}$ normal to the ship-hull surface Σ^H points outside the ship (into the water).

Classical Neumann-Kelvin boundary-value problem

The spatial component $\varphi(\boldsymbol{\xi})$ of the flow potential (9.1a) associated with the free-waterplane flow model is determined by the NK boundary-value problem (1.35), now restated for ease of reference. The flow potential $\varphi(\boldsymbol{\xi})$ satisfies the Laplace equation

$$\nabla^2_{\boldsymbol{\xi}} \varphi \equiv (\partial^2_\xi + \partial^2_\eta + \partial^2_\zeta)\varphi = 0 \ \text{ in } \ \mathcal{D} \tag{9.3a}$$

where $\mathcal{D}$ denotes the flow region outside the ship, the far-field condition

$$\nabla_{\boldsymbol{\xi}} \varphi \to 0 \ \text{ as } \ \boldsymbol{\xi} \to \infty \ , \tag{9.3b}$$

and the free-surface and ship-hull surface boundary conditions

$$\partial_\zeta \varphi + (\mathrm{i} f_\epsilon + F\partial_\xi)^2 \varphi = \mathrm{i} f p^F + F p^F_\xi - q^F \ \text{ at } \ \Sigma^F \tag{9.3c}$$

$$\text{and } \ \mathbf{n} \cdot \nabla_{\boldsymbol{\xi}} \varphi = q^H \ \text{ at } \ \Sigma^H \ . \tag{9.3d}$$

The Froude number F and the non-dimensional wave frequency f in (9.3c) are defined by (1.32). The flux q^H at the ship-hull surface Σ^H and the pressure p^F and flux q^F at the free surface Σ^F are *presumed known* in the general boundary-value problem (9.3) that is considered in this chapter.

Green function for a ship advancing through regular waves

The Green function $G(\boldsymbol{\xi}, \mathbf{x})$ associated with the Laplace equation (9.3a), the far-field condition (9.3b) and the boundary condition (9.3c) at the free surface satisfies the far-field condition

$$G \to 0 \ \text{ as } \ \boldsymbol{\xi} \to \infty \tag{9.4a}$$

and the field equations and free-surface boundary conditions

$$\left\{ \begin{array}{l} \nabla^2_{\boldsymbol{\xi}} G = \delta(\xi - x)\,\delta(\eta - y)\,\delta(\zeta - z) \text{ in } \zeta < 0 \\ \partial_\zeta G + (\mathrm{i} f_\epsilon - F\partial_\xi)^2 G = 0 \text{ at } \zeta = 0 \end{array} \right\} \text{ if } z < 0 \tag{9.4b}$$

$$\text{or } \left\{ \begin{array}{l} \nabla^2_{\boldsymbol{\xi}} G = 0 \text{ in } \zeta < 0 \\ \partial_\zeta G + (\mathrm{i} f_\epsilon - F\partial_\xi)^2 G = \\ \quad -\delta(\xi - x)\,\delta(\eta - y) \text{ at } \zeta = 0 \end{array} \right\} \text{ if } z = 0\ . \tag{9.4c}$$

The Green function $G(\boldsymbol{\xi}, \mathbf{x})$ defined by (9.4) represents the potential of the flow that is created at a point $(\xi, \eta, \zeta \le 0)$ by a source located at a point $(x, y, z < 0)$ or a flux across the free surface at $(x, y, z = 0)$. These pulsating singularities (source or flux) steadily advance along the ξ axis at a (nondimensional) speed $-F$, in accordance with the term $-F\partial_\xi$ in the free-surface boundary conditions in (9.4b-c).

9.2 Neumann-Kelvin boundary-integral flow relations

Green's fundamental relation (6.3) is now applied, in the flow region bounded by the surface Σ defined by (9.2) and Fig.9.1, to the Green function $G(\boldsymbol{\xi}, \mathbf{x})$ determined by (9.4) and the flow potential $\varphi(\boldsymbol{\xi})$ determined by the Neumann-Kelvin boundary-value problem (9.3).

Three complementary boundary-integral relations

Green's relation (6.3) with $\psi(\boldsymbol{\xi}) = G(\boldsymbol{\xi}, \mathbf{x})$, the Laplace equation (9.3a), the far-field boundary conditions (9.3b) and (9.4a) and the boundary condition (9.3d) at the hull surface yield

$$\begin{aligned} \int_{\mathcal{D}} dv\, \varphi\, \nabla^2_{\boldsymbol{\xi}} G = & \int_{\Sigma^F} d\xi\, d\eta\, (\varphi\, \partial_\zeta G - G\, \partial_\zeta \varphi) \\ & + \int_{\Sigma^H} da\, (q^H G - \varphi\, \mathbf{n} \cdot \nabla_{\boldsymbol{\xi}} G) \end{aligned} \tag{9.5}$$

where $G \equiv G(\boldsymbol{\xi}, \mathbf{x})$ and $\varphi \equiv \varphi(\boldsymbol{\xi})$ as was already noted. Furthermore, $da \equiv da(\boldsymbol{\xi})$ and $q^H \equiv q^H(\boldsymbol{\xi})$ denote the differential element of area or the hull-flux at a point $\boldsymbol{\xi}$ of the hull surface Σ^H, and $dv \equiv dv(\boldsymbol{\xi})$ is the differential element of volume at a point $\boldsymbol{\xi} \in \mathcal{D}$.

The identity

$$\begin{aligned} \varphi\, \partial_\zeta G - G\, \partial_\zeta \varphi = & \varphi \left[\partial_\zeta G + (\mathrm{i} f_\epsilon - F\partial_\xi)^2 G \right] - G \left[\partial_\zeta \varphi + (\mathrm{i} f_\epsilon + F\partial_\xi)^2 \varphi \right] \\ & + F\, \partial_\xi \left[F(G \partial_\xi \varphi - \varphi\, \partial_\xi G) + 2\,\mathrm{i} f_\epsilon G \varphi \right] \end{aligned}$$

applied in the integral over the free surface Σ^F in (9.5), together with the free-surface boundary condition (9.3c), Stokes' theorem and the far-field conditions (9.3b) and (9.4a), yield

$$\int_{\mathcal{D}} dv\ \varphi\,\nabla^2_{\boldsymbol{\xi}} G - \int_{\Sigma^F} d\xi\, d\eta\ \varphi\left[\partial_\zeta G + (\mathrm{i} f_\epsilon - F\partial_\xi)^2 G\right] =$$
$$F\int_\Gamma d\eta\,[F(G\,\partial_\xi\varphi - \varphi\,\partial_\xi G) + 2\,\mathrm{i} f_\epsilon G\varphi] + \int_{\Sigma^H} da\left[q^H G - \varphi\ \mathbf{n}\cdot\nabla_{\boldsymbol{\xi}} G\right]$$
$$+\int_{\Sigma^F} d\xi\, d\eta\left[q^F - F p^F_\xi - \mathrm{i} f p^F\right] G \tag{9.6}$$

where the mean ship waterline Γ is oriented in the clockwise direction when viewed from above the free surface as is shown in Fig.9.1.

The flow potential $\varphi \equiv \varphi(\boldsymbol{\xi})$ in the integrals over $\mathcal{D}$ and Σ^F on the left side of (9.6) is now expressed as $\varphi = (\varphi - \phi) + \phi$ where $\phi \equiv \varphi(\mathbf{x})$ is the flow potential at the source-point $\mathbf{x}$ in the Green function $G(\boldsymbol{\xi}, \mathbf{x})$. The relations

$$\int_{\mathcal{D}} dv\,(\varphi - \phi)\,\nabla^2_{\boldsymbol{\xi}} G = 0 \ \text{ and}$$
$$\int_{\Sigma^F} d\xi\, d\eta\,(\varphi - \phi)\left[\partial_\zeta G + (\mathrm{i} f_\epsilon - F\partial_\xi)^2 G\right] = 0\ ,$$

which follow from the relations (9.4b-c) and (6.6), yield

$$\int_{\mathcal{D}} dv\ \varphi\,\nabla^2_{\boldsymbol{\xi}} G - \int_{\Sigma^F} d\xi\, d\eta\ \varphi\left[\partial_\zeta G + (\mathrm{i} f_\epsilon - F\partial_\xi)^2 G\right] = \phi\ C(\mathbf{x}) \tag{9.7a}$$
$$\text{where}\ \ C(\mathbf{x}) \equiv \int_{\mathcal{D}} dv\,\nabla^2_{\boldsymbol{\xi}} G - \int_{\Sigma^F} d\xi\, d\eta\left[\partial_\zeta G + (\mathrm{i} f_\epsilon - F\partial_\xi)^2 G\right]\ . \tag{9.7b}$$

Equations (9.4b-c) yield

$$C(\mathbf{x}) = \left\{\begin{matrix} 1 \\ 0 \\ 1/2 \end{matrix}\right\} \text{ if } \mathbf{x} \in \left\{\begin{matrix} \mathcal{D}\cup\Sigma^F \\ \mathcal{D}_i \cup \Sigma^F_i \\ \Sigma^H \cup \Gamma \end{matrix}\right\} \tag{9.8a}$$

where $\mathcal{D}\cup\Sigma^F$ and $\mathcal{D}_i \cup \Sigma^F_i$ denote the 3D regions and the portions of the free-surface plane $\zeta = 0$ that are located strictly outside or inside the mean wetted ship-hull surface $\Sigma^H \cup \Gamma$. The relations (9.6) and (9.7a) yield

$$C(\mathbf{x})\,\phi = \int_{\Sigma^H} da\left[q^H G - \varphi\ \mathbf{n}\cdot\nabla_{\boldsymbol{\xi}} G\right]$$
$$+ F\int_\Gamma d\eta\,[F(G\,\partial_\xi\varphi - \varphi\,\partial_\xi G) + 2\,\mathrm{i} f_\epsilon G\varphi] + \phi^{\Sigma^F} \tag{9.8b}$$
$$\text{where}\ \ \phi^{\Sigma^F} \equiv \int_{\Sigma^F} d\xi\, d\eta\left[q^F - F p^F_\xi - \mathrm{i} f p^F\right] G\ . \tag{9.8c}$$

Explicit solution in a special case

In the special (and simplest) case when no ship-hull surface Σ^H exists, both the relations (9.7b) and (9.8a) yield $C = 1$ in the entire flow region $z \leq 0$, and the boundary-integral relation (9.8b) *explicitly* determines the velocity potential of the flow created by a distribution of pressure $p^F(\xi, \eta)$ and/or flux $q^F(\xi, \eta)$ at the free surface Σ^F as

$$\phi = \phi^{\Sigma^F} \equiv \int_{\Sigma^F} d\xi \, d\eta \, \big[\, q^F - F p^F_\xi - \mathrm{i} f p^F \, \big] G \ . \tag{9.9}$$

This explicit expression for the velocity potential ϕ of the flow created by a prescribed distribution of pressure p^F and/or flux q^F at the free surface Σ^F can also be directly obtained via Fourier transformation of the reduced boundary-value problem defined by (9.3a-c).

Equivalent single weakly-singular boundary-integral relation

Expressions (9.8) yield three boundary-integral identities that hold inside, outside or at the ship-hull surface. An equivalent boundary-integral identity that holds everywhere in the lower half space $z \leq 0$ is now obtained. In accordance with expression (9.7b), the complementary function

$$C_i(\mathbf{x}) \equiv \int_{\mathcal{D}_i} dv \, \nabla^2_{\boldsymbol{\xi}} G - \int_{\Sigma^F_i} d\xi \, d\eta \, \big[\, \partial_\zeta G + (\mathrm{i} f_\epsilon - F \partial_\xi)^2 G \, \big] \tag{9.10a}$$

is defined. Equations (9.4b-c) yield

$$C_i(\mathbf{x}) = \left\{ \begin{array}{c} 0 \\ 1 \\ 1/2 \end{array} \right\} \text{ if } \mathbf{x} \in \left\{ \begin{array}{c} \mathcal{D} \cup \Sigma^F \\ \mathcal{D}_i \cup \Sigma^F_i \\ \Sigma^H \cup \Gamma \end{array} \right\} \ . \tag{9.10b}$$

The relations (9.8a) and (9.10b) show that one has

$$C(\mathbf{x}) + C_i(\mathbf{x}) = 1 \tag{9.11}$$

at every point $\mathbf{x}$ in the lower half space $z \leq 0$.

The divergence theorem applied in (9.10a) yields

$$C_i(\mathbf{x}) = \int_{\Sigma^H} da \, \mathbf{n} \cdot \nabla_{\boldsymbol{\xi}} G + f_\epsilon^2 \int_{\Sigma^F_i} d\xi \, d\eta \, G - F \int_{\Sigma^F_i} d\xi \, d\eta \, \partial_\xi \, (F \partial_\xi - 2 \, \mathrm{i} f_\epsilon) G \ .$$

Stokes' theorem finally yields the alternative expression

$$C_i(\mathbf{x}) = \int_{\Sigma^H} da \, \mathbf{n} \cdot \nabla_{\boldsymbol{\xi}} G + f_\epsilon^2 \int_{\Sigma^F_i} d\xi \, d\eta \, G + F \int_{\Gamma} d\eta \, (F \partial_\xi - 2 \, \mathrm{i} f_\epsilon) G \tag{9.12}$$

where the waterline Γ is oriented as in Fig.9.1.

Addition of the term $C_i\,\phi$ on the left and right sides of (9.8b), with (9.11) or (9.12) used on the left or right sides, yields the boundary-integral relation

$$\begin{aligned}\phi = &\int_{\Sigma^H} da\,\Big[\,q^H\,G + (\phi-\varphi)\,\mathbf{n}\cdot\nabla_{\boldsymbol{\xi}}\,G\,\Big] + f_\epsilon^2\,\phi\int_{\Sigma_i^F} d\xi\,d\eta\;G \\ &+ F\int_\Gamma d\eta\,\left[\,FG\,\partial_\xi\varphi + (\phi-\varphi)(F\,G_\xi - 2\,\mathrm{i}\,f_\epsilon\,G)\right] \\ &+ \int_{\Sigma^F} d\xi\,d\eta\,\left[\,q^F - F p_\xi^F - \mathrm{i}\,f\,p^F\,\right] G\;. \end{aligned} \tag{9.13}$$

The boundary-integral relation (9.13) holds at every point $(x, y, z \le 0)$ and is equivalent to the three relations (9.8) with $C(\mathbf{x}) = 1$, 0 or 1/2 for points $\mathbf{x}$ in the flow region $\mathcal{D}\cup\Sigma^F$, the region $\mathcal{D}_i\cup\Sigma_i^F$ inside the ship, or at the ship-hull surface $\Sigma^H\cup\Gamma$. The term $\phi-\varphi\equiv\varphi(\mathbf{x})-\varphi(\boldsymbol{\xi})$ in (9.13) vanishes if the points $\boldsymbol{\xi}$ and $\mathbf{x}$ in the Green function $G(\boldsymbol{\xi},\mathbf{x})$ coincide. The singularities in the integrands

$$\varphi\;\mathbf{n}\cdot\nabla_{\boldsymbol{\xi}}\,G\;\text{ and }\;\varphi\,G_\xi \tag{9.14a}$$

of the integrals over the hull surface Σ^H or the waterline Γ in (9.8b) are then weakened in the integrands

$$(\phi-\varphi)\,\mathbf{n}\cdot\nabla_{\boldsymbol{\xi}}\,G\;\text{ and }\;(\phi-\varphi)\,G_\xi \tag{9.14b}$$

of the corresponding integrals in (9.13). As a result, the hull-surface or waterline integrals of the functions (9.14b) are continuous at the ship-hull surface $\Sigma^H\cup\Gamma$, whereas the corresponding integrals of the functions (9.14a) are discontinuous, in accordance with the jump in the value of $C(\mathbf{x})$ across the surface $\Sigma^H\cup\Gamma$.

9.3 Neumann-Kelvin flow representation and particular cases

The boundary-integral relation (9.13), with f_ϵ denoted as f, finally yields

$$\begin{aligned}\left[1 - f^2\int_{\Sigma_i^F} d\xi\,d\eta\,G\right]\phi = &\int_{\Sigma^F} d\xi\,d\eta\,\left[\,q^F - F p_\xi^F - \mathrm{i}\,f\,p^F\,\right] G \\ &+ \int_{\Sigma^H} da\,\Big[\,q^H\,G + (\phi-\varphi)\,\mathbf{n}\cdot\nabla_{\boldsymbol{\xi}}\,G\,\Big] \\ &+ F\int_\Gamma d\eta\,\left[\,FG\,\partial_\xi\varphi + (\phi-\varphi)(F\,G_\xi - 2\,\mathrm{i}\,f\,G)\right]\;. \end{aligned} \tag{9.15}$$

This boundary-integral flow representation is called **Neumann-Kelvin (NK) flow representation** hereafter. **[9,2]**

FIVE PARTICULAR CASES

In the particular case of a **ship that steadily advances in calm water**, one has $f = 0$ and the NK flow representation (9.15) becomes

$$\phi = \int_{\Sigma^F} d\xi\, d\eta \left[q^F - F p^F_\xi \right] G + \int_{\Sigma^H} da \left[q^H G + (\phi - \varphi)\, \mathbf{n} \cdot \nabla_{\boldsymbol{\xi}} G \right] + F^2 \int_\Gamma d\eta \left[G\, \partial_\xi \varphi + (\phi - \varphi) G_\xi \right] \ . \tag{9.16}$$

In the particular case of a **stationary body in regular waves**, i.e. in the special case $F = 0$, the line integral around the body waterline Γ in the Neumann-Kelvin flow representation (9.15) disappears, and (9.15) becomes

$$\left[1 - f^2 \int_{\Sigma^F_i} d\xi\, d\eta\, G \right] \phi = \int_{\Sigma^F} d\xi\, d\eta \left[q^F - \mathrm{i} f p^F \right] G + \int_{\Sigma^H} da \left[q^H G + (\phi - \varphi)\, \mathbf{n} \cdot \nabla_{\boldsymbol{\xi}} G \right] \tag{9.17}$$

in agreement with the boundary-integral flow representation defined by (8.18) and (8.12).

In the particular case of a **body that is fully submerged under the free-surface plane** $\zeta = 0$, the integral over the waterplane Σ^F_i and the integral around the ship waterline Γ in the Neumann-Kelvin flow representation (9.15) disappear. This flow representation then becomes

$$\phi = \int_{\Sigma_F} d\xi\, d\eta \left[q^F - F p^F_\xi - \mathrm{i} f p^F \right] G + \int_{\Sigma_H} da \left[q^H G + (\phi - \varphi)\, \mathbf{n} \cdot \nabla_{\boldsymbol{\xi}} G \right] \tag{9.18}$$

where Σ_F denotes the *entire* plane $\zeta = 0$, and the (closed) surface of the fully submerged body is denoted as Σ_H.

If no body surface Σ_H exists, the flow representation (9.18) becomes

$$\phi = \int_{\Sigma_F} d\xi\, d\eta \left[q^F - F p^F_\xi - \mathrm{i} f p^F \right] G \tag{9.19}$$

in agreement with expression (9.9) for the potential ϕ of the **flow created by a free-surface distribution of pressure p^F and/or flux q^F.**

The Neumann-Kelvin flow representation (9.15) is significantly different for the general case $Ff \neq 0$ and the particular cases $f = 0$ or $F = 0$. In particular, the Neumann-Kelvin flow representations (9.15) and (9.16) for a ship that advances through regular waves or in calm water contain line

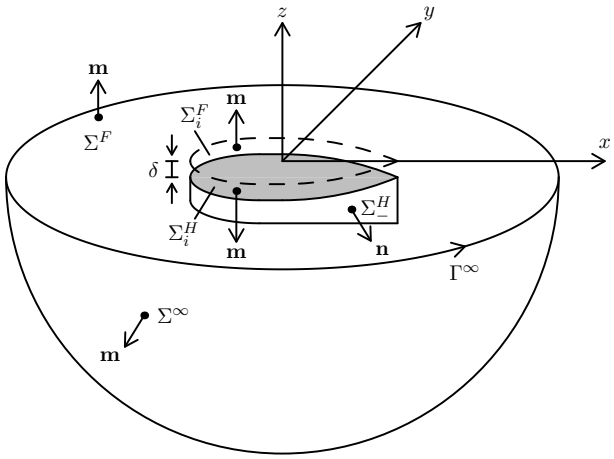

Figure 9.2: Boundary surface $\Sigma \equiv \Sigma^\infty \cup \Sigma^F \cup \Sigma_i^F \cup \Sigma_i^H \cup \Sigma_-^H$ related to the rigid-waterplane linear flow model. The unit vector $\mathbf{m}$ normal to the boundary surface Σ points outside the flow region, whereas the unit vector $\mathbf{n} = -\mathbf{m}$ normal to the ship hull surface Σ_-^H points outside the ship.

integrals around the ship waterline Γ and these waterline integrals involve the flow potential φ and its derivative $\partial_\xi \varphi$, whereas the Neumann-Kelvin representation (9.17) for an offshore structure in waves does not contain a waterline integral and the flow potential φ only appears at the hull surface Σ^H. The boundary-integral flow representations (9.15) and (9.16) for a ship that steadily advances through regular waves or in calm water are then much more complicated than the boundary-integral flow representation (9.17) for wave diffraction-radiation by a stationary body.

9.4 Basic rigid-waterplane (RW) flow model and RW flow representation

The flow representation (9.18) for a general *closed* body surface Σ_H that is *fully submerged* under the free-surface plane $\zeta = 0$ is now applied to a particular type of submerged bodies. Specifically, the body surface

$$\Sigma_H \equiv \Sigma_-^H \cup \Sigma_i^H \,, \tag{9.20a}$$

where Σ_i^H denotes a rigid horizontal lid that closes the open body surface Σ_-^H as is illustrated in Fig.9.2, is considered. The free surface Σ_F associated

with this special submerged closed body consists of the entire plane $\zeta = 0$ and is given by

$$\Sigma_F \equiv \Sigma^F \cup \Sigma_i^F \tag{9.20b}$$

where Σ_i^F denotes the portion of the free surface that is above the rigid body lid Σ_i^H as is shown in Fig.9.2.

The free-surface and hull-surface boundary conditions (9.3c-d) yield

$$\partial_\zeta \varphi + (\mathrm{i} f_\epsilon + F\partial_\xi)^2 \varphi = \left\{ \begin{array}{c} \mathrm{i} f p^F + F p_\xi^F - q^F \\ 0 \end{array} \right\} \text{ at } \left\{ \begin{array}{c} \Sigma^F \\ \Sigma_i^F \end{array} \right\} \tag{9.21a}$$

$$\text{and } \left\{ \begin{array}{c} \mathbf{n} \cdot \nabla_{\boldsymbol{\xi}} \varphi = q^H \\ \varphi_\zeta = q_i^H = 0 \end{array} \right\} \text{ at } \left\{ \begin{array}{c} \Sigma_-^H \\ \Sigma_i^H \end{array} \right\} . \tag{9.21b}$$

The flow representation (9.18) for a general submerged closed body then becomes

$$\phi = \phi^{\Sigma^F} + \phi_-^H + \phi_i^H \quad \text{where} \tag{9.22a}$$

$$\phi^{\Sigma^F} \equiv \int_{\Sigma^F} d\xi\, d\eta \left[q^F - F p_\xi^F - \mathrm{i} f p^F \right] G \, , \tag{9.22b}$$

$$\phi_-^H \equiv \int_{\Sigma_-^H} da \left[q^H G + (\phi - \varphi)\, \mathbf{n} \cdot \nabla_{\boldsymbol{\xi}} G \right] \tag{9.22c}$$

$$\text{and} \quad \phi_i^H \equiv \int_{\Sigma_i^H} da\, (\phi - \varphi)\, G_\zeta \, . \tag{9.22d}$$

This flow representation holds for any submergence depth δ (large or small) of the horizontal rigid lid Σ_i^H below the free surface. The rigid-waterplane (RW) linear flow model defined in section 8.4 and in Fig.9.2 considers the special case when the rigid horizontal lid Σ_i^H of the closed body $\Sigma_-^H \cup \Sigma_i^H$ is submerged at an infinitesimally small depth $0 < \delta \ll 1$.

In the limit $\delta \to 0$, one has $\Sigma_-^H \to \Sigma^H$ and $\Sigma_i^H \to \Sigma_i^F$. The boundary-integral flow representation (9.22) then becomes

$$\phi = \phi^{\Sigma^F} + \phi^H + \phi_i^F \quad \text{where} \tag{9.23a}$$

$$\phi^{\Sigma^F} \equiv \int_{\Sigma^F} d\xi\, d\eta \left[q^F - F p_\xi^F - \mathrm{i} f p^F \right] G \, , \tag{9.23b}$$

$$\phi^H \equiv \int_{\Sigma^H} da \left[q^H G + (\phi - \varphi)\, \mathbf{n} \cdot \nabla_{\boldsymbol{\xi}} G \right] \text{ with } q^H \equiv \mathbf{n} \cdot \nabla \varphi \, , \tag{9.23c}$$

$$\phi_i^F \equiv \int_{\Sigma_i^F} d\xi\, d\eta\, (\phi - \varphi)\, G_\zeta = \int_{\Sigma_i^F} d\xi\, d\eta\, (\phi - \varphi)\, (f + \mathrm{i} F \partial_\xi)^2 G \, . \tag{9.23d}$$

The free-surface boundary conditions in (9.4b-c) were used in (9.23d).

The **RW flow representation** defined by (9.23) does not contain a line integral around the ship waterline Γ, but includes the surface integral

ϕ_i^F over the ship waterplane Σ_i^F. Thus, the RW flow representation (9.23) yields an integral equation that determines the flow potential φ over the *extended* closed ship hull surface $\Sigma^H \cup \Sigma_i^F$.

9.5 2D-flow at the ship waterplane, and RW-hw and RW-h flow representations

The flow within the thin water-layer $-\delta < z \leq 0$ is now analyzed based on the *assumption* that the boundary conditions

$$\partial_\zeta \varphi = 0 \text{ at } \Sigma_i^H \quad \text{and} \tag{9.24a}$$

$$\partial_\zeta \varphi + (\mathrm{i} f_\epsilon + F\partial_\xi)^2 \varphi = 0 \text{ at } \Sigma_i^F \tag{9.24b}$$

are both satisfied, and that the flow in the thin water-layer $-\delta < z \leq 0$ is two dimensional and hence determined by a flow potential $\varphi(\xi, \eta)$ that satisfies the 2D Laplace equation. One then has

$$\varphi_{\xi\xi} + \varphi_{\eta\eta} = 0 \text{ if } (\xi, \eta, 0) \in \Sigma_i^F \text{ and } -\delta < \zeta \leq 0 \tag{9.25a}$$

$$\text{and } F^2\varphi_{\xi\xi} + 2\,\mathrm{i}\, f F \varphi_\xi - f^2\varphi = 0 \text{ if } \boldsymbol{\xi} \in \Sigma_i^F \tag{9.25b}$$

where f_ϵ is denoted as f in (9.25b). In the particular case of an offshore structure in regular waves, one has $F = 0$ and (9.25b) becomes

$$\varphi = 0 \quad \text{if } \boldsymbol{\xi} \in \Sigma_i^F \tag{9.26}$$

in agreement with (8.32).

Analysis of 2D flow in the thin water-layer above the rigid lid Σ_i^H

The general solution of equation (9.25b) in the **general case** $f/F \neq 0$ is

$$\varphi = [H_1(\eta) + \xi H_2(\eta)]\, e^{-\mathrm{i}\xi f/F}$$

where $H_1(\eta)$ and $H_2(\eta)$ are undetermined functions. The Laplace equation (9.25a) then yields

$$H_1''(\eta) + \xi H_2''(\eta) = (f/F)^2 [H_1(\eta) + \xi H_2(\eta)] + 2\,\mathrm{i}\,(f/F) H_2(\eta)\ .$$

This equation, which holds for all values of ξ, yields

$$H_2'' - (f/F)^2 H_2 = 0 \text{ and } H_1'' - (f/F)^2 H_1 = 2\,\mathrm{i}\,(f/F) H_2\ .$$

If $f/F \neq 0$, one then has

$$H_2 = C_2^+ e^{\eta f/F} + C_2^- e^{-\eta f/F} \text{ and}$$

$$H_1 = C_1^+ e^{\eta f/F} + C_1^- e^{-\eta f/F} + \mathrm{i}\,\eta \left[C_2^+ e^{\eta f/F} - C_2^- e^{-\eta f/F} \right]$$

where $C_2^{\pm}$ and $C_1^{\pm}$ are undetermined. The potential φ of the 2D flow within the thin layer of water between the surfaces Σ_i^H and Σ_i^F is then given by

$$\begin{aligned}\varphi = &\left[C_1^+ + C_2^+(\xi + \mathrm{i}\,\eta)\right] e^{-\mathrm{i}\,(\xi+\mathrm{i}\,\eta)\,f/F} \\ &+ \left[C_1^- + C_2^-(\xi - \mathrm{i}\,\eta)\right] e^{-\mathrm{i}\,(\xi-\mathrm{i}\,\eta)\,f/F} \quad \text{if } f/F \neq 0\ . \end{aligned} \tag{9.27}$$

The particular solutions $C_1^{\pm} = 0$ and $C_2^{\pm} = 0$ yield the 'no-flow' solution (9.26).

In the **special case** $f/F = 0$, i.e. for a ship that steadily advances in calm water, equations (9.25) yield

$$\varphi_{\xi\xi} = 0 \ \text{ and } \ \varphi_{\eta\eta} = 0 \ \text{ if } \ \boldsymbol{\xi} \in \Sigma_i^F\ . \tag{9.28a}$$

The potential φ of the 2D flow within the thin layer of water between the surfaces Σ_i^H and Σ_i^F is then given by

$$\varphi = C_0 + C_1\,\xi + C_2\,\eta + C_3\,\xi\,\eta \ \text{ if } \ f/F = 0 \tag{9.28b}$$

where C_0, C_1, C_2 and C_3 are undetermined. The particular solutions $C_n = 0$ with $0 \le n \le 3$ yield the 'no-flow' solution (9.26). The 2D flow velocity defined by (9.28b) at a point $(\xi, \eta) \in \Sigma_i^F$ is given by

$$(\partial_\xi \varphi, \partial_\eta \varphi) = (C_1, C_2) + C_3(\eta, \xi)$$

where (C_1, C_2) evidently is a uniform stream and $C_3(\eta, \xi)$ corresponds to a stagnation flow within the corners defined by the lines $\eta = \pm\xi$.

RW-hw FLOW REPRESENTATION

The waterplane integral ϕ_i^F in the **basic RW flow representation** (9.23) is now considered. The first waterplane-integral expression in (9.23d) yields

$$\phi_i^F \equiv \int_{\Sigma_i^F} d\xi\, d\eta\, (\phi - \varphi)\, G_\zeta = \int_{\Sigma_i^F} d\xi\, d\eta\, (\phi - \varphi) \left[\nabla_{\boldsymbol{\xi}}^2\, G^\zeta - (\partial_\xi^2 + \partial_\eta^2)\, G^\zeta\right]$$

where $^\zeta$ means integration with respect to ζ. The Poisson and Laplace equations in (9.4b-c) yield

$$\phi_i^F = \int_{\Sigma_i^F} d\xi\, d\eta\, (\varphi - \phi)\, (\partial_\xi^2 + \partial_\eta^2)\, G^\zeta = \int_{\Sigma_i^F} d\xi\, d\eta\, (\varphi - \phi)\, \widetilde{\nabla}_{\boldsymbol{\xi}} \cdot \widetilde{\nabla}_{\boldsymbol{\xi}}\, G^\zeta$$

where $\widetilde{\nabla}_{\boldsymbol{\xi}} \equiv (\partial_\xi, \partial_\eta)$. The relation

$$(\varphi - \phi)\, \widetilde{\nabla}_{\boldsymbol{\xi}} \cdot \widetilde{\nabla}_{\boldsymbol{\xi}}\, G^\zeta = \widetilde{\nabla}_{\boldsymbol{\xi}} \cdot \left[(\varphi - \phi)\, \widetilde{\nabla}_{\boldsymbol{\xi}}\, G^\zeta - G^\zeta\, \widetilde{\nabla}_{\boldsymbol{\xi}}\, \varphi\right] + G^\zeta\, \widetilde{\nabla}_{\boldsymbol{\xi}} \cdot \widetilde{\nabla}_{\boldsymbol{\xi}}\, \varphi$$

where one has $\widetilde{\nabla}_{\boldsymbol{\xi}} \cdot \widetilde{\nabla}_{\boldsymbol{\xi}} \varphi = \varphi_{\xi\xi} + \varphi_{\eta\eta} = 0$ in accordance with the Laplace equation (9.25a) associated with a 2D flow in the thin water-layer above the rigid lid Σ_i^H that closes the ship-hull surface Σ_-^H in the rigid-waterplane flow model. The 2D divergence theorem finally yields

$$\phi_i^F = -\int_\Gamma d\ell \left[q^\Gamma \, G^\zeta + (\phi - \varphi^\Gamma) \, \boldsymbol{\nu} \cdot \nabla_{\boldsymbol{\xi}} G^\zeta \right] \text{ where } q^\Gamma \equiv \boldsymbol{\nu} \cdot \nabla_{\boldsymbol{\xi}} \varphi^\Gamma \quad (9.29)$$

and the unit vector $\boldsymbol{\nu} \equiv (\nu^x, \nu^y, 0)$ is normal to the waterline Γ and points into the water, like the unit vector $\mathbf{n}$ normal to the ship-hull surface Σ^H. The notation φ^Γ in expression (9.29) emphasizes the fact that the flow potential φ is evaluated at the ship waterline Γ in this expression. The waterline integral (9.29) is simpler than the waterline integral in the Neumann-Kelvin representation (9.15). In particular, the waterline integral in the Neumann-Kelvin representation (9.15) involves the derivative $\partial_\xi \varphi$ of the flow potential φ whereas the rigid-waterplane flow representation defined by (9.23a-c) and (9.29) only involves φ.

The boundary-integral representation (9.23a-c), (9.29) contains both the integral (9.23b) over the ship-**h**ull surface Σ^H and the integral (9.29) over the ship **w**aterline Γ, and is then identified as the **RW-hw boundary-integral flow representation**.

RW-h FLOW REPRESENTATION

The integrands of the hull-surface and waterline integrals (9.23c) and (9.29) in the RW-hw flow representation are identical except for the fact that the Green function G in the hull-surface integral (9.23c) is replaced by G^ζ in the waterline integral (9.29). The similarity of the integrands of the hull-surface and waterline integrals (9.23b) and (9.29) in the RW-hw flow representation suggest that the waterline integral (9.29) can be combined with the hull-surface integral (9.23b) as is most readily shown for a wall-sided ship-hull surface Σ^H and is now considered.

Expressions (9.23c) and (9.29) yield

$$\phi^H + \phi_i^F = \int_{\Sigma^H} da \, A^H - \int_\Gamma d\ell \, A^\Gamma \text{ where} \quad (9.30a)$$

$$A^H \equiv q^H G + (\phi - \varphi) \, \mathbf{n} \cdot \nabla_{\boldsymbol{\xi}} G \text{ with } q^H \equiv \mathbf{n} \cdot \nabla_{\boldsymbol{\xi}} \varphi \text{ and} \quad (9.30b)$$

$$A^\Gamma \equiv q^\Gamma \, G^\zeta + (\phi - \varphi^\Gamma) \, \boldsymbol{\nu} \cdot \nabla_{\boldsymbol{\xi}} G^\zeta \text{ with } q^\Gamma \equiv \boldsymbol{\nu} \cdot \nabla_{\boldsymbol{\xi}} \varphi^\Gamma \, . \quad (9.30c)$$

The waterline-integral representation of the potential ϕ_i^F in (9.30a) can be

expressed as the hull-surface integral

$$\phi_i^F = -\int_{\Sigma^H} da\; \partial_\zeta \big(E\, A^\Gamma \big) = -\int_{\Sigma^H} da\; \big(E\, A_\zeta^\Gamma + E_\zeta\, A^\Gamma \big) \tag{9.31a}$$

$$\text{where} \quad E \equiv E(\zeta) \equiv e^{-9\,\zeta^2/d_*^2} \tag{9.31b}$$

and d_* is a fraction of the nondimensional draft D/L of the ship. The function $E(\zeta)$ vanishes rapidly as $\zeta \to -\infty$ and one has $E(0) = 1$ and $E_\zeta(0) = 0$. Expressions (9.30a) and (9.31) then yield

$$\phi^H + \phi_i^F = \int_{\Sigma^H} da\; A_\Gamma^H \;\; \text{where} \;\; A_\Gamma^H \equiv A^H - E\, A_\zeta^\Gamma - E_\zeta\, A^\Gamma \tag{9.32}$$

and A^H, A^Γ and E are defined by expressions (9.30b-c) and (9.31b), which show that one has $A_\Gamma^H = 0$ at Γ. Thus, the integrand A_Γ^H of the surface integral (9.32) vanishes at the ship waterline Γ, which implies numerical cancellations between the hull-surface integral (9.23c) and the waterline integral (9.29) or the equivalent waterplane integral (9.23d).

The RW flow representation defined by (9.23a-b) and (9.32) only contains an integral over the ship-hull surface Σ^H, i.e. does not contain a line integral around the ship waterline Γ, although the integrand A_Γ^H in (9.32) involves the flow potential φ^Γ at Γ. The flow representation defined by (9.23a-b) and (9.32) is then identified as the **RW-h flow representation**.

9.6 No-flow at the ship waterplane, and NN flow representation

The **RW flow representation** (9.23) associated with the basic rigid-waterplane (RW) linear flow model allows a flow within the thin sheet of water above the rigid lid Σ_i^H. A flow at the ship waterplane Σ_i^F is also allowed, but presumed 2D, in the **RW-hw flow representation** defined by (9.23a-c) and (9.29) and in the **RW-h flow representation** defined by (9.23a-b) and (9.32) with (9.31b) and (9.30b-c). The special case in which *no flow* is allowed at the ship waterplane Σ_i^F is now considered.

The no-flow assumption in the rigid-waterplane flow model

Thus, the rigid-waterplane (**RW**) linear flow model with the fundamental waterplane restriction

$$\varphi(\boldsymbol{\xi}) = 0 \;\text{ if }\; \boldsymbol{\xi} \in \Sigma_i^F \tag{9.33}$$

in the limit $\delta = 0$ is now considered.

The assumption (9.33) may arguably be justified by the fact that the direction of the unit vector $\mathbf{n}$ normal to the body surface $\Sigma_-^H \cup \Sigma_i^H$ is discontinuous along the waterline Γ, and the flow velocity can therefore be unbounded at Γ; Indeed, an unbounded flow velocity at Γ can arguably be avoided if the 'no-flow' restriction (9.33) is imposed within the thin sheet of water between the rigid lid Σ_i^H and the waterplane Σ_i^F. Moreover, the cancellations between the contributions of the ship-hull surface Σ^H and the waterplane Σ_i^F noted in section 9.5 arguably also suggest that the restriction (9.33) might be a reasonable assumption. Lastly, the assumption that the thin sheet of water above the rigid lid Σ_i^H is a 'dead-water' region can be argued to imply that the flows around the closed body surface $\Sigma_-^H \cup \Sigma_i^H$ and the free-surface piercing ship-hull surface Σ^H are practically identical, as is essentially presumed in the rigid-waterplane linear flow model. **[9,3]**

The restriction $\varphi = 0$ at the interior waterplane Σ_i^F does not necessarily imply that $\varphi = 0$ along the waterline Γ or at the free surface Σ^F outside Γ because the flow potential $\varphi(\xi, \eta, \zeta = 0)$ may be discontinuous across Γ. Such a case can easily be imagined. E.g. if θ denotes the angle between the interior waterplane Σ_i^F and the vector that joins a point $\mathbf{x}^\Gamma \in \Gamma$ to a point $\mathbf{x}$ in the vicinity of $\mathbf{x}^\Gamma$, one has $\theta = 0$ and $\sin(\theta/2) = 0$ if $\mathbf{x} \in \Sigma_i^F$, $\theta = \pi$ and $\sin(\theta/2) = 1$ if $\mathbf{x} \in \Sigma^F$, and $\theta = \pi/2$ and $\sin(\theta/2) = 1/\sqrt{2}$ for a point $\mathbf{x} \in \Sigma^H$ if the hull surface Σ^H is vertical at $\mathbf{x}$. Thus, the value of the function $\sin(\theta/2)$ depends on the direction of approach to the point $\mathbf{x}^\Gamma \in \Gamma$. Such a behavior, or more complicated and stronger singularities of the flow potential φ at the waterline Γ cannot be ruled out as a result of incompatibilities between the hull-surface boundary condition and the linearized free-surface boundary condition. **[9,4]**

Neumann-Noblesse (NN) flow representation

The restriction (9.33) applied in expression (9.23d) yields

$$\phi_i^F = \phi \, C^\Gamma \quad \text{where} \tag{9.34a}$$

$$C^\Gamma = \int_{\Sigma_i^F} d\xi \, d\eta \; G_\zeta = \int_{\Sigma_i^F} d\xi \, d\eta \; (f + \mathrm{i} F \partial_\xi)^2 G \; . \tag{9.34b}$$

Expressions (8.34a) and (8.35) yield the alternative expression

$$C^\Gamma = -\int_\Gamma d\ell \; \boldsymbol{\nu} \cdot \nabla_{\boldsymbol{\xi}} \, G^\zeta \; . \tag{9.34c}$$

Expression (9.34c) and the second expression in (9.34b) are continuous in the entire lower half space $z \leq 0$. However, the first expression in (9.34b) is discontinuous across the waterplane Σ_i^F.

The flow representation (9.23a-c) with expression (9.34a) for the potential ϕ_i^F readily yield

$$\big(1 - C^\Gamma\big)\,\phi = \phi^{\Sigma^F} + \phi^H \tag{9.35a}$$

where the potentials ϕ^{Σ^F} and ϕ^H and the function $C^\Gamma(\mathbf{x})$ are defined by expressions (9.23b-c) and (9.34b-c) as

$$\phi^{\Sigma^F} \equiv \int_{\Sigma^F} d\xi\, d\eta \,\big[\, q^F - F\, p_\xi^F - \mathrm{i}\, f\, p^F \,\big]\, G \;, \tag{9.35b}$$

$$\phi^H \equiv \int_{\Sigma^H} da \,\Big[\, q^H G + (\phi - \varphi)\, \mathbf{n}\cdot\nabla_{\boldsymbol{\xi}}\, G \Big] \;\text{ and} \tag{9.35c}$$

$$C^\Gamma = -\int_\Gamma d\ell\; \boldsymbol{\nu}\cdot\nabla_{\boldsymbol{\xi}}\, G^\zeta = \int_{\Sigma_i^F} d\xi\, d\eta\, (f + \mathrm{i} F\partial_\xi)^2 G \;. \tag{9.35d}$$

The boundary-integral flow representation (9.35) holds in the entire lower half space $z \le 0$. This flow representation only involves the flow potential $\varphi \equiv \varphi(\boldsymbol{\xi})$ at the ship-hull surface Σ^H, and hence provides an integral equation that determines the unknown potential $\phi \equiv \varphi(\mathbf{x})$ at Σ^H for a ship that steadily advances through regular waves or in calm water, as well as for a stationary body in regular waves. Indeed, the flow representation (9.35) is identical to the flow representation (8.36) obtained in chapter 8 for diffraction-radiation of regular waves by an offshore structure. The flow representation (9.35) was obtained, over 40 years ago, in Noblesse (1983) for the particular case of diffraction-radiation of regular water waves by a stationary body and is then identified as the **NN flow representation**.

Flow-field point x outside the ship-hull surface

The NN flow representation (9.35) can be expressed as

$$\phi = \phi^{\Sigma^F} + \int_{\Sigma^H} da \,\Big[\, q^H G - \varphi\; \mathbf{n}\cdot\nabla_{\boldsymbol{\xi}}\, G \Big] + C\,\phi$$
$$\text{where}\;\; C \equiv \int_{\Sigma_i^F} d\xi\, d\eta\; G_\zeta + \int_{\Sigma^H} da\; \mathbf{n}\cdot\nabla_{\boldsymbol{\xi}}\, G$$

is the flux through the closed surface $\Sigma_i^F \cup \Sigma^H$ due to a submerged source, or a flux through the free-surface plane, at the singularity point $\mathbf{x}$ in the Green function G. One has $C = 0$ if $\mathbf{x} \in (\mathcal{D} \cup \Sigma^F)$. Thus, the flow representation (9.35) expresses the flow potential $\phi \equiv \varphi(\mathbf{x})$ at a point $\mathbf{x}$ in the flow region *outside* the ship-hull surface as

$$\phi = \phi^{\Sigma^F} + \int_{\Sigma^H} da \,\Big[\, q^H G - \varphi\; \mathbf{n}\cdot\nabla_{\boldsymbol{\xi}}\, G \Big] \tag{9.36}$$

where the flow potential $\varphi \equiv \varphi(\boldsymbol{\xi})$ at Σ^H is determined by the NN boundary-integral equation (9.35).

9.7 Alternative linear flow models and boundary-integral flow representations

Four alternative linear flow models, and five related alternative boundary-integral flow representations, are considered in sections 9.2-9.6. These linear flow models and flow representations are

(i) the classical NK (Neumann-Kelvin) linear flow model and **NK flow representation** (9.15) considered in sections 9.1-9.3,

(ii) the basic RW (Rigid-Waterplane) flow model and the corresponding **RW flow representation** (9.23) considered in section 9.4,

(iii) the RW flow model with a *2D flow assumption at the ship waterplane* and the two related **RW-hw flow representation** (9.23a-c), (9.29) and **RW-h flow representations** (9.23a-b), (9.32) given in section 9.5,

(iv) and the NN linear flow model and **NN flow representation** (9.35), based on the RW flow model with a *no-flow restriction at the ship waterplane*, analyzed in section 9.6.

The NK flow representation (9.15) contains a line integral around the ship waterline Γ that involves the unknown flow potential φ and its derivative $\partial_\xi \varphi$. Thus, this flow representation determines $\varphi(\mathbf{x})$ at $(\Sigma^H \cup \Gamma)$ via an integro-differential equation, whereas the four flow representations obtained from three variants of the rigid-waterplane flow model do not involve $\partial_\xi \varphi$ and determine $\varphi(\mathbf{x})$ via integral equations.

The RW and RW-hw flow representations involve a surface integral over the ship waterplane Σ_i^F or a line integral around the ship waterline Γ. The RW-h flow representation does not contain a line integral around Γ. However, this flow representation involves the flow potential φ at Γ.

The NN flow representation includes neither a waterline nor a waterplane integral, and does not involve the flow potential φ at Γ. Indeed, C^Γ in (9.35a) is a function of $\mathbf{x}$ that is explicitly defined via the alternative expressions (9.35d). Thus, the NN flow representation (9.35) yields an integral equation that determines φ at the ship-hull surface Σ^H.

Differences between the alternative flow representations considered above are ultimately related to the fact that they stem from different linear flow models. In particular, the ship waterline Γ in the **NK** flow model is the intersection curve of two surfaces: the free surface Σ^F and the mean wetted ship-hull surface Σ^H, where the linear free-surface boundary condition (9.3c) or the hull-surface boundary condition (9.3d) are applied. However, in the **RW-hw**, **RW-h** and **NN** flow models, the waterline Γ separates three surfaces: the free surface Σ^F, the hull surface Σ^H and the ship waterplane Σ_i^F where different boundary conditions hold: the free-surface condition (9.3c), the hull-surface condition (9.3d), and either the 2D flow condition (9.25) or the no-flow condition (9.33). Although the flow potentials φ determined

by the five alternative flow representations defined in sections 9.2-9.6 all satisfy the Laplace equation and identical boundary conditions at the free surface and at the ship-hull surface, differences or incompatibilities between these boundary conditions may result in different local behaviors of the flow potential, and possibly different flow singularities, at Γ. **[9,4]** and **[9,5]**.

As is noted at the end of chapter 8, the classical NK approach and the alternative approach based on the rigid-waterplane flow model correspond to a reversal of the order of the two processes 'apply Green's identity in a flow region' and 'consider the limit $\delta \to 0$' in rigid-waterplane model. Specifically, in the NK linear flow model (called free-waterplane model in chapter 8), Green's identity is applied in the flow region that is defined in the limit $\delta = 0$ of the rigid-waterplane model. However, Green's identity is applied in the flow region defined for $0 < \delta$, and the limit $\delta \to 0$ of the boundary-integral flow representation is considered in the rigid-waterplane model. This linear flow model allows alternative assumptions about the flow in the thin layer of water $-\delta < \zeta \leq 0$ above the rigid lid that closes the ship hull in this flow model.

The NK and NN flow representations

The NK flow representation (9.15) can be expressed as

$$\left(1 - C_*^\Gamma\right) \phi = \phi^{\Sigma^F} + \phi^H + \phi^\Gamma \text{ where} \tag{9.37a}$$

$$\phi^\Gamma \equiv F \int_\Gamma d\eta \, [F(G\,\partial_\xi \varphi - \varphi\,\partial_\xi G) + 2\,\mathrm{i} f\, G\,\varphi\,] \tag{9.37b}$$

and the potentials ϕ^{Σ^F} and ϕ^H are defined by (9.23b-c). Moreover, C_*^Γ in (9.37a) is given by

$$\begin{aligned} C_*^\Gamma &\equiv f^2 \int_{\Sigma_i^F} d\xi\, d\eta\; G + F \int_\Gamma d\eta\, (F\, G_\xi - 2\,\mathrm{i} f\, G) \\ &= \int_{\Sigma_i^F} d\xi\, d\eta\, \left[\, f^2 G - F\,\partial_\xi\, (F\, G_\xi - 2\,\mathrm{i} f\, G)\right] = \int_{\Sigma_i^F} d\xi\, d\eta\; G_\zeta = C^\Gamma \end{aligned}$$

where Stokes' theorem, the free-surface boundary condition in (9.4b), and (9.34b) were used. The potential ϕ^Γ defined by (9.37b) and the waterline integral in (9.8b) are identical. Thus, the NK flow representation (9.15) contains the waterline integral ϕ^Γ, which does not appear in the NN flow representation (9.35). The NK and NN flow representations (9.15) and (9.35) define different flow potentials $\phi \equiv \varphi(\mathbf{x})$ unless the integral (9.37b) around the ship waterline is nil. This waterline integral is nil if $\varphi = 0$ at Γ but may not be nil in general. Thus, the NK and NN flow representations might determine different flow potentials $\phi \equiv \varphi(\mathbf{x})$. **[9,5]**

The NN flow representation (9.35) evidently is considerably simpler than the NK representation (9.15). In particular, the NK flow representations associated with an offshore structure in regular waves or a ship that advances in calm water or through regular waves differ significantly, as is shown in section 9.3, whereas the NN flow representation (9.35) holds for a ship that advances in calm water or through waves, as well as for an offshore structure in waves as is shown in chapter 8. **[9,6]**.

9.8 Neumann-Michell (NM) flow model for a ship that advances in calm water

Four alternative linear flow models—the classical NK model, the basic RW model, and the RW model with '2D-flow' or 'no-flow' assumptions at the ship waterplane—have already been considered **[9,7]**. Other linear flow models can be considered, as is now illustrated for a ship that steadily advances in calm water.

The NK flow model and boundary-integral flow representation

In the special case $f = 0$ now considered, the NK boundary-integral flow representation (9.16) can be expressed as

$$\phi = \int_{\Sigma^F} d\xi\, d\eta \left[q^F - F\, p_\xi^F \right] G + \psi^H + \int_{\Sigma^H} da\, (\phi - \varphi)\, \mathbf{n} \cdot \nabla_{\boldsymbol{\xi}}\, G$$
$$+ F^2 \int_\Gamma d\eta\, (\phi - \varphi)\, G_\xi + \psi^\Gamma \quad \text{where} \tag{9.38a}$$

$$\psi^H \equiv \int_{\Sigma^H} da\, G\, q^H \quad \text{and} \quad \psi^\Gamma \equiv F^2 \int_\Gamma d\eta\, G\, \partial_\xi \varphi \ . \tag{9.38b}$$

The hull-surface flux q^H and the linear free-surface elevation z^F for a ship that advances in calm water are determined by (1.36) and (1.37a) as

$$q^H = F\, n^x \quad \text{and} \quad z^F = F\, \partial_\xi \varphi \ .$$

The potentials ψ^H and ψ^Γ defined by (9.38b) then become

$$\psi^H \equiv F \int_{\Sigma^H} da\ G\, n^x \quad \text{and} \quad \psi^\Gamma \equiv F \int_\Gamma d\eta\ G\, z^F \ . \tag{9.39}$$

The NM flow model and boundary-integral flow representation

In the classical NK linear flow model, Σ^H in (9.39) is the mean wetted ship-hull surface below the undisturbed free-surface plane $\zeta = 0$. However, Σ^H is

taken as the wetted hull surface below the actual free surface $\zeta = z^F$ in the alternative linear flow model—called Neumann-Michell (NM) model—that is now considered. Indeed, the difference between these two wetted hull surfaces yields a *linear* contribution to the hull-surface potential ψ^H that arguably should not be ignored in a consistent linear flow model. Thus, the hull-surface potential ψ^H defined by (9.39) is now expressed as

$$\psi^H = \psi_0^H + \psi_*^H \quad \text{where} \quad \psi_0^H \equiv F \int_{\Sigma_0^H} da\, G\, n^x$$

represents the contribution of the mean wetted ship-hull surface, denoted as Σ_0^H for clarity, and ψ_*^H accounts for the contribution of the narrow band of water between the undisturbed free-surface plane $\zeta = 0$ and the linear approximation to the actual free surface $\zeta = z^F \approx F\, \partial_\xi \varphi$. The relation

$$n^x\, da = -\, t^y\, d\ell\, d\zeta\,,$$

where the unit vector $\mathbf{t} \equiv (t^x, t^y, 0)$ is tangent to the waterline Γ and oriented like Γ, yields

$$\psi_*^H \approx -F \int_\Gamma d\ell\; t^y\, G \int_0^{z^F} d\zeta = -F \int_\Gamma d\ell\; t^y\, G\, z^F\,.$$

This expression and expression (9.39) for ψ^Γ show that one has $\psi_*^H = -\psi^\Gamma$.

Thus, the waterline integral ψ^Γ in the NK flow representation (9.38a) and the contribution ψ_*^H of the narrow band of water between the undisturbed free-surface plane $\zeta = 0$ and the free surface $\zeta = z^F$ in the hull-surface potential ψ^H cancel out, and the NK boundary-integral flow representation (9.16) then becomes

$$\begin{aligned}\phi = &\int_{\Sigma^F} d\xi\, d\eta \left[\, q^F - F\, p_\xi^F \,\right] G + \int_{\Sigma^H} da \left[\, q^H\, G + (\phi - \varphi)\, \mathbf{n} \cdot \nabla_{\boldsymbol{\xi}}\, G \right] \\ &+ F^2 \int_\Gamma d\eta\, (\phi - \varphi)\, G_\xi \end{aligned} \tag{9.40}$$

where Σ^H is the mean wetted ship-hull surface. The boundary-integral flow representation (9.40) associated with the Neumann-Michell (NM) linear flow model is called **NM flow representation**. **[9,8]**

Hogner's explicit approximation

An important approximation to the flow created by a common displacement ship, for which one has $\phi^{\Sigma^F} = 0$, that steadily advances in calm water is

$$\phi \approx F \int_{\Sigma^H} da\; n^x\, G\,. \tag{9.41}$$

This approximation, proposed by Hogner in 1932 as a composite of Michell's famous 'thin-ship approximation' and the similar 'flat-ship approximation' proposed by Havelock, is also closely related to the NN flow representation (9.36). Specifically, Hogner's approximation (9.41) follows from (9.36) and the ship-hull surface boundary condition $q^H = Fn^x$ if the approximation $\varphi \approx 0$ is invoked. This approximation is reasonable for common displacement ships, which are streamlined slender bodies that create relatively small flow disturbances and for which one has $n^x = O(B/L_s)$ and $\varphi = O(BD/L_s^2)$ where L_s is the length and B and D are the beam or the draft of the ship.

Hogner's approximation (9.41) *explicitly* determines the flow created by a ship in terms of the Froude number F and n^x, i.e. the speed and the length of the ship, and the shape of the ship hull. Indeed, Hogner's approximation is among the most remarkable and beautiful results in ship hydrodynamics. In spite of its great simplicity, Hogner's explicit approximation (9.41) is realistic and useful for several notable practical applications. [**9,9**]

Other flow models and theories

As is noted in section 1.2, the analysis expounded in the book is associated with the Kelvin-Michell linear free-surface boundary condition, which is based on the simplest, and arguably the most realistic, assumption that the velocity $\nabla\Phi$ of the flow created by a ship is significantly smaller than the ship speed V_s. However, the nonlinear kinematic and dynamic free-surface boundary conditions given in section 1.2 can also be linearized based on alternative linearization assumptions. In particular, the velocity $\nabla\Phi$ of the flow created by a ship can be assumed to be a small perturbation of the flow around the ship in the infinite or zero-gravity limits. Alternative theories of flows around ships, notably approximate theories that do not involve the formulation of a boundary-integral flow representation, have also been considered in a broad literature. [**9,10**] and [**9,11**]

Although nonlinear effects are ignored in the linear analysis considered in the book, nonlinearities have important local effects. In particular, the bow wave of a ship that steadily advances in calm water is greatly influenced by nonlinearities [**9,12**]. Moreover, the linear theory of potential flow around a ship that advances in calm water predicts short waves that in reality are too steep to exist due to nonlinearities [**9,13**]. Despite these limitations, linear potential flow theory is mostly realistic and widely useful, and can also be corrected to account for nonlinearities [**9,14**].

9.9 Conclusion

In summary, four alternative linear models of potential flow around a ship that steadily advances through regular waves, and five related boundary-integral flow representations, are considered in this chapter. These alternative flow models are the classical Neumann-Kelvin (NK) model, the basic rigid-waterplane (RW) flow model and two related flow models, which either allow a 2D flow or disallow any flow at the ship waterplane. In the special case of a ship that advances in calm water, a fifth linear flow model called Neumann-Michell (NM) model has also been considered. A notable common feature of all the alternative boundary-integral flow representations given in this chapter is that they only involve weakly singular dipoles $(\varphi - \phi)\, \nabla_{\boldsymbol{\xi}}\, G$ and consequently define flow potentials that are continuous at the ship-hull surface Σ^H. **[8,2]**

The NN flow representation (9.35) associated with the rigid-waterplane model and the additional 'no-flow restriction' (9.33) at the waterplane Σ_i^F stands out due to its remarkable simplicity. Specifically, the function $C^\Gamma(\mathbf{x})$ in (9.35a) is explicitly defined as an integral over the ship's waterline Γ or waterplane Σ_i^F by the alternative expressions (9.35d), and the flow representation (9.35) only involves the unknown flow potential φ at the ship-hull surface Σ^H. Thus, the flow representation (9.35) yields an integral equation that determines the unknown flow potential at the hull surface Σ^H. This flow representation holds for the general case $Ff \neq 0$ as well as the particular case $F = 0$ considered in chapter 8 and the particular case $f = 0$ considered in section 9.8. The waterline integral that defines $C^\Gamma(\mathbf{x})$ in (9.35d) can be decomposed into Rankine and Fourier components, which can be evaluated via the relations (7.56) and the Fourier-Kochin method expounded in chapters 10–12.

The flow representation (9.35) relies on the restriction (9.33), which imposes that the thin sheet of water above the rigid lid that closes a free-surface piercing hull in the rigid-waterplane flow model is a 'dead-water' region. This 'no-flow' constraint arguably precludes flow singularities along the waterline, and intuitively ensures that the flows around a free-surface piercing ship-hull surface Σ^H and the corresponding submerged body surface $\Sigma_-^H \cup \Sigma_i^H$ defined in the rigid-waterplane flow model are practically equivalent. Moreover, the waterplane condition (9.33) is consistent with the fact that the flow around Σ^H does not determine a flow inside Σ^H (outside the flow region), which can then be freely specified and in particular can be chosen nil.

The occurrence of irregular frequencies can be avoided in the manner explained in section 8.6 for the NN flow representation, which can also be readily applied to the alternative boundary-integral flow representations considered in chapter 9.

Chapter 10

Basic Rankine-Fourier decomposition and Fourier-Kochin method

The boundary-integral flow representations given in the previous chapter express the flow potential ϕ via distributions of the Green function G and its gradient $\nabla_{\boldsymbol{\xi}} G$ over the free surface Σ^F, the hull surface Σ^H, and the waterplane Σ_i^F and/or the waterline Γ of the ship. The Green function G is defined in chapter 7 in terms of Rankine singularities and a Fourier superposition of elementary wave functions. This fundamental Rankine-Fourier decomposition of G and $\nabla_{\boldsymbol{\xi}} G$ is now applied to similarly decompose the flow potential ϕ determined by the boundary-integral flow representation (9.35) in terms of Rankine and Fourier components. The flow representation (9.35) is considered for a ship that steadily advances through regular waves in deep water and for diffraction-radiation of regular waves by an offshore structure in water of uniform finite depth. The two special cases of a ship that steadily advances in calm water and wave diffraction-radiation of regular waves by an offshore structure in deep water only involve simple modifications of the two more general cases considered in this chapter, and accordingly are not explicitly considered.

10.1 Rankine-Fourier decomposition of flow around a ship advancing through waves

Green functions G associated with potential flows around an offshore structure in regular waves or a ship that advances through waves or in calm water can be expressed as

$$4\pi G = -1/r + H^R + G^F = G^R + G^F \text{ where} \tag{10.1a}$$

$$r \equiv \sqrt{h^2 + (\zeta - z)^2} \text{ with } h \equiv \sqrt{(\xi - x)^2 + (\eta - y)^2} \tag{10.1b}$$

and the Rankine and Fourier components H^R and G^F denote harmonic functions that are defined in terms of elementary (free-space) Rankine sources or a Fourier superposition of elementary plane waves.

For a ship that steadily advances through regular waves, now considered, the Rankine and Fourier components G^R and G^F are defined by (7.6) as

$$G^R = -1/r + 1/r' \text{ where } r' \equiv \sqrt{h^2 + (\zeta + z)^2} \text{ and} \tag{10.1c}$$

$$G^F = \frac{1}{\pi} \int_{-\pi}^{\pi} d\gamma \int_0^{\infty} dk \; \frac{e^{k\,(z+\zeta) \,+\, \mathrm{i}\,[\,\alpha\,(x-\xi) + \beta\,(y-\eta)\,]}}{(f + F\alpha)^2/k - 1 + \mathrm{i}\,\epsilon\,\mathrm{sign}(f + F\alpha)} \tag{10.1d}$$

$$\text{with } (\alpha, \beta) = k\,(\cos\gamma, \sin\gamma) \text{ and } \epsilon = +0 \; . \tag{10.1e}$$

Expressions (10.1b-c) show that one has

$$G^R = 0 \text{ at } \Sigma^F \, . \tag{10.2}$$

As is explained in Chapter 7, expressions (10.1c) and (10.1d) correspond to a Rankine-Fourier decomposition that is optimal for a ship that advances in regular waves. However, the Rankine-Fourier decomposition (10.1c-d) is not optimal in the special cases $F = 0$ or $f = 0$, as is also explained in chapter 7. The Rankine-Fourier decomposition (10.1c-d) is used in the present chapter. The modified optimal Rankine-Fourier decomposition that is also optimal in the limits $F \to 0$ or $f \to 0$ is considered in chapter 12.

The Rankine-Fourier decomposition (10.1) of the Green function is now applied to the flow representation (9.35). Thus, the flow representation

$$\left[\, 1 - C^{\Gamma} \,\right] \phi = \phi^H + \phi^{\Sigma^F} \text{ where} \tag{10.3a}$$

$$C^{\Gamma} \equiv -\int_{\Gamma} d\ell \; \boldsymbol{\nu} \cdot \nabla_{\boldsymbol{\xi}} \, G^{\zeta} \; , \tag{10.3b}$$

$$\phi^H \equiv \int_{\Sigma^H} da \left[\, q^H G + (\phi - \varphi)\, \mathbf{n} \cdot \nabla_{\boldsymbol{\xi}} \, G \,\right] \text{ and} \tag{10.3c}$$

$$\phi^{\Sigma^F} \equiv \int_{\Sigma^F} d\xi \, d\eta \, \left[\, q^F - F p_{\xi}^F - \mathrm{i} f p^F \,\right] G \tag{10.3d}$$

is considered. The unit vectors $\mathbf{n} \equiv (n^x, n^y, n^z)$ and $\boldsymbol{\nu} \equiv (\nu^x, \nu^y, 0)$ normal to the hull surface Σ^H or the waterline Γ point outside the ship.

The free-surface potential ϕ^{Σ^F}, the hull-surface potential ϕ^H and the function C^Γ in the flow representation (10.3) are expressed as

$$\phi_F^R + \phi_F^F \equiv \int_{\Sigma^F} d\xi\, d\eta \left[\, q^F - F p_\xi^F - \mathrm{i} f p^F \,\right] (G^R + G^F) \;, \tag{10.4a}$$

$$\phi_H^R + \phi_H^F \equiv \int_{\Sigma^H} da \left[q^H (G^R + G^F) + (\phi - \varphi)\, \mathbf{n} \cdot \nabla_{\boldsymbol{\xi}} (G^R + G^F) \right] \;, \tag{10.4b}$$

$$C_\Gamma^R + C_\Gamma^F \equiv -\int_\Gamma d\ell\; \boldsymbol{\nu} \cdot \nabla_{\boldsymbol{\xi}} (G^{R\zeta} + G^{F\zeta}) \;. \tag{10.4c}$$

The Rankine components ϕ_F^R, ϕ_H^R, C_Γ^R and the Fourier components ϕ_F^F, ϕ_H^F, C_Γ^F defined by (10.4) and (10.1) are successively considered below.

Rankine components

Expressions (10.4), (10.1b-c), (10.2) and (7.56) yield

$$\phi_F^R = 0 \;, \tag{10.5a}$$

$$4\pi \phi_H^R = \int_{\Sigma^H} da \left[q^H \left(\frac{-1}{r} + \frac{1}{r'} \right) + (\phi - \varphi) \left(\frac{\mathbf{n} \cdot \mathbf{r}}{r^3} - \frac{\mathbf{n} \cdot \mathbf{r}'}{(r')^3} \right) \right] \quad \text{where}$$

$$\mathbf{r} \equiv (\xi - x, \eta - y, \zeta - z) \;\text{ and }\; \mathbf{r}' \equiv (\xi - x, \eta - y, \zeta + z) \;, \tag{10.5b}$$

$$C_\Gamma^R(\mathbf{x}) = \frac{1}{2\pi} \int_\Gamma d\ell\; \frac{\nu^x(\xi - x) + \nu^y(\eta - y)}{(\sqrt{h^2 + z^2} - z)\sqrt{h^2 + z^2}} \;. \tag{10.5c}$$

Fourier components

The Fourier components ϕ_F^F, ϕ_H^F, C_Γ^F defined by (10.4) and (10.1d-e) are defined via distributions of the Fourier component G^F in (10.1a) and its gradient $\nabla_{\boldsymbol{\xi}} G^F$. Specifically, expressions (10.4) yield

$$\phi_F^F \equiv \int_{\Sigma^F} d\xi\, d\eta \left[\, q^F - F p_\xi^F - \mathrm{i} f p^F \,\right] G^F \;, \tag{10.6a}$$

$$\phi_H^F \equiv \int_{\Sigma^H} da \left[q^H G^F + (\phi - \varphi)\, \mathbf{n} \cdot \nabla_{\boldsymbol{\xi}} G^F \right] \tag{10.6b}$$

$$\text{and}\;\; C_\Gamma^F \equiv -\int_\Gamma d\ell\; \boldsymbol{\nu} \cdot \nabla_{\boldsymbol{\xi}} G^{F\zeta} \tag{10.6c}$$

where G^F, $\nabla_{\boldsymbol{\xi}} G^F$ and $G^{F\zeta}$ are given by

$$\left\{ \begin{array}{c} G^F \\ G^F_\xi \\ G^F_\eta \\ G^F_\zeta \\ G^{F\zeta} \end{array} \right\} = \frac{1}{\pi} \int_{-\pi}^{\pi} d\gamma \int_0^\infty dk \left\{ \begin{array}{c} 1 \\ -\mathrm{i}\,\alpha \\ -\mathrm{i}\,\beta \\ k \\ 1/k \end{array} \right\} \frac{e^{\,k\,(z+\zeta)\,+\,\mathrm{i}\,[\,\alpha\,(x-\xi)\,+\,\beta\,(y-\eta)\,]}}{(f+F\alpha)^2/k - 1 + \mathrm{i}\,\epsilon\,\mathrm{sign}(f+F\alpha)} \tag{10.7}$$

in accordance with (10.1d).

10.2 The usual Green-function method

The usual Green-function method involves two main steps. The first step consists in a 'Fourier integration' to evaluate the Fourier components $G^F(\boldsymbol{\xi}, \mathbf{x})$ and $\nabla_{\boldsymbol{\xi}} G^F(\boldsymbol{\xi}, \mathbf{x})$ defined by the singular double Fourier integrals (10.7). The subsequent second step is a 'space integration' to integrate G^F and $\nabla_{\boldsymbol{\xi}} G^F$ over the free surface Σ^F, the hull surface Σ^H, and the waterline Γ in accordance with expressions (10.6).

The first 'Fourier-integration' step is now considered. In the simplest case of diffraction-radiation of regular waves by an offshore structure in deep water, one has $F = 0$ and the functions G^F and $\nabla_{\boldsymbol{\xi}} G^F$ are functions of the two nondimensional variables

$$z^\omega \equiv f^2(z+\zeta) \;\text{ and }\; h^\omega \equiv f^2 h \;\text{ where }\; h \equiv \sqrt{(x-\xi)^2 + (y-\eta)^2}\ .$$

The functions G^F and $\nabla_{\boldsymbol{\xi}} G^F$ associated with wave diffraction-radiation by an offshore structure in water of uniform depth D are functions of the three nondimensional variables z^ω, h^ω and $d^\omega \equiv f^2 d \equiv \omega^2 D/g$. For a ship that steadily advances in calm water, one has $f = 0$ and the functions G^F and $\nabla_{\boldsymbol{\xi}} G^F$ are functions of the three nondimensional coordinates

$$x^V \equiv (x-\xi)/F^2\ ,\ \ y^V \equiv (y-\eta)/F^2 \;\text{ and }\; z^V \equiv (z+\zeta)/F^2\ .$$

The functions G^F and $\nabla_{\boldsymbol{\xi}} G^F$ associated with a ship that advances through regular waves are functions of $\tau \equiv Ff = V_s\,\omega/g$ and the three coordinates $x-\xi, y-\eta, z+\zeta$ made nondimensional with respect to the lengths g/ω^2, V_s^2/g or V_s/ω in accordance with (1.33).

These Green functions, defined by the singular double Fourier integrals (10.7) as was already noted, have been widely studied, especially for the simplest cases $F = 0$ and $f = 0$ in deep water. In particular, alternative Fourier integral representations, near-field and far-field series expansions,

one-dimensional Taylor series and even global analytical approximations have been given for the functions G^F and $\nabla_{\boldsymbol{\xi}} G^F$ associated with the simplest cases $F = 0$ or $f = 0$. Numerical methods, notably methods based on analytical series expansions or polynomial approximations in complementary contiguous regions and methods based on table interpolation associated with coordinate and function transformations, for evaluating G^F and $\nabla_{\boldsymbol{\xi}} G^F$ have also been developed. These various analytical studies and numerical methods are reported in a huge literature [**10,1**].

The second 'space-integration' step in the usual Green function method consists in integrating the Fourier components G^F and $\nabla_{\boldsymbol{\xi}} G^F$ of the Green function G and its gradient $\nabla_{\boldsymbol{\xi}} G$ over the panels (flat or curved triangles or quadrilaterals) and segments that approximate the ship-hull surface Σ^H and its waterline Γ in common numerical implementations based on a panel method. If a distribution of pressure and/or flux is applied at the free surface Σ^F in the vicinity of Γ, G^F and $\nabla_{\boldsymbol{\xi}} G^F$ must also be integrated over free-surface panels. Accurate numerical integration of G^F and $\nabla_{\boldsymbol{\xi}} G^F$ requires particular attention because G^F and $\nabla_{\boldsymbol{\xi}} G^F$ involve complicated singularities at the origin $\xi - x = 0$, $\eta - y = 0$, $\zeta + z = 0$.

The usual Green-function method is not considered in this book because both the 'Fourier-integration' step and the 'space-integration' step involve considerable complexities, especially for the general case $Ff \neq 0$ and in finite water-depth. Moreover, this classical approach requires complicated analysis for every particular class of flows and hence lacks generality.

An inherently more general and simpler alternative, called Fourier-Kochin (FK) method, to the usual Green-function method is considered. The order in which the 'Fourier-integration' and the 'space-integration' steps are performed in the usual Green-function method is reversed in the FK method. A main recommendation of the FK method is that it is readily applicable to a general dispersion function associated with plane waves for a wide class of dispersive media, as is shown in the next chapter.

10.3 Fourier-Kochin representation of Fourier components

Expressions (10.7) for G^F and $\nabla_{\boldsymbol{\xi}} G^F$ can readily be used to express the Fourier components ϕ_F^F, ϕ_H^F and C_Γ^F defined by (10.6) as

$$\begin{Bmatrix} \phi_F^F \\ \phi_H^F \\ C_\Gamma^F \end{Bmatrix} = \frac{1}{\pi} \int_{-\pi}^{\pi} d\gamma \int_0^\infty dk \begin{Bmatrix} A_F \\ A_H \\ A_\Gamma \end{Bmatrix} \frac{e^{\,k\,z\,+\,\mathrm{i}\,(\alpha\,x\,+\,\beta\,y)}}{(f+F\alpha)^2/k - 1 + \mathrm{i}\,\epsilon\,\mathrm{sign}(f+F\alpha)} \tag{10.8}$$

where A_F, A_H and A_Γ are defined as

$$A_F \equiv \int_{\Sigma^F} d\xi\, d\eta \left[\, q^F - F\, p^F_\xi - \mathrm{i}\, f\, p^F \,\right] \mathcal{E}\ , \tag{10.9a}$$

$$A_H \equiv \int_{\Sigma^H} da \left[\, q^H + \left\{ k\, n^z - \mathrm{i}\,(\alpha\, n^x + \beta\, n^y) \right\} (\phi - \varphi) \right] e^{\,k\,\zeta}\, \mathcal{E}\ , \tag{10.9b}$$

$$A_\Gamma \equiv \mathrm{i} \int_\Gamma d\ell\ \frac{\alpha\, \nu^x + \beta\, \nu^y}{k}\ \mathcal{E} \tag{10.9c}$$

$$\text{with}\ \ \mathcal{E} \equiv e^{\,-\mathrm{i}\,(\alpha\,\xi + \beta\,\eta)}\ \ \text{and}\ \ k \equiv \sqrt{\alpha^2 + \beta^2}\ . \tag{10.9d}$$

Expressions (10.8) and (10.9) for the Fourier components ϕ^F_F, ϕ^F_H and C^F_Γ are called Fourier-Kochin representation hereafter. The amplitude functions A_F, A_H and A_Γ in the Fourier-Kochin representation are called Kochin functions or amplitude functions. These Kochin functions are functions of the Fourier variables α and β and are denoted as $A(\alpha, \beta)$ hereafter.

10.4 Fourier-Kochin representation for diffraction-radiation of regular waves in water of uniform finite depth

The Fourier-Kochin (FK) representation (10.8)-(10.9) given in the previous section for a ship that steadily advances through regular waves in deep water is now considered for diffraction and radiation of regular waves by a stationary body in water of uniform finite depth. The optimal Rankine-Fourier decomposition (7.33) of the Green function for offshore structures in finite water-depth is defined by (7.33) as

$$G^F = \frac{1}{\pi} \int_{-\pi}^{\pi} d\gamma \int_0^\infty dk\ \frac{A^\zeta\, A^z\, e^{\,\mathrm{i}\,[\alpha\,(x-\xi) + \beta\,(y-\eta)]}}{1 - (k/f^2)\tanh(k\,d) + 2\,\mathrm{i}\,\epsilon/f} \quad \text{where} \tag{10.10a}$$

$$A^\zeta \equiv 2\cosh[k\,(\zeta + d)]\,/\,e^{\,k\,d}\ \ \text{and} \tag{10.10b}$$

$$A^z \equiv \left[1 + \frac{k}{f^2}\right] \frac{\cosh[k\,(z+d)]}{2\cosh(k\,d)} + \left[\frac{1}{2} - e^{\,-k/f^2}\right] \left[1 - \frac{k}{f^2}\tanh(k\,d)\right] e^{\,k\,z}\ . \tag{10.10c}$$

Expression (10.10a) readily yields

$$\begin{Bmatrix} G^F \\ G^F_\xi \\ G^F_\eta \\ G^F_\zeta \end{Bmatrix} = \frac{1}{\pi} \int_{-\pi}^{\pi} d\gamma \int_0^\infty dk \begin{Bmatrix} 1 \\ -\mathrm{i}\,\alpha \\ -\mathrm{i}\,\beta \\ k\tanh[k(\zeta + d)] \end{Bmatrix} \frac{A^\zeta\, A^z\, e^{\,\mathrm{i}\,[\alpha\,(x-\xi) + \beta\,(y-\eta)]}}{1 - (k/f^2)\tanh(k\,d) + \mathrm{i}\,\epsilon} \tag{10.11}$$

where the inconsequential positive term $2/f$ in $2\,\mathrm{i}\,\epsilon/f$ is omitted.

Expressions (10.6) and (10.11) show that the Fourier-Kochin representation (10.8)-(10.9) associated with a ship that steadily advances through waves is modified as

$$\begin{Bmatrix} \phi_F^F \\ \phi_H^F \\ C_\Gamma^F \end{Bmatrix} = \frac{1}{\pi}\int_{-\pi}^{\pi} d\gamma \int_0^\infty dk\, \frac{\cosh(k\,d)}{e^{\,k\,d}/2} \begin{Bmatrix} A_F \\ A_H \\ A_\Gamma \end{Bmatrix} \frac{A^z\, e^{\,\mathrm{i}\,(\alpha\,x+\beta\,y)}}{1-(k/f^2)\tanh(k\,d)+\mathrm{i}\,\epsilon} \tag{10.12}$$

where the Kochin functions A_F, A_H and A_Γ are defined as

$$A_F \equiv \int_{\Sigma^F} d\xi\, d\eta\, \big[\, q^F - F\, p_\xi^F - \mathrm{i}\, f\, p^F \,\big]\, \mathcal{E}\ , \tag{10.13a}$$

$$A_H \equiv \int_{\Sigma^H} da\, \big[\, q^H + \{T k\, n^z - \mathrm{i}\,(\alpha\, n^x + \beta\, n^y)\}\,(\phi-\varphi)\big]\, \frac{\cosh[k\,(\zeta+d)]}{\cosh(k\,d)}\, \mathcal{E}\ , \tag{10.13b}$$

$$A_\Gamma \equiv \mathrm{i}\,\tanh(k\,d) \int_\Gamma d\ell\, \frac{\alpha\,\nu^x + \beta\,\nu^y}{k}\, \mathcal{E} \tag{10.13c}$$

$$\text{with}\ \ \mathcal{E} \equiv e^{\,-\,\mathrm{i}\,(\alpha\,\xi+\beta\,\eta)}\ \ ,\ \ T \equiv \tanh[k(\zeta+d)]\ \ ,\ \ k \equiv \sqrt{\alpha^2+\beta^2}\ . \tag{10.13d}$$

10.5 The Fourier-Kochin method

The three Kochin functions defined by (10.9) in deep water or (10.13) in finite water-depth are determined via a space integration of the elementary wave functions

$$\mathcal{E} \equiv e^{\,-\,\mathrm{i}\,(\alpha\,\xi+\beta\,\eta)}\ \ ,\ \ e^{\,k\,\zeta}\,\mathcal{E}\ \ \text{or}\ \ \cosh[k\,(\zeta+d)]\,\mathcal{E} \tag{10.14}$$

over the free surface Σ^F and the ship-hull surface Σ^H and waterline Γ. This space (surface and line) integration of smooth ordinary functions evidently is incomparably simpler than the space integration of the Green function G^F and its gradient $\nabla_{\boldsymbol{\xi}}\, G^F$, which contain intricate singularities, that is required in the usual Green function method. The Kochin functions defined by (10.9) or (10.13) do not involve the wave frequency f or the Froude number F, which only appear in the Fourier integrals (10.8) or (10.12). Thus, the Fourier-Kochin (FK) method avoids the daunting analytical and numerical complexities associated with the evaluation and subsequent space integration of G^F and $\nabla_{\boldsymbol{\xi}}\, G^F$. However, these compelling advantages of the FK method require the evaluation of the double Fourier integrals (10.8) or (10.12) for amplitude functions that correspond to general distributions of singularities, rather than for a point source in the usual Green-function method.

Thus, the 'space-integration' required to determine the Kochin function is a trivial task in the Fourier-Kochin method, but the 'Fourier-integration' involves the evaluation of the singular double Fourier integrals (10.8) or (10.12) for a *general* Kochin function associated with a general distribution of the elementary wave functions (10.14). Specifically, the fundamental task in the Fourier-Kochin method consists in evaluating the Fourier integral

$$\phi^F(\mathbf{x}) = \frac{1}{\pi}\int_{-\pi}^{\pi} d\gamma \int_0^{\infty} dk\, \frac{\mathcal{A}(\alpha,\beta;z)\, e^{\,\mathrm{i}\,(\alpha\, x + \beta\, y)}}{\Delta(\alpha,\beta) + \mathrm{i}\,\epsilon\,\Delta_1(\alpha,\beta)} \quad \text{where } \epsilon = +0\ , \tag{10.15}$$

$\mathcal{A}(\alpha,\beta;z)$ denotes a general amplitude (or Kochin) function, and

$$\Delta(\alpha,\beta) \equiv (f + F\alpha)^2/k - 1 \ \text{ and } \ \Delta_1(\alpha,\beta) \equiv \text{sign}(f + F\alpha) \tag{10.16a}$$

$$\text{or} \quad \Delta(\alpha,\beta) \equiv 1 - (k/f^2)\tanh(k\,d) \ \text{ and } \ \Delta_1(\alpha,\beta) \equiv 1 \tag{10.16b}$$

are the dispersion functions associated with a ship that advances through regular waves in deep water or diffraction-radiation of regular waves by an offshore structure **[10,2]**.

The Fourier-Kochin representations given in this chapter for a ship that steadily advances through regular waves in deep water and for diffraction-radiation of regular waves by an offshore structure in finite water-depth can readily be formulated for various similar problems—notably for a ship that steadily advances in calm water and wave diffraction-radiation by an offshore structure in deep water—involving diffraction-radiation of plane dispersive waves. Accordingly, the Fourier integral (10.15) is considered in the next chapter for *general* dispersion functions $\Delta(\alpha,\beta)$ and $\Delta_1(\alpha,\beta)$, rather than the specific dispersion functions (10.16), and a *general* amplitude function $\mathcal{A}(\alpha,\beta;z)$. An analytical representation of the singular double Fourier integral (10.15) that provides an *exact* decomposition of ϕ^F into waves and a non-oscillatory local disturbance is given in chapter 11.

Chapter 11

Waves and local-effects decomposition in a general dispersive medium

As is explained in the previous chapter, the basic core issue of the Fourier-Kochin method consists in evaluating the singular double Fourier integrals

$$\phi^F(\mathbf{x}) = \frac{1}{\pi}\int_{-\pi}^{\pi} d\gamma \int_0^{\infty} dk\, \frac{\mathcal{A}(\alpha,\beta;z)\, e^{\,\mathrm{i}\,(\alpha\, x\,+\,\beta\, y)}}{\Delta\,(\alpha,\beta) + \mathrm{i}\,\epsilon\Delta_1(\alpha,\beta)} \quad \text{or} \tag{11.1a}$$

$$\phi^F(\mathbf{x}) = \frac{1}{\pi}\int_{-\infty}^{\infty} d\beta \int_{-\infty}^{\infty} d\alpha\, \frac{\mathcal{A}(\alpha,\beta;z)\, e^{\,\mathrm{i}\,(\alpha\, x\,+\,\beta\, y)}}{\Delta\,(\alpha,\beta) + \mathrm{i}\,\epsilon\,\Delta_1(\alpha,\beta)} \quad \text{where } \epsilon = +0\,. \tag{11.1b}$$

The double Fourier integrals (11.1) are considered in this chapter for general functions Δ and Δ_1 and a general (although preferably not *rapidly* oscillatory) amplitude function $\mathcal{A}$.

The functions Δ and Δ_1 in (11.1) correspond to dispersion functions associated with dispersive waves that propagate in a plane, like the waves created by ships or offshore structures of primary interest in this book. Other examples of waves that propagate in a plane are the waves created by an airplane landing over a very large floating elastic offshore structure, and the waves created by a truck or a submarine traveling over or below an ice sheet. Indeed, offshore structures in regular waves, ships advancing in calm water or through regular waves, and bodies moving over or below an elastic structure create disturbances (flow, deflection) that can be expressed in terms of Fourier representations of the form (11.1), and these disturbances consist of both waves and non-oscillatory local disturbances. Thus, the singular double Fourier integrals (11.1) are an essential element of

the mathematical and numerical analysis of forcing effects in a wide range of dispersive media [**11,1**]. The amplitude function $\mathcal{A}$ in the Fourier integrals (11.1) is associated with a *general forcing*.

Direct numerical evaluation of the singular double Fourier integrals (11.1) for $\epsilon = +0$ is difficult and impractical. Direct numerical evaluation of (11.1) for $0 < \epsilon \ll 1$ is feasible, but impractical. Indeed, a practical and accurate method for evaluating the singular double Fourier integrals (11.1) requires an analytical approach, as is considered in this chapter [**11,2**].

The Fourier integral (11.1b) is now considered and is expressed as

$$\phi^F(\mathbf{x}) = \frac{1}{\pi}\int_{-\infty}^{\infty} d\beta\, e^{\,\mathrm{i}\,\beta\, y}\, I^F(\beta, x) \;\text{ where} \tag{11.2a}$$

$$I^F(\beta, x) \equiv \int_{-\infty}^{\infty} d\alpha\, \frac{\mathcal{A}(\alpha,\beta)\, e^{\,\mathrm{i}\,\alpha\, x}}{\Delta(\alpha,\beta) + \mathrm{i}\,\epsilon\,\Delta_1(\alpha,\beta)} \;. \tag{11.2b}$$

The singular Fourier integral (11.2b) is analyzed for $\epsilon = +0$, a general amplitude function $\mathcal{A}$ and general real functions Δ and Δ_1. These two functions are dispersion functions in the book, although the analysis expounded in the next section is general.

11.1 A basic singular Fourier integral

The Fourier variable β in expression (11.2b) is inconsequential and the basic singular Fourier integral

$$I^F(x) \equiv \int_{-\infty}^{\infty} d\alpha\, \frac{\mathcal{A}(\alpha)\, e^{\,\mathrm{i}\,\alpha\, x}}{\Delta(\alpha) + \mathrm{i}\,\epsilon\,\Delta_1(\alpha)} \;\text{ with }\; \epsilon = +0 \tag{11.3}$$

is then analyzed in this section [**11,3**]. As was already noted, $\Delta(\alpha)$ and $\Delta_1(\alpha)$ are general real functions, and the amplitude function $\mathcal{A}(\alpha)$ likewise is general (but does not oscillate very fast). In the limit $\epsilon = +0$ considered in (11.3), the integrand of the integral I^F is singular at the roots of the function $\Delta(\alpha)$. These roots are denoted as $\alpha = \alpha_*$ hereafter.

The limit $\epsilon = +0$

The limit $\epsilon = +0$ of the integral (11.3) is first considered. One has

$$\frac{1}{\Delta + \mathrm{i}\,\epsilon\,\Delta_1} = \frac{1}{\Delta} - \frac{\mathrm{i}\,\epsilon\,\Delta_1/\Delta}{\Delta + \mathrm{i}\,\epsilon\,\Delta_1} = \frac{1}{\Delta} - \frac{\mathrm{i}\,\epsilon\,\Delta_1}{\Delta^2 + \epsilon^2\Delta_1^2} - \frac{\epsilon^2\Delta_1^2/\Delta}{\Delta^2 + \epsilon^2\Delta_1^2} \;. \tag{11.4}$$

If $\Delta \neq 0$, the last two terms on the right side of expression (11.4) vanish in the limit $\epsilon = 0$. Thus, the only contribution of these two terms stems from

the roots $\alpha = \alpha_*$ of the equation $\Delta(\alpha) = 0$. The function $\mathcal{A}\, e^{\,\mathrm{i}\,\alpha\, x}$ in (11.3) can then be taken as $\mathcal{A}^* e^{\,\mathrm{i}\,\alpha_*\, x}$, and the functions Δ_1 and Δ can be taken as Δ_1^* and $\Delta_\alpha^*(\alpha - \alpha_*)$, in the last two terms on the right side of (11.4).

Hereafter, $\mathcal{A}^*$, Δ_1^* and Δ_α^* denote the values of the functions $\mathcal{A}(\alpha)$, $\Delta_1(\alpha)$ or $\Delta_\alpha(\alpha)$ at the root $\alpha = \alpha_*$. This notation in which a superscript $(\cdot)^*$ or a subscript $(\cdot)_*$ denotes a function $(\cdot)$ evaluated at the root $\alpha = \alpha_*$ of the function $\Delta(\alpha) = 0$ is used hereafter in this chapter and in chapter 12.

The decomposition (11.4) applied in the integral (11.3) yields

$$I^F = I_0^F - \sum_{\alpha_*} (\,\mathrm{i}\, I_1^F + I_2^F)\, \mathcal{A}^* e^{\,\mathrm{i}\,\alpha_*\, x} \;\text{ where }\; I_0^F \equiv \int_{-\infty}^{\infty} d\alpha\, \frac{\mathcal{A}}{\Delta}\, e^{\,\mathrm{i}\,\alpha\, x} \;, \quad (11.5a)$$

$$I_1^F \equiv \int_{-\infty}^{\infty} d\alpha\, \frac{\epsilon\, \Delta_1^*/(\Delta_\alpha^*)^2}{(\alpha - \alpha_*)^2 + (\epsilon\, \Delta_1^*/\Delta_\alpha^*)^2} \;\text{ and} \quad (11.5b)$$

$$I_2^F \equiv \int_{-\infty}^{\infty} d\alpha\, \frac{\epsilon^2\, (\Delta_1^*)^2/\Delta_\alpha^*}{(\Delta_\alpha^*)^2 (\alpha - \alpha_*)^2 + \epsilon^2 (\Delta_1^*)^2}\, \frac{1}{\alpha - \alpha_*} \;. \quad (11.5c)$$

The integrand of the integral (11.5c) is an odd function of $\alpha - \alpha_*$ and one then has $I_2^F = 0$. However, the integral I_1^F is not nil. The change of variable $\alpha - \alpha_* = \epsilon\, |\, \Delta_1^*/\Delta_\alpha^*\, |\, t$ in (11.5b) yields

$$I_1^F = \frac{\mathrm{sign}(\Delta_1^*)}{|\, \Delta_\alpha^*\, |} \int_{-\infty}^{\infty} dt\, \frac{1}{t^2 + 1} = \pi\, \frac{\mathrm{sign}(\Delta_1^*)}{|\, \Delta_\alpha^*\, |} \;.$$

Expression (11.5a) then becomes

$$\begin{aligned} I^F &= I_0^F - \mathrm{i}\, \pi \sum_{\alpha_*} \mathrm{sign}(\Delta_1^*)\, \frac{\mathcal{A}^*}{|\, \Delta_\alpha^*\, |}\, e^{\,\mathrm{i}\,\alpha_*\, x} \\ &= I_0^F - \mathrm{i}\, \pi \sum_{\alpha_*} \mathrm{sign}(\Delta_1^* \Delta_\alpha^*)\, \frac{\mathcal{A}^*}{\Delta_\alpha^*}\, e^{\,\mathrm{i}\,\alpha_*\, x} \quad (11.6a) \\ \text{where }\; I_0^F &= \int_{-\infty}^{\infty} d\alpha\, \frac{\mathcal{A}}{\Delta}\, e^{\,\mathrm{i}\,\alpha\, x} \;. \quad (11.6b) \end{aligned}$$

The integrand of the integral I_0^F defined by (11.6b) is singular at the roots of $\Delta = 0$. These singularities yield a dominant far-field contribution according to Fourier analysis [**11,4**]. Therefore it is crucial to explicitly determine this far-field contribution and to formally combine it with the contribution of the term $\mathrm{i}\, \epsilon\, \Delta_1$ in (11.3). Indeed, it is shown further on that the dominant contributions of the term $\mathrm{i}\, \epsilon\, \Delta_1$ in (11.3) and of the roots $\alpha = \alpha_*$ in expression (11.6b) can cancel out in some regions of the physical space, e.g. ahead of a ship that advances in calm water.

Basic decomposition into singular and regular components

The singular integral (11.6b) is now considered. One has

$$\frac{\mathcal{A}}{\Delta}\, e^{\,\mathrm{i}\,\alpha\, x} = \mathcal{A}^L\, e^{\,\mathrm{i}\,\alpha\, x} + \sum_{\alpha_*} \frac{\Lambda\, e^{\,\mathrm{i}\,(\alpha-\alpha_*)\, x}}{\Delta^*_\alpha\,(\alpha-\alpha_*)}\, \mathcal{A}^*\, e^{\,\mathrm{i}\,\alpha_*\, x} \ \text{ where} \tag{11.7}$$

$$\mathcal{A}^L \equiv \frac{\mathcal{A}}{\Delta} - \sum_{\alpha_*} \frac{\Lambda\, \mathcal{A}^*}{\Delta^*_\alpha\,(\alpha-\alpha_*)} \ \text{ and } \ \Lambda \equiv e^{\,-\mu_*^2\,(\alpha-\alpha_*)^2/4} \tag{11.8a}$$

is a localizing function of effective width determined by the real positive number μ_*. The function $\mathcal{A}^L$ can be expressed in the form

$$\mathcal{A}^L = \frac{\mathcal{A}-\mathcal{A}^*}{\Delta} + \frac{\mathcal{A}^*}{\Delta^*_\alpha}\left[\frac{\Delta^*_\alpha\,(\alpha-\alpha_*)-\Delta}{\Delta\,(\alpha-\alpha_*)} + \frac{1-\Lambda}{\alpha-\alpha_*}\right] + \sum_{\alpha_{**}\neq\alpha_*} \frac{\mathcal{A}^{**}\, e^{\,-\mu_{**}^2\,(\alpha_{**}-\alpha_*)^2/4}}{\Delta^{**}_\alpha}\,(\alpha_{**}-\alpha_*)$$

where the summation $\sum_{\alpha_{**}\neq\alpha_*}$ is performed over all the roots of $\Delta = 0$ other than the root $\alpha = \alpha_*$. Moreover, $\mathcal{A}^{**}$ and Δ^{**}_α denote the values of the functions $\mathcal{A}(\alpha)$ and $\Delta_\alpha(\alpha)$ at the root $\alpha = \alpha_{**}$. This expression for the function $\mathcal{A}^L$ shows that $\mathcal{A}^L$ is finite at the root $\alpha = \alpha_*$ and given by

$$\mathcal{A}^L_* = \frac{\mathcal{A}^*_\alpha}{\Delta^*_\alpha} - \frac{\mathcal{A}^*\Delta^*_{\alpha\alpha}}{2\,(\Delta^*_\alpha)^2} + \sum_{\alpha_{**}\neq\alpha_*} \frac{\mathcal{A}^{**}\, e^{\,-\mu_{**}^2\,(\alpha_{**}-\alpha_*)^2/4}}{\Delta^{**}_\alpha\,(\alpha_{**}-\alpha_*)}\ . \tag{11.8b}$$

Expressions (11.6b) and (11.7) yield

$$I_0^F = I_0^S + I_0^R \ \text{ where } \ I_0^R \equiv \int_{-\infty}^{\infty} d\alpha\ \mathcal{A}^L\, e^{\,\mathrm{i}\,\alpha\, x} \tag{11.9a}$$

$$\text{and } \ I_0^S \equiv \sum_{\alpha_*} \frac{\mathcal{A}^*}{\Delta^*_\alpha}\, e^{\,\mathrm{i}\,\alpha_*\, x} \int_{-\infty}^{\infty} dt\ \frac{e^{\,-\mu_*^2\, t^2/4\,+\,\mathrm{i}\, t\, x}}{t}\ . \tag{11.9b}$$

The change of variable $t\, x = \theta$ yields

$$\int_{-\infty}^{\infty} dt\ \frac{e^{\,-\mu_*^2\, t^2/4\,+\,\mathrm{i}\, t\, x}}{t} = 2\,\mathrm{i}\,\mathrm{sign}(x) \int_0^{\infty} d\theta\ \frac{\sin\theta}{\theta}\, e^{\,-\mu_*^2\,\theta^2/(2\,|\,x\,|)^2}$$
$$= \mathrm{i}\,\mathrm{sign}(x) \int_0^{\infty} dt\ \frac{\sin(2\,|x|\sqrt{t}/\mu_*)}{t}\ e^{-t} = \mathrm{i}\,\pi\,\mathrm{sign}(x)\,\mathrm{erf}\left[\frac{|\,x\,|}{\mu_*}\right]$$

where $\mathrm{erf}(\cdot)$ is the error function. It then follows from (11.9b) that one has

$$I_0^S = \sum_{\alpha_*} \mathrm{i}\,\pi\,\mathrm{sign}(x)\,\mathrm{erf}\left[\frac{|\,x\,|}{\mu_*}\right] \frac{\mathcal{A}^*}{\Delta^*_\alpha}\ e^{\,\mathrm{i}\,\alpha_*\, x}$$
$$= \sum_{\alpha_*} \mathrm{i}\,\pi\,\mathrm{erf}\left[\frac{x}{\mu_*}\right] \frac{\mathcal{A}^*}{\Delta^*_\alpha}\ e^{\,\mathrm{i}\,\alpha_*\, x}\ . \tag{11.10}$$

Expressions (11.6), (11.9a) and (11.10) yield

$$I^F = I_0^R + \sum_{\alpha_*} \mathrm{i}\,\pi\,[\,\mathrm{erf}(x/\mu_*) - \mathrm{sign}(\Delta_1^*\Delta_\alpha^*)\,]\;\frac{\mathcal{A}^*}{\Delta_\alpha^*}\;e^{\,\mathrm{i}\,\alpha_*\,x}$$

where I^F is the integral (11.3) and I_0^R is defined by (11.9a) and (11.8).

11.2 Fundamental analytical representation

Thus, the singular Fourier integral (11.3) can finally be expressed as

$$I^F(x) \equiv \int_{-\infty}^{\infty} d\alpha\;\frac{\mathcal{A}(\alpha)\;e^{\,\mathrm{i}\,\alpha\,x}}{\Delta(\alpha) + \mathrm{i}\,\epsilon\,\Delta_1(\alpha)} = I^W(x) + I^L(x) \;\text{ where} \tag{11.11a}$$

$$I^W(x) \equiv \sum_{\alpha_*} \mathrm{i}\,\pi\,[\,\mathrm{erf}(x/\mu_*) - \mathrm{sign}(\Delta_1^*\Delta_\alpha^*)\,]\;\frac{\mathcal{A}^*}{\Delta_\alpha^*}\;e^{\,\mathrm{i}\,\alpha_*\,x} \;\text{ and} \tag{11.11b}$$

$$I^L(x) \equiv \int_{-\infty}^{\infty} d\alpha\;\mathcal{A}^L\,e^{\,\mathrm{i}\,\alpha\,x} \;\text{ with }\; \mathcal{A}^L = \frac{\mathcal{A}}{\Delta} - \sum_{\alpha_*} \frac{\mathcal{A}^*\,e^{\,-\mu_*^2\,(\alpha-\alpha_*)^2/4}}{\Delta_\alpha^*\,(\alpha-\alpha_*)} \tag{11.11c}$$

$$\text{and }\; \mathcal{A}_*^L = \frac{\mathcal{A}_\alpha^*}{\Delta_\alpha^*} - \frac{\mathcal{A}^*\Delta_{\alpha\alpha}^*}{2\,(\Delta_\alpha^*)^2} + \sum_{\alpha_{**}\neq\alpha_*} \frac{\mathcal{A}^{**}\,e^{\,-\mu_{**}^2\,(\alpha_{**}-\alpha_*)^2/4}}{\Delta_\alpha^{**}\,(\alpha_{**}-\alpha_*)}\;. \tag{11.11d}$$

The summation $\sum_{\alpha_*}$ in expressions (11.11b-c) is performed over all the roots $\alpha = \alpha_*$ of the equation $\Delta(\alpha) = 0$ and the summation $\sum_{\alpha_{**}\neq\alpha_*}$ in (11.11d) is performed over all the roots of $\Delta = 0$ other than the root $\alpha = \alpha_*$.

As was already noted, Δ_1^*, Δ_α^*, $\Delta_{\alpha\alpha}^*$, $\mathcal{A}^*$ and $\mathcal{A}_\alpha^*$ in (11.11b-d) denote the values of the functions $\Delta_1(\alpha)$, $\Delta_\alpha(\alpha)$, $\Delta_{\alpha\alpha}(\alpha)$, $\mathcal{A}(\alpha)$ or $\mathcal{A}_\alpha(\alpha)$ at the root $\alpha = \alpha_*$, and $\mathcal{A}^{**}$ and Δ_α^{**} similarly denote the values of the functions $\mathcal{A}(\alpha)$ and $\Delta_\alpha(\alpha)$ at the root $\alpha = \alpha_{**}$. Moreover, μ_* and μ_{**} denote the values of the parameter μ that correspond to the roots α_* or α_{**}. The function $\mathcal{A}^L$ is finite (indeed smooth) at the root α_* and the Fourier integral I^L defined by (11.11c) therefore is not singular, unlike the basic Fourier integral I^F defined by (11.11a). Specifically, the (finite) value $\mathcal{A}_*^L$ of the function $\mathcal{A}^L$ at the root $\alpha = \alpha_*$ is given by (11.11d).

The identity (11.11) expresses the singular integral I^F as the sum of a wave function I^W and a regular (non-singular) integral I^L. This identity does not involve approximations, i.e. is *exact*, and holds for $\epsilon = +0$ (rather than for $0 < \epsilon \ll 1$) and for *general* functions $\mathcal{A}$, Δ and Δ_1.

The error function in expression (11.11b) and the exponential function in expressions (11.11c-d) involve the positive real numbers μ_* or μ_{**}. Thus, the components I^W and I^L in the decomposition (11.11a) involve μ_* and μ_{**}, although the integral I^F defined by (11.11a) does not involve μ_* or μ_{**}.

Different choices for μ_* and μ_{**} therefore yield alternative decompositions $I^F = I^W + I^L$ and the identity (11.11) defines a family of decompositions $I^F = I^W + I^L$. Indeed μ can be chosen arbitrarily from a strictly mathematical standpoint. However, the next section shows that the identity (11.11) is best suited for accurate numerical evaluation and practical applications if μ is well chosen.

11.3 Main features of a general waves and local-effects decomposition

Essential features of the decomposition $I^F = I^W + I^L$ given by (11.11) are explained in this section. The case when the equation $\Delta(\alpha) = 0$ has a single root α_* is considered for simplicity, and μ_* is then simply denoted as μ.

The two fundamental limits $\mu = 0$ and $\mu = \infty$

The two interesting special choices $\mu = 0$ and $\mu = \infty$ are studied first.

In the limit $\mu \to \infty$, expressions (11.11) yield

$$I^F = I^W_\infty + I^L_\infty \text{ where} \tag{11.12a}$$

$$I^W_\infty = -\,\mathrm{i}\,\pi\,\mathrm{sign}(\Delta^*_1)\,\mathcal{A}^* e^{\,\mathrm{i}\,\alpha_*\,x}/|\,\Delta^*_\alpha\,| \tag{11.12b}$$

$$\text{and } I^L_\infty = PV\int_{-\infty}^{\infty} d\alpha\,\frac{\mathcal{A}}{\Delta}\,e^{\,\mathrm{i}\,\alpha\,x}\ . \tag{11.12c}$$

PV in (11.12c) represents the Cauchy principal value of the integral.

In the limit $\mu \to 0$, expressions (11.11) become

$$I^F = I^W_0 + I^L_0 \text{ where} \tag{11.13a}$$

$$I^W_0 = \mathrm{i}\,\pi\,[\,\mathrm{sign}(x) - \mathrm{sign}(\Delta^*_1\,\Delta^*_\alpha)\,]\,\mathcal{A}^*\,e^{\,\mathrm{i}\,\alpha_*\,x}/\Delta^*_\alpha \tag{11.13b}$$

$$\text{and } I^L_0 = \int_{-\infty}^{\infty} d\alpha\left[\frac{\mathcal{A}}{\Delta} - \frac{\mathcal{A}^*/\Delta^*_\alpha}{\alpha - \alpha_*}\right] e^{\,\mathrm{i}\,\alpha\,x}\ . \tag{11.13c}$$

A simple illustrative example

Important features of the general identity (11.11) and the two related special cases (11.12-11.13) are now illustrated for a simple special case. Specifically, the case

$$\mathcal{A} = e^{-\,\alpha^2}\ ,\ \ \Delta_1 = 1 \text{ and } \Delta = \alpha - \alpha_* \text{ with } \alpha_* = 1$$

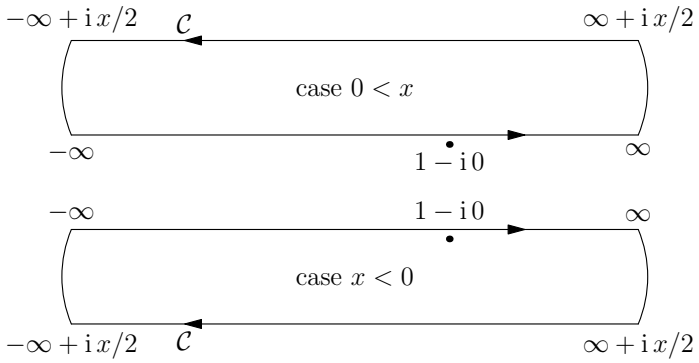

Figure 11.1: Integration contour in the complex plane $\alpha = \alpha_r + \mathrm{i}\,\alpha_i$ used to evaluate the integral I defined by (11.14a) for $0 < x$ (top) or $x < 0$ (bottom).

is considered. The derivative of the function $\Delta(\alpha)$ is $\Delta_\alpha = 1$. Expressions (11.11) then become

$$I^F = \int_{-\infty}^{\infty} d\alpha \, \frac{e^{-\alpha^2 + \mathrm{i}\,\alpha\,x}}{\alpha - 1 + \mathrm{i}\,0} = I^W + I^L \text{ where} \tag{11.14a}$$

$$I^W \equiv \mathrm{i}\,\pi\,[\mathrm{erf}(x/\mu) - 1]\, e^{\,\mathrm{i}\,x}/e \text{ and} \tag{11.14b}$$

$$I^L \equiv \int_{-\infty}^{\infty} d\alpha \, \frac{e^{-\alpha^2} - e^{-\mu^2(\alpha-1)^2/4 - 1}}{\alpha - 1} \, e^{\,\mathrm{i}\,\alpha\,x} \, . \tag{11.14c}$$

Expressions (11.12) and (11.13) similarly become

$$I^W_\infty = -\mathrm{i}\,\pi \, \frac{e^{\,\mathrm{i}\,x}}{e} \;\; , \;\; I^L_\infty = PV \int_{-\infty}^{\infty} d\alpha \, \frac{e^{-\alpha^2 + \mathrm{i}\,\alpha\,x}}{\alpha - 1} \text{ and} \tag{11.15a}$$

$$I^W_0 = \mathrm{i}\,\pi\,[\mathrm{sign}(x) - 1] \, \frac{e^{\,\mathrm{i}\,x}}{e} \;\; , \;\; I^L_0 = \int_{-\infty}^{\infty} d\alpha \, \frac{e^{-\alpha^2} - 1/e}{\alpha - 1} \, e^{\,\mathrm{i}\,\alpha\,x} \, . \tag{11.15b}$$

The integral I^F defined by (11.14a) can be evaluated via the classical contour integration technique in the complex plane $\alpha = \alpha_r + \mathrm{i}\,\alpha_i$. Specifically, the contour of integration depicted in Fig. 11.1 is considered. This integration contour does not enclose a pole if $x > 0$, but encloses the pole $\alpha = 1 - \mathrm{i}\,0$ if $x < 0$. One has $-\alpha^2 + \mathrm{i}\,\alpha\,x = -(\alpha_r^2 + x^2/4)$ along the path $\alpha = \alpha_r + \mathrm{i}\,x/2$ with $-\infty < \alpha_r < \infty$. The connections between this path of integration and the real axis $-\infty < \alpha_r < \infty$, $\alpha_i = 0$ yield a nil contribution. One then obtains the representation

$$I^F = I^W_c + I^L_c \text{ where } I^W_c = \mathrm{i}\,\pi\,[\mathrm{sign}(x) - 1]\, e^{\,\mathrm{i}\,x}/e \tag{11.16a}$$

$$\text{and } I^L_c \equiv \int_{-\infty}^{\infty} d\alpha \, \frac{e^{-(\alpha^2 + x^2/4)}}{\alpha - 1 + \mathrm{i}\,x/2} \;\; . \tag{11.16b}$$

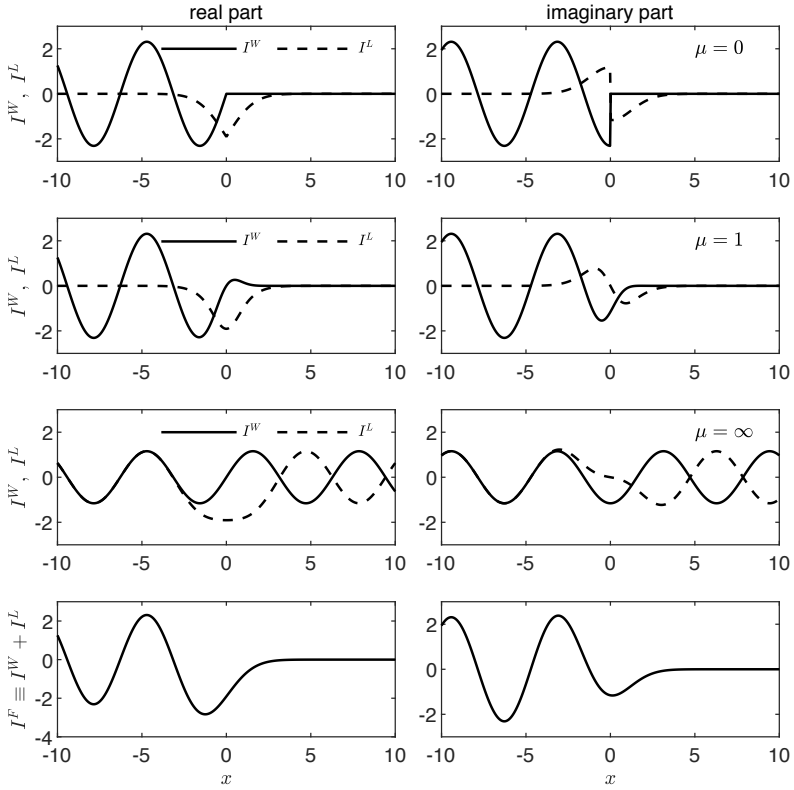

Figure 11.2: Functions $I^W(x)$ and $I^L(x)$ defined by expressions (11.14) with $\mu = 1$ (second row) and expressions (11.15a) or (11.15b), which correspond to $\mu = \infty$ (third row) or $\mu = 0$ (top row). The bottom row depicts the corresponding function $I^F(x) = I^W(x) + I^L(x)$, which is independent of μ.

The change of variable $\alpha_r \to \alpha$ was performed in the integral (11.16b). The wave components I_c^W in (11.16a) and I_0^W in (11.15b) are identical, and one also has $I_c^L = I_0^L$ as can be verified.

Thus, the decomposition $I_0^W + I_0^L$, which corresponds to the special case $\mu = 0$ in the decomposition $I^W + I^L$ given by (11.14), is equivalent to the classical technique of contour integration in the complex α plane, and the decomposition $I_\infty^W + I_\infty^L$ associated with the special case $\mu = \infty$ amounts to taking the principal value of the singular integral I^F as is noted in (11.12). **[11,5]**

Influence of the parameter μ

The functions $I^W(x)$, $I^L(x)$ and $I^F(x) = I^W(x) + I^L(x)$ defined by expressions (11.15a) or (11.15b), which correspond to $\mu = \infty$ or $\mu = 0$ as was just noted, and expressions (11.14) with $\mu = 1$ are depicted in Fig. 11.2. This figure illustrates the already-noted fact that different choices of μ in (11.14) yield different components I^W and I^L but has no effect on the sum $I^F = I^W + I^L$, which is depicted in the bottom row of Fig. 11.2. This figure therefore provides a numerical verification of the identity (11.14).

The bottom row of Fig. 11.2 also shows that the function I^F decays rapidly as $x \to +\infty$ and is negligible in the region $0 < x$ except in a small near-field region in the vicinity of $x = 0$. Moreover, Fig. 11.2 shows that one has $I^L \approx -I^W$ for $0 < x$ in the special case $\mu = \infty$, in accordance with the identity $I^F = I^W + I^L$. Thus, expressions (11.14c) associated with the limit $\mu \to \infty$ and the principal-value integral I^L correspond to a decomposition $I^W + I^L$ that involves numerical cancellations or additions of oscillatory functions in half the physical space, specifically in $0 < x$ or in $x < 0$ in the example considered in (11.14) and in Fig. 11.2. The decomposition (11.15a) associated with the choice $\mu = \infty$ in (11.14b-c) therefore is poorly suited for numerical evaluation.

Expression (11.14b) yields $I^W \approx 0$ and hence $I^F \approx I^L$ if $2 < x/\mu$, as is illustrated in Fig. 11.2. Numerical cancellations between the components I^W and I^L in the identity $I^F = I^W + I^L$ therefore only occur within a region of width $|x| \approx 2\mu$. This region is small if μ is chosen small, but is large if μ is large.

The 'near-field region' $|x| < 2\mu$, where unwanted numerical cancellations between the components I^W and I^L in the identity $I^F = I^W + I^L$ can occur, vanishes as $\mu \to 0$. Indeed, the component I_0^W in expressions (11.15b), which correspond to the limit $\mu \to 0$, is nil for $0 \leq x$. Expression (11.15b) for the component I_0^W shows that I_0^W is not smooth at $x = 0$, as can also be observed in Fig. 11.2. This figure shows that the integral I_0^L likewise is not smooth at $x = 0$, although the sum $I^F = I_0^W + I_0^L$ is smooth. The choice $\mu = 0$, while much preferable to the choice $\mu = \infty$, yields a decomposition that is not smooth and therefore not fully satisfactory. Indeed, a positive value of μ in (11.14) is required to obtain a decomposition $I^F = I^W + I^L$ that is smooth, in accordance with the error function $\mathrm{erf}(x/\mu)$ and as is illustrated in Fig. 11.2 for $\mu = 1$.

Thus, the parameter μ should not be chosen too small, to avoid excessively sharp variations of the components I^W and I^L, or too large to avoid numerical cancellations between the components I^W and I^L in large regions of the physical space. The simple illustrative example considered in this section suggests that the special case $\mu = 0$ is essentially equivalent to the classical technique of contour integration in the complex plane. This tech-

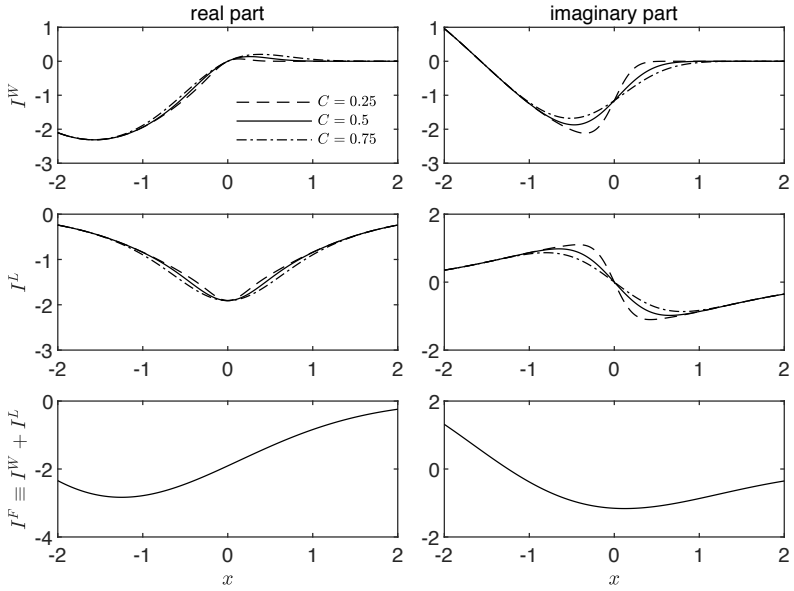

Figure 11.3: Functions $I^W(x)$, $I^L(x)$ and $I^F(x) = I^W(x) + I^L(x)$ defined by expressions (11.14a-b) and (11.20) with $\alpha_* = 1$ for $C = 0.25$, 0.5 and 0.75.

nique yields a discontinuity in the wave component I^W because a pole is either inside or outside an integration contour, whereas a *smooth* transition is allowed in the fundamental decomposition (11.11). Indeed, the error function in expression (11.14b) is replaced by the sign function in (11.15b).

11.4 Optimal decomposition into waves and local effects

The localizing function $e^{-\mu_*^2(\alpha-\alpha_*)^2/4}$ in expression (11.11c) is negligible outside the 'dispersion strip' defined as

$$-5/\mu_* \leq \alpha - \alpha_* \leq 5/\mu_* \ . \tag{11.17}$$

This dispersion strip is wide if μ_* is small, narrow if μ_* is large. Indeed, the integral I^L defined by (11.11c) is singular in the limit $\mu \to \infty$, which corresponds to the principal value of a singular integral in accordance with (11.12c).

The approximation

$$\mathrm{erf}(x/\mu_*) \approx \mathrm{sign}(x/\mu_*) = \mathrm{sign}(x) \ \text{ if } \ 2 < |x|/\mu_*$$

shows that the function

$$\Theta \equiv \mathrm{erf}(x/\mu_*) - \mathrm{sign}(\Delta_1^* \Delta_\alpha^*) \tag{11.18a}$$

in expression (11.11b) for the function I^W is given by

$$\Theta \approx \mathrm{sign}(x) - \mathrm{sign}(\Delta_1^* \Delta_\alpha^*) \text{ if } 2 < |x|/\mu_* \,. \tag{11.18b}$$

This approximation shows that the influence of the parameter μ_* on the component I^W, and hence also on the component I^L, in the decomposition $I^F = I^W + I^L$ is insignificant in the far-field region $2\mu_* < |x|$. The extent of the 'near-field region' $|x| < 2\mu_*$ of influence of μ_* on the components I^W and I^L in the decomposition $I^F = I^W + I^L$ vanishes as $\mu_* \to 0$, but is unbounded if $\mu_* \to \infty$.

Thus, small/large values of μ_* yield wide/narrow dispersion strips (in the Fourier plane) and small/large regions (in the physical plane) where the components I^W and I^L are significantly influenced by μ_*. Moreover, unwanted numerical cancellations between the components I^W and I^L occur within a wide region $|x| < 2\mu_*$ if μ_* is large, as is illustrated in Fig. 11.2 for the extreme case $\mu_* = \infty$.

The width $|x| \approx 2\mu_*$ of the near-field region should then be chosen relatively small in comparison to the wavelength $2\pi/\alpha_*$ that corresponds to the root α_* of the equation $\Delta = 0$. In particular, the width of the near-field region is equal to $1/6$ of the wavelength $2\pi/|\alpha_*|$ if μ_* is chosen as $\mu_* = C/|\alpha_*|$ with $C = \pi/6 \approx 1/2$. An optimal waves and local-effects decomposition is then obtained if the parameter μ_* in (11.11b-d) is chosen as

$$\mu_* = C/|\alpha_*| \quad \text{with} \quad C \approx 1/2 \,. \tag{11.19}$$

This choice yields a *smooth* decomposition of the singular integral I^F into a wave component I^W and a component I^L that represents a *non-oscillatory local* component, as is illustrated in Fig. 11.2. Smaller values of C yield sharper variations of the wave and local components I^W and I^L within narrower near-field regions. In particular, these two components are not smooth, even though the sum $I^W + I^L$ is smooth, in the limit $C = 0$. **[11,6]**

The functions $I^W(x)$, $I^L(x)$ and $I^F(x) = I^W(x) + I^L(x)$ defined by (11.14) and (11.19), where one has $\alpha_* = 1$ and $\mu_* = \mu = C$, are depicted in Fig. 11.3 for $C = 0.25, 0.5$ and 0.75. This figure shows that the decomposition (11.11) is not overly sensitive to the choice of the parameter μ. Fig. 11.3 also shows that satisfactory decompositions are obtained for values of $C \approx 1/2$ in expression (11.19). This value of C is considered to be nearly optimal.

Special case and general expression for μ_*

Expression (11.19) yields $\mu_* = \infty$ if $\alpha_* = 0$. This special case, in which the function $\Delta(\alpha)$ in (11.3) has a root $\alpha_* = 0$, occurs for instance for the

dispersion function associated with a ship that advances through regular waves considered in chapter 5. An unbounded value of μ_* in the special case $\alpha_* = 0$ is avoided if expression (11.19) is modified as

$$\mu_* = C/\alpha_m^* \text{ where } C \approx 1/2 \ , \ \alpha_m^* \equiv \sqrt{\alpha_*^2 + \alpha_s^2} \tag{11.20}$$

and α_s denotes a significant value of α associated with the function $\Delta(\alpha)$, as is illustrated in the next section for the dispersion function relevant to a ship that advances through regular waves.

11.5 Open dispersion curves expressed in Cartesian form

The fundamental general analytical representation (11.11) is now applied to the singular double Fourier integrals (11.2) and (11.1b) associated with dispersion curves $\Delta(\alpha, \beta) = 0$ expressed in the Cartesian form $\alpha = \alpha_*(\beta)$ with $-\infty < \beta < +\infty$.

Expressions (11.1b), (11.2) and (11.11) readily yield

$$\phi^F(\mathbf{x}) \equiv \frac{1}{\pi} \int_{-\infty}^{\infty} d\beta \int_{-\infty}^{\infty} d\alpha \, \frac{\mathcal{A}(\alpha, \beta) \, e^{\,\mathrm{i}\,(\alpha\, x + \beta\, y)}}{\Delta(\alpha, \beta) + \mathrm{i}\,\epsilon\, \Delta_1(\alpha, \beta)} \tag{11.21a}$$

$$= \phi^W(\mathbf{x}) + \phi^L(\mathbf{x}) \tag{11.21b}$$

where $\phi^W(\mathbf{x})$ and $\phi^L(\mathbf{x})$ respectively represent waves and a nonoscillatory local disturbance.

The wave component $\phi^W(\mathbf{x})$ in the decomposition (11.21b) is given by

$$\phi^W \equiv \sum_{\alpha_*} \mathrm{i} \int_{-\infty}^{\infty} d\beta \; \Theta \; \frac{\mathcal{A}^*}{\Delta_\alpha^*} \, e^{\,\mathrm{i}\,(\alpha_*\, x + \beta\, y)} \tag{11.22a}$$

$$\text{where } \Theta = \mathrm{erf}(\alpha_m^* \, x/C) - \mathrm{sign}(\Delta_1^* \, \Delta_\alpha^*) \tag{11.22b}$$

$$\text{with } \alpha_m^* = \sqrt{\alpha_*^2 + \alpha_s^2} \text{ and } C \approx 1/2 \tag{11.22c}$$

in accordance with (11.20), and erf is the error function. The summation $\sum_{\alpha_*}$ is performed over all the roots $\alpha = \alpha_*(\beta)$ of the dispersion relation $\Delta(\alpha, \beta) = 0$ and thus accounts for the contribution of all the dispersion curves defined by the dispersion relation. The functions $\mathcal{A}(\alpha, \beta)$, $\mathcal{A}_\alpha(\alpha, \beta)$, $\Delta_\alpha(\alpha, \beta)$, $\Delta_1(\alpha, \beta)$ evaluated at the (dispersion) curve $\alpha = \alpha_*(\beta)$ are denoted as

$$\left\{ \begin{matrix} \mathcal{A}^* \equiv \mathcal{A}^*(\beta) \equiv \mathcal{A}(\alpha_*, \beta) \\ \mathcal{A}_\alpha^* \equiv \mathcal{A}_\alpha^*(\beta) \equiv \mathcal{A}_\alpha(\alpha_*, \beta) \end{matrix} \right\} \quad \left\{ \begin{matrix} \Delta_\alpha^* \equiv \Delta_\alpha^*(\beta) \equiv \Delta_\alpha(\alpha_*, \beta) \\ \Delta_1^* \equiv \Delta_1^*(\beta) \equiv \Delta_1(\alpha_*, \beta) \end{matrix} \right\}$$

in (11.22a-b).

The local component $\phi^L(\mathbf{x})$ in the decomposition (11.21b) is given by the double Fourier integral

$$\phi^L(\mathbf{x}) \equiv \frac{1}{\pi}\int_{-\infty}^{\infty} d\beta \int_{-\infty}^{\infty} d\alpha \; \mathcal{A}^L(\alpha,\beta)\, e^{\,\mathrm{i}\,(\alpha\, x + \beta\, y)} \tag{11.23a}$$

$$\text{where } \mathcal{A}^L \equiv \frac{\mathcal{A}}{\Delta} - \sum_{\alpha_*} \frac{\mathcal{A}^*\, e^{-C^2(\alpha-\alpha_*)^2/(2\alpha_m^*)^2}}{\Delta_\alpha^*\,(\alpha-\alpha_*)} \;. \tag{11.23b}$$

The function $\mathcal{A}^L(\alpha,\beta)$ is finite at the dispersion curves $\alpha = \alpha_*(\beta)$ where the functions $\mathcal{A}^L(\alpha_*,\beta) \equiv \mathcal{A}_*^L(\beta) \equiv \mathcal{A}_*^L$ are defined by (11.8b) as

$$\mathcal{A}_*^L = \frac{\mathcal{A}_\alpha^*}{\Delta_\alpha^*} - \frac{\mathcal{A}^*\Delta_{\alpha\alpha}^*}{2\,(\Delta_\alpha^*)^2} + \sum_{\alpha_{**}\neq\alpha_*} \frac{\mathcal{A}^{**}\, e^{-C^2\,(\alpha_{**}-\alpha_*)^2/(2\,\alpha_m^{**})^2}}{\Delta_\alpha^{**}\,(\alpha_{**}-\alpha_*)} \tag{11.23c}$$

where the summation $\sum_{\alpha_{**}\neq\alpha_*}$ is performed over all the roots of $\Delta = 0$ other than the root $\alpha = \alpha_*$.

An optimal decomposition—in which the component ϕ^W given by the single Fourier integrals (11.22) represents the waves defined by the singular double integral in (11.21) and the double integral (11.23) represents a non-oscillatory local disturbance, and the components ϕ^W and ϕ^L are smooth—is obtained if C is chosen as $C \approx 1/2$ in (11.22b) and (11.23b-c). The wavenumber α_s in (11.22c) can be taken as $\alpha_s = 0$ for dispersion curves $\Delta\,(\alpha,\beta)$ that do not cross the axis $\alpha = 0$, but should be taken as a significant small wavenumber α_s for a dispersion curve that crosses the axis $\alpha = 0$. E.g., for a ship that steadily advances through regular waves at $1/4 < \tau$, the dispersion curve IO^+ located in the region $-k_i^- \leq \alpha < \infty$ intersects the axis $\alpha = 0$, and $\alpha_s = k_i^-$ is an obvious choice.

Expressions (11.21-11.23) associated with dispersion curves expressed in the Cartesian form $\alpha = \alpha_*(\beta)$ can readily be applied to dispersion curves expressed in the Cartesian form $\beta = \beta_*(\alpha)$ via the substitution $\alpha \longleftrightarrow \beta$.

11.6 Closed dispersion curve expressed in polar form

Application of the fundamental decomposition (11.11) to the general integral (11.1a) associated with the polar representation (k,γ) is not as straightforward because the wavenumber k varies within the range $0 \leq k < \infty$ in (11.1a), whereas the range of integration is $-\infty < \alpha < \infty$ in (11.1b) and (11.2). This application is now considered. Specifically, this section considers the case of a *closed* dispersion curve, defined as $k = k_*(\gamma)$, that *surrounds the origin* $k = 0$ of the Fourier plane, such as the inner dispersion curve I depicted in Fig.5.2 related to flows around ships steadily advancing in regular waves at $\tau < 1/4$.

Analysis

One has

$$\phi^F = \phi^F_+ + \phi^F_- \text{ where} \tag{11.24a}$$

$$\phi^F_+ = \frac{1}{\pi}\int_0^\pi d\gamma \int_0^\infty dk\ \frac{\mathcal{A}(k,\gamma)\, e^{\,\mathrm{i}\,k\,(x\,\cos\gamma + y\,\sin\gamma)}}{\Delta\,(k,\gamma) + \mathrm{i}\,\epsilon\,\Delta_1(k,\gamma)} \tag{11.24b}$$

$$\text{and } \phi^F_- = \frac{1}{\pi}\int_{-\pi}^0 d\gamma' \int_0^\infty dk'\ \frac{\mathcal{A}(k',\gamma')\, e^{\,\mathrm{i}\,k'(x\,\cos\gamma' + y\,\sin\gamma')}}{\Delta\,(k',\gamma') + \mathrm{i}\,\epsilon\,\Delta_1(k',\gamma')}\ .$$

The changes of variables $\gamma' = \gamma - \pi$ and $k' = -k$ in the expression for ϕ^F_- yield

$$\phi^F_- = \frac{1}{\pi}\int_0^\pi d\gamma \int_{-\infty}^0 dk\ \frac{\mathcal{A}(-k,\gamma-\pi)\, e^{\,\mathrm{i}\,k\,(x\,\cos\gamma + y\,\sin\gamma)}}{\Delta\,(-k,\gamma-\pi) + \mathrm{i}\,\epsilon\,\Delta_1(-k,\gamma-\pi)}\ . \tag{11.24c}$$

Expressions (11.24) yield

$$\phi^F(\mathbf{x}) = \frac{1}{\pi}\int_0^\pi d\gamma\ I^F(\gamma,\mathbf{x}) \text{ where} \tag{11.25a}$$

$$I^F(\gamma,\mathbf{x}) \equiv \int_{-\infty}^\infty dk\ \frac{\widehat{\mathcal{A}}(k,\gamma)\, e^{\,\mathrm{i}\,k\,(x\,\cos\gamma + y\,\sin\gamma)}}{\widehat{\Delta}\,(k,\gamma) + \mathrm{i}\,\epsilon\,\widehat{\Delta}_1(k,\gamma)} \tag{11.25b}$$

and the functions $\widehat{\mathcal{A}}$, $\widehat{\Delta}$ and $\widehat{\Delta}_1$ are defined as

$$\widehat{\mathcal{A}}(k,\gamma) = \begin{cases} \mathcal{A}(k,\gamma) & \text{if } 0 \le k \\ \mathcal{A}(-k,\gamma-\pi) & \text{if } k < 0 \end{cases} \tag{11.26a}$$

$$\widehat{\Delta}\,(k,\gamma) = \begin{cases} \Delta\,(k,\gamma) & \text{if } 0 \le k \\ \Delta\,(-k,\gamma-\pi) & \text{if } k < 0 \end{cases} \tag{11.26b}$$

$$\widehat{\Delta}_1(k,\gamma) = \begin{cases} \Delta_1(k,\gamma) & \text{if } 0 \le k \\ \Delta_1(-k,\gamma-\pi) & \text{if } k < 0 \end{cases} \tag{11.26c}$$

Expression (11.26b) yields

$$\widehat{\Delta}_k(k,\gamma) = \begin{cases} \Delta_k(k,\gamma) & \text{if } 0 \le k \\ -\Delta_k(-k,\gamma-\pi) & \text{if } k < 0 \end{cases} \tag{11.26d}$$

and the roots of the dispersion relation $\widehat{\Delta}(k,\gamma) = 0$ are $k = k_*(\gamma)$ and $k = -k_*(\gamma-\pi)$ where $0 \le \gamma \le \pi$ and $0 < k_*$.

The integral I^F defined by (11.25b) is of the form (11.3) and (11.11a) with the substitutions

$$x \longrightarrow x\,\cos\gamma + y\,\sin\gamma\ ,\ \ \alpha \longrightarrow k \text{ and } (\mathcal{A},\Delta,\Delta_1) \longrightarrow (\widehat{\mathcal{A}},\widehat{\Delta},\widehat{\Delta}_1)\ .$$

Moreover, expression (11.19) becomes

$$\mu_*(\gamma) = C/k_*(\gamma) \;\text{ with }\; C \approx 1/2\;. \tag{11.27}$$

Expressions (11.25-11.27) and (11.11) then yield

$$\phi^F(\mathbf{x}) = \frac{1}{\pi}\int_{-\pi}^{\pi} d\gamma \int_0^\infty dk\; \frac{\mathcal{A}(k,\gamma)\, e^{\,\mathrm{i}\,k\,(x\,\cos\gamma + y\,\sin\gamma)}}{\Delta\,(k,\gamma) + \mathrm{i}\,\epsilon\,\Delta_1(k,\gamma)} \tag{11.28a}$$

$$= \phi^W(\mathbf{x}) + \phi^L(\mathbf{x})\;. \tag{11.28b}$$

The wave component $\phi^W(\mathbf{x})$ in (11.28b) is given by

$$\begin{aligned}\phi^W = \mathrm{i}\int_0^\pi d\gamma \Big[&\Theta^+\, \frac{\mathcal{A}(k_*^+,\gamma)}{\Delta_k(k_*^+,\gamma)}\; e^{\,\mathrm{i}\,k_*^+\,(x\,\cos\gamma + y\,\sin\gamma)} \\ &- \Theta^-\, \frac{\mathcal{A}(k_*^-,\gamma-\pi)}{\Delta_k(k_*^-,\gamma-\pi)}\; e^{-\,\mathrm{i}\,k_*^-\,(x\,\cos\gamma + y\,\sin\gamma)} \Big]\end{aligned} \tag{11.29}$$

where $k_*^+ \equiv k_*(\gamma)$, $k_*^- \equiv k_*(\gamma-\pi)$,

$\Theta^+ \equiv \mathrm{erf}\,\big[k_*^+(x\cos\gamma + y\sin\gamma)/C\big] - \mathrm{sign}[\,\Delta_1(k_*^+,\gamma)\,\Delta_k(k_*^+,\gamma)]$,

$\Theta^- \equiv \mathrm{erf}\,\big[k_*^-(x\cos\gamma + y\sin\gamma)/C\big] + \mathrm{sign}[\,\Delta_1(k_*^-,\gamma-\pi)\,\Delta_k(k_*^-,\gamma-\pi)]$.

The change of variable $\gamma - \pi \to \gamma$ in the second term in (11.29) finally yields

$$\phi^W(\mathbf{x}) = \mathrm{i}\int_{-\pi}^{\pi} d\gamma\; \Theta\; \frac{\mathcal{A}(k_*,\gamma)}{\Delta_k(k_*,\gamma)}\; e^{\,\mathrm{i}\,k_*\,(x\,\cos\gamma + y\,\sin\gamma)} \tag{11.30a}$$

where $k_* = k_*(\gamma)$ and (11.30b)

$$\Theta \equiv \mathrm{erf}[\,k_*\,(x\cos\gamma + y\sin\gamma)/C\,] - \mathrm{sign}[\,\Delta_1(k_*,\gamma)\,\Delta_k(k_*,\gamma)]\;. \tag{11.30c}$$

The local-effect component $\phi^L(\mathbf{x})$ in (11.28b) is given by

$$\begin{aligned}\phi^L &= \frac{1}{\pi}\int_0^\pi d\gamma \int_{-\infty}^\infty dk\; \mathcal{A}^L(k,\gamma)\; e^{\,\mathrm{i}\,k\,(x\,\cos\gamma + y\,\sin\gamma)} \;\text{ where} \\ \mathcal{A}^L &= \frac{\widehat{\mathcal{A}}(k,\gamma)}{\widehat{\Delta}\,(k,\gamma)} - \frac{\mathcal{A}(k_*^+,\gamma)\; e^{-C^2(k/k_*^+ - 1)^2/4}}{(k-k_*^+)\,\Delta_k(k_*^+,\gamma)} \\ &\qquad + \frac{\mathcal{A}(k_*^-,\gamma-\pi)\; e^{-C^2(k/k_*^- + 1)^2/4}}{(k+k_*^-)\,\Delta_k(k_*^-,\gamma-\pi)}\;.\end{aligned} \tag{11.31}$$

The changes of variables $\gamma - \pi \to \gamma$ and $k \to -k$ in the lower half $0 \le \gamma \le \pi$, $-\infty < k \le 0$ of the region of integration in the integral (11.31) finally yield

$$\phi^L(\mathbf{x}) = \frac{1}{\pi}\int_{-\pi}^{\pi} d\gamma \int_0^\infty dk\ \mathcal{A}^L(k,\gamma)\ e^{\,\mathrm{i}\,k\,(x\,\cos\gamma + y\,\sin\gamma)} \tag{11.32a}$$

$$\text{where } \mathcal{A}^L = \frac{\mathcal{A}(k,\gamma)}{\Delta(k,\gamma)} - \frac{\mathcal{A}(k_*^+,\gamma)\ e^{-C^2(k/k_*^+-1)^2/4}}{(k-k_*^+)\,\Delta_k(k_*^+,\gamma)} + \frac{\mathcal{A}(k_*^-,\gamma-\pi)\,e^{-C^2(k/k_*^-+1)^2/4}}{(k+k_*^-)\,\Delta_k(k_*^-,\gamma-\pi)} \tag{11.32b}$$

$$\text{with } k_*^+ \equiv k_*(\gamma) \text{ and } k_*^- \equiv k_*(\gamma-\pi)\ . \tag{11.32c}$$

Summary

In summary, the general singular double Fourier integral defined by (11.28) is expressed as the sum of a wave component ϕ^W and a local-effect component ϕ^L. Thus, one has

$$\phi^F(\mathbf{x}) = \frac{1}{\pi}\int_{-\pi}^{\pi} d\gamma \int_0^\infty dk\ \frac{\mathcal{A}(k,\gamma)\ e^{\,\mathrm{i}\,k\,(x\,\cos\gamma + y\,\sin\gamma)}}{\Delta\,(k,\gamma) + \mathrm{i}\,\epsilon\,\Delta_1(k,\gamma)} \tag{11.33a}$$

$$= \phi^W(\mathbf{x}) + \phi^L(\mathbf{x})\ . \tag{11.33b}$$

The wave component ϕ^W in (11.33b) is expressed by (11.30) as

$$\phi^W(\mathbf{x}) = \mathrm{i}\int_{-\pi}^{\pi} d\gamma\ \Theta\ \frac{\mathcal{A}(k_*,\gamma)}{\Delta_k(k_*,\gamma)}\ e^{\,\mathrm{i}\,k_*\,(x\,\cos\gamma + y\,\sin\gamma)} \tag{11.34a}$$

$$\text{where } k_* = k_*(\gamma) \text{ and} \tag{11.34b}$$

$$\Theta \equiv \mathrm{erf}[\,k_*\,(x\cos\gamma + y\sin\gamma)/C\,] - \mathrm{sign}[\,\Delta_1(k_*,\gamma)\,\Delta_k(k_*,\gamma)]\ . \tag{11.34c}$$

The local-effect component ϕ^L in (11.33b) is expressed by (11.32) as

$$\phi^L(\mathbf{x}) = \frac{1}{\pi}\int_{-\pi}^{\pi} d\gamma \int_0^\infty dk\ \mathcal{A}^L(k,\gamma)\ e^{\,\mathrm{i}\,k\,(x\,\cos\gamma + y\,\sin\gamma)} \tag{11.35a}$$

$$\text{where } \mathcal{A}^L = \frac{\mathcal{A}(k,\gamma)}{\Delta(k,\gamma)} - \frac{\mathcal{A}(k_*^+\gamma)\ e^{-C^2(k/k_*^+-1)^2/4}}{(k-k_*^+)\,\Delta_k(k_*^+,\gamma)} + \frac{\mathcal{A}(k_*^-,\gamma-\pi)\ e^{-C^2(k/k_*^-+1)^2/4}}{(k+k_*^-)\,\Delta_k(k_*^-,\gamma-\pi)} \tag{11.35b}$$

$$\text{with } k_*^+ \equiv k_*(\gamma) \text{ and } k_*^- \equiv k_*(\gamma-\pi)\ . \tag{11.35c}$$

The function $\mathcal{A}^L(k,\gamma)$ is finite at the dispersion curve $k = k_*(\gamma)$ where the function $\mathcal{A}^L(k_*,\gamma) \equiv \mathcal{A}_*^L(\gamma) \equiv \mathcal{A}_*^L$ is given by

$$\mathcal{A}_*^L = \frac{\mathcal{A}_k(k_*^+,\gamma)}{\Delta_k(k_*^+,\gamma)} - \frac{\mathcal{A}(k_*^+,\gamma)\,\Delta_{kk}(k_*^+,\gamma)}{2\,\Delta_k^2(k_*^+,\gamma)} + \frac{\mathcal{A}(k_*^-,\gamma-\pi)\,e^{-C^2(k_*^+/k_*^-+1)^2/4}}{(k_*^+ + k_*^-)\,\Delta_k(k_*^-,\gamma-\pi)} \tag{11.35d}$$

Expressions (11.35) with $C \approx 1/2$ yield a smooth decomposition into waves and local effects.

11.7 Conclusion

Expressions (11.21-11.23) can be applied to a general amplitude function $\mathcal{A}(\alpha, \beta)$, i.e. a general applied forcing, and general dispersion functions $\Delta(\alpha, \beta)$ and $\Delta_1(\alpha, \beta)$ associated with dispersion curves $\Delta = 0$ expressed in the Cartesian form $\alpha = \alpha_*(\beta)$ with $-\infty < \beta < +\infty$. Expressions (11.33-11.35) similarly hold for a general amplitude function $\mathcal{A}(k,\gamma)$ and general dispersion functions $\Delta(k,\gamma)$ and $\Delta_1(k,\gamma)$ associated with a single closed dispersion curve $\Delta = 0$ that contains the origin $k = 0$ of the Fourier plane and is expressed in the polar form $k = k_*(\gamma)$ with $-\pi \leq \gamma \leq \pi$.

The fundamental relations (11.21-11.23) and (11.33-11.35) express the singular double Fourier integrals (11.21a) and (11.33a) in terms of wave components $\phi^W(\mathbf{x})$ and non-oscillatory local disturbances $\phi^L(\mathbf{x})$. These decompositions are exact and nearly optimal. The wave components ϕ^W in the decompositions (11.21b) and (11.33b) are expressed as single Fourier integrals along the dispersion curves defined by the dispersion relations $\Delta(\alpha, \beta) = 0$ or $\Delta(k,\gamma) = 0$, and the local-effects components ϕ^L are defined by double Fourier integrals with integrands that are everywhere finite, notably along the dispersion curves $\Delta = 0$ and at the origin $k = 0$ of the Fourier plane, and vanish as $k \to \infty$. Thus, the Fourier integrals that define the wave component ϕ^W and the local component ϕ^L in the decompositions $\phi^F = \phi^W + \phi^L$ are suited for accurate numerical evaluation.

Chapter 12

Waves and local flow created by a general singularity distribution

The fundamental analytical representations given in the previous chapter for a general dispersive medium and a general amplitude (Kochin) function are now applied to the specific dispersion functions Δ and Δ_1 that are associated with five classes of flows in ship and offshore hydrodynamics: diffraction-radiation of regular waves by offshore structures in water of uniform finite depth or in deep water, and flow around a ship that steadily advances in calm water or through regular waves in the regimes $0 \leq \tau < 1/4$ or $0.3 \leq \tau$.

The Fourier component ϕ^F, called Fourier potential in this chapter, in the Rankine-Fourier decomposition $\phi = \phi^R + \phi^F$ is considered for a *general* Kochin function; e.g. the Kochin functions A_F, A_H and A_Γ in (10.12) or the Kochin function associated with the Fourier-Kochin representation of the flow created by a distribution of singularities such as a distribution of sources over a flat triangle.

Thus, *exact* analytical representations of the Fourier potential ϕ^F as the sum of a wave component ϕ^W and a local-flow component ϕ^L are given in this chapter for five classes of flows in ship and offshore hydrodynamics. These flow representations provide a simple basis suited for accurate evaluation of the Fourier potential ϕ^F that corresponds to the Kochin function associated with a general distribution of singularities [**12,1**].

12.1 Diffraction-radiation of regular waves by offshore structures in finite water depth

The Fourier-Kochin representation (10.12) associated with diffraction-radiation of regular waves by an offshore structure in finite water-depth shows that the dispersion functions Δ and Δ_1 in (11.33a) are given by

$$\Delta(k) = 1 - (k/f^2)\tanh(k\,d) \quad \text{and} \quad \Delta_1 = 1\ . \tag{12.1a}$$

The dispersion relation $\Delta = 0$ has a single root $k = k_*$, which is determined by the equation

$$k_* \tanh(k_* d) = f^2\ . \tag{12.1b}$$

Thus, one has a single dispersion curve: the circle $k = k_*$ centered at the origin $k = 0$ of the Fourier plane.

Expression (10.12) shows that the Fourier-Kochin representation of the Fourier potential ϕ^F associated with the optimal Rankine-Fourier decomposition defined by (7.32) and (7.33) and a *general* Kochin function $A(k,\gamma)$ can be expressed as

$$\phi^F(\mathbf{x}) \equiv \frac{1}{\pi}\int_{-\pi}^{\pi} d\gamma \int_0^{\infty} dk\ \frac{\cosh(k\,d)}{e^{k\,d}/2}\ \frac{A^z(k,z)\ e^{\,\mathrm{i}\,(\alpha\,x+\beta\,y)}}{1-(k/f^2)\tanh(k\,d)+\mathrm{i}\,\epsilon}\ A(k,\gamma) \tag{12.2a}$$

where the function $A^z(k,z)$ is defined by expression (7.33c) as

$$A^z \equiv \left[1+\frac{k}{f^2}\right]\frac{\cosh[k(z+d)]}{2\cosh(k\,d)} + \left[\frac{1}{2} - e^{-k/f^2}\right]\left[1-\frac{k}{f^2}\tanh(k\,d)\right]e^{k\,z}\ . \tag{12.2b}$$

The function A^z also involves the water-depth d and the wave frequency f, but these two parameters are not explicitly noted for shortness. The Kochin function $A(k,\gamma)$ in (12.2a) can be associated with any distribution of singularities. In particular, A can be taken as the Kochin function associated with a distribution of sources or dipoles over a panel, or as the Kochin functions A_F, A_H or A_Γ in (10.12).

The Fourier potential ϕ^F defined by (12.2) is of the form (11.33a) with the function $\mathcal{A}(k,\gamma)$ defined as

$$\mathcal{A}(k,\gamma) \equiv \frac{\cosh(k\,d)}{e^{k\,d}/2}\ A^z(k,z)\ A(k,\gamma)\ . \tag{12.3}$$

Expressions (12.1a) show that one has

$$-\,f^2\,\Delta_k = \frac{\sinh(k\,d)+k\,d/\cosh(k\,d)}{\cosh(k\,d)} \quad \text{and} \quad -\,\mathrm{sign}(\Delta_1\,\Delta_k) = 1\ . \tag{12.4}$$

Fourier potential associated with a general Kochin function

Expressions (11.33-11.35) applied to (12.2a) yield

$$\phi^F(\mathbf{x}) \equiv \frac{1}{\pi}\int_{-\pi}^{\pi} d\gamma \int_0^\infty dk\, \frac{\cosh(k\,d)}{e^{\,k\,d}/2}\, \frac{A^z(k,z)\, e^{\,\mathrm{i}\,k\,(x\,\cos\gamma + y\,\sin\gamma)}}{1-(k/f^2)\tanh(kd)+\mathrm{i}\,\epsilon}\, A(k,\gamma) \quad (12.5a)$$

$$= \phi^W(\mathbf{x}) + \phi^L(\mathbf{x}) \ . \quad (12.5b)$$

The wave component ϕ^W in (12.5b) is given by

$$\frac{\mathrm{i}\,\phi^W(\mathbf{x})}{f^2} \equiv \widehat{A}_*\, A^z_* \int_{-\pi}^{\pi} d\gamma\, \Theta\, e^{\,\mathrm{i}\,k_*\,(x\,\cos\gamma + y\,\sin\gamma)}\, A_*(\gamma) \quad (12.6a)$$

$$\text{where } \ \Theta \equiv 1 + \mathrm{erf}[\,k_*\,(x\cos\gamma + y\sin\gamma)/C\,] \ , \quad (12.6b)$$

$A_*(\gamma) \equiv A(k=k_*,\gamma)$ and k_* is the root of the dispersion relation (12.1b). Moreover, A^z_* is defined by (12.2b) as

$$A^z_* \equiv A^z(k_*,z) = \frac{1+\tanh(k_*d)}{2\tanh(k_*d)}\, \frac{\cosh[k_*(z+d)]}{\cosh(k_*d)} \quad (12.6c)$$

$$\text{and } \ \widehat{A}_* \equiv \widehat{A}(k_*d) \equiv \frac{2\cosh^2(k_*d)/e^{\,k_*\,d}}{\sinh(k_*d)+k_*d/\cosh(k_*d)} \ . \quad (12.6d)$$

The local-flow component ϕ^L in (12.5b) is given by

$$\phi^L(\mathbf{x}) \equiv \frac{1}{\pi}\int_{-\pi}^{\pi} d\gamma \int_0^\infty dk\, e^{\,\mathrm{i}\,k\,(x\,\cos\gamma + y\,\sin\gamma)}\, A^L(k,\gamma) \ \text{ where} \quad (12.7a)$$

$$A^L(k,\gamma) \equiv \frac{\cosh(k\,d)}{e^{\,k\,d}/2}\, \frac{A^z(k,z)\, A(k,\gamma)}{1-(k/f^2)\tanh(k\,d)}$$

$$-\widehat{A}_*\, A^z_* \left[\frac{e^{-C^2(1-k/k_*)^2/4}}{k_*/f^2 - k/f^2}\, A_*(\gamma) + \frac{e^{-C^2(1+k/k_*)^2/4}}{k_*/f^2 + k/f^2}\, A_*(\gamma-\pi) \right] . \quad (12.7b)$$

In the common case of an amplitude function $A(k,\gamma)$ that satisfies the relation $A(k,\gamma-\pi) = \overline{A(k,\gamma)}$ where an overline means complex conjugate, the change of variable $\gamma \to \gamma-\pi$ in the portion $-\pi \le \gamma \le 0$ of the range of integration in the Fourier integral (12.7a) yields

$$\phi^L(\mathbf{x}) \equiv \frac{2}{\pi}\,\mathrm{Re}\int_0^{\pi} d\gamma \int_0^\infty dk\, e^{\,\mathrm{i}\,k\,(x\,\cos\gamma + y\,\sin\gamma)}\, A^L(k,\gamma) \quad (12.7c)$$

where $A^L(k,\gamma)$ is given by (12.7b).

A nearly optimal waves and local-flow decomposition $\phi^W + \phi^L$ is obtained if $C \approx 1/2$. The function $A(k,\gamma)$ in (12.5a), (12.6a) and (12.7b) denotes a general amplitude function, notably the Kochin function associated with any distribution of singularities. The general flow representation (12.5-12.7) is associated with the optimal Rankine-Fourier decomposition defined by (7.32) and (7.33).

Deep-water limit

In the deep-water limit $d \to \infty$, the dispersion function (12.1a) and the radius k_* of the dispersion circle defined by the root of the dispersion relation (12.1b) become

$$\Delta = 1 - k/f^2 \quad \text{and} \quad k_* = f^2 \ .$$

This expression for k_* and expressions (12.6d), (12.6c) and (12.2b) yield

$$\widehat{A}_* = 1 \ , \ \ A^z_* = e^{\,f^2 z} \ \text{ and } \ A^z = \Big[1 + e^{-k/f^2}(k/f^2 - 1)\Big]\, e^{\,k\,z} \ .$$

Expressions (12.5) then become

$$\begin{aligned} \phi^F(\mathbf{x}) &\equiv \frac{1}{\pi}\int_{-\pi}^{\pi} d\gamma \int_0^\infty dk\, \frac{1 - e^{-k/f^2}(1 - k/f^2)}{1 - k/f^2 + \mathrm{i}\,\epsilon}\, e^{\,k\,z + \mathrm{i}\,k\,(x\,\cos\gamma + y\,\sin\gamma)} A(k,\gamma) \\ &= \phi^W(\mathbf{x}) + \phi^L(\mathbf{x}) \ . \end{aligned} \tag{12.8}$$

The wave component ϕ^W in (12.8) is determined by (12.6) as

$$\frac{\mathrm{i}\,\phi^W(\mathbf{x})}{f^2} \equiv e^{\,f^2 z} \int_{-\pi}^{\pi} d\gamma\, \Theta\, e^{\,\mathrm{i}\,f^2\,(x\,\cos\gamma + y\,\sin\gamma)}\, A_*(\gamma) \tag{12.9a}$$

$$\text{where } \ \Theta \equiv 1 + \mathrm{erf}[\, f^2(x\cos\gamma + y\sin\gamma)/C\,] \tag{12.9b}$$

and $A_*(\gamma) \equiv A(k = f^2, \gamma)$. Finally, the local-flow component ϕ^L in (12.8) is determined by (12.7) as

$$\phi^L(\mathbf{x}) \equiv \frac{1}{\pi}\int_{-\pi}^{\pi} d\gamma \int_0^\infty dk\, e^{\,\mathrm{i}\,k\,(x\,\cos\gamma + y\,\sin\gamma)}\, A^L(k,\gamma) \ \text{ where} \tag{12.10a}$$

$$\begin{aligned} A^L(k,\gamma) &\equiv \frac{1 - e^{-k/f^2}(1 - k/f^2)}{1 - k/f^2}\, e^{\,k\,z}\, A(k,\gamma) \\ &- e^{\,f^2 z}\left[\frac{e^{-C^2(1-k/f^2)^2/4}}{1 - k/f^2}\, A_*(\gamma) + \frac{e^{-C^2(1+k/f^2)^2/4}}{1 + k/f^2}\, A_*(\gamma - \pi)\right] . \end{aligned} \tag{12.10b}$$

If the amplitude function $A(k,\gamma)$ satisfies the relation $A(k,\gamma - \pi) = \overline{A(k,\gamma)}$, (12.10a) becomes

$$\phi^L(\mathbf{x}) \equiv \frac{2}{\pi}\,\mathrm{Re}\int_0^{\pi} d\gamma \int_0^\infty dk\, e^{\,\mathrm{i}\,k\,(x\,\cos\gamma + y\,\sin\gamma)}\, A^L(k,\gamma) \tag{12.10c}$$

where $A^L(k,\gamma)$ is given by (12.10b). Expressions (12.8-12.10), obtained in the foregoing as the deep-water limit of (12.5-12.7), evidently can also be obtained from (11.33-11.35).

12.2 Ship steadily advancing in calm water

The optimal Rankine-Fourier decomposition (7.16) of the Green function associated with a ship that steadily advances in calm water is used in this section. The polar representation (7.16b) of the Fourier component G^F is expressed in the equivalent Cartesian form

$$G^F = \frac{1}{\pi}\int_{-\infty}^{\infty} d\beta \int_{-\infty}^{\infty} d\alpha \; \widehat{A}(\alpha,\beta)\; \frac{e^{\,k\,(z+\zeta)\,+\,\mathrm{i}\,[\,\alpha\,(x-\xi)\,+\,\beta\,(y-\eta)\,]}}{\Delta\,(\alpha,\beta) + \mathrm{i}\,\epsilon\,\Delta_1(\alpha,\beta)} \tag{12.11}$$

where the function $\widehat{A}(\alpha,\beta)$ and the dispersion functions $\Delta\,(\alpha,\beta)$ and $\Delta_1(\alpha,\beta)$ are given by

$$\widehat{A}(\alpha,\beta) \equiv 1 + e^{-F^2 k}(F^2\alpha^2/k - 1)\;, \tag{12.12a}$$

$$\Delta\,(\alpha,\beta) \equiv F^2\alpha^2 - k \quad \text{and} \quad \Delta_1(\alpha,\beta) \equiv \mathrm{sign}(\alpha)\;. \tag{12.12b}$$

These expressions show that the value $\widehat{A}_*$ of the function $\widehat{A}$ at a dispersion curve $\Delta = 0$ is

$$\widehat{A}_* = 1\;. \tag{12.12c}$$

The Fourier-Kochin representation of the Fourier component $\phi^F(\mathbf{x})$ that corresponds to the Fourier component (12.11) associated with an optimal Rankine-Fourier decomposition $G^R + G^F$ of G is then defined as

$$\phi^F(\mathbf{x}) = \frac{1}{\pi}\int_{-\infty}^{\infty} d\beta \int_{-\infty}^{\infty} d\alpha \; \frac{\widehat{A}(\alpha,\beta)\; e^{\,k\,z\,+\,\mathrm{i}\,(\alpha\,x\,+\,\beta\,y)}}{F^2\alpha^2 - k + \mathrm{i}\,\epsilon\,\mathrm{sign}(\alpha)}\; A(\alpha,\beta) \tag{12.13}$$

where $A(\alpha,\beta)$ is a Kochin function associated with a general distribution of singularities and $\widehat{A}(\alpha,\beta)$ is defined by (12.12a).

The dispersion relation $\Delta\,(\alpha,\beta) = 0$ defines two dispersion curves, which are symmetric about the axis $\alpha = 0$ and are expressed in the Cartesian form

$$\alpha = \pm\alpha_*(\beta) \;\text{ where }\; F^2\alpha_* \equiv \sqrt{1/2 + \sqrt{1/4 + (F^2\beta)^2}} \tag{12.14}$$

and $-\infty < \beta < \infty$. These dispersion curves are depicted in Fig.4.1.

At the dispersion curves $\alpha = \pm\alpha_*$, one has

$$\Delta^*_\alpha = \frac{2(F^2\alpha)^2 - 1}{F^2\alpha}\;,\; \mathrm{sign}(\Delta^*_\alpha) = \mathrm{sign}(\alpha) \text{ and } \mathrm{sign}(\Delta^*_1\,\Delta^*_\alpha) = 1 \tag{12.15}$$

where (12.12b) was used.

The wave component ϕ^W that corresponds to the Fourier potential ϕ^F defined by (12.13) is determined from expressions (11.22), (12.12a), (12.12c)

and (12.15) as

$$\mathrm{i}\,\phi^W(\mathbf{x}) = \int_{-\infty}^{\infty} d\beta\,[1-\mathrm{erf}(\alpha_*\,x/C)]\,\frac{e^{F^2\alpha_*^2\,z+\mathrm{i}\,(\alpha_*\,x+\beta\,y)}}{2F^2\alpha_* - 1/(F^2\alpha_*)}\,A(\alpha_*,\beta) \\ -\int_{-\infty}^{\infty} d\beta\,[1-\mathrm{erf}(\alpha_*\,x/C)]\,\frac{e^{F^2\alpha_*^2\,z-\mathrm{i}\,(\alpha_*\,x+\beta\,y)}}{2F^2\alpha_* - 1/(F^2\alpha_*)}\,A(-\alpha_*,-\beta)$$

where the change of variable $\beta \to -\beta$ was made in the last integral. The change of variable $F^2\beta = q\,\sqrt{1+q^2}$ yields $F^2\alpha_* = \sqrt{1+q^2}$ and expressions (12.17), given further on.

The local-flow component ϕ^L that corresponds to the Fourier potential ϕ^F and the wave component ϕ^W is determined from expression (11.23) as

$$\phi^L(\mathbf{x}) = \frac{1}{\pi}\int_{-\infty}^{\infty} d\beta \int_{-\infty}^{\infty} d\alpha\; e^{\mathrm{i}\,(\alpha\,x+\beta\,y)}\,A^L(\alpha,\beta) \;\; \text{where}$$

$$A^L(\alpha,\beta) = \frac{\widehat{A}(\alpha,\beta)\,e^{k\,z}}{F^2\alpha^2-k}\,A(\alpha,\beta) \\ -\frac{e^{F^2\alpha_*^2\,z-C^2(1-\alpha/\alpha_*)^2/4}A(\alpha_*,\beta)}{(\alpha-\alpha_*)\,[\,2F^2\alpha_* - 1/(F^2\alpha_*)\,]} + \frac{e^{F^2\alpha_*^2\,z-C^2(1+\alpha/\alpha_*)^2/4}A(-\alpha_*,\beta)}{(\alpha+\alpha_*)\,[\,2F^2\alpha_* - 1/(F^2\alpha_*)\,]}\;.$$

Expressions (12.12a) and (12.14) for the functions $\widehat{A}(\alpha,\beta)$ and $\alpha_*(\beta)$ yield expressions (12.18), given further on.

Fourier potential associated with a general Kochin function

In summary, one has

$$\phi^F(\mathbf{x}) \equiv \frac{1}{\pi}\int_{-\infty}^{\infty} d\beta \int_{-\infty}^{\infty} d\alpha\;\frac{1+e^{-F^2k}\,(F^2\alpha^2/k-1)}{F^2\alpha^2-k+\mathrm{i}\,\epsilon\,\mathrm{sign}(\alpha)}\,e^{k\,z+\mathrm{i}\,(\alpha\,x+\beta\,y)}\,A(\alpha,\beta) \\ = \phi^W(\mathbf{x}) + \phi^L(\mathbf{x})\;. \qquad (12.16)$$

The wave potential ϕ^W in (12.16) is given by

$$\mathrm{i}\,F^2\phi^W(\mathbf{x}) = \int_{-\infty}^{\infty} dq\,\Big[1-\mathrm{erf}\Big(\sqrt{1+q^2}\,(x/F^2)/C\Big)\Big]\,e^{(1+q^2)\,z/F^2} \\ \Big[\,e^{\mathrm{i}\,\sqrt{1+q^2}\,(x+q\,y)/F^2}A^+(q) - e^{-\mathrm{i}\,\sqrt{1+q^2}\,(x+q\,y)/F^2}A^-(q)\Big] \\ \text{with}\;\; A^{\pm}(q) \equiv A\Big(\alpha = \pm\sqrt{1+q^2}/F^2,\,\beta = \pm\,q\,\sqrt{1+q^2}/F^2\Big)\;. \qquad (12.17)$$

The local-flow potential ϕ^L in (12.16) is given by

$$\phi^L(\mathbf{x}) = \frac{1}{\pi}\int_{-\pi}^{\pi} d\gamma \int_0^\infty dk\; e^{\,\mathrm{i}\,k\,(x\cos\gamma + y\sin\gamma)}\, A^L(\alpha,\beta) \;\text{ where} \tag{12.18a}$$

$$\begin{aligned} A^L(\alpha,\beta) &\equiv \frac{1+e^{-F^2 k}\,(F^2\alpha^2/k-1)}{F^2\alpha^2/k-1}\; e^{k\,z} A(\alpha,\beta) \\ &+ \frac{e^{\,F^2\alpha_*^2\, z - C^2(1-\alpha/\alpha_*)^2/4} A(\alpha_*,\beta)}{(1-\alpha/\alpha_*)\sqrt{1+4\,(F^2\beta)^2}/(F^2 k)} + \frac{e^{\,F^2\alpha_*^2\, z - C^2(1+\alpha/\alpha_*)^2/4} A(-\alpha_*,\beta)}{(1+\alpha/\alpha_*)\sqrt{1+4\,(F^2\beta)^2}/(F^2 k)} \\ \text{with }\; F^2\alpha_* &= \sqrt{1/2+\sqrt{1/4+(F^2\beta)^2}}\;,\; (\alpha,\beta) = k\,(\cos\gamma,\sin\gamma)\;. \end{aligned} \tag{12.18b}$$

In the common case of an amplitude function $A(\alpha,\beta)$ that satisfies the relation $A(-\alpha,-\beta) = \overline{A(\alpha,\beta)}$ where an overline means complex conjugate, (12.17) can be simplified as

$$F^2\phi^W(\mathbf{x}) = 2\,\mathrm{Im}\int_{-\infty}^{\infty} dq\;\Theta\; e^{\,(1+q^2)\,z/F^2 + \mathrm{i}\sqrt{1+q^2}\,(x+q\,y)/F^2} A(q) \tag{12.19a}$$

$$\text{where }\; \Theta \equiv 1-\mathrm{erf}\Big[\sqrt{1+q^2}\,(x/F^2)/C\Big] \;\text{ and} \tag{12.19b}$$

$$A(q) \equiv A\Big(\alpha = \sqrt{1+q^2}/F^2,\, \beta = q\sqrt{1+q^2}/F^2\Big)\;. \tag{12.19c}$$

Similarly, the change of variable $\gamma \to \gamma - \pi$ in the portion $-\pi \le \gamma \le 0$ of the range of integration in the integral (12.18a) yields

$$\phi^L(\mathbf{x}) = \frac{2}{\pi}\,\mathrm{Re}\int_0^{\pi} d\gamma \int_0^\infty dk\; e^{\,\mathrm{i}\,k\,(x\cos\gamma + y\sin\gamma)}\, A^L(\alpha,\beta) \tag{12.19d}$$

where $A^L(\alpha,\beta)$ is given by (12.18b).

12.3 Ship advancing through regular waves in the regime $0.3 \le \tau$

Expressions (7.6) for the Green function associated with a ship that steadily advances through regular waves are used in this section. Section 7.6 shows that these expressions yield an optimal Rankine-Fourier decomposition. The polar representation (7.6c) of the Fourier component G^F in the Rankine-Fourier decomposition (7.6a) is expressed in the equivalent Cartesian form

$$G^F = \frac{1}{\pi}\int_{-\infty}^{\infty} d\beta \int_{-\infty}^{\infty} d\alpha\; \frac{e^{\,k\,(z+\zeta)\,+\,\mathrm{i}\,[\,\alpha\,(x-\xi)\,+\,\beta\,(y-\eta)\,]}}{\Delta\,(\alpha,\beta) + \mathrm{i}\,\epsilon\,\Delta_1(\alpha,\beta)} \tag{12.20}$$

where $k \equiv \sqrt{\alpha^2+\beta^2}$ and the dispersion functions Δ and Δ_1 are given by

$$\Delta\,(\alpha,\beta) \equiv (f+F\alpha)^2 - k \;\text{ and }\; \Delta_1(\alpha,\beta) \equiv \mathrm{sign}(f+F\alpha)\;. \tag{12.21}$$

As in the case of a ship that steadily advances in calm water considered in the previous section, the dispersion relation $\Delta = 0$ defines two open dispersion curves if $1/4 < \tau$. These two dispersion curves, identified as O^- and IO^+ in chapter 5, are located in the regions

$$-\infty < \alpha \leq -k_o^- \text{ and } -k_i^- \leq \alpha < \infty \tag{12.22}$$

where the basic wavenumbers k_o^- and k_i^- are given by (5.8). A constant-β line intersects the dispersion curve O^- at a single point, and this dispersion curve can be represented in the Cartesian form $\alpha = \alpha_*^-(\beta)$ for every value of τ in the range $1/4 < \tau$. However, a constant-β line intersects the dispersion curve IO^+ at three points if $1/4 < \tau \leq \sqrt{2/27} \approx 0.272$ or at a single point if $\sqrt{2/27} < \tau$, as is illustrated in Fig.5.6. This dispersion curve can only be conveniently represented in the Cartesian form $\alpha = \alpha_*^+(\beta)$ if $\tau^\ell \leq \tau$ with $\tau^\ell \approx 0.3$, as is shown in chapter 5.

The regime $0.3 \leq \tau$ is considered in this section, and the two dispersion curves O^- and IO^+ are represented in the Cartesian form

$$\alpha = \alpha_*^-(\beta) \text{ or } \alpha = \alpha_*^+(\beta) \text{ where } -\infty < \beta < \infty \tag{12.23a}$$

and the functions $\alpha_*^\pm(\beta)$ are defined by (5.30) and (5.31). These dispersion curves are depicted in Fig.5.4 and Fig.5.5. The wavenumbers $k_*^\pm(\beta)$ that correspond to the roots $\alpha_*^\pm(\beta)$ are given by

$$k_*^\pm(\beta) = \sqrt{[\,\alpha_*^\pm(\beta)]^2 + \beta^2}\,. \tag{12.23b}$$

Expressions (12.21) yield

$$\Delta_\alpha(\alpha,\beta) = 2\,(\tau + F^2\alpha) - \alpha/k \text{ and } \Delta_1(\alpha,\beta) = \text{sign}(\tau + F^2\alpha)\,. \tag{12.23c}$$

At the dispersion curves $\alpha = \alpha_*^\pm(\beta)$, one has

$$F^2\alpha_*^+ \geq F^2\alpha_*^+(\beta = 0) \equiv -\left(\sqrt{1/4+\tau} - 1/2\right)^2 \text{ and}$$
$$F^2\alpha_*^- \leq F^2\alpha_*^-(\beta = 0) \equiv -\left(\sqrt{1/4+\tau} + 1/2\right)^2$$

where $\alpha_*^\pm(\beta = 0)$ are the roots of the dispersion relation $(f + F\alpha)^2 + \alpha = 0$ for $\beta = 0$. One has

$$\tau + F^2\alpha_*^+ \geq \sqrt{1/4+\tau} - 1/2 > 0\ ,$$
$$\tau + F^2\alpha_*^- \leq -(\sqrt{1/4+\tau} + 1/2) < 0 \text{ and}$$
$$\Delta_\alpha(\alpha_*^-,\beta) \equiv 2\,(\tau + F^2\alpha_*^-) - \alpha_*^-/k_*^- \leq -\sqrt{1+4\tau} < 0$$

where the relation $\alpha_*^-/k_*^- \geq -1$ was used. Moreover, the dispersion relation $(f + F\alpha_*^+)^2 - k_*^+ = 0$ yields

$$\Delta_\alpha(\alpha_*^+,\beta) = 2\,(\tau + F^2\alpha_*^+) - F^2\alpha_*^+/(\tau + F^2\alpha_*^+)^2\,.$$

The function $N(\widehat{\alpha}) \equiv 2\,(\tau + \widehat{\alpha})^3 - \widehat{\alpha}$ is considered for

$$-(\sqrt{1/4+\tau} - 1/2)^2 \leq \widehat{\alpha} \equiv F^2 \alpha_*^+ \ .$$

It can be verified that one has

$$N(\widehat{\alpha}) \geq N(\widehat{\alpha}_0) \equiv \tau - \sqrt{2/27} > 0 \ \text{ where } \ \widehat{\alpha}_0 \equiv 1/\sqrt{6} - \tau \ ,$$

$N'(\widehat{\alpha}) = 0$ and $N''(\widehat{\alpha}) > 0$. One then has $\Delta_\alpha(\alpha_*^+, \beta) > 0$, and

$$\pm\, \Delta_\alpha(\alpha_*^\pm, \beta) > 0 \ \text{ and } \ \pm\, \Delta_1(\alpha_*^\pm, \beta) > 0 \ . \tag{12.23d}$$

Fourier potential associated with a general Kochin function

Expression (12.20) for the Fourier component G^F in the Rankine-Fourier decomposition of the Green function appropriate for a ship that advances through regular waves shows that the Fourier potential ϕ^F that corresponds to a Kochin function $A(\alpha, \beta)$ associated with a given singularity distribution can be expressed as

$$\phi^F(\mathbf{x}) = \frac{1}{\pi} \int_{-\infty}^{\infty} d\beta \int_{-\infty}^{\infty} d\alpha \ \frac{e^{\,k\,z\,+\,\mathrm{i}\,(\alpha\,x\,+\,\beta\,y)}\ A(\alpha,\beta)}{(f+F\alpha)^2 - k + \mathrm{i}\,\epsilon\,\mathrm{sign}(f+F\alpha)} \ . \tag{12.24a}$$

This expression for the Fourier potential ϕ^F is of the form (11.21) and the wave and local-flow potentials ϕ^W and ϕ^L in the decomposition

$$\phi^F(\mathbf{x}) = \phi^W(\mathbf{x}) + \phi^L(\mathbf{x}) \tag{12.24b}$$

can then be obtained from expressions (11.22) and (11.23).

Specifically, the wave potential ϕ^W in expression (12.24b) is determined by (11.22) and (12.23c-d) as

$$\begin{aligned} \mathrm{i}\,\phi^W(\mathbf{x}) = \int_{-\infty}^{\infty} d\beta \Bigg[& \frac{1 - \mathrm{erf}(\alpha_m^+\, x/C)}{2\,(\tau + F^2\alpha_*^+) - \alpha_*^+/k_*^+}\ e^{\,k_*^+ z\,+\,\mathrm{i}\,(\alpha_*^+ x\,+\,\beta\,y)}\ A(\alpha_*^+, \beta) \\ & + \frac{1 + \mathrm{erf}(\alpha_*^-\, x/C)}{2\,(\tau + F^2\alpha_*^-) - \alpha_*^-/k_*^-}\ e^{\,k_*^- z\,+\,\mathrm{i}\,(\alpha_*^- x\,+\,\beta\,y)}\ A(\alpha_*^-, \beta) \Bigg] \end{aligned}$$

$$\text{where } \alpha_m^+(\beta) \equiv \sqrt{(\alpha_*^+)^2 + (k_i^-)^2} \text{ with } k_i^- = f^2/(\sqrt{1/4+\tau} + 1/2)^2 \ . \tag{12.25}$$

Moreover, $\alpha_*^\pm(\beta)$ and $k_*^\pm(\beta)$ are given by (12.23a-b). The modified root α_m^+ is used for the dispersion curve IO^+ because this curve crosses the axis $\alpha = 0$ in accordance with (12.22) and as is illustrated in Fig.5.6. The small wavenumber α_s in expression (11.22c) is taken as the smallest wavenumber k_i^- associated with the dispersion curve IO^+ in (12.25).

The local-flow potential ϕ^L in expression (12.24b) is determined by (11.23) and (12.23c-d) as

$$\phi^L(\mathbf{x}) \equiv \frac{1}{\pi}\int_{-\pi}^{\pi} d\gamma \int_0^\infty dk\; e^{\,\mathrm{i}\,k\,(x\cos\gamma + y\sin\gamma)}\, A^L(\alpha,\beta) \quad \text{where} \tag{12.26a}$$

$$A^L(\alpha,\beta) \equiv \frac{e^{\,k\,z}\, A(\alpha,\beta)}{(f+F\alpha)^2/k - 1} - \frac{e^{\,k_*^+ z - C^2(\alpha-\alpha_*^+)^2/(2\,\alpha_m^+)^2} A(\alpha_*^+,\beta)}{[\,2\,(\tau + F^2\alpha_*^+) - \alpha_*^+/k_*^+\,](\alpha-\alpha_*^+)/k}$$
$$- \frac{e^{\,k_*^- z - C^2(1-\alpha/\alpha_*^-)^2/4}\, A(\alpha_*^-,\beta)}{[\,2\,(\tau + F^2\alpha_*^-) - \alpha_*^-/k_*^-\,](\alpha-\alpha_*^-)/k}$$

$$\text{and } (\alpha,\beta) = k\,(\cos\gamma, \sin\gamma)\;. \tag{12.26b}$$

The Kochin function $A(\alpha,\beta)$ in the Fourier potential ϕ^F and in the corresponding wave and local-flow potentials defined by (12.24a), (12.25) and (12.26) is general. These expressions can then readily be applied to evaluate the waves and the local flow created by any given distribution of singularities. The decomposition (12.24b) is nearly optimal if $C \approx 1/2$.

12.4 Ship advancing through regular waves in the regime $0 \le \tau < 1/4$

Ships advancing through regular waves in the regime $0 \le \tau < 1/4$ are now considered. Two Rankine-Fourier decompositions $G^R + G^F$ of the Green function G associated with this class of flows are given in chapter 7. The Rankine components G^R in these alternative decompositions are defined by (7.42a) or (7.43a-c), which involves two additional elementary Rankine sources. The Fourier components G^F that correspond to these alternative Rankine components G^R are defined by (7.6c) or (7.46) as

$$G^F = \frac{1}{\pi}\int_{-\pi}^{\pi} d\gamma \int_0^\infty dk\; \frac{\widehat{A}(k,\gamma)\; e^{\,k\,(z+\zeta) + \mathrm{i}\,[\,\alpha\,(x-\xi) + \beta\,(y-\eta)\,]}}{(f+F\alpha)^2/k - 1 + \mathrm{i}\,\epsilon\,\mathrm{sign}(f+F\alpha)} \quad \text{where} \tag{12.27a}$$

$$\widehat{A}(k,\gamma) \equiv 1 \;\text{ if }\; G^R = -1/r + 1/r' \quad \text{or} \tag{12.27b}$$

$$\widehat{A}(k,\gamma) \equiv 1 + e^{-F^2 k}\,(1 - e^{-k/f^2})\,[(f+F\alpha)^2/k - 1] \tag{12.27c}$$

$$\text{if }\; G^R = -1/r + 1/r' - 2/r^F + 2/r^{Ff} \tag{12.27d}$$

with r, r', r^F and r^{Ff} given by (7.43b-c). The two alternative representations of the Green function G associated with expressions (12.27b) or (12.27c-d) both correspond to optimal Rankine-Fourier decompositions of the Green function G appropriate for a ship that advances through regular waves.

One has $\widehat{A} = 1$ in (12.27b) and the Rankine component G^R in (12.27b) only contains two Rankine sources, which do not involve the Froude number

F or the (adimensional) wave frequency f. This simpler Rankine-Fourier decomposition is then preferable to the alternative decomposition associated with the Rankine component (12.27d), which involves the two additional Rankine sources $1/r^F$ and $1/r^{Ff}$ that depend on F and f, for most practical applications. Indeed, the simpler Rankine-Fourier decomposition (12.27b) is used in sections 10.1-5.

However, in the limits $F \to 0$ or $f \to 0$, the Rankine-Fourier decomposition $G^R + G^F$ that is associated with the somewhat more complicated Rankine component G^R and function $\widehat{A}$ given by (12.27c-d) is consistent with the optimal Rankine-Fourier decompositions that are given in chapter 7 for the special cases $f = 0$ or $F = 0$. Specifically, the Rankine-Fourier representation (7.44), (7.43) and (7.46) of the Green function associated with a ship steadily advancing through regular waves is consistent with the Rankine-Fourier representations (7.16) and (7.25) that correspond to the special cases $f = 0$ or $F = 0$, whereas these Rankine-Fourier decompositions are not consistent with the limits $f \to 0$ or $F \to 0$ of the simpler Rankine-Fourier decomposition (12.27b) as is shown in section 7.7.

Expression (12.27a) for the Fourier component G^F is considered in this section for a general function $\widehat{A}$ that can be taken as $\widehat{A} = 1$ in accordance with (12.27b) or as the function defined by (12.27c). In the latter case, the value of the function $\widehat{A}$ at the dispersion curves defined by the dispersion relation $(f + F\alpha)^2 = k$ is

$$\widehat{A}_* = 1 \ . \tag{12.28}$$

The Fourier potential $\phi^F(\mathbf{x})$ that corresponds to the Fourier component G^F defined by (12.27a) and a Kochin function $A(\alpha, \beta)$ associated with a general distribution of singularities is then expressed as

$$\phi^F(\mathbf{x}) = \frac{1}{\pi} \int_{-\pi}^{\pi} d\gamma \int_0^\infty dk \ \frac{\widehat{A}(k,\gamma)\, e^{\,k\,z\,+\,\mathrm{i}\,(\alpha\,x\,+\,\beta\,y)}\, A(\alpha,\beta)}{(f+F\alpha)^2/k - 1 + \mathrm{i}\,\epsilon\,\mathrm{sign}(f+F\alpha)} \ . \tag{12.29}$$

In the regime $0 \leq \tau < 1/4$ that is considered in this section, the general Fourier potential (12.29) can be decomposed as

$$\phi^F(\mathbf{x}) = \phi_i^F(\mathbf{x}) + \phi_o^F(\mathbf{x}) \tag{12.30}$$

where the components ϕ_i^F and ϕ_o^F correspond to the components G_i^F and G_o^F in the fundamental decomposition of the Fourier component G^F that is defined by expressions (7.53) as

$$G^F = G_i^F + G_o^F \quad \text{where} \tag{12.31a}$$

$$G_i^F \equiv \frac{1}{\pi} \int_{-\pi}^{\pi} d\gamma \int_0^\infty dk \ \frac{k\,\widehat{A}(k,\gamma)}{\sqrt{1 - 4\,\tau\cos\gamma}} \ \frac{e^{\,k\,(z+\zeta)\,+\,\mathrm{i}\,[\,\alpha\,(x-\xi)\,+\,\beta\,(y-\eta)\,]}}{k_*^i(\gamma) - k + \mathrm{i}\,\epsilon} \ , \tag{12.31b}$$

$$G_o^F \equiv \frac{1}{\pi} \int_{-\pi}^{\pi} d\gamma \int_0^\infty dk \ \frac{k\,\widehat{A}(k,\gamma)}{\sqrt{1 - 4\,\tau\cos\gamma}} \ \frac{e^{\,k\,(z+\zeta)\,+\,\mathrm{i}\,[\,\alpha\,(x-\xi)\,+\,\beta\,(y-\eta)\,]}}{k - k_*^o(\gamma) + \mathrm{i}\,\epsilon\,\mathrm{sign}(\cos\gamma)} \ . \tag{12.31c}$$

The functions $k_*^i \equiv k_*^i(\gamma)$ and $k_*^o \equiv k_*^o(\gamma)$ in (12.31b) or (12.31c) are given by

$$k_*^i/f^2 \equiv 1/(\sqrt{1/4 - \tau\cos\gamma} + 1/2)^2 \quad \text{and} \tag{12.31d}$$

$$F^2 k_*^o \equiv (\sqrt{1/4 - \tau\cos\gamma} + 1/2)^2/\cos^2\gamma \; . \tag{12.31e}$$

Expressions (12.31a-c) readily show that the Fourier potentials $\phi_i^F(\mathbf{x})$ and $\phi_o^F(\mathbf{x})$ in (12.30) are given by

$$\phi_i^F = \frac{1}{\pi}\int_{-\pi}^{\pi} d\gamma \int_0^\infty dk \; \frac{\widehat{A}(k,\gamma)\, k/k_*^i}{\sqrt{1-4\tau\cos\gamma}} \; \frac{e^{k\,z\,+\,\mathrm{i}\,k\,(x\,\cos\gamma\,+\,y\,\sin\gamma)}}{1 - k/k_*^i + \mathrm{i}\,\epsilon} \, A(\alpha,\beta) \; , \tag{12.32a}$$

$$\phi_o^F = \frac{1}{\pi}\int_{-\pi}^{\pi} d\gamma \int_0^\infty dk \; \frac{\widehat{A}(k,\gamma)\, k/k_*^o}{\sqrt{1-4\tau\cos\gamma}} \; \frac{e^{k\,z\,+\,\mathrm{i}\,k\,(x\,\cos\gamma\,+\,y\,\sin\gamma)}}{k/k_*^o - 1 + \mathrm{i}\,\epsilon\,\mathrm{sign}(\cos\gamma)} \, A(\alpha,\beta) \; . \tag{12.32b}$$

The components G_i^F and G_o^F in (12.31a) and the corresponding Fourier potentials (12.32a) and (12.32b) are associated with the inner dispersion curve I located in the inner region $-k_i^- \le \alpha \le k_i^+$ or the outer dispersion curves O^- and O^+ located in the two outer regions $-\infty < \alpha \le -k_o^-$ and $k_o^+ \le \alpha < \infty$ where $k_i^\pm$ and $k_o^\pm$ are defined by (5.8). As is shown in chapter 5 and is illustrated in Fig.5.9 and Fig.5.10, the inner dispersion curve I and the corresponding Fourier potential ϕ_i^F are associated with a system of ring waves that are best scaled with respect to the wave frequency ω, whereas the outer dispersion curves O^+ and O^- and the related Fourier potential ϕ_o^F are associated with two systems of Kelvin-like V waves best scaled with respect to the ship speed V_s.

Wave potential ϕ_i^W associated with ring waves

The closed inner dispersion curve I is conveniently represented in the polar form $k = k_*^i(\gamma)$ where $k_*^i(\gamma)$ is given by (12.31d). The Fourier potential ϕ_i^F associated with the contribution of the inner dispersion curve I and defined by (12.32a) is of the form (11.33a) with

$$\Delta = \sqrt{1-4\tau\cos\gamma}\,(k_*^i - k) \;\; , \;\; \Delta_1 = 1 \tag{12.33a}$$

$$\text{and} \;\; \mathcal{A}(k,\gamma) = \widehat{A}(k,\gamma)\, e^{k\,z}\, k\, A(k,\gamma) \; . \tag{12.33b}$$

One then has

$$\Delta_k = -\sqrt{1-4\tau\cos\gamma} \;\text{ and }\; \mathrm{sign}(\Delta_1\,\Delta_k) = -1 \; . \tag{12.33c}$$

The wave potential ϕ_i^W that corresponds to the Fourier potential (12.32a) is determined by (11.34a) and (12.33) as

$$\mathrm{i}\,\phi_i^W(\mathbf{x}) = \int_{-\pi}^{\pi} d\gamma \; \Theta^i\, k_*^i \; \frac{e^{\,k_*^i\,z\,+\,\mathrm{i}\,k_*^i\,(x\,\cos\gamma\,+\,y\,\sin\gamma)}}{\sqrt{1-4\tau\cos\gamma}} \, A(k_*^i,\gamma) \tag{12.34a}$$

$$\text{where} \;\; \Theta^i = 1 + \mathrm{erf}[\, k_*^i(x\cos\gamma + y\sin\gamma)/C\,] \tag{12.34b}$$

and $k_*^i \equiv k_*^i(\gamma)$ is given by (12.31d).

Wave potential ϕ_o^W associated with V waves

The wave potential ϕ_o^W associated with the outer dispersion curves O^+ and O^- is now considered. The two open outer dispersion curves O^+ and O^- are defined via the Cartesian representation (12.23a). The Fourier potential (12.32b) is then expressed in the equivalent Cartesian form

$$\phi_o^F(\mathbf{x}) = \frac{1}{\pi}\int_{-\infty}^{\infty} d\beta \int_{-\infty}^{\infty} d\alpha \; \frac{\widehat{A}(k,\gamma)\, e^{\,k\,z + \mathrm{i}\,(\alpha\,x + \beta\,y)}\, A(\alpha,\beta)}{\sqrt{1 - 4\tau\,\alpha/k}\,(k - k_*^o) + \mathrm{i}\,\epsilon\,\mathrm{sign}(\alpha)} \;\; . \tag{12.35}$$

The Fourier potential ϕ_o^F defined by (12.35) is of the form (11.21a) with

$$\Delta(\alpha,\beta) = \sqrt{1 - 4\tau\,\alpha/k}\,(k - k_*^o) \;\; , \;\; \Delta_1(\alpha,\beta) = \mathrm{sign}(\alpha) \tag{12.36a}$$

$$\text{and} \;\; \mathcal{A}(\alpha,\beta) = \widehat{A}(k,\gamma)\, e^{\,k\,z}\, A(\alpha,\beta) \;\; . \tag{12.36b}$$

Expression (12.31e) yields

$$\Delta_\alpha(\alpha_*^\pm,\beta) = 2\,(\tau + F^2\alpha_*^\pm) - \alpha_*^\pm/k_*^\pm \;\; , \tag{12.36c}$$

where $\alpha_*^\pm(\beta)$ are the dispersion curves defined by (5.29) and $k_*^\pm(\beta)$ are given by (12.23b).

At the dispersion curves $\alpha = \alpha_*^\pm(\beta)$, one has

$$F^2\alpha_*^+ \geq F^2\alpha_*^+(\beta = 0) \equiv \left(\sqrt{1/4 - \tau} + 1/2\right)^2 \;\; \text{and}$$

$$F^2\alpha_*^- \leq F^2\alpha_*^-(\beta = 0) \equiv -\left(\sqrt{1/4 + \tau} + 1/2\right)^2$$

where $\alpha_*^\pm(\beta = 0)$ are solutions of the dispersion relation $(f + F\alpha)^2 \mp \alpha = 0$ at $\beta = 0$. One has

$$\begin{aligned}
&\tau + F^2\alpha_*^+ \geq 1/2 + \sqrt{1/4 - \tau} > 0 \;\; , \\
&2\,(\tau + F^2\alpha_*^+) - \alpha_*^+/k_*^+ \geq \sqrt{1 - 4\tau} > 0 \;\; \text{and} \\
&\tau + F^2\alpha_*^- \leq -\,(1/2 + \sqrt{1/4 + \tau}) < 0 \;\; , \\
&2\,(\tau + F^2\alpha_*^-) - \alpha_*^-/k_*^- \leq -\sqrt{1 + 4\tau} < 0 \;\; .
\end{aligned}$$

where the relations $\alpha_*^+/k_*^+ \leq 1$ and $\alpha_*^-/k_*^- \geq -1$ were used.

In summary, one has

$$\pm\,\Delta_\alpha(\alpha_*^\pm,\beta) > 0 \;\; \text{and} \;\; \mathrm{sign}(\Delta_1^*\,\Delta_\alpha^*) = 1 \;\; . \tag{12.36d}$$

The wave potential ϕ_o^W that corresponds to the Fourier potential (12.35) is determined by (11.22) and (12.36) as

$$\mathrm{i}\,\phi_o^W(\mathbf{x}) = \int_{-\infty}^{\infty} d\beta \Big[\frac{1-\,\mathrm{erf}(\alpha_*^+ x/C)}{2\,(\tau + F^2\alpha_*^+) - \alpha_*^+/k_*^+}\; e^{\,k_*^+ z + \mathrm{i}\,(\alpha_*^+ x + \beta y)}\, A(\alpha_*^+,\beta) + \frac{1+\,\mathrm{erf}(\alpha_*^- x/C)}{2\,(\tau + F^2\alpha_*^-) - \alpha_*^-/k_*^-}\; e^{\,k_*^- z + \mathrm{i}\,(\alpha_*^- x + \beta y)}\, A(\alpha_*^-,\beta) \Big] \tag{12.37}$$

where $k_*^\pm \equiv k_*^\pm(\beta) \equiv \sqrt{(\alpha_*^\pm)^2 + \beta^2}$ and $\alpha_*^\pm \equiv \alpha_*^\pm(\beta)$ is defined by (5.29).

Local-flow potential ϕ_i^L

The local flow potential ϕ_i^L that corresponds to the potentials (12.32a) and (12.34) is defined by (11.32) and (12.33) as

$$\phi_i^L(\mathbf{x}) = \frac{1}{\pi}\int_{-\pi}^{\pi} d\gamma \int_0^{\infty} dk\; e^{\,\mathrm{i}\,k\,(x\cos\gamma + y\sin\gamma)}\, A_i^L(k,\gamma) \quad \text{where} \tag{12.38a}$$

$$A_i^L(k,\gamma) \equiv \frac{\widehat{A}(k,\gamma)\; e^{\,k\,z}\, A(k,\gamma)}{(k_+^i/k - 1)\sqrt{1-4\,\tau\cos\gamma}} - \frac{e^{\,k_+^i z - C^2(1-k/k_+^i)^2/4}\, A(k_+^i,\gamma)}{(1-k/k_+^i)\sqrt{1-4\,\tau\cos\gamma}} - \frac{e^{\,k_-^i z - C^2(1+k/k_-^i)^2/4}\, A(k_-^i,\gamma-\pi)}{(1+k/k_-^i)\sqrt{1+4\,\tau\cos\gamma}}$$

$$\text{with}\;\; k_+^i \equiv k_*^i(\gamma)\;\; \text{and}\;\; k_-^i \equiv k_*^i(\gamma-\pi)\;. \tag{12.38b}$$

Moreover, $k_*^i \equiv k_*^i(\gamma)$ is given by (12.31d).

Local-flow potential ϕ_o^L

The local flow potential ϕ_o^L that corresponds to the potentials (12.35) and (12.37) is determined by (11.23) and (12.36) as

$$\phi_o^L(\mathbf{x}) = \frac{1}{\pi}\int_{-\infty}^{\infty} d\beta \int_{-\infty}^{\infty} d\alpha\; A_o^L(\alpha,\beta)\; e^{\,\mathrm{i}\,(\alpha x + \beta y)} \quad \text{where} \tag{12.39a}$$

$$A_o^L(\alpha,\beta) \equiv \frac{\widehat{A}(k,\gamma)\, e^{\,k\,z}\, A(\alpha,\beta)}{\sqrt{1-4\,\tau\,\alpha/k}\,(k-k_*^o)} - \frac{e^{\,k_*^+ z - C^2(\alpha/\alpha_*^+ - 1)^2/4}\, A(\alpha_*^+,\beta)}{(\alpha-\alpha_*^+)\,[\,2\,(\tau + F^2\alpha_*^+) - \alpha_*^+/k_*^+\,]} - \frac{e^{\,k_*^- z - C^2(\alpha/\alpha_*^- - 1)^2/4}\, A(\alpha_*^-,\beta)}{(\alpha-\alpha_*^-)\,[\,2\,(\tau + F^2\alpha_*^-) - \alpha_*^-/k_*^-\,]}$$

$$\text{with}\;\; k_*^\pm \equiv k_*^\pm(\beta) \equiv \sqrt{(\alpha_*^\pm)^2 + \beta^2}\;. \tag{12.39b}$$

Moreover, $\alpha_*^\pm \equiv \alpha_*^\pm(\beta)$ is defined by (5.29).

Local-flow potential $\phi^L = \phi_o^L + \phi_i^L$

Expressions (12.38) and (12.39) finally determine $\phi^L = \phi_i^L + \phi_o^L$ as

$$\phi^L(\mathbf{x}) = \frac{1}{\pi}\int_{-\pi}^{\pi} d\gamma \int_0^\infty dk\ A^L(k,\gamma)\ e^{\,\mathrm{i}\,k\,(x\cos\gamma + y\sin\gamma)} \tag{12.40a}$$

where $A^L(k,\gamma) \equiv A_i^L(k,\gamma) + k\,A_o^L(k,\gamma)$ is given by

$$\begin{aligned} A^L(k,\gamma) &= \frac{e^{\,k\,z}\,\widehat{A}(k,\gamma)\,A(k,\gamma)}{(f+F\alpha)^2/k - 1} \\ &- \frac{e^{\,k_+^i\,z - C^2(1-k/k_+^i)^2/4}\,A(k_+^i,\gamma)}{(1-k/k_+^i)\sqrt{1-4\tau\cos\gamma}} - \frac{e^{\,k_-^i\,z - C^2(1+k/k_-^i)^2/4}\,A(k_-^i,\gamma-\pi)}{(1+k/k_-^i)\sqrt{1+4\tau\cos\gamma}} \\ &- \frac{e^{\,k_*^+\,z - C^2(1-\alpha/\alpha_*^+)^2/4}\,A(\alpha_*^+,\beta)}{[\,2\,(\tau+F^2\alpha_*^+) - \alpha_*^+/k_*^+\,](\alpha-\alpha_*^+)/k} \\ &- \frac{e^{\,k_*^-\,z - C^2(1-\alpha/\alpha_*^-)^2/4}\,A(\alpha_*^-,\beta)}{[\,2\,(\tau+F^2\alpha_*^-) - \alpha_*^-/k_*^-\,](\alpha-\alpha_*^-)/k} \\ \text{with}\ \ k_+^i &\equiv k_*^i(\gamma)\ ,\ k_-^i \equiv k_*^i(\gamma-\pi)\ ,\ k_*^\pm \equiv \sqrt{(\alpha_*^\pm)^2+\beta^2} \end{aligned} \tag{12.40b}$$

and $(\alpha,\beta) = k\,(\cos\gamma, \sin\gamma)$. Moreover, $k_*^i(\gamma)$ and $\alpha_*^\pm \equiv \alpha_*^\pm(\beta)$ are defined by (12.31d) and (5.29).

Summary: waves and local-flow decomposition

The decomposition (12.30) and the decompositions

$$\phi_i^F = \phi_i^W + \phi_i^L\ \ ,\ \ \phi_o^F = \phi_o^W + \phi_o^L\ \ \text{and}\ \ \phi^L = \phi_i^L + \phi_o^L$$

show that the flow potential $\phi^F(\mathbf{x})$ given by (12.29), where the Kochin function $A(\alpha,\beta)$ is general, can finally be expressed as

$$\phi^F(\mathbf{x}) = \phi_i^W(\mathbf{x}) + \phi_o^W(\mathbf{x}) + \phi^L(\mathbf{x}) \tag{12.41}$$

where the wave components ϕ_i^W and ϕ_o^W are given by (12.34) or (12.37) and the local-flow component ϕ^L is defined by (12.40).

In the limit $F = 0$, the flow potential (12.41) agrees with the potential $\phi^W + \phi^L$ that is defined by (12.9) and (12.10) and corresponds to diffraction-radiation of regular waves by offshore structures. In the limit $f = 0$, the flow potential (12.41) also agrees with the potential $\phi^W + \phi^L$ given by (12.17-12.18) and associated with a ship that steadily advances in calm water. Thus, the flow representation defined by (12.41) with (12.34), (12.37) and (12.40) is consistent with both the flow representations (12.8-12.10) and (12.16-12.18) in the limits $F = 0$ or $f = 0$.

12.5 Conclusion

The amplitude (Kochin) functions $A(\alpha, \beta)$ or $A(k,\gamma)$ in the expressions for the Fourier potentials ϕ^F and the corresponding wave and local-flow components ϕ^W and ϕ^L given in this chapter for an offshore structure in regular waves and a ship that advances in calm water or through regular waves are associated with Fourier-Kochin flow representations for *general* distributions of singularities, e.g. a source distribution over a panel. Both the wave component ϕ^W and the non-oscillatory local-flow component ϕ^L in the fundamental decomposition $\phi^F = \phi^W + \phi^L$ involve the real number C. Although the sum $\phi^W + \phi^L$ is independent of C, the choice $C \approx 1/2$ is shown in chapter 11 to yield nearly optimal flow decompositions.

The wave components ϕ^W in the flow representations $\phi^F = \phi^W + \phi^L$ are defined by single Fourier integrals with smooth integrands. The local-flow components $\phi^L(\mathbf{x})$ are the double Fourier transforms of amplitude functions A^L/k where the functions $A^L(k,\gamma)$ vanish as $k \to \infty$ and are finite or nil at $k = 0$. Moreover, the functions $A^L(k,\gamma)$ are non-oscillatory and smooth everywhere, notably at the dispersion curves. Thus, the flow representations given in this chapter are suited for accurate numerical evaluation of flows created by general distributions of singularities [**12,2**].

Notes

This chapter gathers the notes marked as **[m,n]** in chapters 1-12. The note **[m,n]** corresponds to note number **n** in chapter number **m**.

[1,1] See e.g., Molin (2023) and Faltinsen (1993).

[1,2] The upper bound (1.9) has a determining influence on the bow wave created by a ship that steadily advances in calm water, notably the boundary between the steady and unsteady bow-wave regimes as is shown in Noblesse et al. (2008b) and Delhommeau et al. (2009).

[1,3] In particular, a perturbation analysis for ambient waves of small amplitude leads to the formulation of a hierarchy of approximations ϕ_1, $\phi_2, \ldots$ and a related sequence of boundary-value problems with free-surface pressure $p^F = p^F_{k+1}$ and body-surface flux $q^H = q^H_{k+1}$ in (1.35d-e) that is defined in terms of the flow potentials $\phi_1, \ldots, \phi_k$ and therefore is known in the boundary-value problem associated with the potential ϕ_{k+1}. This weakly-nonlinear perturbation analysis is used to estimate drift forces, yaw moment and nonlinear wave loads for offshore structures and ships in waves in a broad literature, e.g. Maruo (1960), Newman (1967), Molin (1979), Hunt and Baddour (1981), Chau and Eatock Taylor (1992), Faltinsen (1993), Malenica and Molin (1995), Newman (1996), Rahman (1998), Teng and Kato (2002), Buldakov et al. (2004), Rahman and Mousavizadegan (2005), Molin (2023).

[1,4] The straightforward approach in which a steady or time-harmonic flow is analyzed as a flow that slowly grows from rest at a time $T = -\infty$, as in (1.19) and (1.22), is adopted throughout the book. This approach, used in Lighthill (1967,1978), is equivalent but considerably simpler than the use of a 'radiation condition' or Rayleigh's 'artificial viscosity'. Lighthill's way leads to the generalized elementary waves expounded in Noblesse and Yang (2007) and in chapter 2 of the book.

[1,5] The sinkage and the trim experienced by a freely floating common monohull ship that steadily advances in calm deep water at a moderate Froude number $F \leq 0.45$ can be estimated—without flow computations—

in terms of the ship speed and four basic parameters related to the ship-hull geometry (length, beam, draft and block coefficient) via simple analytical relations, obtained in Ma et al. (2016) by means of an analysis of experimental data and elementary theoretical considerations. Ma et al. (2016) shows that good estimates of sinkage and trim can also be obtained via a simple numerical method. Ma et al. (2017) shows that sinkage and trim effects on the total (viscous and wave) drag of a typical freely floating monohull ship is significant at Froude numbers $0.25 < F$ and can be realistically accounted for in a practical manner that only requires simple potential flow computations for the ship hull in equilibrium position at rest, i.e. without iterative computations for a sequence of hull positions.

[1,6] The classical analysis and decomposition of the flow around an offshore structure undergoing small oscillatory motions in ambient regular waves into a 'wave-diffraction problem' and six 'wave-radiation problems' is explained in e.g. Newman (1977), Faltinsen (1993), Molin (2023) and numerous studies of interactions between regular water waves and floating bodies.

[2,1] The analysis of generalized elementary free waves expounded in chapter 2, notably in sections 2.8 and 2.9, largely follows Noblesse and Yang (2007).

[2,2] Green's fundamental boundary-integral flow representation, given in chapter 6, shows that a closed non-lifting body appears as a dipole in the far field, and accordingly creates a flow velocity proportional to $1/r^3$ as $r \equiv \sqrt{x^2 + y^2 + z^2} \to \infty$.

[2,3] The energy transported via the waves created by a wavemaker (ship or offshore structure) is proportional to the width of the wave front, which increases in proportion to the horizontal distance h from the wavemaker, and moreover is proportional to the square of the wave amplitude a. Thus, the energy radiated by a wavemaker is proportional to $h\,a^2$. It follows that $a \propto 1/\sqrt{h}$ if the energy radiated by the wavemaker is transported without significant loss (e.g. due to wavebreaking, which mostly occurs in the vicinity of the wavemaker).

[2,4] The equivalence, noted in **[1,4]**, between the approach adopted in the book, where a steady or time-harmonic flow is analyzed as a flow that slowly grows from rest at a time $T = -\infty$, and a 'radiation condition' or Rayleigh's 'artificial viscosity' is considered in Noblesse and Yang (2007).

[3,1] The stationary-phase approximation (3.12) was first given by William Thomson (1824-1907), also known as Lord Kelvin, in Thomson (1891) to explain the pattern of far-field waves—now widely known as Kelvin's wake—created by a ship that steadily advances in calm water.

[3,2] Asymptotic approximations of integrals is a classical topic consid-

ered in a broad literature, e.g. Erdélyi (2010), Copson (1965), Bleistein and Handelsman (1986), Wong (1989). The integral (3.9) occurs in the representation of the waves created by a ship that steadily advances in calm water, first analyzed by Kelvin as is noted in **[3,1]**. Accordingly, far-field asymptotic approximations have been extensively studied for this historically important case, now briefly considered. Kelvin's approximations (3.12) holds strictly inside the Kelvin wake that trails a ship steadily advancing in calm water. Havelock's approximation (3.13), given in Havelock (1908), only holds at the cusps of the Kelvin wake. An asymptotic approximation that holds strictly outside the cusps of the Kelvin wake is given in Peters (1949). This asymptotic approximation shows that ship waves decay exponentially outside the cusps of the wake, in accordance with the analysis of the integral (3.9) for the case $\Theta_0' \neq 0$, except in the vicinity of the cusps where the free-surface elevation decays as $1/h^{1/3}$ as $h \to \infty$. Thus, large ship waves can exist outside the Kelvin wake, as is illustrated in Wu et al. (2019b). Kelvin's and Peters approximations both are singular at the cusps of Kelvin's wake, where Havelock's approximation holds. An approximation that combines the Kelvin, Havelock and Peters approximations is given in Wu et al. (2018b) and Liang et al. (2020a). This approximation, called Kelvin-Havelock-Peters (KHP) approximation, is nearly identical to Kelvin's and Peters' approximations inside or outside the cusps of Kelvin's wake, but agrees with Havelock's approximation at the cusps (where Kelvin's and Peters' approximations are singular). A more accurate uniform far-field approximation, which is also finite everywhere, has been given by Chester et al. (1957) and revisited by Borovikov (1994). This approximation involves the Airy function and is then more complicated than the KHP approximation, which only involves ordinary functions. The asymptotic approximations to far-field ship waves given by Kelvin, Havelock, Peters and Chester et al. are considered, applied or extended in a large literature, briefly reviewed in e.g. Liang et al. (2020a).

[3,3] Interferences among the divergent waves created (predominantly) by the bows and the sterns of high-speed vessels, notably longitudinal interferences between the divergent waves created by the bow and the stern of a monohull ship and lateral interferences between the divergent waves created by the twin bows of a catamaran, have been widely studied; e.g. Noblesse et al. (2014b), Zhang et al. (2015c), Miao and Liu (2015), He et al. (2016), Noblesse et al. (2016), Zhu et al. (2017,2018a-b) and Colen and Kolomeisky (2021).

[3,4] Indeed, the Froude number and the submergence depth can have a large, even striking, influence on the appearance of the wave pattern created by a ship that steadily advances in calm deep water, as is illustrated in Wu et al. (2019b). In particular, at high Froude numbers F, e.g. at $F = 1.5$, a ship wave pattern mostly contains divergent waves that are most apparent along rays well inside the cusps of the Kelvin wake due to interferences between

the dominant waves created by the bow and the stern of the ship. A very different wave pattern is observed at low Froude numbers, e.g. at $F = 0.2$, for which the dominant waves are found outside the cusps of the Kelvin wake. Thus, the wave patterns created by surface-piercing or submerged bodies can greatly differ from Kelvin's classical pattern of transverse and divergent waves found inside a 39° wedge trailing a ship.

[4,1] The result that a ship that steadily advances in calm water only creates waves aft of the ship follows from expression (1.19), which defines a steady flow as a flow that slowly grows from rest, and the related analysis expounded in chapter 2. This rigorous analysis proves—without the need for a radiation condition based on observations—that steady ship waves only exist behind a ship.

[4,2] The studies of short waves reported in Wu et al. (2018c,2019a) provide strong evidence that short divergent waves created by a ship that steadily advances in calm deep water are too steep to exist within a broad inner wake with angle roughly equal to a third of Kelvin's 39° wake. The short divergent waves created by a ship bow are also too steep to exist in the vicinity of the fore shoulder of the hull of a ship that steadily advances in calm deep water at Froude numbers smaller than about 0.35, as is shown in He et al. (2020a).

[5,1] The wave patterns created by a ship that steadily advances through regular waves, and the related Green function considered in chapter 7, have been studied in a vast literature; e.g. Haskind (1946), Brard (1948), Stretenski (1954), Hanaoka (1957), Eggers (1957), Havelock (1958), Wehausen and Laitone (1960), Lighthill (1967), Noblesse and Hendrix (1992).

[6,1] John Henry Michell (1863-1940) published his remarkable theory of the wave resistance of a ship that steadily advances in calm water in 1898. This theory, expounded in Michell (1898), was ignored for about thirty years, but became famous and widely used after that long period of initial neglect, and the theory remains useful and relevant for ship design to this day. The theory considers a 'thin ship' with small beam/length ratio. The ship-hull boundary conditions (1.35e) and (1.36) for a ship-hull surface defined as $\eta = \pm b(\xi, \zeta)$, where $b(\xi, \zeta)$ denotes the local beam, yield the boundary condition

$$\partial_\eta \phi = \pm F b_\xi / \sqrt{1 + b_\xi^2 + b_\zeta^2} \text{ at } \eta = \pm b \, .$$

This boundary condition is applied at the ship centerplane $\eta = 0$, rather than at the actual hull surface $\eta = \pm b(\xi, \zeta)$, in Michell's thin-ship theory. The solution of the resulting 'thin-ship' boundary-value problem in the region $-\infty < \xi < \infty, 0 \leq \eta < \infty, -\infty < \zeta \leq 0$ can then be obtained via Fourier transformation. This simple and beautiful theory explicitly determines the flow and the wave drag of a ship in terms of the speed, the length

and the hull-shape of the ship.

[6,2] Analytical solutions of the boundary-value problem (1.35) exist for simple special geometries; e.g. Havelock (1952), Farell (1973), Hulme (1982), Yeung (1982), Wu and Eatock Taylor (1987b,1989), Chatjigeorgiou and Miloh (2014a-b,2015) and Chatjigeorgiou (2013,2018).

[6,3] The method of Green function and boundary-integral representation is due to the extraordinary British mathematical physicist George Green (1793-1841), who was almost entirely self taught. Green's method is largely expounded in Green (1828), a remarkable study that contains all the essential elements—including concepts now known as Green's theorem and Green's functions—of the method of Green function and boundary-integral representation. This method, expounded in the book for flows around ships and offshore structures, is widely used in engineering and physics. A biography of George Green is given in Cannel (1993,1999).

[6,4] A brief introduction to generalized functions and Fourier analysis is given in Lighthill (1958).

[7,1] The complementary 'Fourier-space' and 'physical-space' analyses expounded in sections 7.2–7.6 largely follow Noblesse (2001a-b). The optimal Rankine-Fourier decompositions $G^R + G^F$ given by (7.16) and (7.25), and the related consistent Rankine-Fourier decomposition (7.43) and (7.46) are also given in that study. The optimal Rankine-Fourier decomposition (7.32)-(7.33) is given in Wu et al. (2021).

[7,2] Expressions (7.53) are given in He et al. (2022a) and are primarily due to the book's second author.

[7,3] Several studies of the Green function G associated with a ship that steadily advances through regular waves and of the corresponding far-field wave patterns are listed in **[5,1]**. This Green function and the integration of G and its gradient over hull-surface panels and waterline segments have been widely considered; e.g., Bessho (1977), Chang (1977), Inglis and Price (1981,1982), Guevel and Bougis (1982), Wu and Eatock Taylor (1987a,1989), Iwashita and Ohkusu (1989,1092), Ohkusu and Iwashita (1989), Noblesse and Hendrix (1990,1992), Zong and Huang (1991), Du et al. (1999), Guilbaud et al. (2001), Chen and Wu (2001), Maury et al. (2003), Noblesse and Yang (2004), Chapchap et al. (2011), Xu and Dong (2011), Hong et al. (2016), Chen and Liang (2016), Yang et al. (2019a-b) and He et al. (2020c,2021a,2022a).

[7,4] The Green function associated with a ship that steadily advances in calm deep water, and the integration of G and its gradient over hull-surface panels and waterline segments, are considered in a broad literature, which begins with Michell's celebrated study of the wave resistance of a ship in Michell (1898) and includes Havelock (1932), Peters (1949), Lunde

(1951), Kostyukov (1959), Wehausen and Laitone (1960), Wehausen (1973), Standing (1974), Noblesse (1975a,1977,1978a-b), Shen and Farell (1977), Newman (1987a-b), Telste and Noblesse (1989), Day and Doctors (2001), Faltinsen (2005), Zilman(2006). In particular, these studies include three alternative single-integral representations of the Green function and corresponding decompositions into waves and non-oscillatory local flows given in Noblesse (1981), analytical expansions given in Noblesse (1975a,1978a-b) and Newman(1987a-b), and practical methods for evaluating the local-flow component in the Green function given in Ponizy et al. (1994), Noblesse et al. (2009a-b,2011b) and Wu et al. (2016).

[7,5] The Green function associated with diffraction-radiation of regular waves by offshore structures in deep water has been extensively considered in a vast literature, including Havelock (1942), Haskind (1944), Ursell (1949), John (1950), Kochin (1952), Thorne (1953), Haskind (1954), MacCamy (1954), Havelock (1955), Wehausen and Laitone (1960), Kim (1965), Wehausen (1971), Hearn (1977), Martin (1980), Hulme (1982), Wu and Eatock Taylor (1987b). Three complementary single-integral representations of the Green function and related near-field and far-field asymptotic expansions and Taylor series are given in Noblesse (1982). These analytical approximations are the basis of the method for evaluating the Green function and its gradient given in Telste and Noblesse (1986) and Chakrabarti (2001). Other methods include table interpolation associated with function and coordinate transformations given in Ponizy et al. (1994), polynomial approximations within complementary contiguous flow regions given in Newman (1984,1985), Chen (1991), and representations in terms of ordinary differential equations considered in Clément (2013), Shen et al. (2016), Xie et al. (2019). The Green function G for diffraction-radiation of regular water waves is also considered in Wang (1992), Peter and Meylan (2004), Yao et al. (2009), D'elia et al. (2011), Shan and Wu (2018), Shan et al. (2019) and Chen (2015,2019). A comparison of several alternative methods for evaluating this Green function is given in Xie et al. (2018). A particularly simple and efficient method for evaluating G and its gradient is given in Wu et al. (2017,2018a) and validated in Liang et al. (2018a). This method is based on global analytical approximations that are valid within the entire flow region. Liang et al. (2021) shows that higher-order derivatives of G can readily be determined from the Green function and its gradient.

[7,6] The Green function associated with diffraction-radiation of regular waves by an offshore structure in water of uniform finite depth has been extensively studied, and alternative calculation methods exist. These studies and calculation methods include complementary analytical expansions given in John (1950), Pidcock (1985), Linton (1991,1999), Liu et al. (2015), polynomial approximations within complementary contiguous regions given in Newman (1985), Chen (1993) and Mackay (2019), table interpolation used in Delhommeau (1989) and direct numerical integration considered in

Cuer (1989), Liu et al. (2015,2020), Xie et al. (2017), Chen (2020), He et al. (2020b), Wu et al. (2021).

[**8,1**] Sections 8.1–8.3 largely follow Noblesse (1983b), where the boundary-integral flow representation (8.18) is given. Sections 8.4 and 8.5 follow the first author's work, reported in He et al. (2021c).

[**8,2**] Numerical studies of weakly-singular boundary integral equations are given in He et al. (2023b) for potential flows in the zero or infinite gravity limits.

[**8,3**]. Specifically, irregular frequencies correspond to eigensolutions of the interior boundary-value problem with a Dirichlet boundary condition at the body surface.

[**8,4**] The existence of irregular frequencies is demonstrated in Lamb (1932) and John (1949,1950) for diffraction radiation of acoustic or water waves, and is well explained in several subsequent studies, notably in Lau and Hearn (1989) and Liapis (1993) where two effective and practical methods for suppressing irregular frequencies are proposed and applied, and a review of alternative methods for preventing irregular frequencies is also given. Two main classes of methods have been considered to suppress irregular frequencies. These two classes of methods are 'modified integral-operator methods', which essentially consist in formulating an integral equation where the integral operator (kernel) related to the Green function is modified, and 'modified integral-equation-domain methods' in which the body surface where the integral equation is formulated is extended. The first class of methods, i.e. the 'modified integral-operator method', is considered in Burton and Miller (1971), Ursell (1973), Jones (1974), Kleinman and Roach (1974), Ogilvie and Shin (1978), Sayer and Ursell (1980), Ursell (1981), Martin (1981), Kleinman (1982), Wu and Price (1986,1987), Lee and Sclavounos (1989) and Liapis (1993). The 'modified integral-equation-domain method' is adopted in Schenk (1968), Ohmatsu (1975,1983), Rezayat et al. (1986), Lau and Hearn (1989), Lee et al. (1996), Lee and Newman (2005), Malenica and Chen (1998), Sun et al. (2008) and Liang et al. (2020b), where extensive applications of the 'combined boundary-integral equation method' (CBIEM) proposed in Lau and Hearn (1989) are given. An elementary explanation, based on applications of Green's classical identity to the usual 'free-waterplane' linear flow-model and the alternative 'rigid-waterplane' flow model, of the CBIEM is given in chapter 8 of the book.

[**9,1**] The applications of Green's basic identity to the Neumann-Kelvin flow model in sections 9.1–9.3 and to the rigid-waterplane flow model in sections 9.4–9.6 are based on the first author's work. This work was previously reported in He et al. (2019b) and in Noblesse and Yang (2023) where the boundary-integral flow representations (9.15) and (9.23), and the related

RW-hw, RW-h and NN flow representations are obtained in the manner expounded in sections 9.1–9.6. The analysis of the Neumann-Michell flow model given in section 9.8 was previously given in Noblesse et al. (2013b).

[**9,2**] The Neumann-Kelvin (NK) problem and related numerical studies are considered in a broad literature. For the particular case of a ship that steadily advances in calm water, these theoretical and numerical studies include Brard (1972), Guevel et al. (1974,1977), Chang (1979), Tsutsumi (1979), Tsai et al. (1983), Baar (1986), Andrew et al. (1987), Doctors and Beck (1987), Baar and Price (1988), Scragg and Talcott (1988), Marr (1996), Diebold (2007), Noblesse et al. (2013b), Liang et al. (2018b), He et al. (2018a,2021b). Theoretical and numerical studies of the NK problem for a ship that advances through regular waves are reported in e.g. Guevel and Bougis (1982), Inglis and Price (1982), Iwashita and Ohkusu (1989), Wu and Eatock Taylor (1989), Iwashita and Ohkusu (1992), Noblesse and Hendrix (1992), Du et al. (1999), Chapchap et al. (2011), Peng et al. (2015), Hong et al. (2016), He et al. (2019b).

[**9,3**] The restriction (9.26) imposed in chapter 8 for wave diffraction-radiation by a stationary body is a mathematical 'consistency-condition' that ensures consistency of the boundary conditions at the rigid lid Σ_i^H and at the waterplane Σ_i^F in the limit $\delta \to 0$, whereas the particular solution $C_1^{\pm} = 0$ and $C_2^{\pm} = 0$ in (9.27) and the particular solution $C_n = 0$ with $0 \leq n \leq 3$ in (9.28b) are flow-modeling assumptions, as is explained in section 9.7.

[**9,4**] For a ship that steadily advances in calm water, the boundary condition (1.27) at the ship-hull surface Σ^H and the *nonlinear* boundary condition at the free surface Σ^F are shown in Noblesse et al. (1991,2012) to be compatible. However, the boundary condition at the ship-hull surface Σ^H and the *linear* boundary condition (1.21) at the free surface Σ^F have not been shown to be compatible, and indeed likely are not compatible. This feature is also likely to be a main cause of the numerical difficulties associated with solutions of the classical NK boundary-integral flow representation noted in [**9,5**], and is the primary motivation for seeking boundary-integral flow representations that do not involve the flow potential at the waterline of the ship.

[**9,5**] Accurate solutions of the Neumann-Kelvin boundary-integral flow representation are notoriously difficult due to difficulties associated with the line integral around the ship waterline that is present in the NK theory. Marr (1996) summarizes these difficulties by concluding that "the Neumann-Kelvin theory, as it is currently understood, does not give satisfactory wave resistance results for realistic ship hull forms. These results lead to, and reinforce, the suggestion that the problem lies with the waterline integral term; a new treatment of this term may substantially increase the applicability of Neumann-Kelvin theory". Additional evidence of the difficulties

associated with the waterline integral are given in Diebold (2007) and in Liang et al. (2018) where the waterline integral is found to result in an ill-conditioned matrix of influence coefficients. Thus, conclusions about the importance of the waterline integral in the NK theory cannot be stated with certainty. However, the numerical study given in Peng et al. (2015) provides some evidence that the troublesome waterline integral in the NK theory only has a modest influence.

[**9,6**] Indeed, the NN flow representation (9.35) was first given for wave diffraction radiation by an offshore structure in Noblesse (1983b).

[**9,7**] Alternative boundary-integral flow representations that do not include a waterline integral are given in He et al. (2021b,2022b,2023a), where mathematical transformations based on vector Green functions $\mathbf{G}$ associated with the scalar Green function G are used. However, these flow representations are significantly more complicated than the NN flow representation (9.35) based on the rigid-waterplane linear flow model and the no-flow restriction (9.33).

[**9,8**] The Neumann-Michell (NM) theory, proposed in Noblesse et al. (2013b), is applied and validated in Huang et al. (2013), Yang et al. (2013), Zhang et al. (2014,2015a-b), Ma et al. (2016,2017,2018), and is used for hull-form optimization in Huang et al (2014,2015a-b,2016), Huang and Yang (2016), Yang et al. (2014), Yang and Huang (2016), and Wang et al. (2015). The short waves predicted by the NM theory are considered in Wu et al. (2018c,2019a).

[**9,9**] In particular, the Hogner approximation, proposed in Hogner (1932), is shown be useful for hull-form optimization in Percival et al. (2001) and indeed has been widely used for that purpose. This approximation is also useful and has been extensively applied to analyze the influence of wave interferences on the appearance of the far-field pattern of waves created by a ship that steadily advances in calm deep water in Zhang et al. (2015c), He et al. (2016), Noblesse et al. (2016) and Zhu et al. (2017,2018b). Lastly, the Hogner approximation is used to investigate how to filter inconsequential short ship waves in He et al. (2018b,2019a,2020a).

[**9,10**] Linearization of the free-surface boundary condition about the flow around a ship hull and its mirror image with respect to the plane of the undisturbed free surface, as in the 'infinite-gravity' limit $g = \infty$, is considered in e.g. Ogilvie (1968), Hermans (1974), Baba (1975), Baba and Takekuma (1975), Newman(1976) and Nakatake and Yamazaki (1976).

[**9,11**] Approximate analytical theories based on geometrical assumptions—specifically thin-ship, flat-ship, slender-ship or deep-submergence assumptions—have been extensively considered. In particular, for a ship that steadily advances in calm water, the thin-ship approximation, first proposed in Michell (1898), has been considered and

applied in numerous studies, e.g. Wigley (1926), Yeung (1972), Wehausen (1973), Standing (1974), Noblesse (1975a-b,1978a), Noblesse and Dagan (1976), Day and Doctors (2001), Noblesse et al. (2006,2008a,2009a,2011a), Doctors (2015). Slender-ship approximations are given and applied in Hogner (1932), Noblesse (1983a), Percival et al. (2001). Flows around fully-submerged bodies are considered in e.g. Havelock (1932), Farell (1973), Wang (1986), Chatjigeorgiou (2013). For ship motions in waves, the strip theory and related 2D flow approximations, which take advantage of the fact that ships are slender bodies, are widely used.

[9,12] Analytical, numerical and experimental studies of ship bow waves and the related overturning bow wave and unsteady bow wave regimes, are considered in Noblesse et al. (2006,2008a-b,2009a,2011a,2013a,2014a) and Delhommeau et al. (2009).

[9,13] In particular, removal of the unrealistic and inconsequential short divergent waves that are predicted by a linear potential flow analysis of the waves created by a ship that advances in calm water or through regular waves is necessary for numerical implementations. This important issue is considered for a ship that advances through regular waves in section 5.5, where a straightforward method for filtering inconsequential short waves is expounded. The issue is also considered for a ship that advances in calm deep water in Noblesse et al. (2013c), He et al. (2018b,2019a,2020a) and Wu et al. (2018c,2019a). As is noted in **[4,2]**, Wu et al. (2019a) shows that a linear potential flow analysis of the waves due to a ship that advances in calm water predicts short divergent waves that are too steep to exist in reality within an inner Kelvin wake with angle that is about a third of the 39° Kelvin-wake angle, and He et al. (2020a) shows that a linear potential flow analysis also predicts waves that are too steep to exist in reality around the shoulder of common displacement ships at Froude numbers smaller than about 0.35.

[9,14] The influence of nonlinearities in the free-surface boundary condition on the wave drag, the sinkage, the trim, and the wave profile along the hull of four ship models is studied in Ma et al. (2018), which also considers simple (post-processing) nonlinear corrections (that require no additional flow computations) to the Neumann-Michell (NM) theory—based on the Kelvin-Michell linear free-surface condition—to approximately account for nonlinear effects. This study shows that nonlinear effects are relatively small. However, an important exception to this general finding is that the wave drag of a bulbous ship is greatly reduced due to the nonlinear component of the pressure in the Bernoulli relation. This important nonlinear effect, readily included in potential flow theory via a post-processing correction that accounts for the nonlinear component of the pressure in the Bernoulli relation, also yields a small increase of the sinkage. Moreover, free-surface nonlinearities can have appreciable, although not large, effects

on the wave profile. These nonlinear effects can be approximately taken into account via a simple transformation of the linear wave profile. Indeed, the flow computations for the four ship models considered in Ma et al. (2018) suggest that simple post-processing nonlinear corrections of the NM theory yield numerical predictions of the wave drag, the sinkage, the trim and the wave profile that agree well with experimental measurements, and compare favorably with predictions given by more complex computational methods.

[**10,1**] This literature is briefly reviewed in [**7,3**]-[**7,6**].

[**10,2**] The Fourier-Kochin (FK) approach is formulated in Kochin (1952) and Wehausen and Laitone (1960). This approach has been used extensively to represent and evaluate the waves created by a ship that advances in calm water, e.g. Zhang et al. (2015c), He et al. (2016,2020a), Zhu et al. (2017,2018a-b), Wu et al. (2018c,2019a-b). A mixed approach, in which the waves and the local flow are evaluated via the FK method or the usual usual Green function method, is used in Noblesse et al. (2013b), Huang et al. (2013) and Ma et al. (2017,2018), where the local flow is evaluated via the simple global analytical approximations given in Noblesse et al. (2011b) and Wu et al. (2016). The FK approach has also been used more generally to represent both the waves and the non-oscillatory local flow—i.e. the entire free-surface flow disturbance rather than only the wave component—created by an offshore structure in waves or a ship that advances in calm water or through regular waves. This more general application of the Fourier-Kochin method is considered in Noblesse and Yang (1995), Noblesse et al. (1999), Noblesse (2001a-b,2002), Chen (2013), He et al. (2020b-c,2021a,2022a) and Wu et al. (2021). The FK method is applied to diffraction and radiation about stationary floating bodies in Ugurlu and Guedes Soares (2021).

[**11,1**] Many important engineering problems—besides those considered in the book—involve plane dispersive waves and have been widely considered; e.g., Squire et al. (1995,1996), Cadby and Linton (2000), Khabakhpasheva and Korobkin (2002), Squire (2008), Pogorelova (2011), Sturova (2013), Meng (2017), Pogorelova et al. (2018), Hao et al. (2020).

[**11,2**] The analysis given in this chapter largely follows sections 7 and 8 in He et al. (2022a).

[**11,3**] The analysis expounded in sections 11.1-2 is closely related to the analysis previously given in Noblesse and Chen (1995,1997), Noblesse and Yang (1996) and Noblesse et al. (1996,1999). However, a major difference is that the analysis expounded in sections 11.1-2 considers the common case of a dispersion curve that is defined in Cartesian form. This analysis, and its extension to multiple dispersion curves defined in Cartesian form and to closed dispersion curves defined in polar form given in sections 11.5-6, yields general analytical representations suited for practical applications and accurate numerical evaluation.

[**11,4**] See e.g. Lighthill (1958).

[**11,5**]. The representation of a singular double Fourier integral in terms of a single Fourier integral, which typically represents the contribution of pole(s) inside an integration contour in the complex plane, and the Cauchy principle value of a singular double Fourier integral is widely found in the literature; e.g. in many expressions for Green functions given in Wehausen and Laitone (1960) and in the method used in Chen (2015,2019).

[**11,6**]. The important issues related to the influence of the parameter μ considered in sections 11.3 and 11.4 are not fully understood in Noblesse and Chen (1995,1997), Noblesse and Yang (1996) and Noblesse et al. (1996,1999), which essentially assume narrow dispersion strips.

[**12,1**] This chapter follows sections 9-13 of He et al. (2022a), which is closely related to He et al. (2020b-c,2021a) and Wu et al. (2021). However, the flow representations given in chapter 12 are not identical to the expressions given in He et al. (2022a) because the function e^{kz} for deep water, or the corresponding function for finite water-depth, is included in the amplitude function A in He et al. (2022a) but is more properly explicitly accounted for in the modified expressions that are given in chapter 12.

[**12,2**] Numerical illustrations and verifications for uniform distributions of sources and dipoles over rectangular panels are given in He et al. (2020b-c,2021a) and Wu et al. (2021).

Bibliography

Andrew, R.N., Baar, J.J.M., Price, W.G., 1988. Prediction of ship wavemaking resistance and other steady flow parameters using Neumann-Kelvin theory. Trans. R. Inst. Nav. Archit. 130, 119-133.

Baar, J.J.M., 1986. A three-dimensional linear analysis of steady ship motion in deep water (PhD Thesis). Brunel Univ., Uxbridge, UK.

Baar, J.J.M., Price, W.G., 1988. Developments in the calculation of the wavemaking resistance of ships. Proc. R. Soc. London. Ser. A Math. Phys. Sci. 416, 115-147.

Baba, E., 1975. Blunt bow forms and wave breaking. Presented at the 1st STAR Symp. Ship Technol. Res., Washington DC, USA.

Baba, E., Takekuma, K., 1975. A study on free-surface flow around bow of slowly moving full forms. J. Soc. Nav. Archit. Jpn. 137, 1-10.

Bessho, M., 1977. On the fundamental singularity in the theory of ship motions in a seaway. Mem. Def. Acad. Jpn. 17, 95-105.

Bleistein, N., Handelsman, R.A., 1986. Asymptotic Expansions of Integrals. Dover Publications, New York.

Borovikov, V.A., 1994. Uniform Stationary Phase Method. Institution Electrical Engineers, London.

Brard, R., 1948. Introduction à l'étude théorique du tangage en marche. Bull. Assoc. Tech. Marit. Aeronaut. 4, 455-479.

Brard, R., 1972. The representation of a given ship form by singularity distributions when the boundary condition on the free surface is linearized. J. Ship Res. 16, 79-92.

Buldakov, E.V., Eatock-Taylor, R., Taylor, P.H., 2004. Local and far-field surface elevation around a vertical cylinder in unidirectional steep wave groups. Ocean Eng. 31, 833-864.

Burton, A.J., Miller, G.F., 1971. The application of integral equation methods to the numerical solution of some exterior boundary-value problems. Proc. R. Soc. London. Ser. A Math. Phys. Sci. 323, 201-210.

Cadby, J.R., Linton, C.M., 2000. Three-dimensional water-wave scattering in two-layer fluids. J. Fluid Mech. 423, 155-173.

Cannell, D.M., 1993. George Green, Mathematician and Physicist, 1793-1841: The Background to His Life and Work. Continuum Int.

Publication Group Ltd., London.

Cannell, D.M., 1999. George Green: an enigmatic mathematician. Am. Math. Mon. 106, 136-151.

Chakrabarti, S.K., 2001. Application and verification of deepwater Green function for water waves. J. Ship Res. 45, 187-196.

Chang, M.S., 1977. Computations of three-dimensional ship motions with forward speed, in: Proc. 2nd Int. Conf. Numer. Ship Hydrodyn. Berkeley, CA, USA, pp. 124-135.

Chang, M.S., 1979. Wave resistance predictions by using a singularity method, in: Proc. Workshop Ship Wave-Resist. Comput. Bethesda, MD, USA, pp. 202-214.

Chapchap, A., Ahmed, F.M., Hudson, D.A., Temarel, P., Hirdaris, S.E., 2011. The influence of forward speed and nonlinearities on the dynamic behaviour of a container ship in regular waves. Trans. R. Inst. Nav. Archit. 153, 137-148.

Chatjigeorgiou, I.K., 2013. The analytic solution for hydrodynamic diffraction by submerged prolate spheroids in infinite water depth. J. Eng. Math. 81, 47-65.

Chatzigeorgiou, I.K., 2018. Analytical Methods in Marine Hydrodynamics. Cambridge Univ. Press, Cambridge.

Chatjigeorgiou, I.K., Miloh, T., 2014a. Hydrodynamics of submerged prolate spheroids advancing under waves: Wave diffraction with forward speed. J. Fluids Struct. 49, 202-222.

Chatjigeorgiou, I.K., Miloh, T., 2014b. Wave resistance and diffraction by spheroidal vessels in shallow water. Q. J. Mech. Appl. Math. 67, 525-552.

Chatjigeorgiou, I.K., Miloh, T., 2015. Radiation and oblique diffraction by submerged prolate spheroids in water of finite depth. J. Ocean Eng. Mar. Energy 1, 3-18.

Chatjigeorgiou, I.K., Mavrakos, S.A., Miloh, T., 2013. On the wave resistance of an immersed prolate spheroid in infinite water depth, in: Proc. 28th Int. Workshop Water Waves Floating Bodies. Marseille, France.

Chau, F.P., Eatock Taylor, R., 1992. Second-order wave diffraction by a vertical cylinder. Journal of Fluid Mechanics 240, 571-599.

Chen, X.B., 1991. Free surface Green function and its approximation by polynomial series (Bureau Veritas' Res. Rep. No. 641 DTO/XC). Bureau Veritas, France.

Chen, X.B., 1993. Evaluation de la fonction de Green du problème de diffraction/radiation en profondeur d'eau finie-une nouvelle méthode rapide et précise, in: Proc. 4e J. Hydrodyn. Nantes, France, pp. 371-384.

Chen, X.B., Liang, H., 2016. Wavy properties and analytical modeling of free-surface flows in the development of the multi-domain method. J. Hydrodyn. Ser. B 28, 971-976.

Chen, X.B., Wu, G.X., 2001. On singular and highly oscillatory properties of the Green function for ship motions. J. Fluid Mech. 445,

77-91.

Chen, Z.M., 2013. Harmonic function expansion for translating Green functions and dissipative free-surface waves. Wave Motion 50, 282-294.

Chen, Z.M., 2015. Regular wave integral approach to numerical simulation of radiation and diffraction of surface waves. Wave Motion 52, 171-182.

Chen, Z.M., 2019. Straightforward integration for free surface Green function and body wave motions. Eur. J. Mech. B. Fluids 74, 10-18.

Chen, Z.M., 2020. New formulation of the finite depth free surface Green function. J. Eng. Math. 123, 129-147.

Chester, C., Friedman, B., Ursell, F., 1957. An extension of the method of steepest descents. Math. Proc. Cambridge Philos. Soc. 53, 599-611.

Clément, A.H., 2013. A second order ordinary differential equation for the frequency domain Green function, in: Proc. 28th Int. Workshop Water Waves Floating Bodies. Marseille, France.

Colen, J., Kolomeisky, E.B., 2021. Kelvin-Froude wake patterns of a traveling pressure disturbance. Eur. J. Mech. B. Fluids 85, 400-412.

Copson, E.T., 1965. Asymptotic Expansions. Cambridge Univ. Press, Cambridge.

Cuer, M., 1989. Computation of a Green's function for the three-dimensional linearized transient gravity waves problem. IMPACT Comput. Sci. Eng. 1, 313-325.

Day, A.H., Doctors, L.J., 2001. Rapid estimation of near- and far-field wave wake from ships and application to hull-form design and optimization. J. Ship Res. 45, 73-84.

Delhommeau, G., 1989. Amélioration des performances des codes de calcul de diffraction-radiation au premier ordre, in: Proc. 2e J. Hydrodyn. Nantes, France, pp. 69-88.

Delhommeau, G., Guilbaud, M., David, L., Yang, C., Noblesse, F., 2009. Boundary between unsteady and overturning ship bow wave regimes. J. Fluid Mech. 620, 167-175.

D'elía, J., Battaglia, L., Storti, M., 2011. A semi-analytical computation of the Kelvin kernel for potential flows with a free surface. Comput. Appl. Math. 30, 267-287.

Diebold, L., 2007. Study of the Neumann-Kelvin problem for one hemisphere, in: Proc. 22nd Int. Workshop Water Waves Floating Bodies. Plitvice, Croatia, pp. 57-60.

Doctors, L.J., 2015. Hydrodynamics of High-Performance Marine Vessels. CreateSpace Independent Publishing Platform, Charleston, SC.

Doctors, L.J., Beck, R.F., 1987. Numerical aspects of the Neumann-Kelvin problem. J. Ship Res. 31, 1-13.

Du, S.X., Hudson, D.A., Price, W.G., Temarel, P., 1999. Comparison of numerical evaluation techniques for the hydrodynamic analysis of a ship travelling in waves. Trans. R. Inst. Nav. Archit. 141, 236-258.

Eggers, K., 1957. Über das Wellenbild einer pulsierenden Störung in

Translation. Schiffu. Hafen. 9, 874-878.

Erdélyi, A., 2010. Asymptotic Expansions. Dover Publications, New York.

Faltinsen, O.M., 1993. Sea Loads on Ships and Offshore Structures. Cambridge Univ. Press, Cambridge.

Faltinsen, O.M., 2005. Hydrodynamics of High-Speed Marine Vehicles. Cambridge Univ. Press, Cambridge.

Farell, C., 1973. On the wave resistance of a submerged spheroid. J. Ship Res. 17, 1-11.

Green, G., 1889. An essay on the application of mathematical analysis to the theories of electricity and magnetism. Printed for the author, by T. Wheelhouse, Nottingham.

Guevel, P., Bougis, J., 1982. Ship-motions with forward speed in infinite depth. Int. Shipbuild. Prog. 29, 103-117.

Guevel, P., Vaussy, P., Kobus, J.M., 1974. The distribution of singularities kinematically equivalent to a moving hull in the presence of a free surface. Int. Shipbuild. Prog. 21, 311-324.

Guevel, P., Delhommeau, G., Cordonnier, J.P., 1977. Numerical solution of the Neumann-Kelvin problem by the method of singularities, in: Proc. 2nd Int. Conf. Numer. Ship Hydrodyn. Berkeley, CA, USA, pp. 107-123.

Guilbaud, M., Boin, J.P., Ba, M., 2001. Frequency domain numerical and experimental investigation of forward speed radiation by ships, in: Proc 23rd Symp. Nav. Hydrodyn. Val de Reuil, France, pp. 385-401.

Hanaoka, T., 1957. Theoretical investigation concerning ship motion in regular waves, in: Proc. Symp. Behav. Ships Seaway. Wageningen, The Netherlands.

Hao, L., Pan, Z., Wu, B., 2020. Green function of steady forward speed with ice cover. Eur. J. Mech. B. Fluids 83, 15-23.

Haskind, M.D., 1944. The oscillation of a body immersed in heavy fluid. Philos. Mag. 8, 287-300.

Haskind, M.D., 1946. The hydrodynamic theory of ship oscillations in rolling and pitching. Prikl. Mat. Mekh. 10, 33-66.

Haskind, M., 1954. On wave motion of a heavy fluid. Prikl. Mat. Mekh. 18, 15-26.

Havelock, T.H., 1932. The theory of wave resistance. Proc. R. Soc. London. Ser. A Math. Phys. Sci. 138, 339-348.

Havelock, T.H., 1942. The damping of the heaving and pitching motion of a ship. London, Edinburgh, Dublin Philos. Mag. J. Sci. 33, 666-673.

Havelock, T.H., 1952. The moment on a submerged solid of revolution moving horizontally. Q. J. Mech. Appl. Math. 5, 129-136.

Havelock, T.H., 1955. Waves due to a floating sphere making periodic heaving oscillations. Proc. R. Soc. London. Ser. A Math. Phys. Sci. 231, 1-7.

Havelock, T.H., 1958. The effect of speed of advance upon the damping

of heave and pitch. Trans. R. Inst. Nav. Archit. 100, 131-135.

He, J., Zhang, C., Zhu, Y., Zou, L., Li, W., Noblesse, F., 2016. Interference effects on the Kelvin wake of a catamaran represented via a hull-surface distribution of sources. Eur. J. Mech. B. Fluids 56, 1-12.

He, J., Zhu, Y., Ma, C., Yang, C.-J., Li, W., Noblesse, F., 2018a. Boundary integral representations of steady flow around a ship. Eur. J. Mech. B. Fluids 72, 152-163.

He, J., Fan, S., Wang, J., Yang, C.-J., Li, W., Noblesse, F., 2018b. Analytical relations for filtering negligible short ship waves. Appl. Ocean Res. 79, 215-227.

He, J., Wu, H., Ma, C., Yang, C.-J., Zhu, R.-C., Li, W., Noblesse, F., 2019a. Froude number, hull shape, and convergence of integral representation of ship waves. Eur. J. Mech. B. Fluids 78, 216-229.

He, J., Zhu, Y., Wu, H., Yang, C.-J., Li, W., Noblesse, F., 2019b. Boundary-integral representations for ship motions in regular waves. J. Eng. Math. 114, 115-129.

He, J., Wu, H., Yang, C.-J., Zhu, R.-C., Li, W., Noblesse, F., 2020a. Why can steep short waves occur at a ship waterline and how to filter them in a practical way? Eur. J. Mech. B. Fluids 83, 164-174.

He, J., Wu, H., Zhu, R.-C., Yang, C.-J., Noblesse, F., 2020b. Practical flow-representations for arbitrary singularity-distributions in ship and offshore hydrodynamics, with applications to steady ship waves and wave diffraction-radiation by offshore structures. Eur. J. Mech. B. Fluids 83, 24-41.

He, J., Wu, H., Zhu, R.-C., Yang, C.-J., Noblesse, F., 2020c. Practical evaluation of flows due to arbitrary singularity distributions in the 3D theory of ship motions in regular waves at $\tau < 1/4$. Eur. J. Mech. B. Fluids 83, 212-225.

He, J., Wu, H., Zhu, R.-C., Yang, C.-J., Noblesse, F., 2021a. Practical evaluation of flows due to arbitrary singularity distributions in the 3D theory of ship motions in regular waves at $0.3 \leq \tau$. Eur. J. Mech. B. Fluids 85, 8-20.

He, J., Wu, H., Yang, C.-J., Zhu, R.-C., Li, W., Noblesse, F., 2021b. Boundary-integral representation sans waterline integral for flows around ships steadily advancing in calm water. Eur. J. Mech. B. Fluids 89, 259-266.

He, J., Wu, H., Yang, C.-J., Zhu, R.-C., Li, W., Noblesse, F., 2021c. Diffraction-radiation of regular water waves and irregular frequencies: a straightforward flow-modeling approach and analysis. Eur. J. Mech. B. Fluids 90, 7-14.

He, J., Yang, C.-J., Noblesse, F., 2022a. Optimal fourier-kochin flow representations in ship and offshore hydrodynamics: Theory. Eur. J. Mech. B. Fluids 93, 137-159.

He, J., Zhu, R.-C., Noblesse, F., 2022b. An alternative linear flow model and boundary integral flow representation for ship motions in regular

waves. Eur. J. Mech. B. Fluids 94, 190-199.

He, J., Yang, C.-J., Zhu, R.-C., Noblesse, F., 2023a. Alternative flow models, vector Green functions and boundary integral flow representations in ship and offshore hydrodynamics. Ocean Eng. 270, 113630.

He, J., Zhu, R.-C., Yang, C.-J., 2023b. Potential-flow computations in infinite or zero gravity limits via a weakly singular boundary integral equation. Ocean Eng. 282, 115047.

Hearn, G.E., 1977. Alternative methods of evaluating Green's function in three-dimensional ship-wave problems. J. Ship Res. 21, 89-93.

Hermans, A.J., 1974. A matching principle in non-linear ship wave theory at low Froude number (Delft Prog. Rep. Ser. F Vol. 1).

Hogner, E., 1932. Schiffsform und Wellenwiderstand, in: Kempf, G., Foerster, E. (Eds.), Hydromechanische Probleme Des Schiffsantriebs. Springer, Berlin, Heidelberg, pp. 99-114.

Hong, L., Zhu, R.-C., Miao, G.-P., Fan, J., 2016. Study on Havelock form translating-pulsating source Green's function distributing on horizontal line segments and its applications. Ocean Engineering 124, 306-323.

Huang, F., Yang, C., 2016. Hull form optimization of a cargo ship for reduced drag. J. Hydrodyn. Ser. B 28, 173-183.

Huang, F., Yang, C., Noblesse, F., 2013. Numerical implementation and validation of the Neumann-Michell theory of ship waves. Eur. J. Mech. B. Fluids 42, 47-68.

Huang, F., Kim, H., Yang, C., 2014. A new method for ship bulbous bow generation and modification, in: Proc. 24th Int. Ocean Polar Eng. Conf. Busan, Korea, pp. 823-830.

Huang, F., Wang, L., Yang, C., Royce, R., 2015a. Hull form optimization of a TriSWACH for reduced drag. Presented at the 13th Int. Conf. Fast Sea Transp., Washington DC, USA.

Huang, F., Wang, L., Yang, C., 2015b. Hull form optimization for reduced drag and improved seakeeping using a surrogate-based method, in: Proc. 25th Int. Ocean Polar Eng. Conf. Kona, Hawaii, USA, pp. 931-938.

Huang, F., Wang, L., Yang, C., 2016. A new improved artificial bee colony algorithm for ship hull form optimization. Eng. Optim. 48, 672-686.

Hulme, A., 1982. The wave forces acting on a floating hemisphere undergoing forced periodic oscillations. J. Fluid Mech. 121, 443-463.

Hunt, J.N., Baddour, R.E., 1981. The diffraction of nonlinear progressive waves by a vertical cylinder. Q. J. Mech. Appl. Math. 34, 69-87.

Inglis, R., 1981. Calculation of the velocity potential of a translating, pulsating source. Trans. R. Inst. Nav. Archit. 123, 163-175.

Inglis, R.B., Price, W.G., 1982. A three-dimensional ship motion theory: the hydrodynamic coefficients with forward speed. Trans. R. Inst. Nav. Archit. 124, 141-157.

Iwashita, H., Ohkusu, M., 1989. Hydrodynamic forces on a ship moving with forward speed in waves. J. Soc. Nav. Archit. Jpn. 166, 187-205.

Iwashita, H., Ohkusu, M., 1992. The Green function method for ship

motions at forward speed. Ship Technol. Res. 39, 3-21.

John, F., 1949. On the motion of floating bodies. I. Commun. Pure Appl. Math. 2, 13-57.

John, F., 1950. On the motion of floating bodies II. Simple harmonic motions. Commun. Pure Appl. Math. 3, 45-101.

Jones, D.S., 1974. Integral equations for the exterior acoustic problem. Q. J. Mech. Appl. Math. 27, 129-142.

Khabakhpasheva, T.I., Korobkin, A.A., 2002. Hydroelastic behaviour of compound floating plate in waves. J. Eng. Math. 44, 21-40.

Kim, W.D., 1965. On the harmonic oscillations of a rigid body on a free surface. J. Fluid Mech. 21, 427-451.

Kleinman, R.E., 1982. On the mathematical theory of the motion of floating bodies: an update (Rep. No. DTNSRDC-82/074). David W. Taylor Naval Ship Res. Dev. Center, Bethesda, MD, USA.

Kleinman, R.E., Roach, G.F., 1974. Boundary integral equations for the three-dimensional Helmholtz equation. SIAM Rev. 16, 214-236.

Kochin, N.E., 1952. The theory of waves generated by oscillations of a body under the free surface of a heavy incompressible fluid. English transl., in: Soc. Nav. Archit. Mar. Eng. Tech. Res. Bull. No. 1-10. Soc. Nav. Archit. Mar. Eng., New York.

Kostyukov, A.A., 1968. Theory of ship waves and wave resistance. English transl. E.C.I, Iowa City, Iowa.

Lamb, H., 1932. Hydrodynamics. Cambridge Univ. Press, Cambridge.

Lau, S.M., Hearn, G.E., 1989. Suppression of irregular frequency effects in fluid-structure interaction problems using a combined boundary integral equation method. Int. J. Numer. Methods Fluids 9, 763-782.

Lee, C.-H., Newman, J.N., Zhu, X., 1996. An extended boundary integral equation method for the removal of irregular frequency effects. Int. J. Numer. Methods Fluids 23, 637-660.

Lee, C.-H., Newman, J., 2005. Computation of wave effects using the panel method, in: Numerical Models in Fluid-Structure Interaction. WIT Press, pp. 211-251.

Lee, C.-H., Sclavounos, P.D., 1989. Removing the irregular frequencies from integral equations in wave-body interactions. J. Fluid Mech. 207, 393-418.

Liang, H., Wu, H., Noblesse, F., 2018a. Validation of a global approximation for wave diffraction-radiation in deep water. Appl. Ocean Res. 74, 80-86.

Liang, H., Chen, X.B., Feng, X., 2018b. Wave-making problem by a vertical cylinder: Neumann-Kelvin theory versus Neumann-Michell theory, in: Proc. 33rd Int. Workshop Water Waves Floating Bodies. Guidel-Plages, France.

Liang, H., Wu, H., He, J., Noblesse, F., 2020a. Kelvin-Havelock-Peters approximations to a classical generic wave integral. Appl. Math. Modell. 77, 950-962.

Liang, H., Ouled Housseine, C., Chen, X.B., Shao, Y., 2020b. Efficient methods free of irregular frequencies in wave and solid/porous structure interactions. J. Fluids Struct. 98, 103130.

Liang, H., Shao, Y., Chen, J., 2021. Higher-order derivatives of the Green function in hyper-singular integral equations. Eur. J. Mech. B. Fluids 86, 223-230.

Liapis, S., 1993. A method for suppressing the irregular frequencies from integral equations in water wave-structure. Interaction problems. Comput. Mech. 12, 59-68.

Lighthill, M.J., 1958. An Introduction to Fourier Analysis and Generalised Functions. Cambridge Univ. Press, Cambridge.

Lighthill, M.J., 1967. On waves generated in dispersive systems by travelling forcing effects, with applications to the dynamics of rotating fluids. J. Fluid Mech. 27, 725-752.

Lighthill, M.J., 1978. Waves in Fluids. Cambridge Univ. Press, Cambridge.

Linton, C.M., 1991. Radiation and diffraction of water waves by a submerged sphere in finite depth. Ocean Eng. 18, 61-74.

Linton, C.M., 1999. Rapidly convergent representations for Green' functions for Laplace' equation. Proc. R. Soc. London. Ser. A Math. Phys. Eng. Sci. 455, 1767-1797.

Liu, Y., Iwashita, H., Hu, C., 2015. A calculation method for finite depth free-surface green function. Int. J. Nav. Archit. Ocean Eng. 7, 375-389.

Liu, Y., Cong, P., Gou, Y., Yoshida, S., Kashiwagi, M., 2020. Enhanced Endo's approach for evaluating free-surface Green's function with application to wave-structure interactions. Ocean Eng. 207, 107377.

Lunde, J.K., 1951. On the linearized theory of wave resistance for displacement ships in steady and accelerated motion. Trans. Soc. Nav. Archit. Mar. Eng. 59, 25-76.

Ma, C., Zhang, C., Chen, X., Jiang, Y., Noblesse, F., 2016. Practical estimation of sinkage and trim for common generic monohull ships. Ocean Eng. 126, 203-216.

Ma, C., Zhang, C., Huang, F., Yang, C., Gu, X.-C., Li, W., Noblesse, F., 2017. Practical evaluation of sinkage and trim effects on the drag of a common generic freely floating monohull ship. Appl. Ocean Res. 65, 1-11.

Ma, C., Zhu, Y., He, J., Zhang, C., Wan, D., Yang, C., Noblesse, F., 2018. Nonlinear corrections of linear potential-flow theory of ship waves. Eur. J. Mech. B. Fluids 67, 1-14.

MacCamy, R.C., 1954. The motion of a floating sphere in surface waves (Rep. Ser. 61 Issue 4). Wave Research Lab., Univ. of Calif., Berkeley.

Mackay, E., 2019. Consistent expressions for the free-surface Green function in finite water depth. Appl. Ocean Res. 93, 101965.

Malenica, S., Chen, X.B., 1998. On the irregular frequencies appearing in wave diffraction-radiation solutions. Int. J. Offshore Polar Eng. 8,

110-114.

Malenica, S., Molin, B., 1995. Third-harmonic wave diffraction by a vertical cylinder. J. Fluid Mech. 302, 203-229.

Marr, G.P., 1996. An investigation of Neumann-Kelvin ship wave theory and its application to yacht design (PhD Thesis). Univ. of Auckland, Auckland, New Zealand.

Martin, D., 1980. Résolution numérique du problème linéarisé de la tenue à la mer. Bull. Assoc. Tech. Marit. Aeronaut.

Martin, P.A., 1981. On the null-field equations for water-wave radiation problems. J. Fluid Mech. 113, 315-332.

Maruo, H., 1960. The drift of a body floating on waves. J. Ship Res. 4, 1-10.

Maury, C., Delhommeau, G., Ba, M., Boin, J.P., Guilbaud, M., 2003. Comparison between numerical computations and experiments for seakeeping on ship models with forward speed. J. Ship Res. 47, 347-364.

Meng, Q.R., Lu, D.Q., 2017. Wave-induced hydrodynamic responses of a rigid body connected with elastic plates floating on a two-layer fluid. J. Fluids Struct. 68, 295-309.

Miao, S., Liu, Y., 2015. Wave pattern in the wake of an arbitrary moving surface pressure disturbance. Phys. Fluids 27, 122102.

Michell, J.H., 1898. The wave-resistance of a ship. London, Edinburgh, Dublin Philos. Mag. J. Sci. 45, 106-123.

Molin, B., 1979. Second-order diffraction loads upon three-dimensional bodies. Appl. Ocean Res. 1, 197-202.

Molin, B., 2023. Offshore Structure Hydrodynamics. Cambridge Univ. Press, Cambridge.

Nakatake, K., Yamazaki, R., 1976. Discussion on the line integral of wave resistance theory, in: Proc. Int. Semin. Wave Resist. Tokyo, Japan, pp. 445-446.

Newman, J.N., 1967. The drift force and moment on ships in waves. J. Ship Res. 11, 51-60.

Newman, J.N., 1976. Linearized wave resistance theory, in: Proc. Int. Semin. Wave Resist. Tokyo, Japan, pp. 31-43.

Newman, J.N., 1977. Marine Hydrodynamics. The MIT Press, Cambridge, MA.

Newman, J.N., 1984. An expansion of the oscillatory source potential. Appl. Ocean Res. 6, 116-117.

Newman, J.N., 1985. Algorithms for the free-surface Green function. J. Eng. Math. 19, 57-67.

Newman, J.N., 1987a. Evaluation of the wave-resistance Green function: Part 1—the double integral. J. Ship Res. 31, 79-90.

Newman, J.N., 1987b. Evaluation of the wave-resistance Green function: part 2—the single integral on the centerplane. J. Ship Res. 31, 145-150.

Newman, J.N., 1996. The second-order wave force on a vertical cylinder. J. Fluid Mech. 320, 417-443.

Noblesse, F., 1975a. The near-field disturbance in the centerplane Havelock source potential, in: Proc. 1st Int. Conf. Numer. Ship Hydrodyn. Gaithersburg, MD, USA, pp. 481-501.

Noblesse, F., 1975b. A perturbation analysis of the wavemaking of a ship, with an interpretation of Guilloton's method. J. Ship Res. 19, 140-148.

Noblesse, F., 1977. The fundamental solution in the theory of steady motion of a ship. J. Ship Res. 21, 82-88.

Noblesse, F., 1978a. The steady wave potential of a unit source, at the centerplane. J. Ship Res. 22, 80-88.

Noblesse, F., 1978b. On the fundamental function in the theory of steady motion of ships. J. Ship Res. 22, 212-215.

Noblesse, F., 1981. Alternative integral representations for the Green function of the theory of ship wave resistance. J. Eng. Math. 15, 241-265.

Noblesse, F., 1982. The Green function in the theory of radiation and diffraction of regular water waves by a body. J. Eng. Math. 16, 137-169.

Noblesse, F., 1983a. A slender-ship theory of wave resistance. J. Ship Res. 27, 13-33.

Noblesse, F., 1983b. Integral identities of potential theory of radiation and diffraction of regular water waves by a body. J. Eng. Math. 17, 1-13.

Noblesse, F., 2001a. Analytical representation of ship waves. Ship Technol. Res. 48, 23-48.

Noblesse, F., 2001b. Velocity representation of free-surface flows and Fourier-Kochin representation of waves. Appl. Ocean Res. 23, 41-52.

Noblesse, F., 2002. Rankine and Fourier-Kochin representation of near-field ship waves. J. Ship Res. 46, 63-79.

Noblesse, F., Dagan, G., 1976. Nonlinear ship-wave theories by continuous mapping. J. Fluid Mech. 75, 347-371.

Noblesse, F., Hendrix, D., 1990. Fourier-Kochin representation of the flow due to a ship advancing in regular waves. Presented at the IUTAM Symp. Dyn. Mar. Veh. Struct. Waves, Brunel Univ., London, UK.

Noblesse, F., Hendrix, D., 1992. On the theory of potential flow about a ship advancing in waves. J. Ship Res. 36, 17-29.

Noblesse, F., Chen, 1995. Decomposition of free-surface effects into wave and near-field components. Ship Technol. Res. 42, 167-185.

Noblesse, F., Yang, C., 1995. Fourier-Kochin formulation of wave diffraction-radiation by ships or offshore structures. Ship Technol. Res. 42, 115-139.

Noblesse, F., Yang, C., 1996. Fourier representation of near-field free-surface flows. Ship Technol. Res. 43, 19-37.

Noblesse, F., Chen, X.B., 1997. Far-field and near-field dispersive waves. Ship Technol. Res. 44, 37-43.

Noblesse, F., Yang, C., 2004. A simple Green function for diffraction-radiation of time-harmonic waves with forward speed. Ship Technol. Res. 51, 35-52.

Noblesse, F., Yang, C., 2007. Elementary water waves. J. Eng. Math. 59, 277-299.

Noblesse, F., Yang, C., 2023. Boundary integral relations for submerged bodies and free-surface piercing ships and offshore structures. Ocean Eng. 280, 114799.

Noblesse, F., Hendrix, D.M., Kahn, L., 1991. Nonlinear local analysis of steady flow about a ship. J. Ship Res. 35, 288-294.

Noblesse, F., Chen, X.B., Yang, C., 1996. Fourier-Kochin theory of free-surface flows, in: Proc. 21st Symp. Nav. Hydrodyn. Trondheim, Norway, pp. 120-135.

Noblesse, F., Chen, X.B., Yang, C., 1999. Generic super Green functions. Ship Technol. Res. 46, 81-92.

Noblesse, F., Hendrix, D., Faul, L., Slutsky, J., 2006. Simple analytical expressions for the height, location, and steepness of a ship bow wave. J. Ship Res. 50, 360-370.

Noblesse, F., Delhommeau, G., Guilbaud, M., Yang, C., 2008a. The rise of water at a ship stem. J. Ship Res. 52, 89-101.

Noblesse, F., Delhommeau, G., Guilbaud, M., Hendrix, D., Yang, C., 2008b. Simple analytical relations for ship bow waves. J. Ship Res. 600, 105-132.

Noblesse, F., Delhommeau, G., Kim, H.Y., Yang, C., 2009a. Thin-ship theory and influence of rake and flare. J. Eng. Math. 64, 49-80.

Noblesse, F., Delhommeau, G., Yang, C., 2009b. Practical evaluation of steady flow resulting from a free-surface pressure patch. J. Ship Res. 53, 137-150.

Noblesse, F., Delhommeau, G., Yang, C., Kim, H.Y., Queutey, P., 2011a. Analytical bow waves for fine ship bows with rake and flare. J. Ship Res. 55, 1-18.

Noblesse, F., Delhommeau, G., Huang, F., Yang, C., 2011b. Practical mathematical representation of the flow due to a distribution of sources on a steadily advancing ship hull. J. Eng. Math. 71, 367-392.

Noblesse, F., Wang, L., Yang, C., 2012. A simple verification test for nonlinear flow calculations around a ship hull steadily advancing in calm water. J. Ship Res. 56, 162-169.

Noblesse, F., Delhommeau, G., Liu, H., Wan, D., Yang, C., 2013a. Ship bow waves. J. Hydrodyn. Ser. B 25, 491-501.

Noblesse, F., Huang, F., Yang, C., 2013b. The Neumann-Michell theory of ship waves. J. Eng. Math. 79, 51-71.

Noblesse, F., Huang, F., Yang, C., 2013c. Evaluation of ship waves at the free surface and removal of short waves. Eur. J. Mech. B. Fluids 38, 22-37.

Noblesse, F., Delhommeau, G., Queutey, P., Yang, C., 2014a. An elementary analytical theory of overturning ship bow waves. Eur. J. Mech. B. Fluids 48, 193-209.

Noblesse, F., He, J., Zhu, Y., Hong, L., Zhang, C., Zhu, R.-C., Yang,

C., 2014b. Why can ship wakes appear narrower than Kelvin's angle? Eur. J. Mech. B. Fluids 46, 164-171.

Noblesse, F., Zhang, C., He, J., Zhu, Y., Yang, C.-J., Li, W., 2016. Observations and computations of narrow Kelvin ship wakes. J. Ocean. Eng. Sci. 1, 52-65.

Ogilvie, T.F., 1968. Wave resistance: the low-speed limit (Dept. Nav. Archit. Mar. Eng. Rep. No. 002). Univ. of Michigan.

Ogilvie, T.F., Shin, Y.S., 1978. Integral-equation solutions for time-dependent free-surface problems. J. Soc. Nav. Archit. Jpn. 143, 41-51.

Ohkusu, M., Iwashita, H., 1989. Evaluation of the Green function for ship motions at forward speed and application to radiation and diffraction problems, in: Proc. 4th Int. Workshop Water Waves Floating Bodies. Oystese, Norway, pp. 16-20.

Ohmatsu, S., 1975. On the irregular frequencies in the theory of oscillating bodies in a free surface (Papers Ship Res. Inst. No. 48). Ship Research Institute, Tokyo, Japan.

Ohmatsu, S., 1983. A new simple method to eliminate the irregular frequencies in the theory of water wave radiation problems. (Papers Ship Res. Inst. No. 70). Ship Research Institute, Tokyo, Japan.

Peng, H., Wang, J., Qiu, W., 2015. Effect of line integral on the computation of forward-speed ship motions, in: Proc. 34th Int. Conf. Offshore Mech. Arct. Eng. St. John's, Newfoundland, Canada.

Percival, S., Hendrix, D., Noblesse, F., 2001. Hydrodynamic optimization of ship hull forms. Appl. Ocean Res. 23, 337-355.

Peter, M.A., Meylan, M.H., 2004. The eigenfunction expansion of the infinite depth free surface Green function in three dimensions. Wave Motion 40, 1-11.

Peters, A.S., 1949. A new treatment of the ship wave problem. Commun. Pure Appl. Math. 2, 123-148.

Pidcock, M.K., 1985. The calculation of Green's functions in three dimensional hydrodynamic gravity wave problems. Int. J. Numer. Methods Fluids 5, 891-909.

Pogorelova, A.V., 2011. Unsteady motion of a source in a fluid under a floating plate. J. Appl. Mech. Tech. Phys. 52, 717-726.

Pogorelova, A.V., Zemlyak, V.L., Kozin, V.M., 2019. Moving of a submarine under an ice cover in fluid of finite depth. J. Hydrodyn. Ser. B 31, 562-569.

Ponizy, B., Noblesse, F., Ba, M., Guilbaud, M., 1994. Numerical evaluation of free-surface Green functions. J. Ship Res. 38, 193-202.

Rahman, M., 1998. Nonlinear hydrodynamic loading on offshore structures. Theor. Comput. Fluid Dyn. 10, 323-347.

Rahman, M., Mousavizadegan, S.H., 2006. Second-order wave loads on offshore structures using the weber's transform method, in: Advances in Fluid Mechanics VI. WIT Press, pp. 435-444.

Rezayat, M., Shippy, D.J., Rizzo, F.J., 1986. On time-harmonic

elastic-wave analysis by the boundary element method for moderate to high frequencies. Comput. Methods Appl. Mech. Eng. 55, 349-367.

Sayer, P., Ursell, F., 1980. An integral-equation method for determining the fluid motion due to a cylinder heaving on water of finite depth. Proc. R. Soc. London. Ser. A Math. Phys. Sci. 372, 93-110.

Schenck, H.A., 1968. Improved integral formulation for acoustic radiation problems. J. Acoust. Soc. Am. 44, 41-58.

Scragg, C.A., Talcott, J.C., 1988. Convergence of the Neumann-Kelvin problem, in: Proc. 3rd Int. Workshop Water Waves Floating Bodies. Woods Hole, MA, USA, pp. 153-156.

Shan, P., Wu, J., 2018. Highly precise approximation of free surface Green function and its high order derivatives based on refined subdomains. Brodogradnja 69, 53-70.

Shan, P., Zhu, R.-C., Wang, F., Wu, J., 2019. Efficient approximation of free-surface Green function and OpenMP parallelization in frequency-domain wave-body interactions. J. Mar. Sci. Technol. 24, 479-489.

Shen, H.-T., Farell, C., 1977. Numerical calculation of the wave integrals in the linearized theory of water waves. J. Ship Res. 21, 1-10.

Shen, Y., Yu, D., Duan, W., Ling, H., 2016. Ordinary differential equation algorithms for a frequency-domain water wave Green's function. J. Eng. Math. 100, 53-66.

Squire, V.A., 2008. Synergies between VLFS hydroelasticity and sea ice research. Int. J. Offshore Polar Eng. 18, 241-253.

Squire, V.A., Dugan, J.P., Wadhams, P., Rottier, P.J., Liu, A.K., 1995. Of ocean waves and sea ice. Annu. Rev. Fluid Mech. 27, 115-168.

Squire, V.A., Hosking, R.J., Kerr, A.D., Langhorne, P.J., 1996. Moving Loads on Ice Plates. Springer Dordrecht.

Standing, R.G., 1974. Phase and amplitude discrepancies in the surface wave due to a wedge-ended hull form. J. Fluid Mech. 62, 625-642.

Sretenskii, L.N., 1954. The motion of a vibrator under the surface of a fluid. Tr. Mosk. Mat. Obs. 3, 3-14.

Sturova, I.V., 2013. Unsteady three-dimensional sources in deep water with an elastic cover and their applications. J. Fluid Mech. 730, 392-418.

Sun, L., Teng, B., Liu, C.F., 2008. Removing irregular frequencies by a partial discontinuous higher order boundary element method. Ocean Eng. 35, 920-930.

Telste, J.G., Noblesse, F., 1986. Numerical evaluation of the Green function of water-wave radiation and diffraction. J. Ship Res. 30, 69-84.

Telste, J.G., Noblesse, F., 1988. The nonoscillatory near-field term in the Green function for steady flow about a ship, in: Proc. 17th Symp. Nav. Hydrodyn. The Hague, The Netherlands, pp. 39-52.

Teng, B., Kato, S., 2002. Third order wave force on axisymmetric bodies. Ocean Eng. 29, 815-843.

Thomson, W., 1891. Popular Lectures and Addresses, Vol. 3. Macmillan and Co., London.

Thorne, R.C., 1953. Multipole expansions in the theory of surface waves. Math. Proc. Cambridge Philos. Soc. 49, 707-716.

Tsai, W., Lin, Y., Liao, C., 1983. Numerical solution of the Neumann-Kelvin problem and its application to ship wave-resistance computations, in: Proc. 2nd DTNSRDC Workshop Ship Wave-Resist. Comput. Bethesda, MD, USA, pp. 233-280.

Tsutsumi, T., 1979. Calculation of the wave resistance of ships by the numerical solution of Neumann-Kelvin problem, in: Proc. Workshop Ship Wave-Resist. Comput. Bethesda, MD, USA, pp. 162-201.

Uğurlu, B., Guedes Soares, C., 2021. Application of the Fourier-Kochin theory for the diffraction and radiation of free-surface waves about stationary floating bodies. Ocean Eng. 227, 108831.

Ursell, F., 1949. On the heaving motion of a circular cylinder on the surface of a fluid. Q. J. Mech. Appl. Math. 2, 218-231.

Ursell, F., 1973. On the exterior problems of acoustics. Math. Proc. Cambridge Philos. Soc. 74, 117-125.

Ursell, F., 1981. Irregular frequencies and the motion of floating bodies. J. Fluid Mech. 105, 143-156.

Wang, S., 1986. Motions of a spherical submarine in waves. Ocean Eng. 13, 249-271.

Wang, R.S., 1992. The numerical approach of three dimensional free-surface Green function and its derivatives. J. Hydrodyn. Ser. A 7, 277-286.

Wang, L., Huang, F., Yang, C., Datla, R., 2015. Hydrodynamic optimization of a wedge hull. Presented at the 13th Int. Conf. Fast Sea Transp., Washington DC, USA.

Wehausen, J.V., Laitone, E.V., 1960. Surface Waves, in: Truesdell, C. (Ed.), Fluid Dynamics. Encyclopedia of Physics. Springer, Berlin, Heidelberg.

Wehausen, J.V., 1971. The motion of floating bodies. Annu. Rev. Fluid Mech. 3, 237-268.

Wehausen, J.V., 1973. The wave resistance of ships. Adv. Appl. Mech. 13, 93-245.

Wigley, W.C.S., 1926. Ship wave resistance. A comparison of mathematical theory with experimental results. Trans. Inst. Nav. Archit. 68, 124-137.

Wong, R., 1989. Asymptotic Approximations of Integrals. Academic Press, Boston.

Wu, G.X., Eatock Taylor, R., 1987a. A Green's function form for ship motions at forward speed. Int. Shipbuild. Prog. 34, 189-196.

Wu, G.X., Eatock Taylor, R., 1987b. The exciting force on a submerged spheroid in regular waves. J. Fluid Mech. 182, 411-426.

Wu, G.X., Eatock Taylor, R., 1989. On the radiation and diffraction of surface waves by submerged spheroids. J. Ship Res. 33, 84-92.

Wu, X.J., Price, W.G., 1986. An equivalent box approximation to

predict irregular frequencies in arbitrarily-shaped three-dimensional marine structures. Appl. Ocean Res. 8, 223-231.

Wu, X.J., Price, W.G., 1987. A multiple Green's function expression for the hydrodynamic analysis of multi-hull structures. Appl. Ocean Res. 9, 58-66.

Wu, H., Zhang, C., Ma, C., Huang, F., Yang, C., Noblesse, F., 2016. Errors due to a practical Green function for steady ship waves. Eur. J. Mech. B. Fluids 55, 162-169.

Wu, H., Zhang, C., Zhu, Y., Li, W., Wan, D., Noblesse, F., 2017. A global approximation to the Green function for diffraction radiation of water waves. Eur. J. Mech. B. Fluids 65, 54-64.

Wu, H., Liang, H., Noblesse, F., 2018a. Wave component in the Green function for diffraction radiation of regular water waves. Appl. Ocean Res. 81, 72-75.

Wu, H., He, J., Zhu, Y., Noblesse, F., 2018b. The Kelvin-Havelock-Peters farfield approximation to ship waves. Eur. J. Mech. B. Fluids 70, 93-101.

Wu, H., He, J., Zhu, Y., Yang, C.-J., Li, W., Noblesse, F., 2018c. Neumann-Michell theory of short ship waves. Eur. J. Mech. B. Fluids 72, 601-615.

Wu, H., Wu, J., He, J., Zhu, R.-C., Yang, C.-J., Noblesse, F., 2019a. Wave profile along a ship hull, short farfield waves, and broad inner Kelvin wake sans divergent waves. Phys. Fluids 31, 047102.

Wu, H., He, J., Liang, H., Noblesse, F., 2019b. Influence of Froude number and submergence depth on wave patterns. Eur. J. Mech. B. Fluids 75, 258-270.

Wu, H., He, J., Zhu, R.-C., Yang, C.-J., Noblesse, F., 2021. Practical representation of flows due to general singularity distributions for wave diffraction-radiation by offshore structures in finite water depth. Eur. J. Mech. B. Fluids 89, 1-14.

Xie, Z., Liu, Y., Falzarano, J., 2017. A more efficient numerical evaluation of the green function in finite water depth. Ocean Syst. Eng. 7, 399-412.

Xie, C., Choi, Y., Rongère, F., Clément, A.H., Delhommeau, G., Babarit, A., 2018. Comparison of existing methods for the calculation of the infinite water depth free-surface Green function for the wave-structure interaction problem. Appl. Ocean Res. 81, 150-163.

Xie, C., Chen, X.B., Clément, A.H., Babarit, A., 2019. A new ordinary differential equation for the evaluation of the frequency-domain Green function. Appl. Ocean Res. 86, 239-245.

Xu, Y., Dong, W., 2011. Study on characteristics of 3-D translating-pulsating source green function of deep-water havelock form and its fast integration method. China Ocean Eng. 25, 365-380.

Yang, C., Huang, F., 2016. An overview of simulation-based hydrodynamic design of ship hull forms. J. Hydrodyn. Ser. B 28, 947-960.

Yang, C., Huang, F., Noblesse, F., 2013. Practical evaluation of the drag of a ship for design and optimization. J. Hydrodyn. Ser. B 25, 645-654.

Yang, C., Huang, F., Kim, H., 2014. Hydrodynamic optimization of a triswach. J. Hydrodyn. Ser. B 26, 856-864.

Yang, C., Huang, F., Wang, L., 2016. A NURBS-based modification technique for bulbous bow generation and hydrodynamic optimization, in: Proc. 31st Symp. Nav. Hydrodyn. Monterey, CA, USA, pp. 11-16.

Yang, Y., Zhu, R.-C., Hong, L., Huang, S., 2019a. A semi-analytical high-order translating-pulsating source method for forward-speed ship motions. Ocean Eng. 182, 627-644.

Yang, Y., Zhu, R.-C., Hong, L., 2019b. A frequency-domain hybrid HOBEM for motion responses and added resistance of ships sailing in head and oblique waves. Ocean Eng. 194, 106637.

Yao, X.-L., Sun, S.-L., Wang, S.-P., Yang, S.-T., 2009. The research on the highly efficient calculation method of 3-D frequency-domain Green function. J. Mar. Sci. Appl. 8, 196-203.

Yeung, R.W., 1972. Sinkage and trim in first-order thin-ship theory. J. Ship Res. 16, 47-59.

Yeung, R.W., 1981. Added mass and damping of a vertical cylinder in finite-depth waters. Appl. Ocean Res. 3, 119-133.

Zhang, C., Noblesse, F., Wan, D., 2014. Partial validation and verification of the Neumann-Michell theory of ship waves, in: Proc. 11th Int. Conf. Hydrodyn. Singapore.

Zhang, C., He, J., Ma, C., Noblessse, F., Wan, D., Huang, F., Yang, C., 2015a. Validation of the Neumann-Michell theory for two catamarans, in: Proc. 25th Int. Ocean Polar Eng. Conf. Kona, Hawaii, USA, pp. 1018-1024.

Zhang, C., He, J., Zhu, Y., Li, W., Noblesse, F., Huang, F., Yang, C., 2015b. Stationary phase and numerical evaluation of far-field and near-field ship waves. Eur. J. Mech. B. Fluids 52, 28-37.

Zhang, C., He, J., Zhu, Y., Yang, C.-J., Li, W., Zhu, Y., Lin, M., Noblesse, F., 2015c. Interference effects on the Kelvin wake of a monohull ship represented via a continuous distribution of sources. Eur. J. Mech. B. Fluids 51, 27-36.

Zhu, Y., Wu, H., Ma, C., He, J., Li, W., Wan, D., Noblesse, F., 2017. Michell and Hogner models of far-field ship waves. Appl. Ocean Res. 68, 194-203.

Zhu, Y., He, J., Wu, H., Li, W., Noblesse, F., Delhommeau, G., 2018a. Elementary ship models and farfield waves. Eur. J. Mech. B. Fluids 67, 231-241.

Zhu, Y., Wu, H., He, J., Zhang, C., Li, W., Noblesse, F., 2018b. Hogner model of wave interferences for farfield ship waves in shallow water. Appl. Ocean Res. 73, 127-140.

Zilman, G., 2006. Forces exerted on a hovercraft by a moving pressure

distribution: robustness of mathematical models. J. Ship Res. 50, 38-48.

Zong, Z., Huang, D., 1991. Numerical studies on potential of a 3-D pulsating source in uniform stream. J. Hydrodyn. Ser. A 6, 55-63.

$$q^H \equiv \mathbf{n}\cdot\nabla_{\boldsymbol{\xi}}\,\varphi$$

$$\begin{aligned}
&\mathrm{Re}\,\varphi(\boldsymbol{\xi})\,e^{-\mathrm{i}\,f_\epsilon t} \text{ where } f_\epsilon \equiv f+\mathrm{i}\,\epsilon \text{ with } \epsilon=+0\\
&\nabla_{\boldsymbol{\xi}}\,\varphi\to 0 \text{ as } \boldsymbol{\xi}\to\infty \qquad\qquad f\equiv\omega\sqrt{L/g}\\
&\nabla^2_{\boldsymbol{\xi}}\,\varphi\equiv(\partial^2_\xi+\partial^2_\eta+\partial^2_\zeta)\,\varphi=0 \text{ in } \mathcal{D}\\
&\partial_\zeta\,\varphi+(\mathrm{i}\,f_\epsilon+F\partial_\xi)^2\varphi=0 \text{ at } \Sigma^F\\
&\mathbf{n}\cdot\nabla_{\boldsymbol{\xi}}\,\varphi=q^H \text{ at } \Sigma^H \qquad\qquad F\equiv V/\sqrt{gL}
\end{aligned}$$

$$\begin{aligned}
&G(\boldsymbol{\xi},\mathbf{x}) \quad \text{defined as:} \qquad G\to 0 \text{ as } \boldsymbol{\xi}\to\infty\\
&\left\{\begin{array}{l}\nabla^2_{\boldsymbol{\xi}}G=\delta(\xi-x)\,\delta(\eta-y)\,\delta(\zeta-z) \text{ in } \zeta<0\\ \partial_\zeta G+(\mathrm{i}\,f_\epsilon-F\partial_\xi)^2G=0 \text{ at } \zeta=0\end{array}\right\}\text{ if } z<0\\
&\left\{\begin{array}{l}\nabla^2_{\boldsymbol{\xi}}G=0 \text{ in } \zeta<0\\ \partial_\zeta G+(\mathrm{i}\,f_\epsilon-F\partial_\xi)^2G=-\,\delta(\xi-x)\,\delta(\eta-y) \text{ at } \zeta=0\end{array}\right\}\text{ if } z=0
\end{aligned}$$

$$\Delta\equiv(f+F\alpha)^2-k\equiv(f+Fk\cos\gamma)^2-k$$

$$0\le\mu^*\le\infty \quad\Longrightarrow$$

$\mu^*=0$ and $\mu^*=\infty$

$$\begin{aligned}
&\mu^*\to\infty \quad\Longrightarrow\quad I^F=I^W_\infty+I^L_\infty\\
&I^W_\infty=-\,\mathrm{i}\,\pi\,\mathrm{sign}(\Delta^*_1)\,\mathcal{A}^*e^{\,\mathrm{i}\,\alpha_*\,x}/|\,\Delta^*_\alpha\,|\\
&I^L_\infty=PV\!\int_{-\infty}^{\infty}\!d\alpha\,\frac{\mathcal{A}}{\Delta}\,e^{\,\mathrm{i}\,\alpha\,x}
\end{aligned}$$

$$\begin{aligned}
&\mu^*=0 \quad\Longrightarrow\quad I^F=I^W_0+I^L_0\\
&I^W_0=\mathrm{i}\,\pi\,[\,\mathrm{sign}(x)-\mathrm{sign}(\Delta^*_1\,\Delta^*_\alpha)\,]\,\mathcal{A}^*\,e^{\,\mathrm{i}\,\alpha_*\,x}/\Delta^*_\alpha\\
&I^L_0=\int_{-\infty}^{\infty}\!d\alpha\left[\frac{\mathcal{A}}{\Delta}-\frac{\mathcal{A}^*/\Delta^*_\alpha}{\alpha-\alpha_*}\right]e^{\,\mathrm{i}\,\alpha\,x}
\end{aligned}$$

$$\mathcal{A} = e^{-\alpha^2} \;\; , \;\; \Delta_1 = 1 \;\; , \;\; \Delta = \alpha - 1$$

$$I^F = \int_{-\infty}^{\infty} d\alpha \; \frac{e^{-\alpha^2 + \mathrm{i}\,\alpha\, x}}{\alpha - 1 + \mathrm{i}\,0} = I^W + I^L$$
$$I^W \equiv \mathrm{i}\,\pi\,[\mathrm{erf}(x/\mu) - 1]\; e^{\,\mathrm{i}\,x}/e$$
$$I^L \equiv \int_{-\infty}^{\infty} d\alpha \; \frac{e^{-\alpha^2} - e^{-\mu^2(\alpha-1)^2/4 - 1}}{\alpha - 1} \; e^{\,\mathrm{i}\,\alpha\, x}$$

$$I^W_\infty = -\,\mathrm{i}\,\pi \; \frac{e^{\,\mathrm{i}\,x}}{e} \;\; , \;\; I^L_\infty = PV \int_{-\infty}^{\infty} d\alpha \; \frac{e^{-\alpha^2 + \mathrm{i}\,\alpha\, x}}{\alpha - 1}$$
$$I^W_0 = \mathrm{i}\,\pi\,[\mathrm{sign}(x) - 1] \; \frac{e^{\,\mathrm{i}\,x}}{e} \;\; , \;\; I^L_0 = \int_{-\infty}^{\infty} d\alpha \; \frac{e^{-\alpha^2} - 1/e}{\alpha - 1} \; e^{\,\mathrm{i}\,\alpha\, x}$$

$$\phi^F(\mathbf{x}) \equiv \frac{1}{\pi} \int_{-\infty}^{\infty} d\beta \int_{-\infty}^{\infty} d\alpha \; \frac{\mathcal{A}(\alpha,\beta)\; e^{\,\mathrm{i}\,(\alpha\, x + \beta\, y)}}{\Delta(\alpha,\beta) + \mathrm{i}\,\epsilon\,\Delta_1(\alpha,\beta)} = \phi^W(\mathbf{x}) + \phi^L(\mathbf{x})$$

$$\phi^F(\mathbf{x}) \equiv \frac{1}{\pi} \int_{-\pi}^{\pi} d\gamma \int_0^{\infty} dk \; \frac{\cosh(k\,d)}{e^{\,k\,d}/2} \; \frac{A^z(k,z)\; e^{\,\mathrm{i}\,k\,(x\,\cos\gamma + y\,\sin\gamma)}}{1 - (k/f^2)\tanh(kd) + \mathrm{i}\,\epsilon} \; A(k,\gamma)$$

$$\frac{\mathrm{i}\,\phi^W(\mathbf{x})}{f^2} \equiv \widehat{A}_*\, A^z_* \int_{-\pi}^{\pi} d\gamma \; \Theta \; e^{\,\mathrm{i}\,k_*\,(x\,\cos\gamma + y\,\sin\gamma)}\, A_*(\gamma)$$
$$\text{where} \;\; \Theta \equiv 1 + \mathrm{erf}[\,k_*\,(x\cos\gamma + y\sin\gamma)/C\,]$$

$$\phi^L(\mathbf{x}) \equiv \frac{2}{\pi}\,\mathrm{Re} \int_0^{\pi} d\gamma \int_0^{\infty} dk \; e^{\,\mathrm{i}\,k\,(x\,\cos\gamma + y\,\sin\gamma)}\; A^L(k,\gamma) \quad \text{where}$$
$$A^L(k,\gamma) \equiv \frac{1 - e^{-k/f^2}(1 - k/f^2)}{1 - k/f^2} \; e^{\,k\,z}\, A(k,\gamma)$$
$$- e^{\,f^2 z} \left[\frac{e^{-C^2(1-k/f^2)^2/4}}{1 - k/f^2} \; A_*(\gamma) + \frac{e^{-C^2(1+k/f^2)^2/4}}{1 + k/f^2} \; A_*(\gamma - \pi) \right]$$

$$\Delta \;,\; \Delta_1 \;\&\; \mathcal{A}$$